Dissertation
submitted to the
Combined Faculties for the Natural Sciences and for Mathematics
of the Ruperto-Carola University of Heidelberg, Germany
for the degree of
Doctor of Natural Sciences

presented by

MSc. Octavian Postavaru
born in Tulcea, Romania

Oral examination: 8$^{\text{th}}$ December 2010

To Dan, Raica and Silviu Postavaru.
This thesis is for you.

STRONG-FIELD RELATIVISTIC PROCESSES IN HIGHLY CHARGED IONS

Referees: **Prof. Dr. Christoph H. Keitel**
Prof. Dr. Sandra P. Klevansky

ZUSAMMENFASSUNG

In der vorliegenden Arbeit untersuchen wir durch starke Felder hervorgerufene relativistische Prozesse in hochgeladenen Ionen. Im ersten Teil der Arbeit studieren wir die Resonanzfluoreszenz von Laser-getriebenen Ionen im relativistischen Bereich, indem wir die zeitabhängige Master-Gleichung in einem Mehrniveaumodell lösen. Unser ab initio Ansatz, basierend auf der Dirac-Gleichung, ermöglicht es hochrelativistische Ionen zu untersuchen und liefert folglich eine präzise Methode, um korrelierte relativistische Dynamik, Phänomene der Quantenelektrodynamik gebundener Zustände und Kerneffekte durch die Anwendung von kohärentem Röntgenlicht zu überprüfen. Atomare Dipol- oder Multipolmomente können bis zu nie da gewesener Genauigkeit bestimmt werden, indem das durch Interferenz verschmälerte Fluoreszenzspektrum gemessen wird. Desweiteren untersuchen wir die Niveaustruktur von schweren Wasserstoff-ähnlichen Ionen in Laserfeldern. Die Wechselwirkung mit dem Lichtfeld führt zu dynamischen Verschiebungen der elektrischen Energieniveaus, was relevant ist für Spektroskopieexperimente. Die elektrischen Zustände werden vollständig relativistisch behandelt durch die Dirac-Gleichung. Unser Formalismus geht über die Dipolapproximation hinaus und berücksichtigt Nicht-Dipoleffekte wie Retardierung und die Wechselwirkung mit den Magnetfeldkomponenten des Laserfeldes. Wir konnten Wirkungsquerschnitte für die zwischen-Schalen trielektrische Rekombination (TR) und den quadruelektrischen Rekombinationsprozess vorhersagen, welche experimentell mit Hilfe von Elektronenstrahl-Ionenfallen bestätigt wurden, hauptsächlich für C-artige Ionen von Ar, Fe und Kr. Für Kr^{30+} wurden Zwischen-Schalen TR-Beiträge von nahezu 6% zur gesamten resonanten Photorekombinationsrate gefunden.

ABSTRACT

In this thesis we investigate strong-field relativistic processes in highly charged ions. In the first part, we study resonance fluorescence of laser-driven highly charged ions in the relativistic regime by solving the time-dependent master equation in a multi-level model. Our ab initio approach based on the Dirac equation allows for investigating highly relativistic ions, and, consequently, provides a sensitive means to test correlated relativistic dynamics, bound-state quantum electrodynamic phenomena and nuclear effects by applying coherent light with x-ray frequencies. Atomic dipole or multipole moments may be determined to unprecedented accuracy by measuring the interference-narrowed fluorescence spectrum. Furthermore, we investigate the level structure of heavy hydrogenlike ions in laser beams. Interaction with the light field leads to dynamic shifts of the electronic energy levels, which is relevant for spectroscopic experiments. We apply a fully relativistic description of the electronic states by means of the Dirac equation. Our formalism goes beyond the dipole approximation and takes into account non-dipole effects of retardation and interaction with the magnetic field components of the laser beam. We predicted cross sections for the inter-shell trielectronic recombination (TR) and quadruelectronic recombination processes which have been experimentally confirmed in electron beam ion trap measurements, mainly for C-like ions, of Ar, Fe and Kr. For Kr^{30+}, inter-shell TR contributions of nearly 6% to the total resonant photorecombination rate were found.

In connection with the work performed during the thesis, the following paper was published or accepted in refereed journals:

- C. Beilmann, O. Postavaru, L. H. Arntzen, R. Ginzel, C. H. Keitel, V. Mäckel, P. H. Mokler, M. C. Simon, H. Tawara, I. I. Tupitsyn, J. Ullrich, J. R. Crespo López-Urrutia, and Z. Harman, *Intershell trielectronic recombination with K-shell excitation in* Kr^{30+}, Phys. Rev. A 80, 050702(R) (2009)
- C. Beilmann, P. H. Mokler, S. Bernitt, Z. Harman, C. H. Keitel, O. Postavaru, J. Ullrich, and J. R. Crespo López-Urrutia, *Resonant high-order electronic recombination in medium-Z highly charged ions*, J. Phys: Conf. Ser., accepted (2010)
- O. Postavaru, Z. Harman, C. H. Keitel, *High-precision metrology of highly charged ions via relativistic resonance fluorescence*, Phys. Rev. Letter 106, 033001 (2011)

Results from work on the thesis currently in preparation:

- O. Postavaru, Z. Harman, C. H. Keitel, *Relativistic light-shifts in hydrogen-like ions*
- O. Postavaru, Z. Harman, C. H. Keitel, *Relativistic theory of resonance fluorescence in three-level systems*

DECLARATION

The work in this thesis is based on research carried out at the Max Planck Institute for Nuclear Physics (MPIK) in Heidelberg, Germany, within the Theory Division of Prof. Dr. Christoph H. Keitel, *Theoretical Quantum Dynamics in Intense Laser Fields*. No part of this thesis has been submitted elsewhere for any other degree or qualification and it is all my own work unless referenced to the contrary in the text.

Contents

List of Figures

–I–

INTRODUCTION

In the present thesis, we theoretically investigate strong-field dynamical processes in highly charged ions. Highly charged ions (HCI) are ions in high charge states, i.e. with most of the shell electrons removed. An example of a highly charged ion is e.g. carbonlike (C-like) krypton (see Fig. 1.1), which was also studied in this work and in our experimental collaboration (see Chapter 4). Research with these exotic ions is motivated by several areas of science. The strong Coulomb field of the nucleus allows tests of quantum electrodynamics in the strongest electromagnetic fields accessible. Due to the large overlap of the electronic probability density with the nuclear matter, nuclear effects on the electronic shell can also be effectively investigated in such species, and nuclear properties can be inferred through experiments with ions in high charge states. For example, one can find HCI in cosmic matter, or produce them artificially in the laboratory by means of Tokamak plasmas or electron beam ion traps (EBITs) .

Quantum electrodynamics (QED) is the best confirmed field theory in physics. QED has an enormous success in predicting the electrons properties in weak fields. Approximately 50 years ago, Lamb and Rutherford observed for the first time a shift, the Lamb shift, in the atomic structure scheme of the hydrogen atom. Now QED effects like the Lamb shift can be calculated with high accuracy. The nuclear Coulomb field increasing with the charge number Z determines the atomic strucutre of an ion. Thus, a primary goal of research with HCI is to explore the behavior of electrons in the strongest electromagnetic fields accessible to experimental investigation. The QED phenomena in intense fields can be studied by measuring electron binding energies. One can test the QED predictions comparing them with the experimentally determined level energies. Due to the strong nuclear Coulomb field, the HCI cannot be described perturbatively. Therefore, one needs to turn to a non-perturbative treatment and apply the exact wave functions and propagators corresponding to the strong central nuclear field. Also, the appearance of poles in the Green's functions due to bound states and the presence of the negative Dirac continuum introduces further issues that need to be accounted for in a rigorous theoretical treatment of such systems.

Uranium is the heaviest element in which QED effects can be studied in the laboratory: the transuranium elements are radioactive and usually short lived, forbidding a conclusive experimental study of the electron shell. Heavy lithium-like ions are particularly well suited because the electron-electron interaction contributions can be calculated reliably and the relatively low atomic excitation energies are strongly influenced by QED effects.

HCI do not occur naturally on Earth, but they are highly present in the universe, since astrophysical plasmas such as those in stars have usually very high temperatures. This motivates to investigate HCI from an astrophysical point of view. The radiation from HCI is intense and may be detected on the Earth or in space laboratories, therefore, recorded electromagnetic spectra of HCI may deliver information for a better understanding of astrophysical processes.

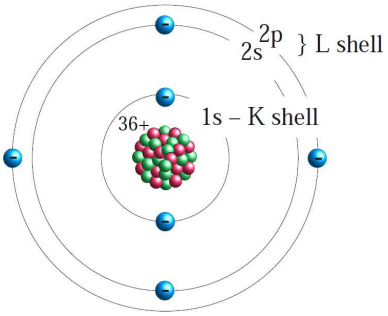

Figure 1.1: An example of a highly charged atomic ion: carbon-like krypton. Its charge number is Z=36, just like that of the neutral krypton atom, and its shell consists of six electrons just like in the case of the carbon atom. The ions net charge is therefore $q = +30e$, with e being the elementary charge, and the ion is denoted as Kr^{30+}.

Research with HCI is also motivated by its interest for controlled nuclear fusion, which may be the dominant source of energy used by mankind in the future. In Tokamak plasmas, atoms from the wall of the chamber are constantly ionized to high charge states. Also, gases such as argon and krypton are artifically injected into the plasma: through energetic collisions within the electron beam, they lose most of their shell electrons, and become highly charged. During this process, and through photorecombination, x rays are emitted, which works to cool the plasma. This gives one an additional degree of freedom to control the thermodynamics of the hot plasma. Furthermore, the emission lines originating from HCI provide an important plasma diagnostic tool. The competing processes of collisional excitation and ionization and radiative and collisional de-excitation and recombination of HCI in a plasma are defined by the plasma parameters such as composition, temperature and density. Such a situation can only very approximately be described by plasma models and is nowadays treated by involved numerical simulations, for which respective precise atomic data from theoretical calculations or experiments is a prerequisite.

The discovery of the parity non-conservation (PNC) – the lack of left-right mirror symmetry – in the beta decay of ^{60}Co by Wu and co-workers about forty years ago marked an important landmark in the history of physics. The parity non-conservation in cesium atoms has lead to the discovery of the nuclear anapole moment. Even for physics beyond the Standard Model, parity non-conservation could be used as an important probe. A further increase in sensitivity to PNC phenomena are expected from theoretical and experimental studies involving highly charged ions: the inner-shell electrons mostly influenced by PNC effects can be most effectively addressed in heavy few-electron systems. Experiments with highly charged uranium ions to explore this field are currently planned at FAIR to be constructed as an extension of the GSI facility at Darmstadt, Germany.

After this general overview about the relevance of HCI in physics, in the following we give a more detailed summary of the topics discussed in this thesis:

In Chapter 2, we develop a fully relativistic theory of resonance fluorescence. In the process of resonance fluorescence, a two- or many-level atomic system is driven by a laser field, and the power spectrum is measured. In principle, if the field is monochromatic, we expect the atom to absorb and to re-emit photons at the same frequency. The spectral width of the fluorescent light is given by the natural decay width of the upper state. The situation becomes more complicated when the intensity of light increases and the Rabi frequency becomes comparable to the transition linewidth. In this situation, due to the Stark splitting, the sidebands start to show up in the spectrum of fluorescence radiation. This is the so-called Mollow spectrum.

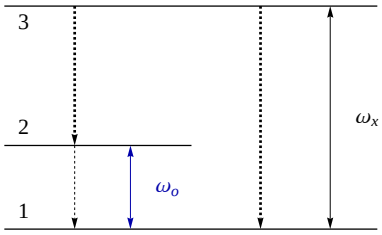

Figure 1.2: Level scheme of an atomic three-level system driven by two different laser fields. In the relativistic ionic systems studied in our work, the transition between the uppermost level 3 and the ground state 1 has energies in the keV range and is driven by an x-ray laser (frequency ω_x). Level 1 and 2 are hyperfine-split ground state sublevels with transition energies in the eV range, and are connected by an optical laser (frequency ω_o). The thick arrows represent fast (electric dipole) spontaneous decay channels and the thin arrows represent slow (magnetic dipole) decay transitions.

In the case of atomic systems with higher nuclear charges or in the case of certain transitions, the usual non-relativistic treatment is not valid. Not only do the electronic wave functions differ significantly from the Schrödinger wave functions, but also the interaction with the light field is modified. Therefore, we formulate an ab initio description that is inherently relativistic, i.e. it is based on the Dirac equation. Such a formalism is especially needed in the case of inner-shell transitions of highly charged ions. These transitions can nowadays or in the near future be driven by x-ray lasers or coherent x-ray light created by high harmonic generation schemes, therefore, the understanding of the relativistic resonance fluorescence spectrum is mandatory.

The theoretical description of resonance fluorescence is not only interesting on its own but it also lays the foundation of laser spectroscopic methods. High-precision optical laser spectroscopy is a versatile tool to investigate correlated relativistic quantum dynamics, the testing of fundamental theories like quantum electrodynamics (QED) [8, 39] or parity non-conservation in atomic systems, as summarized previously. In the regime of heavy few-electron systems, however, the accuracy of optical spectroscopy can seldom be exploited due to the scarcity of low-frequency transitions. With the advent of modern short-wavelength laser systems, the accuracy and versatility of laser spectroscopy may be combined with the increased sensitivity to relativistic and QED effects and nuclear properties at higher nuclear charges and for inner-shell transitions. Brilliant x-ray light has recently enabled to study transitions in the x-ray regime. Coherent light with photon energies over 10 keV becomes experimentally accessible in the near future [1, 2], allowing for an extension to heavier systems and the exploitation of coherence properties.

We study resonance fluorescence of laser-driven highly charged ions in the relativistic regime by solving the time-dependent master equation in a multi-level model. Our ab initio approach may provide a sensitive spectroscopic tool by applying coherent light with x-ray frequencies. In the scheme we put forward, atomic dipole or multipole moments may be determined to unprecedented accuracy by measuring the interference-narrowed fluorescence spectrum. To this end, we develop a theoretical formalism for relativistic resonance fluorescence of a three-level atomic configuration driven by two fields, namely, a short-wavelength laser and a long-wavelength light source in the optical regime. This scheme is illustrated in Fig. 1.2. In such a three-level setting, the linewidth of the spontaneous transition of interest may be rendered much narrower than the natural linewidth, with the simultaneous increase of the total emitted intensity by orders of magnitude. Due to this effect, the determination of atomic multipole moments by means of the detection of the fluorescence spectrum is anticipated to largely increase in accuracy.

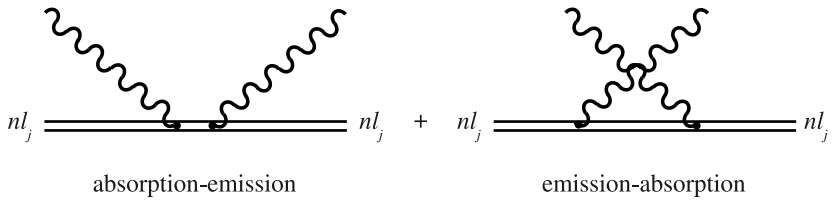

Figure 1.3: Diagrams illustrating the second-order light shift effect with bound relativistic electrons. The double lines represent Furry-picture electronic wave functions and propagators, i.e. solutions of the Dirac equation with the Coulomb nuclear potential. The wavy lines represent emitted or absorbed real photons from the laser field.

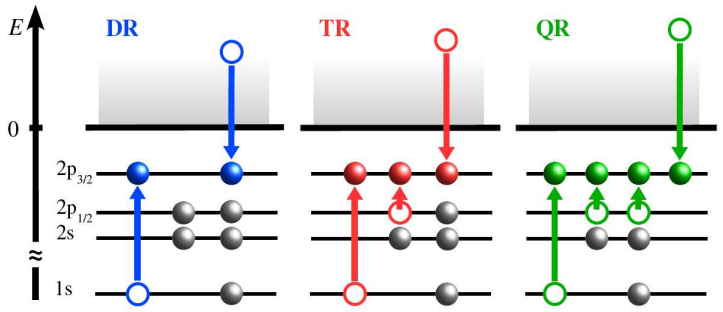

Figure 1.4: Scheme of resonant electron recombination processes in a six-electron ion: In DR (blue diagram) one bound electron is excited by the captured electron, in TR (red diagram) two and in QR (green diagram) three electrons are promoted by the captured electron.

Furthermore, we investigate in Chapter 3 the level structure of heavy hydrogenlike ions in laser beams with off-resonant frequencies. In heavy ions, the electrons are tightly bound by the Coulomb potential of the nucleus, which prohibits ionization even by strong lasers. However, interaction with the light field leads to dynamic shifts of the electronic energy levels. The dominant diagrams are illustrated in Fig. 1.3. Here we again apply a relativistic description of the electronic states by means of the Dirac equation. Theoretical investigation so far apply non-relativistic approaches and are restricted to electric dipole transitions. Our relativistic generalization allows one to extend the field of investigations to stronger laser fields, higher frequencies – e.g., x-ray lasers [27] –, and to the highest nuclear charges. Interaction with the monofrequent laser field is treated by time-dependent perturbation theory. Our formalism goes beyond the Stark long-wavelength dipole approximation and takes into account non-dipole effects of retardation and interaction with the magnetic field components of the laser beam. The resulting level shifts are relevant for experiments at present and near-future laser facilities.

In Chapter 4, we develop a relativistic theoretical formalism and summarize the computational scheme used for the description of resonant many-body recombination processes. Such processes provide a viable alternative to laser spectroscopy: the ions are excited by beams of electrons rather than photons, which allows the experimental study of transitions with keV energies even without the use of large-scale x-ray sources such as synchrotrons or free electron lasers. The most fundamental resonant recombination process is dielectronic recombination (DR). In this two-step process, a free electron is captured into a bound state of the ion with the simultaneous excitation of a second, bound electron. This inverse Auger process is followed by a radiative de-excitation of the so-formed state, completing the photorecombina-

tion process. This process is illustrated in the first panel of Fig. 1.4. DR often represents the dominant pathway for populating excited states in plasmas and, consequently, for inducing easily observable x-ray emission lines which are used as diagnostic tools for fusion plasmas (whereby Kr as well as Ar were chosen as ideal candidates) [22,80], triggering a range of DR studies with highly charged Kr ions [11,29,66]. From a more fundamental point of view, the selectivity of DR [13] allows testing stringently sophisticated atomic structure and dynamics calculations, in particular of relativistic and QED effects in strong electromagnetic fields.

Beyond the well-known DR, resonant recombination processes involving higher-order correlations are relevant, too. Here, as displayed in Fig. 1.4, two or even three bound electrons can be simultaneously excited by the resonantly captured electron in trielectronic or even quadruelectronic recombination (TR and QR, respectively). It is important to mention that in general TR and QR offer new photorecombination channels and their contribution to the radiative cooling of Tokamak and astrophysical plasmas needs to be considered in the theoretical modeling. We calculated TR and QR resonance energies and cross sections in the framework of the multiconfiguration Dirac-Fock (MCDF) method, which can be regarded as a relativistic generalization of the Hartree-Fock scheme and will be also briefly described in Chapter 4.

We investigate trielectronic recombination with simultaneous excitation of a K-shell and a L-shell electron, hence involving three active electrons. Our theoretical prediction triggered experimental activities at the electron beam ion trap facility of the Max Planck Institute for Nuclear Physics. The TR process was identified in the x-ray emission spectrum of recombining highly charged Kr, Fe and Ar ions trapped in the EBIT. An energy resolution three times higher than any reported for this collision energy range around 10 keV resulted in the separation of the associated lines from the stronger dielectronic resonances. For Kr^{30+}, inter-shell TR contributions of nearly 6% to the total resonant photorecombination rate were found, and even higher contributions in the case of the lighter elements of Ar and Fe are deduced from both theoretical and experimental spectra.

In Chapter 5, conclusions and a brief outlook including proposals concerning possible future theoretical and experimental work are given. Some additional derivations and intermediate results are presented in the Appendix.

–II–

RELATIVISTIC THEORY OF RESONANCE FLUORESCENCE IN A TWO- AND THREE-LEVEL SYSTEM

2.1 Introduction

High-precision laser spectroscopy has resulted in crucial advancements in our understanding of nature. In particular, optical laser spectroscopy (OS) is a versatile tool to investigate correlated relativistic quantum dynamics, the testing of fundamental theories like quantum electrodynamics (QED) [8, 39] or parity non-conservation in atomic systems. The determination of atomic dipole or multipole moments via lifetime measurements by means of, e.g., visible emission spectroscopy [53], approaching the accuracy of one per thousand, sheds light on QED effects like the electron anomalous magnetic moment. Isotope shifts (IS) in atomic spectra which has been providing valuable insight into the collective structure of nuclei: for example, recently, isotope shifts were determined two-photon Doppler-free spectroscopy and by collinear laser spectroscopy [31, 69]. Beyond purely nuclear effects, the interaction of the correlated motion of electrons and that of the nucleus can be studied in IS measurements: recently, relativistic effects on nuclear recoil [73] have been measured in visible forbidden transitions of the few-electron argon ions by a trapped-ion method [77].

In the regime of heavy few-electron systems, however, the accuracy of optical spectroscopy can seldom be exploited due to the scarcity of low-frequency transitions. Therefore, one has to apply other techniques. Measuring the $2s \leftrightarrow 2p$ x-ray emission lines of highly charged uranium ions confined in an electron beam ion trap allowed testing strong-field QED on the two-loop level [8] and delivered a new value for the radius of the radioactive isotope ^{235}U [26]. Recently, a method based on the storage ring measurement of dielectronic recombination spectra has yielded the change of the mean square charge radius for Nd isotopes [12, 21].

With the advent of modern short-wavelength laser systems, the accuracy and versatility of laser spectroscopy may be combined with the increased sensitivity to relativistic and QED effects and nuclear properties at higher nuclear charges and for inner-shell transitions. Brilliant x-ray light has recently enabled to study transitions in the soft x-ray regime in the intermediate range of nuclear charges [27]. Coherent light with photon energies over 10 keV becomes experimentally accessible in the near future [1], allowing for an extension to heavier systems and the exploitation of coherence properties. This would also ask for the validity of numerous quantum control schemes of resonance fluorescence [48, 61, 64, 71, 81, 82] for concrete systems in the relativistic regime.

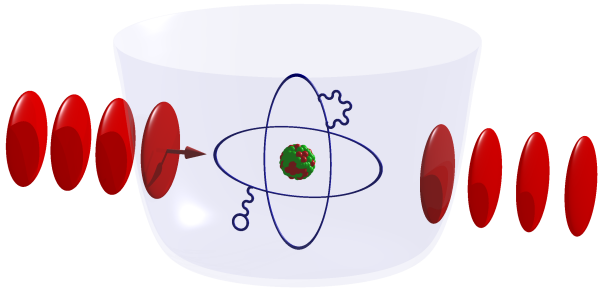

Figure 2.1: Schematic setup of a resonance fluorescence experiment with trapped highly charged ions: the ions are trapped in the electromagnetic potential of an EBIT, Paul trap or Penning trap, and a laser beam is directed through the ion cloud. Emitted photons (not shown) are registered with a detector or spectrometer.

In the present work, we investigate the possibility of measuring atomic transition dipole – or multipole – moments and transition energies via relativistic resonance fluorescence of a three-level atomic configuration driven by two fields, namely, a short-wavelength laser and a long-wavelength light source in the optical regime. In such a three-level setting, the linewidth of the spontaneous transition of interest may be rendered much narrower than the natural linewidth, with the simultaneous increase of the total emitted intensity by orders of magnitude. Due to this effect, the determination of atomic multipole moments by means of the detection of the fluorescence spectrum is anticipated to increase in accuracy by several orders of magnitude.

As relativistic effects on the bound electronic wave function increase rapidly with the nuclear charge number Z, one needs to formulate a fully relativistic theory of coherent laser-atom interaction based on the Dirac equation [23]. Not only do the electronic wave functions differ significantly from the Schrödinger wave functions, but also the interaction with the laser light is modified. For example, magnetic dipole transitions, which are non-relativistically forbidden even in the visible range, can only be explained by a relativistic theory. An approach via the time-dependent numerical solution of the Dirac equation was recently employed to describe ionization phenomena [43]. For our purposes, one needs to go beyond this approach and incorporate radiative relaxation in bound-bound transitions. These transitions can nowadays or in the near future be driven by x-ray or soft x-ray lasers, therefore, the understanding of the relativistic resonance fluorescence spectrum is indispensable.

2.2 The spectrum of resonance fluorescence in two-level approximation

In the process of the resonance fluorescence, an atomic system is driven by a laser field, and the power spectrum of the emitted radiation is measured. If the field is monochromatic, we expect the atom to absorb and to re-emit photons at the same frequency. The spectral width of the fluorescent light is given by the natural decay width of the upper state. The situation becomes more complicated when the Rabi frequency associated with the driving field becomes comparable to, or larger than the transition linewidth. In this situation, due to the Stark splitting, the sidebands start emerging in the spectrum of emitted radiation. These sidebands, together with the central peak, form the so-called Mollow spectrum.

2.2.1 Description of the model and equations of motion

In this section, we are interested in the evolution of a two-level system driven by an incident field of arbitrary strength whose carrier frequency ω is resonant or nearly resonant with the atomic transition. The aim is to calculate the complete power spectrum of the radiation spontaneously emitted by the atomic system ('atom'). The atom is assumed to be isolated and fixed in position.

Let us consider the interaction of a laser having the frequency ω with a two-level atomic system. We consider $|a\rangle$ being the upper state, and $|b\rangle$ the lower state of the atom. Considering $\mathscr{H}_0$ the unperturbed Hamiltonian, the following eigenvalue equations hold for the states: $\mathscr{H}_0|a\rangle = \hbar\omega_a|a\rangle$ and $\mathscr{H}_0|b\rangle = \hbar\omega_b|b\rangle$. The most general wave function of a two-level system has the form [72]

$$|\Psi(t)\rangle = C_a(t)|a\rangle + C_b(t)|b\rangle\,. \tag{2.1}$$

The coefficient C_a is the probability amplitude to find the atom in state $|a\rangle$, and C_b to find it in the state $|b\rangle$. The total Hamiltonian is the sum of unperturbed and the interaction Hamiltonians, i.e., $\mathscr{H} = \mathscr{H}_0 + \mathscr{H}_1$. One may use the closure property $|a\rangle\langle a| + |b\rangle\langle b| = 1$ in order to get the relation [72]

$$\begin{aligned} \mathscr{H}_0 &= (|a\rangle\langle a| + |b\rangle\langle b|)\mathscr{H}_0(|a\rangle\langle a| + |b\rangle\langle b|) \\ &= \hbar\omega_a|a\rangle\langle a| + \hbar\omega_b|b\rangle\langle b|\,. \end{aligned} \tag{2.2}$$

One can use the same trick in order to put the interaction Hamiltonian $\mathscr{H}_1$ in the form [72]

$$\begin{aligned} \mathscr{H}_1 &= -exE(t) \\ &= -e(|a\rangle\langle a| + |b\rangle\langle b|)x(|a\rangle\langle a| + |b\rangle\langle b|)E(t) \\ &= -(\gamma_{ab}|a\rangle\langle b|e^{-i\omega t} + \gamma_{ba}|b\rangle\langle a|e^{-i\omega t})\mathscr{E}\,, \end{aligned} \tag{2.3}$$

where $\gamma_{ab} = e\langle a|x|b\rangle$ is the transition matrix element and $E(t) = \mathscr{E}(e^{-i\omega t} + e^{i\omega t})$ is the field. We kept the conservative terms only, all other being neglected in the rotating wave approximation. In the above equation we consider that the electric field is linearly polarized along the x-axis. It is easy to derive the Hamiltonian of a two-level system interacting with a classical field as

$$\mathscr{H} = \sum_{i=1}^{2} \varepsilon_i|i\rangle\langle i| + \Omega_R(e^{-i\omega t}|2\rangle\langle 1| + e^{i\omega t}|1\rangle\langle 2|)\,. \tag{2.4}$$

The energies of the stationary states are denoted by ε_i (i=1,2). Ω_R is the Rabi frequency, that depends on the atomic matrix element as well as on the strength of the laser field.

In order to extract a piece of the system's information from a state vector $|\Psi\rangle$, we calculate the quantum mechanical expectation value of a given operator O,

$$\langle O\rangle_{\mathrm{QM}} = \langle\Psi|O|\Psi\rangle\,. \tag{2.5}$$

Usualy we may only know the probability P_Ψ that the system is in the state $|\Psi\rangle$. In this sitauations, we should do the ensemble average over many replica systems that have been similarly prepared

$$\langle\langle O\rangle_{\mathrm{QM}}\rangle_{\mathrm{ensemble}} = \mathrm{Tr}(O\rho)\,, \tag{2.6}$$

with

$$\rho = \sum_{\Psi} P_\Psi|\Psi\rangle\langle\Psi|\,. \tag{2.7}$$

If one can write $\rho = |\Psi_0\rangle\langle\Psi_0|$, than we call $|\Psi_0\rangle$ a pure state. It is easy to see that $\mathrm{Tr}(\rho^2) = 1$.

Starting with the Schrödinger equation, one can write the equation for the density matrix as

$$|\dot{\Psi}\rangle = -\frac{i}{\hbar}\mathscr{H}|\Psi\rangle\,. \tag{2.8}$$

From Eq. (2.7) one may get

$$\dot{\rho} = \sum_{\Psi} P_{\Psi}(|\dot{\Psi}\rangle\langle\Psi| + |\Psi\rangle\langle\dot{\Psi}|)\,, \tag{2.9}$$

considering P_Ψ time independent. Using Eq. (2.8) to replace $|\dot{\Psi}\rangle$ and $\langle\dot{\Psi}|$ in Eq.(2.9) we get the reversible part of the Liouville equation

$$\dot{\rho} = -\frac{i}{\hbar}[\mathscr{H}, \rho]\,. \tag{2.10}$$

The Liouville equation in the interaction picture is

$$\dot{\rho'} = -\frac{i}{\hbar}[\mathscr{H}_1', \rho']\,, \tag{2.11}$$

with

$$\mathscr{H}_1' = \hbar\Omega_R(|2\rangle\langle 1|e^{i\Delta t} + |1\rangle\langle 2|e^{-i\Delta t})\,, \tag{2.12}$$

and $\Delta = \omega_{21} - \omega$. The prime denotes that we are dealing with the interaction picture. Now we do the following transformation:

$$R_{ii} = \rho_{ii}\,(i = 1, 2), \quad R_{12} = \rho_{12}e^{i\Delta t}\,, \tag{2.13}$$

and this allows us to write the master equation in terms of R_{ij}. In the case of the irreversible part of the master equation, the equation is more complicated [61]

$$\dot{\rho}'_{irrev} \equiv \Lambda\rho' = \sum_{i,j}[|i\rangle\langle j|\rho'|j\rangle\langle i|(A_{jiij} + A^*_{jiij}) - |j\rangle\langle j|\rho' A_{jiij} - \rho'|j\rangle\langle j|A^*_{jiij}]\,, \tag{2.14}$$

with the A_{jiij} being the complex rate constants, the μ_{ij} being the polarization decay rates and the $\Delta\Omega_{ij}$ frequency shifts. They are defined as [61]

$$\begin{aligned} \Gamma_{ij} &= A_{jiij} + A^*_{jiij}\,, \\ \mu_{ij} &= \sum_k \Re(A_{ikki} + A^*_{jkkj}) = \frac{1}{2}\sum_k(\Gamma_{ik} + \Gamma_{jk})\,, \\ \Delta\Omega_{ij} &= -\sum_k \Im(A_{jkkj} + A^*_{ikki})\,. \end{aligned} \tag{2.15}$$

We shell neglect possible elastic collisions in the following, i.e., we set $A_{iiii} = 0$.

The full master equation reads

$$\dot{\rho'} = -\frac{i}{\hbar}[\mathscr{H}_1', \rho'] + \Lambda\rho'\,. \tag{2.16}$$

Written in terms of the variable R_{ij}, Eq. (2.16) becomes

$$\begin{aligned} \frac{dR_{12}}{d\tau} &= (i\tilde{\Delta} - \tilde{\gamma}_{12})R_{12} + 2i\beta R_{22} - i\beta\,, \\ \frac{dR_{22}}{d\tau} &= -i\beta R_{12} + i\beta R_{21} - (1 + \tilde{\Gamma}_{12})R_{22} + 1\,, \end{aligned} \tag{2.17}$$

with

$$R_{11} = 1 - R_{22}\text{and} \quad R_{21} = R_{12}^{*}\,. \tag{2.18}$$

In Eqs. (2.17) we used the notation $\tau = \Gamma_{21}t$, and $\beta = \Omega_R/\Gamma_{21}$. All other quantities labeled with a tilde are scaled to Γ_{21}. The master equation in terms of Ψ is

$$\frac{d}{d\tau}\Psi = L\Psi + I\,, \tag{2.19}$$

with the components

$$\Psi_1 = R_{12}\,, \quad \Psi_2 = R_{21}\,, \quad \Psi_3 = R_{22}\,, \tag{2.20}$$

and L is an (3×3) matrix

$$L = \begin{pmatrix} i\tilde{\Delta} - \tilde{\gamma}_{12} & 0 & 2i\beta \\ 0 & -i\tilde{\Delta} - \tilde{\gamma}_{21} & -2i\beta \\ -i\beta & i\beta & -(1 + \tilde{\Gamma}_{12}) \end{pmatrix}. \tag{2.21}$$

The components of I are

$$I_1 = -i\beta\,, \quad I_2 = i\beta\,, \quad I_3 = 1\,. \tag{2.22}$$

Applying the regression theorem one gets

$$\hat{\Psi}(z) = M(z)\Psi(\tau_0) + \frac{1}{z}M(z)I\,, \tag{2.23}$$

or

$$\hat{\Psi}_i(z) = \sum_j M_{ij}(z)\Psi_j(\tau_0) + \frac{1}{z}\sum_j M_{ij}(z)I_j\,, \tag{2.24}$$

with

$$M = (z - L)^{-1}\,. \tag{2.25}$$

The Eq. (2.19) for the steady-state case gives

$$\Psi(\infty) = -L^{-1}I\,, \tag{2.26}$$

or, in component form,

$$\Psi_i(\infty) = -\sum_j (L^{-1})_{ij}I_j\,. \tag{2.27}$$

2.2.2 Electric field operator for spontaneous emission from a single atom

We first discuss the interaction of the quantized radiation field with a two- or three-level atomic system described by a Hamiltonian in the dipole approximation [72]. For a single-mode field it reduces to a particularly simple form. This Hamiltonian provides the simplest illustration of spontaneous emission and an explanation of effects of various kind.

The spontaneous decay of an atomic level is treated by considering the interaction of the atomic levels with the modes in the vacuum state. We examine the state of the field that is generated in the process of emission of a quantum of energy equal to the energy difference between the atomic levels. Such a state may be regarded as a single-photon state.

The Hamiltonian of the interaction in the dipole approximation between an atom and an electromagnetic field is given by:

$$\mathscr{H} = \mathscr{H}_A + \mathscr{H}_F - e\mathbf{r}\mathbf{E}. \tag{2.28}$$

$\mathscr{H}_A$ represents the Hamiltonian operator for the atom without interaction, and $\mathscr{H}_F$ is the Hamiltonian of the radiation field without interaction. The vector $\mathbf{r}$ points from the nucleus to the electron. For relativistic atomic systems, e.g. for a single-electron ion, the Hamiltonian is given by

$$\mathscr{H}_A = c\boldsymbol{\alpha}\boldsymbol{p} + \boldsymbol{\beta}m_0c^2 - \frac{Ze^2}{4\pi\epsilon_0 r}\,. \tag{2.29}$$

In the above equation, $\boldsymbol{\alpha}$ and $\boldsymbol{\beta}$ are the usual Dirac matrices and $\boldsymbol{p}$ is the three-momentum of the electron. We note here that the above treatment can be extended to many-electron atoms in a rather straightforward way.

The free field operator, $\mathscr{H}_F$, is given in the quantized form, i.e., in terms of the creation and annihilation operators

$$\mathscr{H}_F = \sum_{\mathrm{k}} \hbar\nu_{\mathrm{k}} \left(a_{\mathrm{k}}^\dagger a_{\mathrm{k}} + \frac{1}{2} \right)\,. \tag{2.30}$$

If we are introducing the atomic transition operators

$$\sigma_{ij} = |i\rangle\langle j|\,, \tag{2.31}$$

we can write $\mathscr{H}_A$ and $e\mathbf{r}$ as a function of these operators. In the following computation we use the fact that the states $\{|i\rangle\}$ represent a complete set of eigenstates, i.e. $\sum_i |i\rangle\langle i| = 1$. Let us consider the eigenvalue equation $\mathscr{H}_A|i\rangle = E_i|i\rangle$ and then we find the expression for $\mathscr{H}_A$ [72]

$$\mathscr{H}_A = \sum_i E_i|i\rangle\langle i| = \sum_i E_i\sigma_{ii}\,. \tag{2.32}$$

Applying the same procedure, we can express the dipole moment as [72]

$$e\mathbf{r} = \sum_{i,j} e|i\rangle\langle i|\mathbf{r}|j\rangle\langle j| = \sum_{i,j} \gamma_{ij}\sigma_{ij}\,, \tag{2.33}$$

where we introduce the notation $\gamma_{ij} = e\langle i|\mathbf{r}|j\rangle$.

For the atom at the origin, the electric field operator is evaluated in the dipole approximation as

$$\mathbf{E} = \sum_{\mathrm{k}} \hat{\epsilon}_{\mathrm{k}}\mathscr{E}_{\mathrm{k}}(a_{\mathrm{k}} + a_{\mathrm{k}}^\dagger)\,, \tag{2.34}$$

with $\mathscr{E}_{\rm k} = (\hbar\nu_{\rm k}/2\epsilon_0 V)^{1/2}$.

After these considerations, it is easy to see that [72]

$$\mathscr{H} = \sum_{\rm k} \hbar\nu_{\rm k} a_{\rm k}^\dagger a_{\rm k} + \sum_i E_i \sigma_{ii} + \hbar \sum_{i,j} \sum_{\rm k} g_{\rm k}^{ij} \sigma_{ij} (a_{\rm k} + a_{\rm k}^\dagger)\,, \tag{2.35}$$

where

$$g_{\mathbf{k}}^{ij} = -\frac{\gamma_{ij}\hat{\epsilon}_{\mathbf{k}}\mathscr{E}_{\mathbf{k}}}{\hbar}\,. \tag{2.36}$$

In the next calculations, we assume γ_{ij} to be real. For a two-level atomic system, $\gamma_{ab} = \gamma_{ba}$ and one can write

$$g_{\rm k} = g_{\rm k}^{ab} = g_{\rm k}^{ba}. \tag{2.37}$$

Now it is easy to see that

$$\mathscr{H} = \sum_{\rm k} \hbar\nu_{\rm k} a_{\rm k}^\dagger a_{\rm k} + (E_a\sigma_{aa} + E_b\sigma_{bb}) + \hbar \sum_{\rm k} g_{\rm k}(\sigma_{ab} + \sigma_{ba})(a_{\rm k} + a_{\rm k}^\dagger)\,, \tag{2.38}$$

with

$$E_a\sigma_{aa} + E_b\sigma_{bb} = \frac{1}{2}\hbar\omega(\sigma_{aa} - \sigma_{bb}) + \frac{1}{2}(E_a - E_b)\,. \tag{2.39}$$

The conservation of energy between these two states gives $(E_a - E_b) = \hbar\omega$. Using the notation

$$\begin{aligned} \sigma_z &= \sigma_{aa} - \sigma_{bb} = |a\rangle\langle a| - |b\rangle\langle b|, \\ \sigma_+ &= \sigma_{ab} = |a\rangle\langle b|, \\ \sigma_- &= \sigma_{ba} = |b\rangle\langle a|\,, \end{aligned} \tag{2.40}$$

we can put the Hamiltonian (2.38) in the form [72]

$$\mathscr{H} = \sum_{\rm k} \hbar\nu_{\rm k} a_{\rm k}^\dagger a_{\rm k} + \frac{1}{2}\hbar\omega\sigma_z + \hbar \sum_{\rm k} g_{\rm k}(\sigma_+ + \sigma_-)(a_{\rm k} + a_{\rm k}^\dagger)\,. \tag{2.41}$$

It is easy to verify that σ_+, σ_- and σ_z satisfy the spin-$1/2$ algebra of the Pauli matrices, i.e.,

$$\begin{aligned} [\sigma_-, \sigma+] &= -\sigma_z\,, \\ [\sigma_-, \sigma_z] &= 2\sigma_-\,, \\ [\sigma_+, \sigma_z] &= 2\sigma_+\,. \end{aligned} \tag{2.42}$$

We can represent, σ_-, σ_+ and σ_z in the matrix form [72]

$$\sigma_- = \begin{pmatrix} 0 & 0 \\ 1 & 0 \end{pmatrix}, \qquad \begin{pmatrix} 0 & 1 \\ 0 & 0 \end{pmatrix}, \qquad \begin{pmatrix} 1 & 0 \\ 0 & -1 \end{pmatrix}\,. \tag{2.43}$$

The σ_- operator takes an atom from the upper state into a lower state whereas σ_+ promotes an atom in the lower state into the upper state.

In the expression Eq. (2.41) we keep only the conservative terms –rotating-wave approximation–, i.e., $a_{\rm k}^\dagger\sigma_-$ and $a_{\rm k}\sigma_+$. The first term describes the atomic de-excitation with the creation of a photon of mode

k, and the second one describes the atomic excitation with photon annihilation. We get the simplified Hamiltonian

$$\mathscr{H} = \sum_{\mathrm{k}} \hbar\nu_{\mathrm{k}} a_{\mathrm{k}}^{\dagger} a_{\mathrm{k}} + \frac{1}{2}\hbar\omega\sigma_z + \hbar\sum_{\mathrm{k}} g_{\mathrm{k}}(\sigma_+ a_{\mathrm{k}} + a_{\mathrm{k}}^{\dagger}\sigma_-)\,. \tag{2.44}$$

An atom can be excited due to the interaction with a laser, and then it radiates spontaneously in all directions. In order to describe field propagation from an initial point $\mathbf{r_0}$ to a point $\mathbf{r}$, the fluorescent field should be related to the appropriate atomic operator at a retarded time.

In the rotating-wave approximation, the Hamiltonian (see Eq. 2.44) can be written as [72]

$$\mathscr{H} = \frac{\hbar\omega}{2}\sigma_z + \sum_{\mathbf{k},\lambda} \hbar\nu_\kappa a_{\mathbf{k},\lambda}^{\dagger} a_{\mathbf{k},\lambda} + \sum_{\mathbf{k},\lambda} \hbar g_{\mathbf{k},\lambda}\left(a_{\mathbf{k},\lambda}\sigma_+ e^{i\mathbf{k}\mathbf{r}_0} + a_{\mathbf{k},\lambda}^{\dagger}\sigma_- e^{-i\mathbf{k}\mathbf{r}_0}\right)\,. \tag{2.45}$$

The field modes are characterized by the wave vector $\mathbf{k}$ and polarization λ. One can apply the method of slowly-varying operators for the operators $a_{\mathbf{k},\lambda}(t)$ and $\sigma_-(t)$, i.e.,

$$\begin{aligned} a_{\mathbf{k},\lambda}(t) &= \widetilde{a}_{\mathbf{k},\lambda}(t)e^{-i\nu_\kappa t}, \\ \sigma_-(t) &= \widetilde{\sigma}_-(t)e^{-i\omega t}\,. \end{aligned} \tag{2.46}$$

For these operators, the Heisenberg equations of motion can be written as [72]

$$\begin{aligned} \dot{\widetilde{a}}_{\mathbf{k},\lambda}(t) &= -ig_{\mathbf{k},\lambda}\widetilde{\sigma}_-(t)e^{-i(\omega-\nu_\kappa)t - i\mathbf{k}\mathbf{r}_0}, \\ \dot{\widetilde{\sigma}}_-(t) &= \sum_{\mathbf{k},\lambda} ig_{\mathbf{k},\lambda}\sigma_z(t)\widetilde{a}_{\mathbf{k},\lambda}(t)e^{i(\omega-\nu_\kappa)t + i\mathbf{k}\mathbf{r}_0}\,, \end{aligned} \tag{2.47}$$

or in the integral form

$$\begin{aligned} \widetilde{a}_{\mathbf{k},\lambda}(t) &= \widetilde{a}_{\mathbf{k},\lambda}(0) - ig_{\mathbf{k},\lambda}e^{-i(\omega-\nu_\kappa)t - i\mathbf{k}\mathbf{r}_0}\int_0^t dt'\widetilde{\sigma}_-(t')e^{i(\omega-\nu_\kappa)(t-t')}, \\ \widetilde{\sigma}_-(t) &= \widetilde{\sigma}_-(0) + \sum_{\mathbf{k},\lambda} ig_{\mathbf{k},\lambda}e^{i(\omega-\nu_\kappa)t + i\mathbf{k}\mathbf{r}_0}\int_0^t dt'\sigma_z(t')\widetilde{a}_{\mathbf{k},\lambda}(t')e^{-i(\omega-\nu_\kappa)(t-t')}\,. \end{aligned} \tag{2.48}$$

In the right part, the operators at time $t = 0$ represent field and atomic operators in the absence of the interaction. Now we study the field modifications due to the interaction with the atom. The positive frequency part of the electric field is defined as

$$\mathbf{E}^{(+)}(\mathbf{r},t) = \sum_{\mathbf{k},\lambda} \mathscr{E}_{\mathbf{k}}\hat{\epsilon}_{\mathbf{k}}^{(\lambda)} a_{\mathbf{k},\lambda}(t)e^{i\mathbf{k}\mathbf{r}}\,, \tag{2.49}$$

with $\mathscr{E}_{\mathbf{k}} = (\hbar\nu_\kappa/2\epsilon_0 V)^{1/2}$. From the Eqs. (2.46) and (2.48) we can write [72]

$$\mathbf{E}^{(+)}(\mathbf{r},t) = \left(\frac{i}{16\pi^3\epsilon_0}\right)e^{-i\omega t}\int d^3k \sum_{\lambda}\hat{\epsilon}_{\mathbf{k}}^{(\lambda)}[\hat{\epsilon}_{\mathbf{k}}^{\lambda}\cdot\,\hat{\gamma}]\nu_\kappa e^{i\mathbf{k}(\mathbf{r}-\mathbf{r}_0)} \tag{2.50}$$

$$\times \int_0^t dt'\widetilde{\sigma}_-(t')e^{i(\omega-\nu_\kappa)(t-t')}, \tag{2.51}$$

where we have replaced the sum by an integral via

$$\sum_{\mathbf{k}} \to \frac{V}{(2\pi)^3}\int d^3k. \tag{2.52}$$

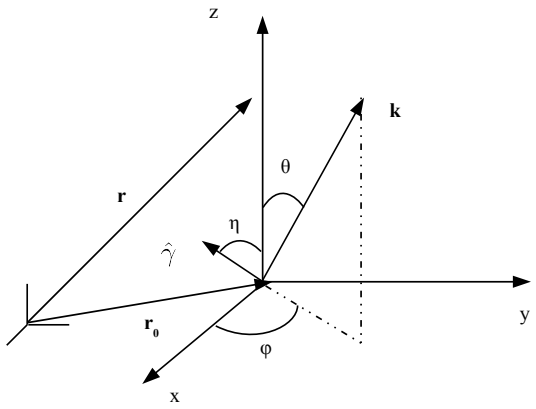

Figure 2.2: The atomic dipole γ and the $\mathbf{k}$-vector of the electric field in polar coordinates. η denotes the angle of the dipole with the z axis.

One can put the vector field operator in the following form [72]

$$\begin{aligned}\mathbf{E}^{(+)}(\mathbf{r},t) &= \left(\frac{i}{16\pi^3\epsilon_0}\right)e^{-i\omega t}\int dkd\theta d\varphi k^2\sin\theta\left[\hat{\gamma}-\frac{\mathbf{k}(\mathbf{k}\cdot\hat{\gamma})}{k^2}\right]\nu_\kappa e^{i\mathbf{k}(\mathbf{r}-\mathbf{r}_0)} \\ &\times \int_0^t dt'\widetilde{\sigma}_-(t')e^{i(\omega-\nu_\kappa)(t-t')}\,,\end{aligned} \tag{2.53}$$

where we used

$$\sum_\lambda \hat{\epsilon}_{\mathbf{k}}^{(\lambda)}\hat{\epsilon}_{\mathbf{k}}^{(\lambda)} = 1-\frac{\mathbf{kk}}{k^2}\,. \tag{2.54}$$

We consider the geometry of the problem as in Fig. 2.2, with the detector along the z-axis. We can transform the vectors $\mathbf{k}$ and $\hat{\gamma}$ in the polar coordinates

$$\begin{aligned}\mathbf{k} &= k(\hat{x}\sin\theta\cos\varphi+\hat{y}\sin\theta\sin\varphi+\hat{z}\cos\theta), \\ \hat{\gamma} &= \gamma(\hat{x}\sin\eta+\hat{z}\cos\eta).\end{aligned} \tag{2.55}$$

In order to perform the integral in Eq. (2.53), first we apply the following results: [72]

$$\begin{aligned}&\int_0^{2\pi}d\varphi\left[\hat{x}\cdot\hat{\gamma}-\frac{(\hat{x}\cdot\mathbf{k})(\mathbf{k}\cdot\hat{\gamma})}{k^2}\right] = \int_0^{2\pi}d\varphi\gamma[\sin\eta-\sin\theta\cos\varphi(\sin\eta\sin\theta\cos\varphi+\cos\eta\cos\theta)] \\ &= 2\pi\gamma\sin\eta(1-\tfrac{1}{2}\sin^2\theta)\,,\end{aligned} \tag{2.56}$$

$$\int_0^{2\pi}d\varphi\left[\hat{y}\cdot\hat{\gamma}-\frac{(\hat{y}\cdot\mathbf{k})(\mathbf{k}\cdot\hat{\gamma})}{k^2}\right] = \int_0^{2\pi}d\varphi\gamma[0-\sin\theta\sin\varphi(\sin\eta\sin\theta\cos\varphi+\cos\eta\cos\theta)] = 0\,, \tag{2.57}$$

$$\begin{aligned}&\int_0^{2\pi}d\varphi\left[\hat{z}\cdot\hat{\gamma}-\frac{(\hat{z}\cdot\mathbf{k})(\mathbf{k}\cdot\hat{\gamma})}{k^2}\right] = \int_0^{2\pi}d\varphi\gamma[\cos\eta-\cos\theta(\sin\eta\sin\theta\cos\varphi+\cos\eta\cos\theta)] \\ &= 2\pi\gamma\cos\eta(1-\cos^2\theta) = 2\pi\gamma\cos\eta\sin^2\theta\,.\end{aligned} \tag{2.58}$$

The integral in Eq. (2.53) can be performed over the variable θ. Using the following identity

$$e^{i\mathbf{k}(\mathbf{r}-\mathbf{r}_0)} = e^{ik|\mathbf{r}-\mathbf{r}_0|\cos\theta}, \tag{2.59}$$

and introducing a new variable $\mu = \cos\theta$, we get the results [72]

$$\begin{aligned} &2\pi\gamma\sin\eta\int_0^\pi d\theta\sin\theta\left(1-\tfrac{1}{2}\sin^2\theta\right)e^{i\mathbf{k}(\mathbf{r}-\mathbf{r}_0)} = 2\pi\gamma\sin\eta\int_{-1}^1 d\mu\left[1-\tfrac{1}{2}(1-\mu^2)\right]e^{ik|\mathbf{r}-\mathbf{r}_0|\mu} \\ &= 2\pi\gamma\sin\eta\left[\frac{e^{ik|\mathbf{r}-\mathbf{r}_0|}-e^{-ik|\mathbf{r}-\mathbf{r}_0|}}{ik|\mathbf{r}-\mathbf{r}_0|}+O\left(\frac{1}{|\mathbf{r}-\mathbf{r}_0|^2}\right)\right], \end{aligned} \tag{2.60}$$

and

$$2\pi\gamma\cos\eta\int_0^\pi d\theta\sin^3\theta e^{i\mathbf{k}(\mathbf{r}-\mathbf{r}_0)} = 2\pi\gamma\cos\eta\int_{-1}^1 d\mu(1-\mu^2)e^{ik|\mathbf{r}-\mathbf{r}_0|\mu} \sim O\left(\frac{1}{|\mathbf{r}-\mathbf{r}_0|^2}\right). \tag{2.61}$$

After this computation, the expression of the positive frequency part of the electric field in the far-field region becomes [72]

$$\begin{aligned} \mathbf{E}^{(+)}(\mathbf{r},t) &= \left(\frac{c\gamma\sin\eta\hat{x}}{8\pi^2\epsilon_0|\mathbf{r}-\mathbf{r}_0|}\right)e^{-i\omega t}\int_0^\infty dkk^2\left(e^{ik|\mathbf{r}-\mathbf{r}_0|}-e^{-ik|\mathbf{r}-\mathbf{r}_0|}\right) \\ &\times \int_0^t dt'\tilde{\sigma}_-(t')e^{i(\omega-\nu_k)(t-t')}. \end{aligned} \tag{2.62}$$

Performing the k-integration, and neglecting the incoming wave contribution, one gets the known expression of $E^{(+)}(\mathbf{r},t)$ [72]

$$E^{(+)}(\mathbf{r},t) = \frac{\omega^2\gamma sin(\eta)}{4\pi\epsilon_0 c^2|\mathbf{r}-\mathbf{r_0}|}\hat{x}\sigma_-\left(t-\frac{|\mathbf{r}-\mathbf{r_0}|}{c}\right). \tag{2.63}$$

For $E^{(-)}(\mathbf{r},t)$, a similar expression can be derived. From the equation (2.63) we can see that the positive-frequency part of the field operator is proportional to σ_- at retarded time.

2.2.3 The spectrum of resonance fluorescence

We are interested in the field emitted by the atom fixed in the position along the x-axis. In the following calculations, the atom is assumed to be isolated. According to the Wiener-Khintchine theorem, the power spectrum $S(\omega_0)$ at some suitably chosen point $\mathbf{r}$ is the Fourier transform of the normally-ordered correlation function of the field $\langle E^{(-)}(\mathbf{r},t)E^{(+)}(\mathbf{r},t+\tau)\rangle$ with respect to τ [72].

$$S(\omega_0) = \frac{1}{2\pi}\lim_{T\to\infty}\frac{1}{T}\int_0^T dt\int_0^T dt'\langle E^{(-)}(t)E^{(+)}(t')\rangle e^{-i\omega_0(t-t')}. \tag{2.64}$$

Demanding the stationary condition, in Eq. (2.64) the correlation function of the field depends only on the time difference $\tau = t - t'$ [72]

$$\begin{aligned} S(\omega_0) &= \frac{1}{2\pi}\lim_{T\to\infty}\frac{1}{T}\int_0^T dt\left(\int_0^t dt'+\int_t^T dt'\right)\langle E^{(-)}(t)E^{(+)}(t')\rangle e^{-i\omega_0(t-t')} \\ &= \frac{1}{2\pi}\lim_{T\to\infty}\frac{1}{T}\int_0^T dt\left[\int_0^t d\tau\langle E^{(-)}(\tau)E^{(+)}(0)\rangle e^{-i\omega_0(\tau)}+\int_0^{T-t} d\tau\langle E^{(-)}(0)E^{(+)}(\tau)\rangle e^{i\omega_0\tau}\right]. \end{aligned} \tag{2.65}$$

If the field operators are correlated only over a short period of time, one can extend the upper limit of the τ-integrations to infinity. Using the property [72]

$$\langle E^{(-)}(\tau)E^{(+)}(0)\rangle = \langle E^{(-)}(0)E^{(+)}(\tau)\rangle^*, \tag{2.66}$$

from Eq. (2.65) one gets

$$S(\omega_0) = \frac{1}{\pi}\mathrm{Re}\int_0^\infty d\tau\langle E^{(-)}(0)E^{(+)}(\tau)\rangle e^{i\omega_0\tau}\,. \tag{2.67}$$

From Eq. (2.63) one obtains the known formula for the power spectrum [72]

$$\langle E^{(-)}(\mathbf{r},t)E^{(+)}(\mathbf{r},t+\tau)\rangle = I_0(\mathbf{r})\langle\sigma_+(t)\sigma_-(t+\tau)\rangle, \tag{2.68}$$

with the quantity

$$I_0(\mathbf{r}) = \left(\frac{\omega^2\gamma\sin\eta}{4\pi\epsilon_0 c^2|\mathbf{r}-\mathbf{r}_0|}\right)^2. \tag{2.69}$$

2.2.4 Calculation of the fluorescence spectrum

We can introduce the polarization operator of the two-level atom as [61]

$$P(\tau) = \gamma_{12}(|1\rangle\langle 2| + |2\rangle\langle 1|)\,, \tag{2.70}$$

where the γ_{ij} are the moduli of the induced transition dipole (multipole) moments. We may define the positive and negative parts of the polarization operator as

$$P^{(+)}(\tau) = \gamma_{12}|1\rangle\langle 2|\,, \quad P^{(-)}(\tau) = \gamma_{21}|2\rangle\langle 1|\,. \tag{2.71}$$

If M, Q and N are elements of a complete set of system operators $\{S_\mu\}$, and if the one-time averages can be expressed in the form

$$\langle M(\tau)\rangle = \sum_\mu O_\mu(\tau,\tau')\langle S_\mu(\tau')\rangle\,, \quad \tau' < \tau\,, \tag{2.72}$$

then the quantum regression theorem [54] states the the two-time expectation values take the form

$$\langle Q(\tau')M(\tau)N(\tau')\rangle = \sum_\mu O_\mu(\tau,\tau')\langle Q(\tau')S_\mu(\tau')N(\tau')\rangle\,, \quad \tau' < \tau\,. \tag{2.73}$$

$O_\mu(\tau,\tau')$ is a complex function of time. If one identifies Q and N with the identity operator, one gets the expression (2.72). One starts with the one-time average of the $P^{(-)}(\tau_1)$ operator

$$\langle P^{(-)}(\tau_1)\rangle = Tr[\rho(\tau_1)\gamma_{12}|2\rangle\langle 1|]\,, \tag{2.74}$$

or, in terms of Ψ_1,

$$\langle P^{(-)}(\tau_1)\rangle = \gamma_{12}e^{i\omega\tau_1}\Psi_1(\tau_1)\,. \tag{2.75}$$

For the elegance of the calculation one may transform Eq. (2.75) in Laplace space. This allows one to express each of the matrix elements $\Psi_i(\tau_1)$ in terms of their initial values $\tau = \tau_0$

$$\langle\hat{P}^{(-)}(z)\rangle = \gamma_{12}\hat{\Psi}_1(z')\,, \tag{2.76}$$

with the transformation $z' = z - i\omega$. Using Eq. (2.24), Eq. (2.76) we can put $\hat{P}^{(-)}(z)$ in the form

$$\langle \hat{P}^{(-)}(z) \rangle = \gamma_{12} \sum_j M_{1j}(z') \Psi_j(\tau_0) + \frac{\gamma_{12}}{z'} \sum_j M_{1j}(z') I_j \,. \tag{2.77}$$

The definition of $\Psi_j(\tau_0)$ is

$$\Psi_1(\tau_0) = e^{-i\omega\tau_0} \rho_{12}(\tau_0) = e^{-i\omega\tau_0} \langle |2\rangle\langle 1| \rangle_{\tau_0} \,. \tag{2.78}$$

This helps us to express $\Psi_j(\tau_0)$ and I_j in the form of expectation values at $\tau = \tau_0$. The regression theorem gives

$$\langle \hat{P}^{(-)}(z) P^{(+)}(\tau_0) \rangle_{\tau_0} = \gamma_{12}^2 M_{11}(z') \Psi_3(\tau_0) e^{-i\omega\tau_0} + \frac{\gamma_{12}^2}{z'} \sum_j M_{1j}(z') \Psi_2(\tau_0) I_j \,. \tag{2.79}$$

In the limiting case of $\tau_0 \to \infty$, the above expression becomes

$$\langle \hat{P}^{(-)}(z) P^{(+)}(\infty) \rangle = \gamma_{12}^2 M_{11}(z') \Psi_3(\infty) + \frac{\gamma_{12}^2}{z'} \sum_j M_{1j}(z') \Psi_2(\infty) I_j \,. \tag{2.80}$$

Eq. (2.80) shows that the spectrum of resonance fluorescence has a structure with a center located at ω, and a magnitude proportional to the atomic transition matrix element. The spectrum has the form

$$f(z) = \frac{A}{z} + g(z) \,, \tag{2.81}$$

where A is independent of z and $g(z)$ is an analytic function of z for $\Re z \geq 0$. The existence of the elastic scattering of the driving fields is reflected in the singularity of the $f(z)$ function. One can define the full correlation function as [61]

$$\hat{\Gamma}(z) \equiv \langle \hat{P}^{(-)}(z) P^{(+)}(\infty) \rangle \,, \tag{2.82}$$

and one can substract the coherent Rayleigh peak using the method in Ref. [61] as

$$\hat{\Gamma}_{\rm incoh}(z) = \hat{\Gamma}(z) - \frac{1}{z'} \lim_{z' \to 0} z' \hat{\Gamma}(z) \,. \tag{2.83}$$

The emission spectrum can be expressed as [61]

$$S(\omega) = \Re \hat{\Gamma}_{incoh}(z)|_{z=i\omega} \,, \tag{2.84}$$

with

$$\hat{\Gamma}_{\rm incoh}(z) = \gamma_{12}^2 M_{11}(z') \Psi_3(\infty) + \gamma_{12}^2 \sum_j N_{1j}(z') \Psi_2(\infty) I_j \,, \tag{2.85}$$

where

$$N_{ij}(z) = (L^{-1}(z - L)^{-1})_{ij} \,. \tag{2.86}$$

2.2.5 Analytic calculation of the spectra in the strong field approximation

It is more convenient to describe the atomic dynamics in a set of dressed atomic states. In the limit when the Rabi frequency is much larger than the decay width, the correlation functions and spectra can be expressed in an analitical form, and this makes possible to have explicit expressions for the line shapes, line widths, and peak heights. We consider the following atomic states:

$$\begin{aligned} |s\rangle &= \frac{1}{\sqrt{1+(\Omega_R/2+\sqrt{1+(\Omega_R/2)^2})^2}}|1\rangle + \frac{\Omega_R/2+\sqrt{1+(\Omega_R/2)^2}}{\sqrt{1+(\Omega_R/2+\sqrt{1+(\Omega_R/2)^2})^2}}|2\rangle\,, \quad (2.87)\\ |t\rangle &= \frac{1}{\sqrt{1+(\Omega_R/2-\sqrt{1+(\Omega_R/2)^2})^2}}|1\rangle + \frac{\Omega_R/2-\sqrt{1+(\Omega_R/2)^2}}{\sqrt{1+(\Omega_R/2-\sqrt{1+(\Omega_R/2)^2})^2}}|2\rangle\,, \end{aligned}$$

where $\Delta_R \equiv \frac{\Delta}{\Omega_R}$. In order to minimize the algebraic effort we limit our considerations to the first order in Δ_R,

$$\begin{aligned} |s\rangle &= (1/\sqrt{2}-\Omega_R/\sqrt{32})|1\rangle + (1/\sqrt{2}+\Omega_R/\sqrt{32})|2\rangle\,, \quad (2.88)\\ |t\rangle &= (1/\sqrt{2}+\Omega_R/\sqrt{32})|1\rangle + (-1/\sqrt{2}+\Omega_R/\sqrt{32})|2\rangle\,. \end{aligned}$$

These states are eigenstates of $\mathscr{H}_1'$ with the eigenvalues

$$\begin{aligned} \mathscr{H}_1'|s\rangle &= \hbar\sqrt{\Omega_R^2+\Delta^2/4}|s\rangle\,, \quad (2.89)\\ \mathscr{H}_1'|t\rangle &= -\hbar\sqrt{\Omega_R^2+\Delta^2/4}|t\rangle\,. \end{aligned}$$

The new matrix L, describing the atomic dynamics, has Ω_R only on the diagonal. The irreversible part of the master equation has contributions for all elements of the L matrix. When the Rabi frequency is sufficiently large, the L matrix is diagonal and we can perform the determination of spectral features analytically.

In the interaction picture one can writte the master equation as

$$\dot{\rho}' = -\frac{i}{\hbar}[\mathscr{H}_1', \rho'] + \Lambda\rho'\,. \quad (2.90)$$

The reversible part of the master equation, Eq. (2.90), has a very simple form:

$$\left(\frac{d}{dt}\right)_{rev}\begin{pmatrix}\rho'_{st}\\ \rho'_{ss}\\ \rho'_{tt}\end{pmatrix} = \begin{pmatrix}-2I\Omega_R\rho'_{st}\\ 0\\ 0\end{pmatrix}\,, \quad (2.91)$$

with the Hermitian symmetry relation $\rho'_{st} = (\rho'_{ts})^*$.

The irreversible part of the master equation is more complicated:

$$\left(\frac{d}{dt}\right)_{irrev}\rho'_{ij} = \sum_{pq}\Lambda_{ijpq}\rho'_{pq}\,, \quad (2.92)$$

where Λ_{ijpq} are some parameters defined in Eq. (2.14). We use the transformation equation $\rho'_{\mu\nu} = \sum_{ij}\langle\mu|i\rangle\rho'_{ij}\langle j|\nu\rangle$ in order to get

$$\left(\frac{d}{dt}\right)_{irrev}\rho'_{\mu\nu} = \sum_{\sigma\tau}\left(\sum_{ijpq}\langle\mu|i\rangle\langle j|\nu\rangle\langle p|\sigma\rangle\langle\tau|q\rangle\Lambda_{ijpq}\right)\rho'_{\sigma\tau} \equiv \sum_{\sigma\tau}\Gamma_{\mu\nu\sigma\tau}\rho'_{\sigma\tau}\,. \quad (2.93)$$

The matrix elements $\langle\mu|i\rangle$ can be calculated using Eq. (2.88). We now consider the limit when the Rabi frequency is much larger than the relaxation rate. We focus on the derivation of an expression for resonance fluorescence with an accuracy of order $1/\Omega_R$. We can define the vector Ψ as

$$\Psi_1 = \rho'_{st}\,, \quad \Psi_2 = \rho'_{ss}\,, \quad \Psi_3 = \rho'_{ts}\,. \tag{2.94}$$

The master equation in terms of Ψ is

$$\frac{d}{dt}\Psi = L\Psi + I\,, \tag{2.95}$$

with the matrix L defined as

$$L = \begin{pmatrix} \Gamma_{stst} - 2I\Omega_R & \Gamma_{stss} - \Gamma_{sttt} & \Gamma_{stts} \\ \Gamma_{ssst} & \Gamma_{ssss} - \Gamma_{sstt} & \Gamma_{ssts} \\ \Gamma_{tsst} & \Gamma_{tsss} - \Gamma_{tstt} & \Gamma_{tsts} + 2I\Omega_R \end{pmatrix}\,, \tag{2.96}$$

and the vector

$$I_1 = \Gamma_{sttt}\,, \quad I_2 = \Gamma_{sstt}\,, \quad I_3 = \Gamma_{tstt}\,. \tag{2.97}$$

In the steady state, it takes the form $\Psi(\infty) = -L^{-1}I$. It is not difficult to see that

$$L^{-1}(\mathscr{O}(1/\Omega_R)) = \begin{pmatrix} 0 & 0 & 0 \\ 0 & \frac{1}{\Gamma_{ssss}-\Gamma_{sstt}} & 0 \\ 0 & 0 & 0 \end{pmatrix}\,, \tag{2.98}$$

so the solution is

$$\Psi_1(\infty) = \Psi_3(\infty) = 0\,, \quad \Psi_2(\infty) = \frac{\Gamma_{sstt}}{\Gamma_{sstt} - \Gamma_{ssss}}\,. \tag{2.99}$$

The deviation from the steady is defined as [61]

$$\delta\Psi = \Psi(t) - \Psi(\infty)\,, \tag{2.100}$$

which fulfils the condition

$$\frac{d}{dt}\delta\Psi = L\delta\Psi I\,. \tag{2.101}$$

Up to corrections of order $1/\Omega_R$, the L_0 in the fluctuation equation Eq. (2.101) has a diagonal form. This approximation can be easily understood if we consider the equations for $\delta\rho'_{\mu\nu}$:

$$\begin{aligned} \frac{d}{dt}\delta\rho'_{st} &= (\Gamma_{stss} - \Gamma_{sttt})\delta\rho'_{ss} + (\Gamma_{stst} - 2I\Omega_R)\delta\rho'_{st} + \Gamma_{stts}\delta\rho'_{ts}\,, \\ \frac{d}{dt}\delta\rho'_{ss} &= (\Gamma_{ssss} - \Gamma_{sstt})\delta\rho'_{ss} + \Gamma_{ssst}\delta\rho'_{st} + \Gamma_{ssts}\delta\rho'_{ts}\,, \\ \frac{d}{dt}\delta\rho'_{ts} &= (\Gamma_{tsss} - \Gamma_{tstt})\delta\rho'_{ss} + \Gamma_{tsst}\delta\rho'_{st} + (\Gamma_{tsts} + 2I\Omega_R)\delta\rho'_{ts}\,. \end{aligned} \tag{2.102}$$

After introducing the notations

$$\delta\rho'_{st} = e^{-2I\Omega_R}R_{st}\,, \quad \delta\rho'_{ts} = e^{2I\Omega_R}R_{ts}\,, \quad \delta\rho'_{ss} = R_{ss}\,, \tag{2.103}$$

we get

$$\begin{aligned}\frac{d}{dt}R_{st} &= \Gamma_{tstt}R_{st} + \mathscr{O}(1/\Omega_R)\,, \\ \frac{d}{dt}R_{ss} &= (\Gamma_{ssss} - \Gamma_{sstt})R_{ss} + \mathscr{O}(1/\Omega_R)\,, \\ \frac{d}{dt}R_{ts} &= \Gamma_{tsts}R_{st} + \mathscr{O}(1/\Omega_R)\,,\end{aligned} \tag{2.104}$$

Dropping the rapidly oscillating terms $\mathscr{O}(1/\Omega_R)$, we may get

$$\begin{aligned}\frac{d}{dt}R_{st} &= (\Gamma_{tstt} - 2I\Omega_R)R_{st}\,, \\ \frac{d}{dt}R_{ss} &= (\Gamma_{ssss} - \Gamma_{sstt})R_{ss}\,, \\ \frac{d}{dt}R_{ts} &= (\Gamma_{tsts} + 2I\Omega_R)R_{st}\,.\end{aligned} \tag{2.105}$$

By doing so, the new matrix L_0 can be obtained after ignoring the off-diagonal elements

$$L_0 = \begin{pmatrix} \Gamma_{stst} - 2I\Omega_R & 0 & 0 \\ 0 & \Gamma_{ssss} - \Gamma_{sstt} & 0 \\ 0 & 0 & \Gamma_{tsts} + 2I\Omega_R \end{pmatrix}. \tag{2.106}$$

One can write Ψ as [see Eq. (2.100)]

$$\frac{d}{dt}\Psi(t) = L_0\Psi(t) + I_\infty\,, \tag{2.107}$$

where $I_\infty = -L_0\Psi(\infty)$, with the components

$$I_{\infty 1} = I_{\infty 3} = 0\,, \quad I_{\infty 2} = \frac{\Gamma_{sstt}}{\Gamma_{sstt} - \Gamma_{ssss}}\,, \tag{2.108}$$

and we get $I_\infty \equiv I_{\infty 2} = \Gamma_{sstt}$.

One can express the $\Gamma_{\mu\nu\sigma\tau}$ in terms of the $\Lambda_{\mu\nu\sigma\tau}$ as

$$\begin{aligned}\Gamma_{stst} &= \tfrac{1}{4}(\Lambda_{1111} - \Lambda_{1112} + \Lambda_{1121} - \Lambda_{1122} - \Lambda_{1211} + \Lambda_{1212} - \Lambda_{1221} + \Lambda_{1222} + \Lambda_{2111} \\ &- \Lambda_{2112} + \Lambda_{2121} - \Lambda_{2122} - \Lambda_{2211} + \Lambda_{2212} - \Lambda_{2221} + \Lambda_{2222})\,, \\ \Gamma_{ssss} &= \tfrac{1}{4}(\Lambda_{1111} + \Lambda_{1112} + \Lambda_{1121} + \Lambda_{1122} + \Lambda_{1211} + \Lambda_{1212} + \Lambda_{1221} + \Lambda_{1222} + \Lambda_{2111} \\ &+ \Lambda_{2112} + \Lambda_{2121} + \Lambda_{2122} + \Lambda_{2211} + \Lambda_{2212} + \Lambda_{2221} + \Lambda_{2222})\,,\end{aligned} \tag{2.109}$$

where

$$\begin{aligned}\Lambda_{1211} &= 0\,, \quad \Lambda_{1212} = -\mu_{12}\,, \quad \Lambda_{1221} = 0\,, \quad \Lambda_{1222} = 0\,, \\ \Lambda_{2111} &= 0\,, \quad \Lambda_{2112} = -\mu_{12}\,, \quad \Lambda_{2121} = 0\,, \quad \Lambda_{2122} = 0\,, \\ \Lambda_{1111} &= -\Gamma_{21}\,, \quad \Lambda_{1112} = 0\,, \quad \Lambda_{1121} = 0\,, \quad \Lambda_{1122} = \Gamma_{12}\,, \\ \Lambda_{2211} &= \Gamma_{21}\,, \quad \Lambda_{2212} = 0\,, \quad \Lambda_{2221} = 0\,, \quad \Lambda_{2222} = -\Gamma_{12}\,.\end{aligned} \tag{2.110}$$

It is easy to see that

$$\begin{aligned}\Gamma_{stst} &= \tfrac{1}{4}(-2\Gamma_{21} + \gamma_x) + \Gamma_{21}\Delta_R/8\,, \quad \Gamma_{ssss} = -\tfrac{1}{4}(\Gamma_{21} + \gamma_x) + \Gamma_{21}\Delta_R/4 \\ \Gamma_{sstt} &= \tfrac{1}{4}(\Gamma_{21} + \gamma_x) + \Gamma_{21}\Delta_R/4\,, \quad \Gamma_{tsts} = -\tfrac{1}{2}(\Gamma_{21} + \gamma_x/2) - \tfrac{1}{4}(\Gamma_{21}/2 + \gamma_x/2)\Delta_R/4\,,\end{aligned} \tag{2.111}$$

where γ_x is the laser's decoherence rate. It was added in the theory to the corresponding polarization decay rate.

One can write the solution of Eq. (2.108)

$$\hat{\Psi}(z) = M^0(z)\Psi(t_0) + \frac{1}{z}M^0(z)I_\infty\,, \tag{2.112}$$

where the matrix M^0 is given as

$$M^0(z) = (z - L_0)^{-1}\,. \tag{2.113}$$

The polarization operator is defined as

$$P^{(+)} = \gamma_{12}|1\rangle\langle 2|\,, \quad P^{(-)} = \gamma_{12}|2\rangle\langle 1|\,. \tag{2.114}$$

Its single-time average is

$$\langle P^{(-)}(t_1)\rangle = \gamma_{12}Tr[\rho'(0)|2\rangle\langle 1|]e^{i\omega t_1}\,. \tag{2.115}$$

Having the results

$$|2\rangle\langle 1|s\rangle = \tfrac{1}{2}|s\rangle + \left(-\tfrac{1}{2} + \Delta_R/4\right)|t\rangle\,, \quad |2\rangle\langle 1|t\rangle = \left(\tfrac{1}{2} + \Delta_R/4\right)|s\rangle - \tfrac{1}{2}|t\rangle\,, \tag{2.116}$$

we can write the expression for $\hat{P}^{(-)}(z)$ as

$$\langle\hat{P}^{(-)}(z)\rangle = \tfrac{1}{2}[2\hat{\Psi}_2(z') - (1 - \Delta_R/2)\,\hat{\Psi}_1(z') + (1 + \Delta_R/2)\,\hat{\Psi}_3(z')] - \frac{1}{2z'}\,, \tag{2.117}$$

where $z' = z - i\omega$. Thus it is easy to write the matrix M^0 as

$$M^0 = \begin{pmatrix} \frac{1}{2i\Omega_R + z - \Gamma_{stst}} & 0 & 0 \\ 0 & \frac{1}{z - \Gamma_{ssss} + \Gamma_{sstt}} & 0 \\ 0 & 0 & \frac{1}{-2i\Omega_R + z - \Gamma_{tsts}}\,. \end{pmatrix} \tag{2.118}$$

Using Eq. (2.112), one can write

$$\begin{aligned} \hat{\Psi}_1(z) &= M^0_{11}(z)\Psi_1(t_0)\,, \quad \hat{\Psi}_2(z) = M^0_{22}(z)\Psi_2(t_0) + \frac{1}{z}M^0_{22}(z)I_{\infty 2}\,, \\ \hat{\Psi}_3(z) &= M^0_{33}(z)\Psi_3(t_0)\,, \end{aligned} \tag{2.119}$$

and then

$$\begin{aligned} \langle\hat{P}^{(-)}(z)\rangle &= \tfrac{1}{2}[2M^0_{22}(z')\Psi_2(t_0) - (1 - \Delta_R/2)M^0_{11}(z')\Psi_1(t_0) \\ &+ (1 + \Delta_R/2)M^0_{33}(z')\Psi_3(t_0)] + \frac{1}{2z'}[M^0_{22}(z')I_{\infty 2} - 1]\,. \end{aligned} \tag{2.120}$$

The regression theorem gives

$$\begin{aligned} \Psi_1(t_0) &\to \gamma_{12}Tr[\rho'(t_0)|\overline{t\rangle\langle s}|1\rangle\langle 2|] = \gamma_{12}Tr[\rho'(t_0)|t\rangle\langle s|\overline{1\rangle\langle 2}|] \\ &= \gamma_{12}\exp(-i\omega t_0)\tfrac{1}{2}\left(\rho'_{st} - (1 - \Delta_R/2)\rho'_{tt}\right)\,, \\ \Psi_2(t_0) &\to \gamma_{12}\exp(-i\omega t_0)\tfrac{1}{2}\left(\rho'_{ss} - (1 - \Delta_R/2)\rho'_{ts}\right)\,, \\ \Psi_3(t_0) &\to \gamma_{12}\exp(-i\omega t_0)\tfrac{1}{2}\left((1 + \Delta_R/2)\rho'_{ss} - \rho'_{ts}\right)\,. \end{aligned} \tag{2.121}$$

With the over-bars we denoted the operators in the interaction picture. In the stationary limit, the off-diagonal elements of $\rho_{\mu\nu}$ vanish and the only nonzero element is $\rho'_{ss} = \Psi_\infty$, as given by Eq. (2.99). In this way, Eq. (2.121) becomes

$$\begin{aligned} \Psi_1(t_0) &\rightarrow -\tfrac{1}{2}\gamma_{12}(1-\Delta_R/2)(1-\Psi_2(\infty))e^{-i\omega t_0}\,, \quad \Psi_2(t_0) \rightarrow \tfrac{1}{2}\gamma_{12}\Psi_2(\infty)e^{-i\omega t_0}\,, \\ \Psi_3(t_0) &\rightarrow \tfrac{1}{2}\gamma_{12}(1+\Delta_R/2)\Psi_2(\infty)e^{-i\omega t_0}\,. \end{aligned} \tag{2.122}$$

For the inhomogeneous part of the equation, we get

$$\begin{aligned} \langle 1\rangle_{t_0} &\rightarrow \langle|1\rangle\langle 2|\rangle_{t_0} = Tr[\rho'(t_0)\overline{1\rangle\langle 2}] \\ &= \tfrac{1}{2}[2\rho_{ss} + (1+\Delta_R/2)\rho_{st} - (1-\Delta_R/2)\rho_{ts} - 1]e^{-i\omega t_0}\,, \end{aligned} \tag{2.123}$$

therefore, we arrive at the result:

$$\begin{aligned} \langle\hat{P}^{(-)}(z)P^{(+)}(\infty)\rangle &= \tfrac{\gamma_{12}}{4}[2M^0_{22}\Psi_2(\infty) + (1-\Delta_R/2)M^0_{11}(1-\Delta_R/2)(1-\Psi_2(\infty)) \\ &+ (1+\Delta_R/2)M^0_{33}(1+\Delta_R/2)\Psi_2(\infty)] - \tfrac{\gamma_{12}}{4z'}(2M^0_{22}I_{\infty 2} - 1)(1-2\Psi_2(\infty))\,. \end{aligned} \tag{2.124}$$

We obtain the final results in the first order of Δ_R as

$$\begin{aligned} \langle\hat{P}^{(-)}(z)P^{(+)}(\infty)\rangle &= \frac{\gamma_{12}}{2}\left[\frac{1}{2z+\Gamma_{21}+\gamma_x} + \frac{1}{4z+2\Gamma_{21}+\gamma_x-8I\Omega_R}\right. \\ &+\left.\frac{1}{4z+2\Gamma_{21}+\gamma_x+8I\Omega_R}\right] + \frac{\gamma_{12}}{4}\left[\frac{2\Gamma_{21}}{(\Gamma_{21}+\gamma_x)(2z+\Gamma_{21}+\gamma_x)} - \frac{\Gamma_{21}+2\gamma_x}{(4z+2\Gamma_{21}+\gamma_x-8I\Omega_R)^2}\right. \\ &+\frac{2(2\Gamma_{21}+\gamma_x)}{(\Gamma_{21}+\gamma_x)(4z+2\Gamma_{21}+\gamma_x-8I\Omega_R)} + \frac{\Gamma_{21}+2\gamma_x}{(4z+2\Gamma_{21}+\gamma_x+8I\Omega_R)^2} \\ &-\left.\frac{2(2\Gamma_{21}+\gamma_x)}{(\Gamma_{21}+\gamma_x)(4z+2\Gamma_{21}+\gamma_x+8I\Omega_R)}\right]\Delta_R + \mathscr{O}(\Delta_R)\,. \end{aligned} \tag{2.125}$$

In the case of a resonant interaction ($\Delta_R = 0$), and an ideal laser without decoherence ($\gamma_x = 0$), we get the well-known formula [72]

$$\langle\hat{P}^{(-)}(z)P^{(+)}(\infty)\rangle = \frac{\gamma_{12}}{2}\left[\frac{1}{2z+\Gamma_{21}} + \frac{1}{4z+2\Gamma_{21}-8I\Omega_R} + \frac{1}{4z+2\Gamma_{21}+8I\Omega_R}\right]\,. \tag{2.126}$$

The emission spectrum will be given by the real part of this expression with the corresponding substitution of the complex energy variable:

$$S(\omega_0) = \Re\langle\hat{P}^{(-)}(z)P^{(+)}(\infty)\rangle|_{z=i(\omega_0-\omega)}\,. \tag{2.127}$$

2.2.6 Appearance of sidebands in the strong field limit

In Fig 2.3 we represent a field with a spectral width of D and a central frequency of ν, scattered on an atom with a characteristic line width Γ and transition frequency ω. The shape of the scattered light depends on the multipole moment created in the atom by the incident field.

The sidebands start emerging in the spectrum of scattered light when the Rabi frequency, Ω_R, becomes larger than the atomic width Γ. The three-peak spectrum is known as the Mollow spectrum [72]. The sidebands are centered at $\nu + \Omega_R$ and $\nu - \Omega_R$.

In order to understand this effect, we consider the so-called dressed atom picture. For the case of a two-level system, the interaction Hamiltonian in rotating-wave approximation is (see Eq. (2.44)) [72]

$$\mathscr{H} = \mathscr{H}_0 + \mathscr{H}_1 = \frac{\hbar\omega}{2}\sigma_z + \hbar\nu a^\dagger a + \hbar g(\sigma_+ a + a^\dagger\sigma_-),\,. \tag{2.128}$$

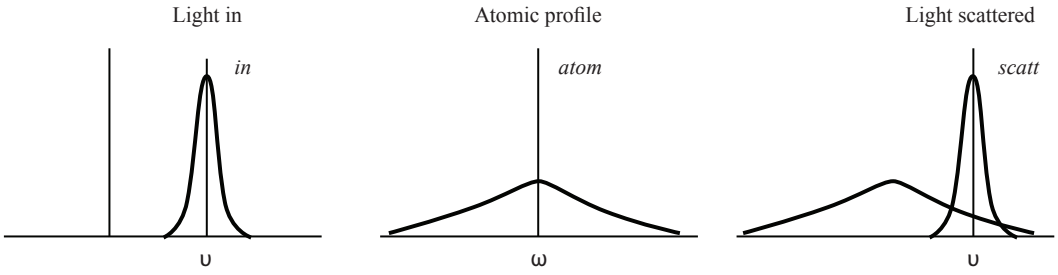

Figure 2.3: The scheme of the scattering of an electromagnetic field with frequency ν and bandwidth D. If $\Gamma \gg D$, the emitted light will have a bandwidth D centered at ν.

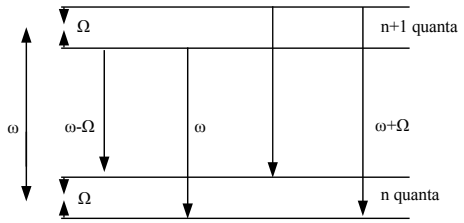

Figure 2.4: Splitting of the atomic states by the dynamic Stark effect. See text for notations and further explanations.

For the present situation, i.e. $\omega = \nu$, one can write the Hamiltonian in the interaction picture [72]

$$\mathscr{H}_1' = \hbar g(\sigma_+ a + a^\dagger \sigma_-)\,. \tag{2.129}$$

The eigenstates of the Hamiltonian are [72]

$$|\pm, n\rangle = \frac{1}{\sqrt{2}}(|a, n\rangle \pm |b, n+1\rangle)\,, \tag{2.130}$$

with the corresponding eigenvalues $+\hbar\Omega_n/2$ and $-\hbar\Omega_n/2$. Ω_n is called the generalized Rabi frequency and it is given by formula $\Omega_n = 2\Omega_R\sqrt{n+1}$. Due to interaction with electromagnetic field the degenaracy of the state $|a, n\rangle$ and $|b, n+1\rangle$ is removed, and they are split into a doublet of dressed states. This effect is called the dynamic Stark splitting. For a large number of photons, the splitting is almost the same for both levels. As one can see in Fig. 2.4, there are only three possible transition with different frequencies, leading to the three-peak Mollow spectrum.

2.3 Calculation of transition matrix elements

The expression for the fluorescence spectrum is now known. What remains is to calculate the corresponding non-relativistic and relativistic matrix elements, i.e. the matrix elements of the radiation field with the Schrödinger or Dirac wave functions which determine the Rabi frequencies and the radiative decay widths. In this section we derive analytical formulas for these quantities.

2.3.1 Electric dipole interaction matrix elements with Schrödinger wave functions

The interaction of a radiation field with a single-electron atom in dipole approximation has the matrix element

$$\boldsymbol{\gamma}_{ab} = e\langle\Phi_a|\hat{\epsilon}\cdot\mathbf{r}|\Phi_b\rangle\,, \tag{2.131}$$

where Ψ_a and Ψ_b are non-relativistic wave functions, solutions of the Schrödinger equation in a Coulomb potential, e is the elementary charge, and $\hat{\epsilon}$ is a unit vector defining the polarization of the electric field component. The subscript a stands collectively for the principal quantum number n_a as well as the angular momentum quantum number l_a and the magnetic quantum number M_a: $a \equiv (n_a, l_a, M_a)$, and the index b plays a similar role. The electric-dipole matrix elements depend on the electric field polarization, thus we need to discuss the *linear*, *left circular* and *right circular* cases.

1° *Linear polarization*

First we consider linear polarization along the z axis, and we calculate this matrix elements in spherical coordinates, $z = r\cos\phi$. In this case the transition matrix element has the form

$$\gamma^z_{ab} = e\langle\Phi_a|\hat{\epsilon}_z\cdot\mathbf{r}|\Phi_b\rangle = e\int d\mathbf{r}\Phi^\dagger_a(\mathbf{r})r\cos\theta\Phi_b(\mathbf{r}) = eRK^z\,. \tag{2.132}$$

1° *Circular polarization*

The definition of right- and left-handed polarization is $\hat{\epsilon}_\pm = \frac{1}{\sqrt{2}}(\hat{\epsilon}_x \pm i\hat{\epsilon}_y)$. In spherical coordinates, i.e. $x = r\sin\theta\cos\phi$ and $y = r\sin\theta\sin\phi$, the transition matrix elements are

$$\begin{aligned}
\gamma^+_{ab} &= e\langle\Phi_a|\hat{\epsilon}_+\cdot\mathbf{r}|\Phi_b\rangle = \tfrac{e}{\sqrt{2}}\int d\mathbf{r}\Phi^\dagger_a(\mathbf{r})\mathbf{r}\cdot(\hat{\epsilon}_x + i\hat{\epsilon}_y)\Phi_b(\mathbf{r}) = \tfrac{e}{\sqrt{2}}R[K^x + iK^y]\,, \qquad (2.133)\\
\gamma^-_{ab} &= e\langle\Phi_a|\hat{\epsilon}_-\cdot\mathbf{r}|\Phi_b\rangle = \tfrac{e}{\sqrt{2}}\int d\mathbf{r}\Phi^\dagger_a(\mathbf{r})\mathbf{r}\cdot(\hat{\epsilon}_x - i\hat{\epsilon}_y)\Phi_b(\mathbf{r}) = \tfrac{e}{\sqrt{2}}\tfrac{e}{\sqrt{2}}R[K^x - iK^y]\,.
\end{aligned}$$

The integral expression of the radial matrix element R is

$$R = \int dr r^3 R_{n_a l_a}(r)R_{n_b l_b}(r)\,. \tag{2.134}$$

For the Coulomb potential of a point-like nucleus with charge $Z|e|$, the bound radial function $R_a(r)$ can be given in an analytical form by means of the generalized Laguerre polynomials:

$$R_a(r) = -\frac{2Z^{3/2}}{n_a^2 a_0^{3/2}}\sqrt{\frac{(n_a - l_a - 1)!}{(n_a + l_a)!}}\left(\frac{2rZ}{a_0 n_a}\right)^{l_a} e^{-rZ/a_0 n_a} L^{2l_a+1}_{n_a - l_a - 1}\left(\frac{2rZ}{a_0 n_a}\right)\,. \tag{2.135}$$

The Bohr radius a_0 is defined $a_0 = \frac{\hbar}{mc\alpha}$, with α being the fine structure constant. The angular matrix elements have the integral representation

$$\begin{aligned}
K^x &= \sqrt{\frac{2\pi}{3}}\int do_r Y^\dagger_{l_a M_a}(\hat{r})(Y_{1-1} - Y_{11})Y_{l_b M_b}(\hat{r})\,, \quad K^z = \sqrt{\frac{2\pi}{3}}\int do_r Y^\dagger_{l_a M_a}(\hat{r})Y_{10}Y_{l_b M_b}(\hat{r})\,,\\
K^y &= \sqrt{\frac{2\pi}{3}}\int do_r Y^\dagger_{l_a M_a}(\hat{r})(Y_{1-1} + Y_{11})Y_{l_b M_b}(\hat{r})\,, \qquad (2.136)
\end{aligned}$$

which can be reduced to the result

$$\begin{aligned}
K^x_1 &= \frac{(-1)^{M_a}}{\sqrt{2}}\sqrt{(2l_a+1)(2l_b+1)}\begin{pmatrix} l_a & 1 & l_b\\ 0 & 0 & 0\end{pmatrix}\left[\begin{pmatrix} l_a & 1 & l_b\\ -M_a & -1 & -M_b\end{pmatrix} - \begin{pmatrix} l_a & 1 & l_b\\ -M_a & 1 & M_b\end{pmatrix}\right]\,,\\
K^y_1 &= \frac{(-1)^{M_a}}{\sqrt{2}}\sqrt{(2l_a+1)(2l_b+1)}\begin{pmatrix} l_a & 1 & l_b\\ 0 & 0 & 0\end{pmatrix}\left[\begin{pmatrix} l_a & 1 & l_b\\ -M_a & -1 & -M_b\end{pmatrix} + \begin{pmatrix} l_a & 1 & l_b\\ -M_a & 1 & M_b\end{pmatrix}\right]\,,\\
K^z_1 &= (-1)^{M_a}\sqrt{(2l_a+1)(2l_b+1)}\begin{pmatrix} l_a & 1 & l_b\\ 0 & 0 & 0\end{pmatrix}\begin{pmatrix} l_a & 1 & l_b\\ -M_a & 0 & M_b\end{pmatrix}\,. \qquad (2.137)
\end{aligned}$$

The final analytical result of radial integration can be expressed in terms of generalized hypergeometric functions as

$$\begin{aligned} R &= \frac{4Z^3}{n_a^2 n_b^2 a_0^3}\sqrt{\frac{(n_a+l_a)!}{(n_a-l_a-1)!}}\sqrt{\frac{(n_b+l_b)!}{(n_b-l_b-1)!}}\left(\frac{2Z}{a_0 n_a}\right)^{l_a}\left(\frac{2Z}{a_0 n_b}\right)^{l_b}\frac{1}{(2l_a+1)}\frac{1}{(2l_b+1)} \\ &\times \sum_{p=0}^{n_a-l_a-1}\frac{(-n_a+l_a+1)_p}{(2l_a+2)_p}\frac{1}{p!}\left(\frac{2Z}{a_0 n_0}\right)^p (3+l_a+l_b+p)!\left(\frac{a_0 n_a n_b}{Z(n_a+n_b)}\right)^{4+l_a+l_b+p} \\ &\times {}_2F_1\left(-n_b+l_b+1, 4+l_a+l_b+p, 2l_b+2; \frac{a_0 n_a n_b}{Z(n_a+n_b)}\right). \end{aligned} \tag{2.138}$$

2.3.2 Relativistic dipole interaction matrix elements in the length gauge

We will work first in the so-called *length gauge*, where the transition matrix elements $\boldsymbol{\gamma}_{ab}$ are defined, similarly to the non-relativistic case, as

$$\boldsymbol{\gamma}_{ab} = e\langle\Phi_a|\hat{\epsilon}\cdot\mathbf{r}|\Phi_b\rangle\,, \tag{2.139}$$

where Ψ_a and Ψ_b are relativistic wave functions, solutions of the Dirac equation in a Coulomb potential, and e is the elementary charge. Because the laser field has a certain polarization, we should again consider all three possibilities.

1° *Linear polarization*

Let us consider the polarization along the z axis, and calculate the matrix elements in spherical coordinates, $z = r\cos\phi$. In this case the transition matrix element has the form

$$\gamma^z_{ab} = e\langle\Phi_a|\hat{\epsilon}_z\cdot\mathbf{r}|\Phi_b\rangle = e\int d\mathbf{r}\Phi^\dagger_a(\mathbf{r})r\cos\theta\Phi_b(\mathbf{r}) = e[R_1K^z_1 + R_2K^z_2]\,. \tag{2.140}$$

2° *Circular polarization*

We consider the right ($\hat{\epsilon}_+$) and left ($\hat{\epsilon}_-$) circular polarization, defined with the polarization unit vectors $\hat{\epsilon}_\pm = \frac{1}{\sqrt{2}}(\hat{\epsilon}_x \pm i\hat{\epsilon}_y)$. In spherical coordinates, i.e. $x = r\sin\theta\cos\phi$ and $y = r\sin\theta\sin\phi$, the transition matrix elements are

$$\begin{aligned} \gamma^+_{ab} &= e\langle\Phi_a|\hat{\epsilon}_+\cdot\mathbf{r}|\Phi_b\rangle = \tfrac{e}{\sqrt{2}}\int d\mathbf{r}\Phi^\dagger_a(\mathbf{r})\mathbf{r}\cdot(\hat{\epsilon}_x + i\hat{\epsilon}_y)\Phi_b(\mathbf{r}) \\ &= \tfrac{e}{\sqrt{2}}[R_1K^x_1 + R_2K^x_2 + iR_1K^y_1 + iR_2K^y_2]\,, \\ \gamma^-_{ab} &= e\langle\Phi_a|\hat{\epsilon}_-\cdot\mathbf{r}|\Phi_b\rangle = \tfrac{e}{\sqrt{2}}\int d\mathbf{r}\Phi^\dagger_a(\mathbf{r})\mathbf{r}\cdot(\hat{\epsilon}_x - i\hat{\epsilon}_y)\Phi_b(\mathbf{r}) \\ &= \tfrac{e}{\sqrt{2}}[R_1K^x_1 + R_2K^x_2 - iR_1K^y_1 - iR_2K^y_2]\,. \end{aligned} \tag{2.141}$$

The radial matrix elements are denoted as

$$R_1 = \int drr^3 G_{n_a\kappa_a}(r)G_{n_b\kappa_b}(r)\,, \quad R_2 = \int drr^3 F_{n_a\kappa_a}(r)F_{n_b\kappa_b}(r)\,, \tag{2.142}$$

and

$$\begin{aligned} K^x_1 &= \int do_r\Omega^\dagger_{\kappa_a M_a}(\hat{r})\sin\theta\cos\phi\Omega_{\kappa_b M_b}(\hat{r})\,, & K^x_2 &= \int do_r\Omega^\dagger_{-\kappa_a M_a}(\hat{r})\sin\theta\cos\phi\Omega_{-\kappa_b M_b}(\hat{r})\,, \\ K^y_1 &= \int do_r\Omega^\dagger_{\kappa_a M_a}(\hat{r})\sin\theta\sin\phi\Omega_{\kappa_b M_b}(\hat{r})\,, & K^y_2 &= \int do_r\Omega^\dagger_{-\kappa_a M_a}(\hat{r})\sin\theta\sin\phi\Omega_{-\kappa_b M_b}(\hat{r})\,, \\ K^z_1 &= \int do_r\Omega^\dagger_{\kappa_a M_a}(\hat{r})\cos\theta\Omega_{\kappa_b M_b}(\hat{r})\,, & K^z_2 &= \int do_r\Omega^\dagger_{-\kappa_a M_a}(\hat{r})\cos\theta\Omega_{-\kappa_b M_b}(\hat{r})\,. \end{aligned} \tag{2.143}$$

To bring the angular part to a simpler form we use the formula [6]

$$\int do_r \Omega^{\dagger}_{\kappa_a M_a}(\hat{r}) Y_{lm}(\hat{r}) \Omega_{\kappa_b M_b}(\hat{r}) = \frac{(-1)^{M_a-1/2}}{\sqrt{4\pi}} \sqrt{(2j_a+1)(2j_b+1)(2l+1)(2l_a+1)(2l_b+1)} \begin{pmatrix} l_a & l_b & l \\ 0 & 0 & 0 \end{pmatrix} \begin{pmatrix} j_a & j_b & l \\ -M_a & M_b & m \end{pmatrix} \begin{Bmatrix} j_a & j_b & l \\ l_b & l_a & 1/2 \end{Bmatrix} . \tag{2.144}$$

Applying Euler's formula, it is easy to see that

$$\sin\theta \sin\phi = i\sqrt{\frac{2\pi}{3}} \left(Y_{1-1} + Y_{11}\right) , \sin\theta\cos\phi = \sqrt{\frac{2\pi}{3}} \left(Y_{1-1} - Y_{11}\right) , \cos\theta = 2\sqrt{\frac{\pi}{3}} Y_{10} , \tag{2.145}$$

and the final result for the angular parts are

$$\begin{aligned} K_1^x &= \frac{(-1)^{M_a-1/2}}{\sqrt{2}} \sqrt{(2j_a+1)(2j_b+1)(2l_a+1)(2l_b+1)} \begin{pmatrix} l_a & l_b & 1 \\ 0 & 0 & 0 \end{pmatrix} \\ &\quad \times \left[\begin{pmatrix} j_a & j_b & 1 \\ -M_a & M_b & -1 \end{pmatrix} - \begin{pmatrix} j_a & j_b & 1 \\ -M_a & M_b & 1 \end{pmatrix} \right] \begin{Bmatrix} j_a & j_b & 1 \\ l_b & l_a & 1/2 \end{Bmatrix} , \end{aligned} \tag{2.146}$$

$$\begin{aligned} K_2^x &= \frac{(-1)^{M_a-1/2}}{\sqrt{2}} \sqrt{(2j_a+1)(2j_b+1)(2l'_a+1)(2l'_b+1)} \begin{pmatrix} l'_a & l'_b & 1 \\ 0 & 0 & 0 \end{pmatrix} \\ &\quad \times \left[\begin{pmatrix} j_a & j_b & 1 \\ -M_a & M_b & -1 \end{pmatrix} - \begin{pmatrix} j_a & j_b & 1 \\ -M_a & M_b & 1 \end{pmatrix} \right] \begin{Bmatrix} j_a & j_b & 1 \\ l'_b & l'_a & 1/2 \end{Bmatrix} , \end{aligned} \tag{2.147}$$

$$\begin{aligned} K_1^y &= i\frac{(-1)^{M_a-1/2}}{\sqrt{2}} \sqrt{(2j_a+1)(2j_b+1)(2l_a+1)(2l_b+1)} \begin{pmatrix} l_a & l_b & 1 \\ 0 & 0 & 0 \end{pmatrix} \\ &\quad \times \left[\begin{pmatrix} j_a & j_b & 1 \\ -M_a & M_b & -1 \end{pmatrix} + \begin{pmatrix} j_a & j_b & 1 \\ -M_a & M_b & 1 \end{pmatrix} \right] \begin{Bmatrix} j_a & j_b & 1 \\ l_b & l_a & 1/2 \end{Bmatrix} , \end{aligned} \tag{2.148}$$

$$\begin{aligned} K_2^y &= i\frac{(-1)^{M_a-1/2}}{\sqrt{2}} \sqrt{(2j_a+1)(2j_b+1)(2l'_a+1)(2l'_b+1)} \begin{pmatrix} l'_a & l'_b & 1 \\ 0 & 0 & 0 \end{pmatrix} \\ &\quad \times \left[\begin{pmatrix} j_a & j_b & 1 \\ -M_a & M_b & -1 \end{pmatrix} + \begin{pmatrix} j_a & j_b & 1 \\ -M_a & M_b & 1 \end{pmatrix} \right] \begin{Bmatrix} j_a & j_b & 1 \\ l'_b & l'_a & 1/2 \end{Bmatrix} , \end{aligned} \tag{2.149}$$

$$\begin{aligned} K_1^z &= (-1)^{M_a-1/2} \sqrt{(2j_a+1)(2j_b+1)(2l_a+1)(2l_b+1)} \begin{pmatrix} l_a & l_b & 1 \\ 0 & 0 & 0 \end{pmatrix} \\ &\quad \times \begin{pmatrix} j_a & j_b & 1 \\ -M_a & M_b & 0 \end{pmatrix} \begin{Bmatrix} j_a & j_b & 1 \\ l_b & l_a & 1/2 \end{Bmatrix} , \end{aligned} \tag{2.150}$$

$$\begin{aligned} K_2^z &= (-1)^{M_a-1/2} \sqrt{(2j_a+1)(2j_b+1)(2l'_a+1)(2l'_b+1)} \begin{pmatrix} l'_a & l'_b & 1 \\ 0 & 0 & 0 \end{pmatrix} \\ &\quad \times \begin{pmatrix} j_a & j_b & 1 \\ -M_a & M_b & 0 \end{pmatrix} \begin{Bmatrix} j_a & j_b & 1 \\ l'_b & l'_a & 1/2 \end{Bmatrix} . \end{aligned} \tag{2.151}$$

The radial integrals can be calculated to yield

$$R_1 = \left(1+\frac{E_a}{mc^2}\right)^{1/2}\left(1+\frac{E_b}{mc^2}\right)^{1/2} U_a U_b [R_1^1 - R_1^2 - R_1^3 + R_1^4]\,, \tag{2.152}$$
$$R_2 = \left(1-\frac{E_a}{mc^2}\right)^{1/2}\left(1-\frac{E_b}{mc^2}\right)^{1/2} U_a U_b [R_1^1 + R_1^2 + R_1^3 + R_1^4]\,,$$

where we introduced the following shorthand notations:

$$\begin{aligned}
R_1^1 &= n_a^r n_b^r (2\lambda_a)^{\gamma_a-1}(2\lambda_b)^{\gamma_b-1}\sum_{m=0}^{n_a^r-1}\frac{(-n_a^r+1)_m}{(2\gamma_a+1)_m}\frac{(2\lambda_a)^m}{m!}\frac{\Gamma(m+\gamma_a+\gamma_b+2)}{(\lambda_a+\lambda_b)^{m+\gamma_a+\gamma_b+2}} \\
&\times\ {}_2F_1\left(m+\gamma_a+\gamma_b+2,-n_b^r+1,2\gamma_b+1;\frac{2\lambda_b}{\lambda_a+\lambda_b}\right)\,, \\
R_1^2 &= n_a^r (N_b-\kappa_b)(2\lambda_a)^{\gamma_a-1}(2\lambda_b)^{\gamma_b-1}\sum_{m=0}^{n_a^r-1}\frac{(-n_a^r+1)_m}{(2\gamma_a+1)_m}\frac{(2\lambda_a)^m}{m!}\frac{\Gamma(m+\gamma_a+\gamma_b+2)}{(\lambda_a+\lambda_b)^{m+\gamma_a+\gamma_b+2}} \\
&\times\ {}_2F_1\left(m+\gamma_a+\gamma_b+2,-n_b^r,2\gamma_b+1;\frac{2\lambda_b}{\lambda_a+\lambda_b}\right)\,, \\
R_1^3 &= (N_a-\kappa_a) n_b^r (2\lambda_a)^{\gamma_a-1}(2\lambda_b)^{\gamma_b-1}\sum_{m=0}^{n_a^r}\frac{(-n_a^r)_m}{(2\gamma_a+1)_m}\frac{(2\lambda_a)^m}{m!}\frac{\Gamma(m+\gamma_a+\gamma_b+2)}{(\lambda_a+\lambda_b)^{m+\gamma_a+\gamma_b+2}} \\
&\times\ {}_2F_1\left(m+\gamma_a+\gamma_b+2,-n_b^r+1,2\gamma_b+1;\frac{2\lambda_b}{\lambda_a+\lambda_b}\right)\,, \\
R_1^4 &= (N_a-\kappa_a)(N_b-\kappa_b)(2\lambda_a)^{\gamma_a-1}(2\lambda_b)^{\gamma_b-1}\sum_{m=0}^{n_a^r}\frac{(-n_a^r)_m}{(2\gamma_a+1)_m}\frac{(2\lambda_a)^m}{m!}\frac{\Gamma(m+\gamma_a+\gamma_b+2)}{(\lambda_a+\lambda_b)^{m+\gamma_a+\gamma_b+2}} \\
&\times\ {}_2F_1\left(m+\gamma_a+\gamma_b+2,-n_b^r,2\gamma_b+1;\frac{2\lambda_b}{\lambda_a+\lambda_b}\right)\,.
\end{aligned} \tag{2.153}$$

Again, for Coulomb potentials, we used the representation of bound radial functions $G_a(r)$ and $F_a(r)$ in terms of confluent hypergeometric functions with negative-integral first argument (see, e.g. Ref. [6]):

$$\begin{aligned}
G_a(r) &= \left(1+\frac{E_a}{mc^2}\right)^{1/2} U_a (A_a - B_a)\,, \\
F_a(r) &= -\left(1-\frac{E_a}{mc^2}\right)^{1/2} U_a (A_a + B_a)\,,
\end{aligned} \tag{2.154}$$

where the eigenenergies are given by the Sommerfeld formula

$$E_a = mc^2\left(1+\frac{(Z\alpha)^2}{\left(n_a - j_a - 1/2 + \sqrt{(j_a+1/2)^2-(Z\alpha)^2}\right)^2}\right)^{-1/2}\,. \tag{2.155}$$

In the above equations, furthermore, the following functions are used:

$$\begin{aligned}
U_a &= \frac{(2\lambda_a)^{3/2}}{\Gamma(2\gamma_a+1)}\left(\frac{\Gamma(2\gamma_a+n_a^r+1)}{4N_a(N_a-\kappa_a)n_a^r!}\right)^{1/2}\,, \\
A_a(r) &= n_a^r\,{}_1F_1(-n_a^r+1,2\gamma_a+1;2\lambda_a r)e^{-\lambda_a r}(2\lambda_a r)^{\gamma_a-1}\,, \\
B_a(r) &= (N_a-\kappa_a)\,{}_1F_1(-n_a^r,2\gamma_a+1;2\lambda_a r)e^{-\lambda_a r}(2\lambda_a r)^{\gamma_a-1}\,.
\end{aligned} \tag{2.156}$$

Here, ${}_1F_1$ is the confluent hyper-geometric function defined by its expansion [3] with coefficients involving Gamma functions:

$$\begin{aligned} {}_1F_1(-n,b;z) &= \sum_{m=0}^{n} \frac{(-n)_m}{(b)_m}\frac{z^m}{m!}\,, \\ (a)_m &= \frac{\Gamma(a+m)}{\Gamma(a)}, \quad (a)_0 \equiv 1\,, \end{aligned} \tag{2.157}$$

and its parameters are

$$\begin{aligned} \lambda_a &= \frac{\sqrt{m^2c^4-E_a^2}}{\hbar c}, \quad N_a = \frac{(n_a^r+\gamma_a)mc^2}{E_a}\,, \\ \gamma_a &= \sqrt{\kappa_a^2-(Z\alpha)^2}, \quad n_a^r = n_a - |\kappa_a|\,, \\ \kappa_a &= \begin{cases} -(l_a+1) & \text{if } j_a = l_a + \frac{1}{2}, \\ l_a & \text{if } j_a = l_a - \frac{1}{2}. \end{cases} \end{aligned} \tag{2.158}$$

As the first argument of the confluent hypergeometric function is an integer, it can be written as a polynomial [3], simplifying the numerical evaluation of the wave function. The spin-angular part of the Dirac wave function is defined by the spherical spinors

$$\Omega_{\kappa_a M_a}(\hat{r}) = \sum_{m_a=-l_a}^{l_a} \sum_{\mu_a=\pm 1/2} C\left(l_a \frac{1}{2} j_a; m_a \mu_a M_a\right) Y_{l_a m_a}(\theta,\phi)\chi_{\mu_a}\,. \tag{2.159}$$

Here, χ_{μ_a} denotes the usual two-component Pauli spinors:

$$\chi_{1/2} = \begin{pmatrix} 1 \\ 0 \end{pmatrix}, \quad \chi_{-1/2} = \begin{pmatrix} 0 \\ 1 \end{pmatrix}\,. \tag{2.160}$$

2.3.3 Relativistic dipole interaction matrix elements in the transverse gauge

The transverse gauge (also called Coulomb gauge) can be regarded as the relativistic generalization of the familiar velocity form. In the following we formulate the atom-field interaction in this gauge. As in the case of the form $\mathbf{r}\cdot\mathbf{E}$, in the case of the $\boldsymbol{\alpha}\cdot\mathbf{A}$ interaction, the transition matrix element can be defined as

$$\boldsymbol{\gamma}_{ab} = \frac{ec}{\omega}\langle\Phi_a|\hat{\epsilon}\cdot\boldsymbol{\alpha}|\Phi_b\rangle\,. \tag{2.161}$$

One should consider also the two cases of *linear* and *circular* polarization for the laser field.

1° *Linear polarization*

For the polarization along the z axis, the matrix elements have the form

$$\boldsymbol{\gamma}_{ab}^z = \frac{ec}{\omega}\langle\Phi_a|\boldsymbol{\alpha}_z|\Phi_b\rangle = \frac{ec}{\omega}\int d\mathbf{r}\Phi_a^\dagger(\mathbf{r})\boldsymbol{\alpha}_z\Phi_b(\mathbf{r}) = -i\frac{ec}{\omega}[R_1K_1^z - R_2K_2^z]\,. \tag{2.162}$$

2° *Circular polarization*

For the right- and left-circular polarization, the matrix elements are

$$\begin{aligned}
\boldsymbol{\gamma}^{+}_{ab} &= \frac{ec}{\omega}\langle\Phi_a|\boldsymbol{\alpha}\cdot\hat{\epsilon}_{+}|\Phi_b\rangle = \frac{1}{\sqrt{2}}\frac{ec}{\omega}\int d\mathbf{r}\Phi^{\dagger}_a(\mathbf{r})\boldsymbol{\alpha}\cdot(\hat{\epsilon}_x + i\hat{\epsilon}_y)\Phi_b(\mathbf{r}) \\
&= -\frac{i}{\sqrt{2}}\frac{ec}{\omega}\{R_1[K_1^x + iK_1^y] - R_2[K_2^x + iK_2^y]\}\,, \\
\boldsymbol{\gamma}^{-}_{ab} &= \frac{ec}{\omega}\langle\Phi_a|\boldsymbol{\alpha}\cdot\hat{\epsilon}_{-}|\Phi_b\rangle = \frac{1}{\sqrt{2}}\frac{ec}{\omega}\int d\mathbf{r}\Phi^{\dagger}_a(\mathbf{r})\boldsymbol{\alpha}\cdot(\hat{\epsilon}_x - i\hat{\epsilon}_y)\Phi_b(\mathbf{r}) \\
&= -\frac{i}{\sqrt{2}}\frac{ec}{\omega}\{R_1[K_1^x - iK_1^y] - R_2[K_2^x - iK_2^y]\}\,,
\end{aligned} \tag{2.163}$$

with the radial parts

$$R_1 \equiv \int dr r^2 G_{n_b\kappa_b}(r)F_{n_a\kappa_a}(r), \quad R_2 \equiv \int dr r^2 F_{n_b\kappa_b}(r)G_{n_a\kappa_a}(r), \tag{2.164}$$

and angular parts

$$\begin{aligned}
K_1^x &= \int do_r \Omega^{\dagger}_{-\kappa_a M_a}(\hat{r})\sigma_x\Omega_{\kappa_b M_b}(\hat{r}), \quad K_2^x = \int do_r \Omega^{\dagger}_{\kappa_a M_a}(\hat{r})\sigma_x\Omega_{-\kappa_b M_b}(\hat{r})\,, \\
K_1^y &= \int do_r \Omega^{\dagger}_{-\kappa_a M_a}(\hat{r})\sigma_y\Omega_{\kappa_b M_b}(\hat{r}), \quad K_2^y = \int do_r \Omega^{\dagger}_{\kappa_a M_a}(\hat{r})\sigma_y\Omega_{-\kappa_b M_b}(\hat{r})\,, \\
K_1^z &= \int do_r \Omega^{\dagger}_{-\kappa_a M_a}(\hat{r})\sigma_z\Omega_{\kappa_b M_b}(\hat{r}), \quad K_2^z = \int do_r \Omega^{\dagger}_{\kappa_a M_a}(\hat{r})\sigma_z\Omega_{-\kappa_b M_b}(\hat{r})\,.
\end{aligned} \tag{2.165}$$

After some lengthy but straightforward calculation, we get the final results for the angular parts:

$$\begin{aligned}
K_1^x &= (-1)^{j_a+j_b-M_b+3/2}\sqrt{(2j_a+1)(2j_b+1)(2l'_a+1)(2l_b+1)}\begin{pmatrix} l'_a & l_b & 0 \\ 0 & 0 & 0 \end{pmatrix}(a_1^1 - a_2^1)\,, \\
K_2^x &= (-1)^{j_a+j_b-M_b+3/2}\sqrt{(2j_a+1)(2j_b+1)(2l_a+1)(2l'_b+1)}\begin{pmatrix} l_a & l'_b & 0 \\ 0 & 0 & 0 \end{pmatrix}(a_1^2 - a_2^2)\,, \\
K_1^y &= -i(-1)^{j_a+j_b-M_b+3/2}\sqrt{(2j_a+1)(2j_b+1)(2l'_a+1)(2l_b+1)}\begin{pmatrix} l'_a & l_b & 0 \\ 0 & 0 & 0 \end{pmatrix}(a_1^1 + a_2^1)\,, \\
K_2^y &= -i(-1)^{j_a+j_b-M_b+3/2}\sqrt{(2j_a+1)(2j_b+1)(2l_a+1)(2l'_b+1)}\begin{pmatrix} l_a & l'_b & 0 \\ 0 & 0 & 0 \end{pmatrix}(a_1^2 + a_2^2)\,, \\
K_1^z &= (-1)^{j_a+j_b-M_b+3/2}\sqrt{(2j_a+1)(2j_b+1)(2l'_a+1)(2l_b+1)}\begin{pmatrix} l'_a & l_b & 0 \\ 0 & 0 & 0 \end{pmatrix}(b_1^1 + b_2^1)\,, \\
K_2^z &= (-1)^{j_a+j_b-M_b+3/2}\sqrt{(2j_a+1)(2j_b+1)(2l_a+1)(2l'_b+1)} \\
&\times \begin{pmatrix} l_a & l'_b & 0 \\ 0 & 0 & 0 \end{pmatrix}(b_1^2 + b_2^2)\,,
\end{aligned} \tag{2.166}$$

where the following notations were used:

$$
\begin{aligned}
a_1^1 &= \begin{pmatrix} l'_a & j_a & 1/2 \\ M_a - 1/2 & -M_a & 1/2 \end{pmatrix} \begin{pmatrix} l_b & j_b & 1/2 \\ M_b + 1/2 & -M_b & -1/2 \end{pmatrix} \begin{pmatrix} l'_a & l_b & 0 \\ -M_a + 1/2 & M_b + 1/2 & 0 \end{pmatrix}, \\
a_2^1 &= \begin{pmatrix} l'_a & j_a & 1/2 \\ M_a + 1/2 & -M_a & -1/2 \end{pmatrix} \begin{pmatrix} l_b & j_b & 1/2 \\ M_b - 1/2 & -M_b & 1/2 \end{pmatrix} \begin{pmatrix} l'_a & l_b & 0 \\ -M_a - 1/2 & M_b - 1/2 & 0 \end{pmatrix}, \\
b_1^1 &= \begin{pmatrix} l'_a & j_a & 1/2 \\ M_a - 1/2 & -M_a & 1/2 \end{pmatrix} \begin{pmatrix} l_b & j_b & 1/2 \\ M_b - 1/2 & -M_b & 1/2 \end{pmatrix} \begin{pmatrix} l'_a & l_b & 0 \\ -M_a + 1/2 & M_b - 1/2 & 0 \end{pmatrix}, \\
b_2^1 &= \begin{pmatrix} l'_a & j_a & 1/2 \\ M_a + 1/2 & -M_a & -1/2 \end{pmatrix} \begin{pmatrix} l_b & j_b & 1/2 \\ M_b + 1/2 & -M_b & -1/2 \end{pmatrix} \begin{pmatrix} l'_a & l_b & 0 \\ -M_a - 1/2 & M_b + 1/2 & 0 \end{pmatrix}, \\
a_1^2 &= \begin{pmatrix} l_a & j_a & 1/2 \\ M_a - 1/2 & -M_a & 1/2 \end{pmatrix} \begin{pmatrix} l'_b & j_b & 1/2 \\ M_b + 1/2 & -M_b & -1/2 \end{pmatrix} \begin{pmatrix} l_a & l'_b & 0 \\ -M_a + 1/2 & M_b + 1/2 & 0 \end{pmatrix}, \\
a_2^2 &= \begin{pmatrix} l_a & j_a & 1/2 \\ M_a + 1/2 & -M_a & -1/2 \end{pmatrix} \begin{pmatrix} l'_b & j_b & 1/2 \\ M_b - 1/2 & -M_b & 1/2 \end{pmatrix} \begin{pmatrix} l_a & l'_b & 0 \\ -M_a - 1/2 & M_b - 1/2 & 0 \end{pmatrix}, \\
b_1^2 &= \begin{pmatrix} l_a & j_a & 1/2 \\ M_a - 1/2 & -M_a & 1/2 \end{pmatrix} \begin{pmatrix} l'_b & j_b & 1/2 \\ M_b - 1/2 & -M_b & 1/2 \end{pmatrix} \begin{pmatrix} l_a & l'_b & 0 \\ -M_a + 1/2 & M_b - 1/2 & 0 \end{pmatrix}, \\
b_2^2 &= \begin{pmatrix} l_a & j_a & 1/2 \\ M_a + 1/2 & -M_a & -1/2 \end{pmatrix} \begin{pmatrix} l'_b & j_b & 1/2 \\ M_b + 1/2 & -M_b & -1/2 \end{pmatrix} \\
&\quad \times \begin{pmatrix} l_a & l'_b & 0 \\ -M_a - 1/2 & M_b + 1/2 & 0 \end{pmatrix}.
\end{aligned} \tag{2.167}
$$

For the radial part we find the final expressions

$$
\begin{aligned}
R_1 &= -\left(1 - \frac{E_a}{mc^2}\right)^{1/2} \left(1 + \frac{E_b}{mc^2}\right)^{1/2} U_a U_b [R_1^1 + R_1^2 - R_1^3 - R_1^4], \\
R_2 &= -\left(1 + \frac{E_a}{mc^2}\right)^{1/2} \left(1 - \frac{E_b}{mc^2}\right)^{1/2} U_a U_b [R_1^1 - R_1^2 + R_1^3 - R_1^4],
\end{aligned} \tag{2.168}
$$

where the following polynomials need to be inserted:

$$
\begin{aligned}
R_1^1 &= n_a^r n_b^r (2\lambda_a)^{\gamma_a - 1} (2\lambda_b)^{\gamma_b - 1} \sum_{m=0}^{n_b^r - 1} \frac{(-n_b^r + 1)_m}{(2\gamma_b + 1)_m} \frac{(2\lambda_b)^m}{m!} \frac{\Gamma(m + \gamma_a + \gamma_b + 1)}{(\lambda_a + \lambda_b)^{m + \gamma_a + \gamma_b + 1}} \\
&\quad \times \; {}_2F_1\left(m + \gamma_a + \gamma_b + 1, -n_a^r + 1, 2\gamma_a + 1; \frac{2\lambda_a}{\lambda_a + \lambda_b}\right),
\end{aligned} \tag{2.169}
$$

$$
\begin{aligned}
R_1^2 &= (N_a - \kappa_a) n_b^r (2\lambda_a)^{\gamma_a - 1} (2\lambda_b)^{\gamma_b - 1} \sum_{m=0}^{n_b^r - 1} \frac{(-n_b^r + 1)_m}{(2\gamma_b + 1)_m} \frac{(2\lambda_b)^m}{m!} \frac{\Gamma(m + \gamma_a + \gamma_b + 1)}{(\lambda_a + \lambda_b)^{m + \gamma_a + \gamma_b + 1}} \\
&\quad \times \; {}_2F_1\left(m + \gamma_a + \gamma_b + 1, -n_a^r, 2\gamma_a + 1; \frac{2\lambda_a}{\lambda_a + \lambda_b}\right),
\end{aligned} \tag{2.170}
$$

$$
\begin{aligned}
R_1^3 &= n_a^r (N_b - \kappa_b) (2\lambda_a)^{\gamma_a - 1} (2\lambda_b)^{\gamma_b - 1} \sum_{m=0}^{n_b^r} \frac{(-n_b^r)_m}{(2\gamma_b + 1)_m} \frac{(2\lambda_b)^m}{m!} \frac{\Gamma(m + \gamma_a + \gamma_b + 1)}{(\lambda_a + \lambda_b)^{m + \gamma_a + \gamma_b + 1}} \\
&\quad \times \; {}_2F_1\left(m + \gamma_a + \gamma_b + 1, -n_a^r + 1, 2\gamma_a + 1; \frac{2\lambda_a}{\lambda_a + \lambda_b}\right),
\end{aligned} \tag{2.171}
$$

$$R_1^4 = (N_a-\kappa_a)(N_b-\kappa_b)(2\lambda_a)^{\gamma_a-1}(2\lambda_b)^{\gamma_b-1}\sum_{m=0}^{n_b^r}\frac{(-n_b^r)_m}{(2\gamma_b+1)_m}\frac{(2\lambda_b)^m}{m!}\frac{\Gamma(m+\gamma_a+\gamma_b+1)}{(\lambda_a+\lambda_b)^{m+\gamma_a+\gamma_b+1}}$$
$$\times \; {}_2F_1\left(m+\gamma_a+\gamma_b+1,-n_a^r,2\gamma_a+1;\frac{2\lambda_a}{\lambda_a+\lambda_b}\right). \tag{2.172}$$

Now, we have all analytical expressions needed to calculate the transition matrix elements.

2.3.4 Magnetic dipole interaction in the transverse gauge

We follow the procedure applied in the previous two subsections. Here we are going beyond the electric dipole approximation, which allows us to describe magnetic transitions and electric transitions of higher multipolarity. We expand the exponential $e^{\pm i\mathbf{kr}}$ in a sum of the electric and magnetic dipole terms (the first two terms)

$$\langle\Phi_a|\boldsymbol{\alpha}\cdot\mathbf{A}|\Phi_b\rangle \simeq \langle\Phi_a|\boldsymbol{\alpha}\cdot\hat{\epsilon}_{\mathbf{k}}\mathcal{A}_{\mathbf{k}}\left(a_{\mathbf{k}}+i\mathbf{k}\cdot\mathbf{r}a_{\mathbf{k}}+a_{\mathbf{k}}^\dagger-i\mathbf{k}\cdot\mathbf{r}a_{\mathbf{k}}^\dagger\right)|\Phi_b\rangle \tag{2.173}$$
$$= \langle\Phi_a|\boldsymbol{\alpha}\cdot\hat{\epsilon}_{\mathbf{k}}\mathcal{A}_{\mathbf{k}}\left(a_{\mathbf{k}}+a_{\mathbf{k}}^\dagger\right)|\Phi_b\rangle + \langle\Phi_a|\boldsymbol{\alpha}\cdot\hat{\epsilon}_{\mathbf{k}}\mathcal{A}_{\mathbf{k}}i\mathbf{k}\cdot\mathbf{r}\left(a_{\mathbf{k}}-a_{\mathbf{k}}^\dagger\right)|\Phi_b\rangle.$$

We recognize the first term as the term for the $E1$ transition, for which

$$\boldsymbol{\gamma}_{ab}^{E1} = \frac{ec}{\omega}\langle\Phi_a|\hat{\epsilon}_\lambda\cdot\boldsymbol{\alpha}|\Phi_b\rangle\,. \tag{2.174}$$

The second term corresponds to a magnetic transition, and the corresponding $\boldsymbol{\gamma}_{ab}$ matrix is defined as

$$\boldsymbol{\gamma}_{ab}^{M1} = \frac{ec}{\omega}\langle\Phi_a|\hat{\epsilon}_\lambda\cdot\boldsymbol{\alpha}i\mathbf{k}\cdot\mathbf{r}|\Phi_b\rangle\,. \tag{2.175}$$

As in the previous calculations, we need to analyze the problem considering the laser polarization.

1° *Linear polarization*

First we take the polarization along the z direction:

$$\boldsymbol{\gamma}_{ab}^z = -e\langle\Phi_a|\hat{\epsilon}_z\cdot\boldsymbol{\alpha}r\cos\theta|\Phi_b\rangle = -e\int d\mathbf{r}\Phi_a^\dagger(\mathbf{r})\boldsymbol{\alpha}_z r\cos\theta\Phi_b(\mathbf{r}) = ie[R_1K_1^z - R_2K_2^z]\,. \tag{2.176}$$

2° *Circular polarization*

In this case, the matrix elements are

$$\boldsymbol{\gamma}_{ab}^+ = -e\langle\Phi_a|\hat{\epsilon}_+\cdot\boldsymbol{\alpha}r\cos\theta|\Phi_b\rangle = -\frac{e}{\sqrt{2}}\int d\mathbf{r}\Phi_a^\dagger(\mathbf{r})\boldsymbol{\alpha}\cdot(\hat{\epsilon}_x+i\hat{\epsilon}_y)r\cos\theta\Phi_b(\mathbf{r}) \tag{2.177}$$
$$= -i\frac{e}{\sqrt{2}}\{R_1[-iK_1^x+K_1^y]+R_2[iK_2^x+K_2^y]\}\,,$$
$$\boldsymbol{\gamma}_{ab}^- = -e\langle\Phi_a|\hat{\epsilon}_-\cdot\boldsymbol{\alpha}r\cos\theta|\Phi_b\rangle = -\frac{e}{\sqrt{2}}\int d\mathbf{r}\Phi_a^\dagger(\mathbf{r})\boldsymbol{\alpha}\cdot(\hat{\epsilon}_x-i\hat{\epsilon}_y)r\cos\theta\Phi_b(\mathbf{r})$$
$$= -i\frac{e}{\sqrt{2}}\{R_1[-iK_1^x-K_1^y]+R_2[iK_2^x-K_2^y]\}\,,$$

with the radial integrals

$$R_1 = \int drr^3G_{n_b\kappa_b}(r)F_{n_a\kappa_a}(r), \quad R_2 = \int drr^3F_{n_b\kappa_b}(r)G_{n_a\kappa_a}(r)\,, \tag{2.178}$$

and angular parts

$$
\begin{aligned}
K_1^x &= \int do_r \Omega^\dagger_{-\kappa_a M_a}(\hat{r})\sigma_x \cos\theta \Omega_{\kappa_b M_b}(\hat{r}) \,, \quad K_2^x = \int do_r \Omega^\dagger_{\kappa_a M_a}(\hat{r})\sigma_x \cos\theta \Omega_{-\kappa_b M_b}(\hat{r}) \,, \\
K_1^y &= \int do_r \Omega^\dagger_{-\kappa_a M_a}(\hat{r})\sigma_y \cos\theta \Omega_{\kappa_b M_b}(\hat{r}) \,, \quad K_2^y = \int do_r \Omega^\dagger_{\kappa_a M_a}(\hat{r})\sigma_y \cos\theta \Omega_{-\kappa_b M_b}(\hat{r}) \,, \\
K_1^z &= \int do_r \Omega^\dagger_{-\kappa_a M_a}(\hat{r})\sigma_z \cos\theta \Omega_{\kappa_b M_b}(\hat{r}) \,, \\
K_2^z &= \int do_r \Omega^\dagger_{\kappa_a M_a}(\hat{r})\sigma_z \cos\theta \Omega_{-\kappa_b M_b}(\hat{r}) \,.
\end{aligned} \tag{2.179}
$$

The integrations can again be performed using group theoretic methods, and yield

$$
\begin{aligned}
K_1^x &= (-1)^{j_a+j_b-M_b+3/2}\sqrt{(2j_a+1)(2j_b+1)(2l'_a+1)(2l_b+1)} \begin{pmatrix} l'_a & l_b & 1 \\ 0 & 0 & 0 \end{pmatrix} (a_1^1 - a_2^1) \,, \\
K_2^x &= (-1)^{j_a+j_b-M_b+3/2}\sqrt{(2j_a+1)(2j_b+1)(2l_a+1)(2l'_b+1)} \begin{pmatrix} l_a & l'_b & 1 \\ 0 & 0 & 0 \end{pmatrix} (a_1^2 - a_2^2) \,, \\
K_1^y &= -i(-1)^{j_a+j_b-M_b+3/2}\sqrt{(2j_a+1)(2j_b+1)(2l'_a+1)(2l_b+1)} \begin{pmatrix} l'_a & l_b & 1 \\ 0 & 0 & 0 \end{pmatrix} (a_1^1 + a_2^1) \,, \\
K_2^y &= -i(-1)^{j_a+j_b-M_b+3/2}\sqrt{(2j_a+1)(2j_b+1)(2l_a+1)(2l'_b+1)} \begin{pmatrix} l_a & l'_b & 1 \\ 0 & 0 & 0 \end{pmatrix} (a_1^2 + a_2^2) \,, \\
K_1^z &= (-1)^{j_a+j_b-M_b+3/2}\sqrt{(2j_a+1)(2j_b+1)(2l'_a+1)(2l_b+1)} \begin{pmatrix} l'_a & l_b & 1 \\ 0 & 0 & 0 \end{pmatrix} (b_1^1 + b_2^1) \,, \\
K_2^z &= (-1)^{j_a+j_b-M_b+3/2}\sqrt{(2j_a+1)(2j_b+1)(2l_a+1)(2l'_b+1)} \\
&\times \begin{pmatrix} l_a & l'_b & 1 \\ 0 & 0 & 0 \end{pmatrix} (b_1^2 + b_2^2) \,,
\end{aligned} \tag{2.180}
$$

with the expressions

$$
\begin{aligned}
a_1^1 &= \begin{pmatrix} l'_a & j_a & 1/2 \\ M_a - 1/2 & -M_a & 1/2 \end{pmatrix} \begin{pmatrix} l_b & j_b & 1/2 \\ M_b + 1/2 & -M_b & -1/2 \end{pmatrix} \begin{pmatrix} l'_a & l_b & 1 \\ -M_a + 1/2 & M_b + 1/2 & 0 \end{pmatrix} , \\
a_2^1 &= \begin{pmatrix} l'_a & j_a & 1/2 \\ M_a + 1/2 & -M_a & -1/2 \end{pmatrix} \begin{pmatrix} l_b & j_b & 1/2 \\ M_b - 1/2 & -M_b & 1/2 \end{pmatrix} \begin{pmatrix} l'_a & l_b & 1 \\ -M_a - 1/2 & M_b - 1/2 & 0 \end{pmatrix} , \\
b_1^1 &= \begin{pmatrix} l'_a & j_a & 1/2 \\ M_a - 1/2 & -M_a & 1/2 \end{pmatrix} \begin{pmatrix} l_b & j_b & 1/2 \\ M_b - 1/2 & -M_b & 1/2 \end{pmatrix} \begin{pmatrix} l'_a & l_b & 1 \\ -M_a + 1/2 & M_b - 1/2 & 0 \end{pmatrix} , \\
b_2^1 &= \begin{pmatrix} l'_a & j_a & 1/2 \\ M_a + 1/2 & -M_a & -1/2 \end{pmatrix} \begin{pmatrix} l_b & j_b & 1/2 \\ M_b + 1/2 & -M_b & -1/2 \end{pmatrix} \begin{pmatrix} l'_a & l_b & 1 \\ -M_a - 1/2 & M_b + 1/2 & 0 \end{pmatrix} , \\
a_1^2 &= \begin{pmatrix} l_a & j_a & 1/2 \\ M_a - 1/2 & -M_a & 1/2 \end{pmatrix} \begin{pmatrix} l'_b & j_b & 1/2 \\ M_b + 1/2 & -M_b & -1/2 \end{pmatrix} \begin{pmatrix} l_a & l'_b & 1 \\ -M_a + 1/2 & M_b + 1/2 & 0 \end{pmatrix} , \\
a_2^2 &= \begin{pmatrix} l_a & j_a & 1/2 \\ M_a + 1/2 & -M_a & -1/2 \end{pmatrix} \begin{pmatrix} l'_b & j_b & 1/2 \\ M_b - 1/2 & -M_b & 1/2 \end{pmatrix} \begin{pmatrix} l_a & l'_b & 1 \\ -M_a - 1/2 & M_b - 1/2 & 0 \end{pmatrix} , \\
b_1^2 &= \begin{pmatrix} l_a & j_a & 1/2 \\ M_a - 1/2 & -M_a & 1/2 \end{pmatrix} \begin{pmatrix} l'_b & j_b & 1/2 \\ M_b - 1/2 & -M_b & 1/2 \end{pmatrix} \begin{pmatrix} l_a & l'_b & 1 \\ -M_a + 1/2 & M_b - 1/2 & 0 \end{pmatrix} , \\
b_2^2 &= \begin{pmatrix} l_a & j_a & 1/2 \\ M_a + 1/2 & -M_a & -1/2 \end{pmatrix} \begin{pmatrix} l'_b & j_b & 1/2 \\ M_b + 1/2 & -M_b & -1/2 \end{pmatrix} \\
&\times \begin{pmatrix} l_a & l'_b & 1 \\ -M_a - 1/2 & M_b + 1/2 & 0 \end{pmatrix} .
\end{aligned} \tag{2.181}
$$

The analytical results for radial integrals can be written in the rather concise form as

$$R_1 = -\left(1-\frac{E_a}{mc^2}\right)^{1/2}\left(1+\frac{E_b}{mc^2}\right)^{1/2} U_a U_b[R_1^1 - R_1^2 + R_1^3 - R_1^4]\,, \tag{2.182}$$
$$R_2 = -\left(1+\frac{E_a}{mc^2}\right)^{1/2}\left(1-\frac{E_b}{mc^2}\right)^{1/2} U_a U_b[R_1^1 + R_1^2 - R_1^3 - R_1^4]\,,$$

where the quantities R_1^i, $i \in \{1,2,3,4\}$, have been given previously in the Eqs. (2.153).

2.3.5 Multipole interaction matrix elements in the transverse gauge

We start using the expansion

$$e^{i\mathbf{kr}} = 4\pi \sum_{lm} i^l j_l(kr) Y^*_{lm}(\hat{k}) Y_{lm}(\hat{r})\,. \tag{2.183}$$

Taking the photons direction along the z-axis, we get

$$\begin{aligned} Y^*_{lm}(\theta = 0\,, \phi = 0) &= Y^*_{l0}(0,0) = \sqrt{\frac{2l+1}{4\pi}} \\ Y^*_{lm,m\neq 0}(0,0) &= 0\,, \end{aligned} \tag{2.184}$$

and with this geometry the expansion of the exponential function simplifies to

$$e^{i\mathbf{kr}} = 4\pi \sum_{l} i^l \sqrt{2l+1}\, j_l(kr) Y_{l0}(\hat{r})\,. \tag{2.185}$$

The matrix element $\boldsymbol{\gamma}_{ab} = \frac{ec}{\omega}\langle \Phi_a | \hat{\epsilon}_\lambda \cdot \boldsymbol{\alpha} e^{i\mathbf{kr}} | \Phi_b \rangle$ can then be written in the form

$$\boldsymbol{\gamma}_{ab} = i\sqrt{4\pi}\frac{ec}{\omega} \sum_{l} i^l \sqrt{2l+1} \langle \Phi_a | \hat{\epsilon}_\lambda \cdot \boldsymbol{\alpha} j_l(kr) Y_{l0}(\hat{r}) | \Phi_b \rangle\,. \tag{2.186}$$

1° *Linear polarization*

For the polarization in the z direction, the matrix element takes the form

$$\begin{aligned} \boldsymbol{\gamma}^z_{ab} &= \sqrt{4\pi}\frac{ec}{\omega} \sum_{l} i^{l+1} \sqrt{2l+1} \langle \Phi_a | \hat{\epsilon}_z \cdot \boldsymbol{\alpha} j_l(kr) Y_{l0}(\hat{r}) | \Phi_b \rangle \\ &= i\sqrt{4\pi}\frac{ec}{\omega} \sum_{l} i^{l+1} \sqrt{2l+1} \int d\mathbf{r} \Phi^\dagger_a(\mathbf{r}) \alpha_z j_l(kr) Y_{l0}(\hat{r}) \Phi_b(\mathbf{r}) \\ &= -\sqrt{4\pi}\frac{ec}{\omega} \sum_{l} i^{l} \sqrt{2l+1} [-R_1 K_1^z + R_2 K_2^z]\,. \end{aligned} \tag{2.187}$$

1° *Circular polarization*

For the case of right- and left-circular polarization, we can express the matrix elements as

$$\begin{aligned}
\boldsymbol{\gamma}^{+}_{ab} &= \sqrt{4\pi}\frac{ec}{\omega}\sum_l i^{l+1}\sqrt{2l+1}\langle\Phi_a|\hat{\epsilon}_+\cdot\boldsymbol{\alpha}j_l(kr)Y_{l0}(\hat{r})|\Phi_b\rangle \qquad (2.188)\\
&= i\sqrt{2\pi}\frac{ec}{\omega}\sum_l i^{l+1}\sqrt{2l+1}\int d\mathbf{r}\Phi^\dagger_a(\mathbf{r})(\hat{\epsilon}_x+i\hat{\epsilon}_y)\boldsymbol{\alpha}j_l(kr)Y_{l0}(\hat{r})\Phi_b(\mathbf{r})\\
&= -\sqrt{2\pi}\frac{ec}{\omega}\sum_l i^{l}\sqrt{2l+1}\{-R_1[K^x_1+iK^y_1]+R_2[K^x_2+iK^y_2]\}\,,\\
\boldsymbol{\gamma}^{-}_{ab} &= \sqrt{4\pi}\frac{ec}{\omega}\sum_l i^{l+1}\sqrt{2l+1}\langle\Phi_a|\hat{\epsilon}_-\cdot\boldsymbol{\alpha}j_l(kr)Y_{l0}(\hat{r})|\Phi_b\rangle\\
&= i\sqrt{2\pi}\frac{ec}{\omega}\sum_l i^{l+1}\sqrt{2l+1}\int d\mathbf{r}\Phi^\dagger_a(\mathbf{r})(\hat{\epsilon}_x-i\hat{\epsilon}_y)\boldsymbol{\alpha}j_l(kr)Y_{l0}(\hat{r})\Phi_b(\mathbf{r})\\
&= -\sqrt{2\pi}\frac{ec}{\omega}\sum_l i^{l}\sqrt{2l+1}\{-R_1[K^x_1-iK^y_1]+R_2[K^x_2-iK^y_2]\}\,,
\end{aligned}$$

with the radial integrals

$$R_1=\int drr^2F_{n_a\kappa_a}(r)j_l(kr)G_{n_b\kappa_b}(r)\,,\quad R_2=\int drr^2G_{n_a\kappa_a}(r)j_l(kr)F_{n_b\kappa_b}(r)\,, \qquad (2.189)$$

and the angular parts

$$\begin{aligned}
K^x_1 &= \int do_r\Omega^\dagger_{-\kappa_aM_a}(\hat{r})\sigma_xY_{l0}\Omega_{\kappa_bM_b}(\hat{r}),\quad K^x_2=\int do_r\Omega^\dagger_{\kappa_aM_a}(\hat{r})\sigma_xY_{l0}\Omega_{-\kappa_bM_b}(\hat{r})\,, \qquad (2.190)\\
K^y_1 &= \int do_r\Omega^\dagger_{-\kappa_aM_a}(\hat{r})\sigma_yY_{l0}\Omega_{\kappa_bM_b}(\hat{r}),\quad K^y_2=\int do_r\Omega^\dagger_{\kappa_aM_a}(\hat{r})\sigma_yY_{l0}\Omega_{-\kappa_bM_b}(\hat{r})\,,\\
K^z_1 &= \int do_r\Omega^\dagger_{-\kappa_aM_a}(\hat{r})\sigma_zY_{l0}\Omega_{\kappa_bM_b}(\hat{r}),\quad K^z_2=\int do_r\Omega^\dagger_{\kappa_aM_a}(\hat{r})\sigma_zY_{l0}\Omega_{-\kappa_bM_b}(\hat{r})\,.
\end{aligned}$$

The results of the integration are

$$\begin{aligned}
K^x_1 &= \frac{(-1)^{j_a+j_b-M_b+3/2}}{\sqrt{4\pi}}\sqrt{(2j_a+1)(2j_b+1)(2l+1)(2l'_a+1)(2l_b+1)}\\
&\times \begin{pmatrix} l'_a & l_b & l\\ 0 & 0 & 0\end{pmatrix}(a^1_1-a^1_2)\,, \qquad (2.191)
\end{aligned}$$

$$K^x_2=\frac{(-1)^{j_a+j_b-M_b+3/2}}{\sqrt{4\pi}}\sqrt{(2j_a+1)(2j_b+1)(2l+1)(2l_a+1)(2l'_b+1)}\begin{pmatrix} l_a & l'_b & l\\ 0 & 0 & 0\end{pmatrix}(a^2_1-a^2_2)\,,$$

$$K^y_1=-i\frac{(-1)^{j_a+j_b-M_b+3/2}}{\sqrt{4\pi}}\sqrt{(2j_a+1)(2j_b+1)(2l+1)(2l'_a+1)(2l_b+1)}\begin{pmatrix} l'_a & l_b & l\\ 0 & 0 & 0\end{pmatrix}(a^1_1+a^1_2)\,,$$

$$K^y_2=-i\frac{(-1)^{j_a+j_b-M_b+3/2}}{\sqrt{4\pi}}\sqrt{(2j_a+1)(2j_b+1)(2l+1)(2l_a+1)(2l'_b+1)}\begin{pmatrix} l_a & l'_b & l\\ 0 & 0 & 0\end{pmatrix}(a^2_1+a^2_2)\,,$$

$$K^z_1=\frac{(-1)^{j_a+j_b-M_b+3/2}}{\sqrt{4\pi}}\sqrt{(2j_a+1)(2j_b+1)(2l+1)(2l'_a+1)(2l_b+1)}\begin{pmatrix} l'_a & l_b & l\\ 0 & 0 & 0\end{pmatrix}(b^1_1+b^1_2)\,,$$

$$K_2^z = \frac{(-1)^{j_a+j_b-M_b+3/2}}{\sqrt{4\pi}}\sqrt{(2j_a+1)(2j_b+1)(2l+1)(2l_a+1)(2l'_b+1)}\begin{pmatrix} l_a & l'_b & l \\ 0 & 0 & 0 \end{pmatrix}(b_1^2+b_2^2)\,,$$

with the angular coefficients defined as

$$\begin{aligned}
a_1^1 &= \begin{pmatrix} l'_a & j_a & 1/2 \\ M_a-1/2 & -M_a & 1/2 \end{pmatrix}\begin{pmatrix} l_b & j_b & 1/2 \\ M_b+1/2 & -M_b & -1/2 \end{pmatrix} \\
&\times \begin{pmatrix} l'_a & l_b & l \\ -M_a+1/2 & M_b+1/2 & 0 \end{pmatrix}, \qquad (2.192)\\
a_2^1 &= \begin{pmatrix} l'_a & j_a & 1/2 \\ M_a+1/2 & -M_a & -1/2 \end{pmatrix}\begin{pmatrix} l_b & j_b & 1/2 \\ M_b-1/2 & -M_b & 1/2 \end{pmatrix}\begin{pmatrix} l'_a & l_b & l \\ -M_a-1/2 & M_b-1/2 & 0 \end{pmatrix}, \\
b_1^1 &= \begin{pmatrix} l'_a & j_a & 1/2 \\ M_a-1/2 & -M_a & 1/2 \end{pmatrix}\begin{pmatrix} l_b & j_b & 1/2 \\ M_b-1/2 & -M_b & 1/2 \end{pmatrix}\begin{pmatrix} l'_a & l_b & l \\ -M_a+1/2 & M_b-1/2 & 0 \end{pmatrix}, \\
b_2^1 &= \begin{pmatrix} l'_a & j_a & 1/2 \\ M_a+1/2 & -M_a & -1/2 \end{pmatrix}\begin{pmatrix} l_b & j_b & 1/2 \\ M_b+1/2 & -M_b & -1/2 \end{pmatrix}\begin{pmatrix} l'_a & l_b & l \\ -M_a-1/2 & M_b+1/2 & 0 \end{pmatrix}, \\
a_1^2 &= \begin{pmatrix} l_a & j_a & 1/2 \\ M_a-1/2 & -M_a & 1/2 \end{pmatrix}\begin{pmatrix} l'_b & j_b & 1/2 \\ M_b+1/2 & -M_b & -1/2 \end{pmatrix}\begin{pmatrix} l_a & l'_b & l \\ -M_a+1/2 & M_b+1/2 & 0 \end{pmatrix}, \\
a_2^2 &= \begin{pmatrix} l_a & j_a & 1/2 \\ M_a+1/2 & -M_a & -1/2 \end{pmatrix}\begin{pmatrix} l'_b & j_b & 1/2 \\ M_b-1/2 & -M_b & 1/2 \end{pmatrix}\begin{pmatrix} l_a & l'_b & l \\ -M_a-1/2 & M_b-1/2 & 0 \end{pmatrix}, \\
b_1^2 &= \begin{pmatrix} l_a & j_a & 1/2 \\ M_a-1/2 & -M_a & 1/2 \end{pmatrix}\begin{pmatrix} l'_b & j_b & 1/2 \\ M_b-1/2 & -M_b & 1/2 \end{pmatrix}\begin{pmatrix} l_a & l'_b & l \\ -M_a+1/2 & M_b-1/2 & 0 \end{pmatrix}, \\
b_2^2 &= \begin{pmatrix} l_a & j_a & 1/2 \\ M_a+1/2 & -M_a & -1/2 \end{pmatrix}\begin{pmatrix} l'_b & j_b & 1/2 \\ M_b+1/2 & -M_b & -1/2 \end{pmatrix}\begin{pmatrix} l_a & l'_b & l \\ -M_a-1/2 & M_b+1/2 & 0 \end{pmatrix}.
\end{aligned}$$

For the radial parts, the results are

$$\begin{aligned}
R_1 &= -\sqrt{\pi}\left(1-\frac{E_a}{mc^2}\right)^{1/2}\left(1+\frac{E_b}{mc^2}\right)^{1/2}U_aU_b\sum_{\alpha=0}^{\infty}\frac{(-1)^\alpha\omega^{2\alpha+l}}{2^{2\alpha+l+1}\alpha!\Gamma(\alpha+l+3/2)} \qquad (2.193)\\
&\times[R_1^1-R_1^2+R_1^3-R_1^4]\,,\\
R_2 &= -\sqrt{\pi}\left(1+\frac{E_a}{mc^2}\right)^{1/2}\left(1-\frac{E_b}{mc^2}\right)^{1/2}U_aU_b\sum_{\alpha=0}^{\infty}\frac{(-1)^\alpha\omega^{2\alpha+l}}{2^{2\alpha+l+1}\alpha!\Gamma(\alpha+l+3/2)}\\
&\times[R_1^1+R_1^2-R_1^3-R_1^4]\,,
\end{aligned}$$

with the quantities

$$
\begin{aligned}
R_1^1 &= n_a^r n_b^r (2\lambda_a)^{\gamma_a-1}(2\lambda_b)^{\gamma_b-1}\sum_{m=0}^{n_a^r-1}\frac{(-n_a^r+1)_m}{(2\gamma_a+1)_m}\frac{(2\lambda_a)^m}{m!}\frac{\Gamma(m+\gamma_a+\gamma_b+1+2\alpha+l)}{(\lambda_a+\lambda_b)^{m+\gamma_a+\gamma_b+1+2\alpha+l}} \\
&\quad {}_2F_1\left(m+\gamma_a+\gamma_b+1+2\alpha+l,-n_b^r+1,2\gamma_b+1;\frac{2\lambda_b}{\lambda_a+\lambda_b}\right), \\
R_1^2 &= n_a^r (N_b-\kappa_b)(2\lambda_a)^{\gamma_a-1}(2\lambda_b)^{\gamma_b-1}\sum_{m=0}^{n_a^r-1}\frac{(-n_a^r+1)_m}{(2\gamma_a+1)_m}\frac{(2\lambda_a)^m}{m!}\frac{\Gamma(m+\gamma_a+\gamma_b+1+2\alpha+l)}{(\lambda_a+\lambda_b)^{m+\gamma_a+\gamma_b+1+2\alpha+l}} \\
&\quad {}_2F_1\left(m+\gamma_a+\gamma_b+1+2\alpha+l,-n_b^r,2\gamma_b+1;\frac{2\lambda_b}{\lambda_a+\lambda_b}\right), \\
R_1^3 &= (N_a-\kappa_a) n_b^r (2\lambda_a)^{\gamma_a-1}(2\lambda_b)^{\gamma_b-1}\sum_{m=0}^{n_a^r}\frac{(-n_a^r+1)_m}{(2\gamma_a+1)_m}\frac{(2\lambda_a)^m}{m!}\frac{\Gamma(m+\gamma_a+\gamma_b+1+2\alpha+l)}{(\lambda_a+\lambda_b)^{m+\gamma_a+\gamma_b+1+2\alpha+l}} \\
&\quad {}_2F_1\left(m+\gamma_a+\gamma_b+1+2\alpha+l,-n_b^r+1,2\gamma_b+1;\frac{2\lambda_b}{\lambda_a+\lambda_b}\right), \\
R_1^4 &= (N_a-\kappa_a)(N_b-\kappa_b)(2\lambda_a)^{\gamma_a-1}(2\lambda_b)^{\gamma_b-1}\sum_{m=0}^{n_a^r}\frac{(-n_a^r+1)_m}{(2\gamma_a+1)_m}\frac{(2\lambda_a)^m}{m!}\frac{\Gamma(m+\gamma_a+\gamma_b+1+2\alpha+l)}{(\lambda_a+\lambda_b)^{m+\gamma_a+\gamma_b+1+2\alpha+l}} \\
&\quad {}_2F_1\left(m+\gamma_a+\gamma_b+1+2\alpha+l,-n_b^r,2\gamma_b+1;\frac{2\lambda_b}{\lambda_a+\lambda_b}\right).
\end{aligned}
\tag{2.194}
$$

For the matrix elements in the case of driving between hyperfine-split atomic levels, which will be necessary later, we are using the formula [52]

$$
\begin{aligned}
\langle n_1' j_1' J' || f_k^{(1)} || n_1 j_1 J\rangle &= (-1)^{j_{1,max}+j_2+J_{min}+k}\sqrt{(2J+1)(2J'+1)} \\
&\quad \times \left\{ \begin{array}{ccc} j_1' & J' & j_2 \\ J & j_1 & k \end{array} \right\} \langle n_1' j_1' || f_k^{(1)} || n_1 j_1\rangle ,
\end{aligned}
\tag{2.195}
$$

where $f_{1,max} = \max\{j_1, j_1'\}$, and $(n_1' n_2' j_1' j_2' J) \equiv (n_1' j_1' J)$, i.e. the n_2', j_2' are omitted. It is then easy to find the transition matrix element

$$
\begin{aligned}
&\gamma_{ab}(n_b j_b I F_b \to n_a j_a I F_a) = (-1)^{j_{max}+I+F_{min}+J}\sqrt{(2F_a+1)(2F_b+1)} \\
&\times \left(\begin{array}{ccc} F_a & J & F_b \\ -M_{F_a} & M_{F_a}-M_{F_b} & M_{F_b} \end{array} \right) \Big/ \left(\begin{array}{ccc} j_a & J & j_b \\ -M_a & M_a-M_b & M_b \end{array} \right) \left\{ \begin{array}{ccc} j_a & F_a & I \\ F_a & j_b & J \end{array} \right\} \\
&\times \gamma_{ab}(n_b j_b \to n_a j_a) ,
\end{aligned}
\tag{2.196}
$$

where $\mathbf{F}_a = \mathbf{j}_a + \mathbf{I}$, with $\mathbf{I}$ being the nuclear angular momentum.

2.4 Calculation of relativistic decay widths

In this section we briefly describe how one can derive formulas for the width of radiative decay involving relativistic electrons [46]. Let us add the interaction Hamiltonian $\mathscr{H}_I$ to $\mathscr{H}$– in general, a many-electronic atomic Hamiltonian –, where $\mathscr{H}_{EM}$ is the electromagnetic Hamiltonian

$$
\mathscr{H} = \mathscr{H}_0 + \mathscr{V}_I + \mathscr{H}_{EM} . \tag{2.197}
$$

The state function Ψ_k represents an eigenfunction of $\mathscr{H}_0 + \mathscr{V}_I$ with the eigenvalue E_k, and $|n_k\rangle$ is an n_k-photon eigenstate of $\mathscr{H}_{EM}$ with the eigenvalue $n_k\hbar\omega$, such that:

$$\begin{aligned} (\mathscr{H}_0 + \mathscr{V}_I)\Psi_k &= E_k\Psi_k\,, \\ \mathscr{H}_{EM}|n_k\rangle &= n_k\hbar\omega|n_k\rangle\,. \end{aligned} \tag{2.198}$$

The product of the state Ψ_k and n_k, i.e. $\Phi_k \equiv \Psi_k|n_k\rangle$ is an eigenstate of $\mathscr{H}$ corresponding to a many-electron atom. The eigenvalue coresponding to this eigenstate of $\mathscr{H}$ is $E_k + n_k\hbar\omega$. Considering the interaction $\mathscr{H}_I$, we are interested in readiative transitons between these states.

The unitary operator $U(t, t_0)$ satisfies [46, 68]

$$\begin{aligned} i\hbar\frac{\partial U(t,t_0)}{\partial t} &= \hat{\mathscr{H}_I}U(t,t_0)\,, \\ U(t_0,t_0) &= I\,, \end{aligned} \tag{2.199}$$

with I being the identity operator. The equivalent integral equation is [68]

$$U(t,t_0) = I - \frac{i}{\hbar}\int_{t_0}^{t} dt_1 \hat{\mathscr{H}_I}(t_1)U(t_1,t_0)\,, \tag{2.200}$$

where $\hat{\mathscr{H}_I}(t_1)$ represents the time-dependent interaction Hamiltonian in the interaction picture. The iterative solution of Eq. (2.200) is [46, 68]

$$\begin{aligned} U(t,t_0) &= I - \frac{i}{\hbar}\int_{t_0}^{t} dt_1 \hat{\mathscr{H}_I}(t_1) + \frac{(-i)^2}{\hbar^2}\int_{t_0}^{t} dt_1 \hat{\mathscr{H}_I}(t_1)\int_{t_0}^{t_1} dt_2 \hat{\mathscr{H}_I}(t_2)U(t_2,t_0) \\ &= \sum_{n=0}^{\infty}\frac{(-i)^n}{\hbar^n}\int_{t_0}^{t} dt_1 \hat{\mathscr{H}_I}(t_1)\int_{t_0}^{t_1} dt_2 \hat{\mathscr{H}_I}(t_2)\cdots\int_{t_0}^{t_{n-1}} dt_n \hat{\mathscr{H}_I}(t_n). \end{aligned} \tag{2.201}$$

By definition $S = U(\infty, -\infty)$, where the interaction $\hat{\mathscr{H}_I}(t)$ is assumed to vanish in the distant past $(t = -\infty)$ and in the future $(t = \infty)$.

We can expand S in powers of $\mathscr{H}_I(t)$, i.e.

$$S = I + \sum_{n=1}^{\infty} S^{(n)}\,, \tag{2.202}$$

with

$$S^{(n)} = \frac{(-i)^n}{\hbar^n}\int_{-\infty}^{\infty} dt_1 \hat{\mathscr{H}_I}(t_1)\int_{-\infty}^{t_1} dt_2 \hat{\mathscr{H}_I}(t_2)\cdots\int_{-\infty}^{t_{n-1}} dt_n \hat{\mathscr{H}_I}(t_n)\,. \tag{2.203}$$

It is easy to see that the first order in $\mathscr{H}_I(t)$ is

$$S \approx I - \frac{i}{\hbar}\int_{-\infty}^{\infty} dt \hat{\mathscr{H}_I}(t)\,, \tag{2.204}$$

and the first-order transition amplitude is

$$S_{fi}^{(1)} = \langle\Phi_f|S^{(1)}|\Phi_i\rangle = -\frac{i}{\hbar}\int_{-\infty}^{\infty} dt\langle\Phi_f^{\dagger}|e^{i\mathscr{H}t/\hbar}\mathscr{H}_I e^{-i\mathscr{H}t/\hbar}|\Phi_i\rangle\,. \tag{2.205}$$

If one introduces the *transition amplitude*

$$T_{fi} = \begin{cases} \langle \Psi_f | \mathscr{H}_I | \Psi_i \rangle, & \text{for absorption of radiation,} \\ \langle \Psi_f | \mathscr{H}_I^\dagger | \Psi_i \rangle, & \text{for emission of radiation.} \end{cases} , \tag{2.206}$$

we can write [46]

$$S_{fi} = -2\pi\delta(E_f - E_i \mp \hbar\omega) T_{fi} \left(\frac{\sqrt{n_i}}{\sqrt{n_i + 1}} \right) , \tag{2.207}$$

For isotropic, unpolarized radiation, the absorption probability per second, $w_{b\to a}$, leading from an initial (lower energy) state a to final (higher energy) state b in presence of n photons of energy $\hbar\omega$ is given in terms of the spectral density function $\rho(\omega)$ as [46]

$$w_{a\to b}^{ab} = \frac{\pi^2 c^3}{\hbar\omega^3} \rho(\omega) \frac{\alpha}{2\pi} \omega \sum_\lambda \int d\Omega_k |T_{ba}|^2 . \tag{2.208}$$

The emission probability per second leading from state b to state a in presence of n photons of energy $\hbar\omega$ is given in terms of $\rho(\omega)$ by [46]

$$w_{b\to a}^{em} = \left(1 + \frac{\pi^2 c^3}{\hbar\omega^3} \rho(\omega) \right) \frac{\alpha}{2\pi} \omega \sum_\lambda \int d\Omega_k |T_{ba}|^2 . \tag{2.209}$$

This probability is given as a sum of two terms, namely, a spontaneous emission term and an induced emission term.

Thus one can see that the determination of the decay width is essentially reduced to the calculation of the transition amplitude T_{ba}, given by

$$T_{ba} = \int d^3 r \Psi_b^\dagger \boldsymbol{\alpha} \cdot \boldsymbol{A}(\boldsymbol{r}, \omega) \Psi_a , \tag{2.210}$$

with the transverse-gauge vector potential $\boldsymbol{A}(\boldsymbol{r}, \omega) = \hat{\epsilon} e^{i\mathbf{k}\cdot\mathbf{r}}$. Afret some computation the transition amplitude can be put in the form [36, 46]

$$T_{ba} = 4\pi \sum_{JM\lambda} i^{J-\lambda} \left[\mathbf{Y}_{JM}^{(\lambda)}(\hat{k}) \cdot \hat{\epsilon} \right] \left[T_{JM}^{(\lambda)} \right]_{ba} , \tag{2.211}$$

where

$$\left[T_{JM}^{(\lambda)} \right]_{ba} = \int d^3 r \Psi_b^\dagger \boldsymbol{\alpha} \cdot \boldsymbol{a}_{JM}^{(\lambda)}(\mathbf{r}) \Psi_a . \tag{2.212}$$

The squared transition amplitude contains terms of the form

$$\left[\mathbf{Y}_{JM}^{(\lambda)}(\hat{k}) \cdot \hat{\epsilon}_\nu \right] \left[\hat{\epsilon}_\nu \cdot \mathbf{Y}_{J'M'}^{(\lambda')}(\hat{k}) \right] , \tag{2.213}$$

and one has to sum these terms over the possible polarization directions $\hat{\epsilon}_\nu$. The result of this summation is [46]

$$\sum_\nu \left[\mathbf{Y}_{JM}^{(\lambda)}(\hat{k}) \cdot \hat{\epsilon}_\nu \right] \left[\hat{\epsilon}_\nu \cdot \mathbf{Y}_{J'M'}^{(\lambda')}(\hat{k}) \right] = \left[\mathbf{Y}_{JM}^{(\lambda)}(\hat{k}) \cdot \mathbf{Y}_{J'M'}^{(\lambda')}(\hat{k}) \right] , \tag{2.214}$$

where we exploited the property that the vector spherical harmonics with $\lambda = 0\,, 1$ are orthogonal to $\hat{k}$. Thus it is easy to integrate this expression over the photon direction

$$\int d\Omega_k \left[\mathbf{Y}^{(\lambda)}_{JM}(\hat{k}) \cdot \mathbf{Y}^{(\lambda')}_{J'M'}(\hat{k})\right] = \delta_{JJ'}\delta_{MM'}\delta_{\lambda\lambda'}\,. \tag{2.215}$$

After this discussion one can cast the transition rate in the following form [46]:

$$w_{ba} = \frac{\alpha}{2\pi}\omega \sum_{\nu} \int d\Omega_k |T_{ba}|^2 = 8\pi\alpha\omega \sum_{JM\lambda} \left|\left[T^{(\lambda)}_{JM}\right]_{ba}\right|^2 . \tag{2.216}$$

The interaction can be written in terms of the transition operator $t^{(\lambda)}_{JM}(\mathbf{r})$ [46]

$$\left[\boldsymbol{\alpha}\cdot\boldsymbol{a}^{(\lambda)}_{JM}(\mathbf{r}) - \frac{1}{c}\Phi_{JM}(\mathbf{r})\right] = i\sqrt{\frac{(2J+1)(J+1)}{4\pi J}}\, t^{(\lambda)}_{JM}(\mathbf{r})\,. \tag{2.217}$$

The reduced matrix elements $\langle i||t^{(\lambda)}_J||j\rangle$ are given in the transverse gauge [46] as

$$\begin{aligned}
\langle\kappa_i||t^{(0)}_J||\kappa_j\rangle &= \langle -\kappa_i||C_J||\kappa_j\rangle \int_0^\infty dr \frac{\kappa_i+\kappa_j}{J+1} j_J(kr)\left[G_i(r)F_j(r) + F_i(r)G_j(r)\right], \qquad (2.218)\\
\langle\kappa_i||t^{(1)}_J||\kappa_j\rangle &= \langle\kappa_i||C_J||\kappa_j\rangle \int_0^\infty dr \left\{-\frac{\kappa_i-\kappa_j}{J+1}\left[j'_J(kr) + \frac{j_J(kr)}{kr}\right]\times\right.\\
&\qquad \left.[F_i(r)G_j(r) + G_i(r)F_j(r)] + J\frac{j_J(kr)}{kr}\left[F_i(r)G_j(r) - G_i(r)F_j(r)\right]\right\},
\end{aligned}$$

and in the so-called Babushkin gauge, which is a relativistic generalization of the nonrelativistic length form [46]:

$$\begin{aligned}
\langle\kappa_i||t^{(1)}_J||\kappa_j\rangle = \langle\kappa_i||C_J||\kappa_j\rangle \int_0^\infty dr \Bigg\{ & j_J(kr)\left[F_i(r)F_j(r) + G_i(r)G_j(r)\right] + \qquad (2.219)\\
& + j_{J+1}(kr)\left[\frac{\kappa_i-\kappa_j}{J+1}\left[F_i(r)G_j(r) + G_i(r)F_j(r)\right] + \left[F_i(r)G_j(r) - G_i(r)F_j(r)\right]\right]\Bigg\}.
\end{aligned}$$

The functions $F_i(r)$ and $G_i(r)$ in the above equations are the large and small components, respectively, of the radial Dirac wave functions for the principal and angular momentum quantum numbers (n_i, κ_i).

Using the Wigner-Eckart theorem [15]

$$\langle\Phi_b|t^{(\lambda)}_{JM}|\Phi_a\rangle = (-1)^{(j_b - m_b)} \begin{pmatrix} j_b & J & j_a \\ -M_b & M & M_a \end{pmatrix} \langle\Phi_b||t^{(\lambda)}_J||\Phi_a\rangle \tag{2.220}$$

the final formula for the decay width is

$$\Gamma_{ba} = 2\alpha\omega\frac{(2J+1)(J+1)}{J}\sum_{J\lambda}|\langle\Phi_b||t^{(\lambda)}_J||\Phi_a\rangle|^2 \sum_{Mm_b}\begin{pmatrix} j_b & J & j_a \\ -M_b & M & M_a \end{pmatrix}^2 . \tag{2.221}$$

In a two-level approximation, all quantum numbers of the initial state are well defined, therefore, no averaging over unresolved quantum numbers has to be performed as in the usual case.

We can express, using the formula (2.195), the decay rate between hyperfine components (F_a, M_{F_a}), (F_b, M_{F_b}) as

$$\begin{aligned}
\Gamma_{ab}(n_a j_a I F_a M_{F_a} \to n_b j_b I F_b M_{F_b}) &= (2F_a+1)(2F_b+1)\begin{pmatrix} F_b & J & F_a \\ -M_{F_b} & M_{F_b} - M_{F_a} & M_{F_a}\end{pmatrix}^2\\
/\begin{pmatrix} j_b & J & j_a \\ -M_b & M_b - M_a & M_a\end{pmatrix}^2 &\begin{Bmatrix} j_b & F_b & I \\ F_a & j_a & J\end{Bmatrix}^2 \Gamma_{ab}(n_a j_a \to n_b j_b)\,, \qquad (2.222)
\end{aligned}$$

2.5 Nuclear proton distributions explored by relativistic resonance fluorescence

A promising application of relativistic resonance fluorescence employing x-ray lasers is the determination of isotope shifts in highly charged ions. In these species, the large mutual overlap of the nuclear matter with inner-shell electrons ensures a large sensitivity of ionic transition energies to the protonic charge distribution. First we summarize the phenomenology of isotope shifts, then, as an application of the relativistic theory of resonance fluorescence in two-level systems presented in the previous sections we discuss our results on isotope shift measurements via x-ray lasers.

2.5.1 Isotope shifts and nuclear charge distribution parameters

Isotope shifts are variations of the electron energies without their splitting. The isotope shifts are caused by two effects, namely, the mass and the field shift. The mass shift – or recoil effect – appears due to the fact that the nuclear mass is finite. In the first approximation, we replace the electron mass (m_e) with the reduced mass [28]

$$\mu = \frac{m_e M_{nuc}}{m_e + M_{nuc}}\,, \tag{2.223}$$

and the energy will be rescaled as [28]

$$E = \frac{\mu}{m_e} E_\infty\,. \tag{2.224}$$

E_∞ is the energy value when we consider the nucleus is infinitely heavy ($M_{nuc} = \infty$). This method does not work in the relativistic case, because the center of the mass cannot be defined geometrically. One needs to do more elaborate calculations in the case of relativistic electrons. In the case of many-electron atoms, correction due to the correlated motion should be included. These relativistic and many-body effects can be taken into account by, e.g., perturbative means by the use of the relativistic recoil operator for a general atomic system of electrons with indices i, j (see Refs. [63, 75], in relativistic units, $\hbar = c = \epsilon_0 = 1$):

$$R_{ij} = \frac{\boldsymbol{p}_i \cdot \boldsymbol{p}_j}{2M} - \frac{Z\alpha}{2Mr_i}\left(\boldsymbol{\alpha}_i + \frac{(\boldsymbol{\alpha}_i \cdot \boldsymbol{r}_i)\boldsymbol{r}_i}{r_i^2}\right) \cdot \boldsymbol{p}_j\,. \tag{2.225}$$

Here, $\boldsymbol{r}_i$ and $\boldsymbol{p}_i$ are the position vector and the momentum operator of the ith electron, respectively, and $\boldsymbol{\alpha}_i$ is the vector of Dirac matrices acting on its bispinor wave function. The isotope-dependent nuclear mass is denoted by M and α is the fine-structure constant. There is no summation convention on i and j. The normal mass shift correction to a given atomic state is obtained as the expectation value $\langle \sum_i R_{ii} \rangle$, whereas the specific mass shift term is given by $\langle \sum_{i \neq j} R_{ij} \rangle$. The first term in Eq. (2.225) corresponds to the mass shift operator also known in the non-relativistic theory.

The other physical effect which can produce isotope shifts is the field or volume shift. In this case the nucleus is not point-like anymore, its charge is distributed within a finite volume. The different distribution of the protons will create an electrostatic potential and will influence the motion of the electrons at short distances.

Several models are in use for the description of the proton distribution. One of them is a spherical nuclear charge distribution, with a good aproximation. In reality the nuclei have a different distribution, and the deviation from spherical distribution determines higher-order electric and magnetic moments. These multipole moments contribute to the splitting of energy levels in an atom, and are so-called hyperfine structure effects.

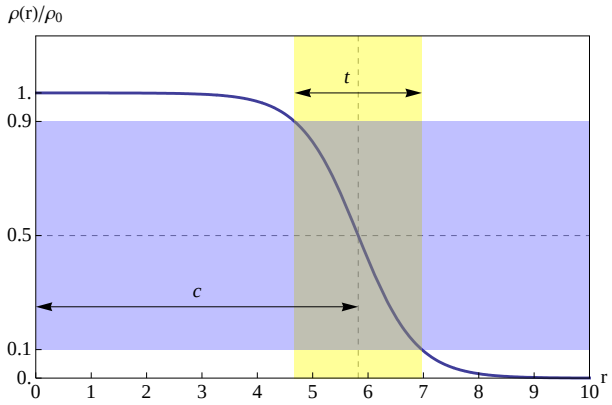

Figure 2.5: The two-parameter Fermi charge distribution normalized by the constant ρ_0 (see text). The half-density radius c and the surface thickness t are indicated. [62]

One of the most studied density function is the two-parameter Fermi distribution

$$\rho_{nuc}(\mathbf{r}) = \frac{\rho_0}{1 + e^{(r-c)/a}}\,, \tag{2.226}$$

where c is the half-density radius. For the case of a spherical distribution, c is a constant and it corresponds to the radius at the half of the maximum value of density. We can introduce the surface thickness of the distribution t as [28]

$$t = 4a \ln 3. \tag{2.227}$$

The normalization condition is

$$\int_0^\infty \rho_{nuc}(r) 4\pi r^2 dr = Ze\,. \tag{2.228}$$

Let us note that the density is essentially ρ_0 when the radius c is much bigger than a. The Fermi distribution is illustrated in Fig. 2.5.

In more complicated cases, when the nuclei are deformed, one should use a four-parameter Fermi charge distribution, where the parameter c is written as [86]

$$c = R_0[1 + \beta_2 Y_{20}(\theta, \phi) + \beta_4 Y_{40}(\theta, \phi)]\,, \tag{2.229}$$

where R_0, β_2 and β_4 are the monopole, quadrupole, hexadecapole parameters, respectively. One can introduce the root mean square (RMS) radius [28]

$$r_{RMS} = \sqrt{\frac{1}{Ze}\int_0^\infty r^2 \rho_{nuc}(r) 4\pi r^2 dr}\,. \tag{2.230}$$

In general, the energy shift also depends on other radial moments [28]

$$\langle r^n \rangle = \frac{1}{Ze}\int_0^\infty \rho_{nuc}(r) 4\pi r^{n+2} dr\,. \tag{2.231}$$

Poisson's equation expresses the relationship between the density distribution and the corresponding nuclear potential [45]

$$\nabla^2 V_{nuc}(r) = -4\pi\rho_{nuc}(r)\,. \tag{2.232}$$

For a spherically symmetrical distribution one gets [47]

$$-rV_{nuc}(r) = 4\pi \left(\int_0^r \rho_{nuc}(s) s^2 ds + r \int_r^\infty \rho_{nuc}(s) s ds \right) , \tag{2.233}$$

if we impose the boundary condition $V_{nuc} \to 0$ for $r \to \infty$.

In many cases, it is sufficient to model the protonic distribution by a homogenous distribution, which has the form [47]

$$\rho_{nuc}(r) = \begin{cases} \rho_0 , & \text{for} \quad r \leq r_{nuc} \\ 0 , & \text{otherwise} \end{cases} , \tag{2.234}$$

and in this case, the nuclear radius may be simply approximated by the empirical form [47]

$$r_{nuc} = (1.0793 A^{1/3} + 0.73587)\text{fm} . \tag{2.235}$$

For a Fermi distribution for a spherically symmetric nucleus, the root mean square radius can be similarly approximated by [47]

$$r_{RMS} = (0.836 A^{1/3} + 0.570)\text{fm} , \tag{2.236}$$

and the surface thickness parameter may be taken constant as $t = 2.30\text{fm}$.

There are four established methods to measure some properties of the nuclear ground-state distribution: elastic electron scattering, optical spectroscopy, K x-ray spectroscopy and muonic atom spectroscopy. In some cases, one needs to use data from different experiments of this type in order to measure some parameters with high precission [28].

1. Elastic electron scattering

In this measurement, the only interaction playing a role is the electromagnetic interaction between the probe electron and the nucleus. We need the electron to be accelerated to some certain energy in order to penetrate the nucleus. Its trajectory will be affected by the nuclear charge distribution. The differential cross section can be measured, and the deviation from the point-like charge distribution is given by the form factor $F(q)$ [28]

$$\left. \frac{d\sigma}{d\Omega} \right|_{exp} = \left. \frac{d\sigma}{d\Omega} \right|_{Mott} |F(q)|^2 , \tag{2.237}$$

with

$$q = \frac{2E}{\hbar c} \sin \frac{\theta}{2} , \tag{2.238}$$

where q is the momentum transfer. The probe electron is in the positive continuum, so it has $E \gg m_e c^2$. The cross section for a pointlike nucleus is called the Mott cross section and it is given by [28]

$$\left. \frac{d\sigma}{d\Omega} \right|_{Mott} = \frac{Z^2 e^4}{4E^4} \frac{\cos^2 \frac{\theta}{2}}{\sin^4 \frac{\theta}{2}} , \tag{2.239}$$

where θ is the scattering angle. If one performs a Bessel-Fourier transform of the form factor, one can get the charge distribution density as [28]

$$F(q) = 4\pi \int_0^\infty \rho_{nuc}(r) j_0(qr) r^2 dr , \quad 0 < q < \infty , \tag{2.240}$$

where $j_0(qr)$ denotes the spherical Bessel function of order zero.

The only possibility of determining the radial dependence of the charge distribution $\rho_{nuc}(r)$ is the electron scattering. All other methods deliver integral quantities of $\rho_{nuc}(r)$. As a result of such experiments it has been concluded that most nuclei have an almost Fermi-like distribution.

2. Optical spectroscopy

In the case of optical spectroscopy, one can only get information about nuclear charge parameters. In these experiments mean-square radii $\delta\langle r^2\rangle$ can be measured, with small correction arising from higher radial moments.

The total shift between two isotopes is the sum of the field effect and the mass effect. So, for two isotopes with the masses A and A', for a transition i of frequency ν we have a frequency shift [28]

$$\delta\nu_i^{AA'} = \delta\nu_{i,MS}^{AA'} + \delta\nu_{i,FS}^{AA'} \,. \tag{2.241}$$

In a spectral line i, the FS variation is [28]

$$\delta\nu_{i,FS}^{AA'} = F_i\lambda^{AA'} \,, \tag{2.242}$$

where F_i represents the electronic factor and

$$\lambda^{AA'} = \delta\langle r^2\rangle^{AA'} + \frac{C_2}{C_1}\delta\langle r^4\rangle^{AA'} + \frac{C_3}{C_1}\delta\langle r^6\rangle^{AA'} + \dots \,, \tag{2.243}$$

with $\delta\langle r^2\rangle^{AA'} = \langle r^2\rangle^{A} - \langle r^2\rangle^{A'}$. The coefficients C_1, C_2, C_3,... are known. There are severel methods in order to determine F_i : a semi-empirical method, using Goudsmit-Fermi Segre method, theoretical with, e.g. a multiconfiguration Dirac-Fock method, or experimentally elpoying the King plot (see [28]).

3. K x-ray spectroscopy

The method is similar to the optical spectroscopy. The formulas (2.241) and (2.243) are still valid. In the case of x-ray transitions with inner-shell electrons, the sensibility of the measurements to nuclear properties is higher.

4. Muonic atom spectroscopy

The muon μ is a particle having a mass 207 time bigger then the electron, and the same spin $\frac{1}{2}$. Because it has a negative charge, it can be bound by a nucleus. The muon is also described by the Dirac equation. There is a big overlap betwen the muonic wave function and the nuclear wave function, so the nuclear size effects become relatively large. The binding energies depend on the nuclear charge distribution, as well the transition energy between atomic levels. So by comparision of the experimental and theoretical spectra [28], one can determine the nuclear parameters.

An additional independent method such as measuring IS by employing x-ray free electron lasers will be by no doubt of great use in extending our knowledge on nuclear electromagnetic properties.

2.5.2 Isotope shifts investigated by means of relativistic resonance fluorescence

In Fig. 2.6 we plot the power spectrum of resonance fluorescence for the case of the $2s \rightarrow 2p_{3/2}$ E1 transition in Li-like uranium (Z=92) ions. The dynamic (AC) Stark shift leads to a splitting of the central peak. At an intensity of 10^{12} W/cm^2, the Rabi frequency of 150 meV is only slightly larger than the natural line width of $\Gamma = 45$ meV. As the figure shows, this leads to a rapid decrease of the fluorescence signal as function of the laser detuning from the transition frequency of the ion, especially when the central peak is considered. This enables the determination of ionic resonance energies with a resolution on the order of the natural line width of the transition. At higher intensities, however, the Rabi frequency which dominates the width of the detected signal peak (see dashed curve on Fig. 2.6) increases, thus corrupting the energy resolution.

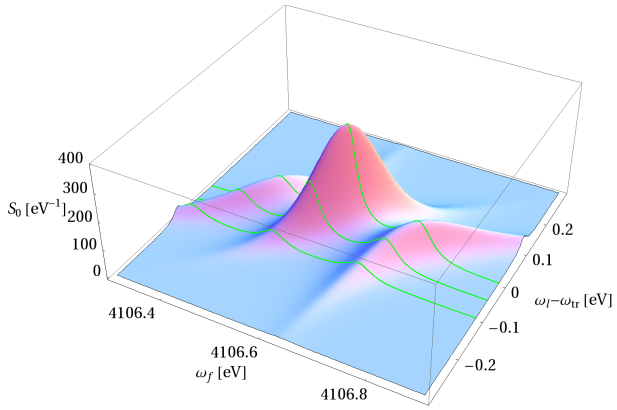

Figure 2.6: Spectrum of fluorescence photons for the $2s$–$2p_{3/2}$ circular (m=3/2–1/2) transition in Li-like U as a function of the fluorescence photon frequency ω_f and the detuning of the laser frequency ω_l from the ionic transition with $\omega_{tr} = 4106.6$ eV. The laser intensity is 10^{12} W/cm^2. The dashed curve shows the frequency-integrated detected signal as a function of the detuning.

In order to deduce nuclear proton distribution parameters via resonance fluorescence spectra, the isotope shifts for a pair of isotopes shall preferably be larger or at least comparable to the width of the fluorescence peaks.

The structure of the relativistic spectra is different from the non-relativistic one due to the spin-orbit interaction and the velocity-dependent electron mass only accounted for in the relativistic theory: the Rabi frequencies depend on the relativistic magnetic sublevels of the upper and lower states, leading to a complex splitting of the usual three-peak Mollow structure.

Current x-ray laser systems such as the LCLS possess a photon beam bandwidth of 200 meV, which is expected to yield an accuracy on the 1 meV level for the IS of the transition mentioned above, thus potentially outperforming the ∼50 meV precision of emission spectroscopy techniques [26] by more than an order of magnitude. Since the only theoretical limitation in our scheme is the rather small natural line width, anticipated improvements of the bandwidth of short-wavelength lasers in the immediate future will allow to push these boundaries even further. Besides the radius, further properties of the nuclear charge distribution such as higher moments, deformation parameters [18] and nuclear polarization contributions may even be accessible. In the optical range, the superior frequency resolution and intensity of existing lasers may be exploited by addressing, e.g., hyperfine transitions in few-electron highly charged ions.

In order to infer nuclear proton radii from experimental IS values, the dependence of the complete fluorescence spectrum on the variation $\delta\langle r^2\rangle$ of the mean square charge radius (averaged over the nuclear volume) is needed. Given the relative simplicity of such few-electron atomic states, this dependence can be calculated to higher precision than in the case of light elements [69]. Such a spectrum is shown in Fig. 2.7 for the case of uranium, delivering directly the radius with respect to that of the ^{238}U isotope.

Laser systems with photon energies of up to a few keV (in the range of Li-like transitions) are presently available [4,27], allowing to excite elements as heavy as U. Future laser facilities are expected to increase the frequency limit to the order of tens of keVs, permitting to directly address the most relativistic very heavy H-like systems. E.g. for the case of Fig. 2.7, experimental photon emission rates are estimated to be on the order of 10^7 $1/s$ per ion at a laser intensity of 10^{12} W/cm^2, providing sufficient count statistics for a high-precision determination of the IS value. Table 2.1 lists values for further elements and charge states.

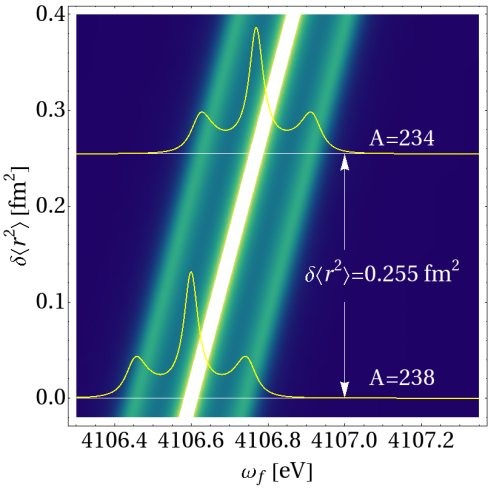

Figure 2.7: Shift of the relativistic resonance fluorescence spectrum as a function of the mean square proton radius variation $\delta\langle r^2\rangle$ for the case of the $2s$–$2p_{3/2}$ transition in Li-like uranium. The spectrum at the bottom corresponds to the reference isotope A=238 and is plotted against the fluorescence photon frequency ω_f around the transition frequency ω_{tr} of 4106.6 eV. The laser intensity is 10^{12} W/cm^2 and the laser detuning is assumed to be 0 for any isotope. See text for more details.

Table 2.1: Parameters for H-like ($1s$–$2p_{1/2}$) and Li-like ($2s$–$2p_{3/2}$) ions. Transition energies, line widths Γ, laser intensities I, and isotope shifts $\Delta\omega_{IS}$, are given. $x(y)$ stands for $x \times 10^y$.

Z	charge state	ω_{tr} [eV]	Γ [eV]	I [W/cm^2]	$\Delta\omega_{IS}$ [eV]
54	H	3.0904(4)	3.03(0)	1(15)	2.96(-2)
	Li	3.6406(2)	1.07(-4)	1(7)	3.44(-3)
60	H	3.8521(4)	5.47(0)	1(16)	3.00(-1)
	Li	5.7763(2)	3.38(-4)	1(8)	3.65(-2)
92	H	9.8065(4)	1.81(1)	1(17)	1.07(0)
	Li	4.1066(3)	4.48(-2)	1(12)	1.70(-1)

2.6 The spectrum of resonance fluorescence in three-level approximation

Resonance fluorescence in a two-level system discussed sofar constitutes the simplest model of bound atomic dynamics. A whole range of new phenomena becomes possible if one extends this picture with a third level and an additional coherent driving. In particular, the quantum manipulation of the system dynamics becomes possible when using a second laser field. In the following we develop a consistent relativistic theory of resonance fluorescence in an atomic three-level system.

2.6.1 Description of the model and equations of motion

The state function of a three-level atom can be written in the form

$$|\Psi(t)\rangle = C_a(t)|a\rangle + C_b(t)|b\rangle + C_c(t)|c\rangle\,. \tag{2.244}$$

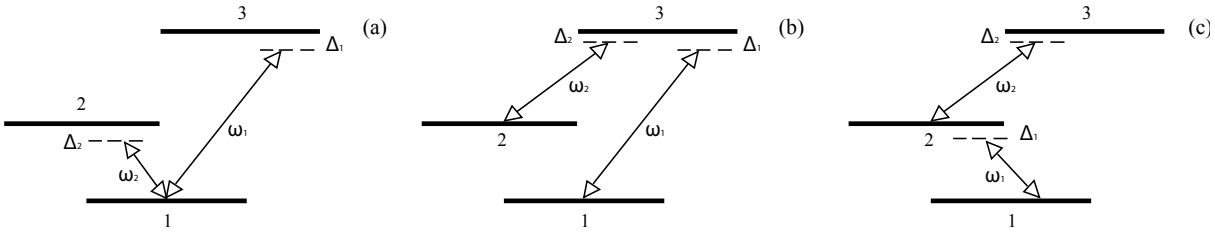

Figure 2.8: Level scheme of an (a) V-system, (b) Λ-system, and (c) Ξ-system. Here, ω_1 and ω_2 are laser frequencies, and Δ_1 and Δ_2 are the corresponding detunings from the atomic transition frequencies.

It is easy to see following the calculations of two-levels atoms that the Hamiltonian of the three-level system interacting with two classical fields is given by [61]

$$\mathscr{H} = \sum_{i=1}^{3} \varepsilon_i |i\rangle\langle i| + \Omega_R^{13}(e^{-i\omega_1 t}|3\rangle\langle 1| + e^{i\omega_1 t}|1\rangle\langle 3|) + \Omega_R^{12}(e^{-i\omega_2 t}|2\rangle\langle 1| + e^{i\omega_2 t}|1\rangle\langle 2|)\,. \quad (2.245)$$

The energies of the stationary states are denoted by ε_i ($i \in \{1,2,3\}$). Ω_R^{12} is the Rabi frequency between the levels $1 \to 2$ and Ω_R^{13} is the Rabi frequency between the levels $1 \to 3$. The operator $|j\rangle\langle i|$ describes the creation of the electronic state in level i and annihilation in level j. ω_1 and ω_2 are the field frequencies between the levels $1 \to 3$ respectively $1 \to 2$. The reversible part of the master equation in the interaction picture has the form [61]

$$\dot{\rho}' = -\frac{i}{\hbar}[\mathscr{H}_1', \rho']\,. \quad (2.246)$$

The prime denotes quantities in the interaction representation. The Hamiltonian in the interaction picture is

$$\mathscr{H}_1' = \hbar\Omega_R^{13}(|3\rangle\langle 1|e^{i\Delta_1 t} + |1\rangle\langle 3|e^{-i\Delta_1 t}) + \hbar\Omega_R^{12}(|2\rangle\langle 1|e^{i\Delta_2 t} + |1\rangle\langle 2|e^{-i\Delta_2 t})\,, \quad (2.247)$$

with

$$\Delta_1 = \omega_{31} - \omega_1\,, \quad \Delta_2 = \omega_{21} - \omega_2\,. \quad (2.248)$$

ω_{31} and ω_{21} are atomic transition frequencies between the levels $1 \to 3$ and $1 \to 2$, respectively. Now we do the following transformation [61]

$$R_{ii} = \rho_{ii}'\,(i = 1,2,3), \quad R_{12} = \rho_{12}' e^{i\Delta_2 t}, \quad R_{13} = \rho_{13}' e^{i\Delta_1 t}, \quad R_{23} = \rho_{23}' e^{i(\Delta_2 - \Delta_2)t}\,, \quad (2.249)$$

with the aim of writing the master equation using the variables R_{ij}.

The full master equation reads

$$\dot{\rho}' = -\frac{i}{\hbar}[\mathscr{H}_1', \rho'] + \Lambda\rho'\,, \quad (2.250)$$

where the irreversible part of Eq. (2.250) is given by Eq. (2.14). Written in terms of the variable R_{ij},

Eq. (2.250) takes the form [61]

$$\begin{aligned}
\frac{dR_{12}}{d\tau} &= i\tilde{\Delta}_2 R_{12} - i\beta_1 R_{32} - i\beta_2(R_{22} - R_{11}) - \tilde{\gamma}_{12} R_{12}\,, \\
\frac{dR_{13}}{d\tau} &= i\tilde{\Delta}_1 R_{13} - i\beta_1(R_{33} - R_{11}) - i\beta_2 R_{23} - \tilde{\gamma}_{13} R_{13}\,, \\
\frac{dR_{22}}{d\tau} &= -i\beta_2(R_{12} - R_{21}) + \tilde{\Gamma}_{12} R_{11} + \tilde{\Gamma}_{32} R_{33} - (\tilde{\Gamma}_{21} + \tilde{\Gamma}_{23}) R_{22}\,, \\
\frac{dR_{23}}{d\tau} &= i(\tilde{\Delta}_1 - \tilde{\Delta}_2) R_{23} + i\beta_1 R_{21} - i\beta_2 R_{13} - \tilde{\gamma}_{23} R_{23}\,, \\
\frac{dR_{33}}{d\tau} &= -i\beta_1(R_{13} - R_{31}) + \tilde{\Gamma}_{13} R_{11} + \tilde{\Gamma}_{23} R_{22} - (1 + \tilde{\Gamma}_{32}) R_{33}\,,
\end{aligned} \tag{2.251}$$

with $R_{11} = 1 - R_{22} - R_{33}$, $R_{21} = R_{12}^*$, $R_{31} = R_{13}^*$ $R_{32} = R_{23}^*$. In Eqs. (2.251) we used the notation $\tau = \Gamma_{31} t$, $\beta_1 = \Omega_R^{13}/\Gamma_{31}$ and $\beta_2 = \Omega_R^{12}/\Gamma_{31}$. All other quantities labeled with a tilde are scaled by Γ_{31}.

The master equation in terms of Ψ is [61]

$$\frac{d}{d\tau}\Psi = L\Psi + I\,, \tag{2.252}$$

with the components

$$\begin{aligned}
\Psi_1 &= R_{12}\,, \quad \Psi_2 = R_{13}\,, \quad \Psi_3 = R_{21}\,, \quad \Psi_4 = R_{22}\,, \\
\Psi_5 &= R_{23}\,, \quad \Psi_6 = R_{31}\,, \quad \Psi_7 = R_{32}\,, \quad \Psi_8 = R_{33}\,,
\end{aligned} \tag{2.253}$$

and L is an 8×8 matrix [61]:

$$L = \begin{pmatrix}
-(\tilde{\gamma}_{12}-i\tilde{\Delta}_2) & 0 & 0 & -2i\beta_2 & 0 & 0 & -i\beta_2 & \\
0 & -(\tilde{\gamma}_{13}-i\tilde{\Delta}_1) & 0 & -i\beta_1 & 0 & 0 & -2i\beta_1 & \\
0 & 0 & -(\tilde{\gamma}_{12}+i\tilde{\Delta}_2) & 2i\beta_2 & 0 & 0 & i\beta_2 & \\
-i\beta_2 & 0 & i\beta_2 & -(\tilde{\Gamma}_{12}+\tilde{\Gamma}_{21}+\tilde{\Gamma}_{23}) & 0 & 0 & -(\tilde{\Gamma}_{12}-\tilde{\Gamma}_{32}) & \\
0 & -i\beta_2 & i\beta_1 & 0 & -[\tilde{\gamma}_{23}-i(\tilde{\Delta}_1-\tilde{\Delta}_2)] & 0 & 0 & \\
0 & 0 & 0 & i\beta_1 & 0 & -(\tilde{\gamma}_{13}+i\tilde{\Delta}_1) & 2i\beta_1 & \\
-i\beta_1 & 0 & 0 & 0 & i\beta_2 & i\beta_2 & 0 & \\
0 & -i\beta_1 & 0 & (\tilde{\Gamma}_{23}-\tilde{\Gamma}_{13}) & 0 & i\beta_1 & -(1+\tilde{\Gamma}_{12}+\tilde{\Gamma}_{13}) &
\end{pmatrix}. \tag{2.254}$$

The components of I are [61]

$$\begin{aligned} I_1 &= i\beta_2\,, \quad I_2 = i\beta_1\,, \quad I_3 = -i\beta_2\,, \quad I_4 = \tilde{\Gamma}_{12}\,, \\ I_5 &= 0\,, \quad I_6 = -i\beta_1\,, \quad I_7 = 0\,, \quad I_8 = \tilde{\Gamma}_{13}\,. \end{aligned} \tag{2.255}$$

2.6.2 The calculation of the spectrum

Like in the case of the two-level atom, in the calculation of the spectra we only need to calculate the atomic correlation function

$$\Gamma(\tau_1, \tau_0) = \langle P^{(-)}(\tau_1) P^{(+)}(\tau_0) \rangle\,. \tag{2.256}$$

We may introduce the polarization operator of the three-level atom as [61]

$$P(\tau) = \gamma_{12}(|1\rangle\langle 2| + |2\rangle\langle 1|) + \gamma_{13}(|1\rangle\langle 3| + |3\rangle\langle 1|)\,, \tag{2.257}$$

where the γ_{ij} are the moduli of the induced transition dipole (or multipole) moments. We can define the positive and negative parts of the polarization operator as [61]

$$\langle P^{(+)}(t)\rangle = \gamma_{12}|1\rangle\langle 2| + \gamma_{13}|1\rangle\langle 3|\,, \quad P^{(-)}(t) = [P^{(+)}(t)]^\dagger\,. \tag{2.258}$$

One starts with one-time average of the $P^{(-)}(\tau_1)$ operator

$$P^{(-)}(\tau_1) = Tr[\rho(\tau_1)(\gamma_{12}(|2\rangle\langle 1| + \gamma_{13}|3\rangle\langle 1|)]\,, \tag{2.259}$$

or in terms of $\Psi_i(\tau_1)$:

$$\langle P^{(-)}(\tau_1)\rangle = \gamma_{12} e^{i\omega_2\tau_1}\Psi_1(\tau_1) + \gamma_{13} e^{i\omega_1\tau_1}\Psi_2(\tau_1)\,. \tag{2.260}$$

For the elegance of the calculation one can start to transform Eq. (2.252) into Laplace space. This allows one to express each of the matrix element $\Psi_i(\tau_1)$ in terms of their initial values $\tau = \tau_0$. We arrive at

$$\langle \hat{P}^{(-)}(z)\rangle = \gamma_{12}\hat{\Psi}_1(z_2) + \gamma_{13}\hat{\Psi}_2(z_1)\,, \tag{2.261}$$

where we did the transformation $z_1 = z - i\omega_1$ and $z_2 = z - i\omega_2$. Using Eq. (2.24) and Eq. (2.261) we can put the average of $\hat{P}^{(-)}(z)$ in the form [61]

$$\langle \hat{P}^{(-)}(z)\rangle = \sum_j [\gamma_{12}M_{1j}(z_2) + \gamma_{13}M_{2j}(z_1)]\Psi_j(\tau_0) + \sum_j \left[\frac{\gamma_{12}}{z_2}M_{1j}(z_2) + \frac{\gamma_{13}}{z_1}M_{2j}(z_1)\right] I_j\,. \tag{2.262}$$

This helps us to express $\Psi_j(\tau_0)$ and I_j in the form of expectation values at $\tau = \tau_0$. The regression theorem gives [61]

$$\begin{aligned} \langle \hat{P}^{(-)}(z)P^{(+)}(\tau_0)\rangle_{\tau_0} &= \gamma_{12}[\gamma_{12}M_{11}(z_2) + \gamma_{13}M_{21}(z_1)]\Psi_4(\tau_0)e^{-i\omega_2\tau_0} \\ &+ \gamma_{13}[\gamma_{12}M_{11}(z_2) + \gamma_{13}M_{21}(z_1)]\Psi_7(\tau_0)e^{-i\omega_1\tau_0} \\ &+ \gamma_{12}[\gamma_{12}M_{12}(z_2) + \gamma_{13}M_{22}(z_1)]\Psi_5(\tau_0)e^{-i\omega_2\tau_0} \\ &+ \gamma_{13}[\gamma_{12}M_{12}(z_2) + \gamma_{13}M_{22}(z_1)]\Psi_8(\tau_0)e^{-i\omega_1\tau_0} \\ &+ \sum_j [\frac{\gamma_{12}}{z_2}M_{1j}(z_2) + \frac{\gamma_{13}}{z_1}M_{2j}(z_1)]I_j[\gamma_{12}\Psi_3(\tau_0)e^{-i\omega_2\tau_0} + \gamma_{13}\Psi_6(\tau_0)e^{-i\omega_1\tau_0}]\,. \end{aligned} \tag{2.263}$$

In the limiting case $\tau_0 \to \infty$, the above expression becomes [61]

$$\langle \hat{P}^{(-)}(z)P^{(+)}(\infty)\rangle_{\tau_0} = \gamma_{12}^2 \left[M_{11}(z_2)\Psi_4(\infty) + M_{12}(z_2)\Psi_5(\infty) + \frac{1}{z_2}\sum_j M_{1j}(z_2)\Psi_3(\infty)I_j \right]$$

$$+\gamma_{13}^2 \left[M_{21}(z_1)\Psi_7(\infty) + M_{22}(z_1)\Psi_8(\infty) + \frac{1}{z_1}\sum_j M_{2j}(z_1)\Psi_6(\infty)I_j \right] . \quad (2.264)$$

Eq. (2.264) shows that the spectrum of resonance fluorescence has a structure with center frequencies located at ω_2 and ω_1, respectively, and magnitudes proportional to the atomic transition matrix elements. The spectrum has the form [61]

$$\hat{\Gamma}_V^{\rm incoh}(z) = \hat{\Gamma}(z) - \frac{1}{z_1}\lim_{z_1\to 0} z_1\hat{\Gamma}(z) - \frac{1}{z_2}\lim_{z_2\to 0} z_2\hat{\Gamma}(z) . \quad (2.265)$$

The emission spectrum can ultimately be expressed as [61]

$$S(\omega) = \Re\hat{\Gamma}_V^{\rm incoh}(z)|_{z=i\omega} , \quad (2.266)$$

with

$$\begin{aligned} \hat{\Gamma}_V^{\rm incoh}(z) &= \gamma_{12}^2[M_{11}(z_2)\Psi_4(\infty) + M_{12}(z_2)\Psi_5(\infty) + \sum_j N_{1j}(z_2)\Psi_3(\infty)I_j] \quad (2.267)\\ &+ \gamma_{13}^2[M_{21}(z_1)\Psi_7(\infty) + M_{22}(z_1)\Psi_8(\infty) + \sum_j N_{2j}(z_1)\Psi_6(\infty)I_j] , \end{aligned}$$

where

$$N_{ij}(z) = (L^{-1}(z-L)^{-1})_{ij} . \quad (2.268)$$

The result of the calculation in the case of the $3 \to 1$ transition in a Λ system (see Fig. 2.8 b)) is [56]

$$\hat{\Gamma}_{\Lambda 1}^{\rm incoh}(z) = \gamma_{13}^2[M_{21}(z_1)\Psi_7(\infty) + M_{22}(z_1)\Psi_8(\infty) + \sum_j N_{2j}(z_1)\Psi_6(\infty)I_j] . \quad (2.269)$$

In the case of the $3 \to 2$ emission one gets [56]

$$\begin{aligned} \hat{\Gamma}_{\Lambda 2}^{\rm incoh}(z) &= \gamma_{23}^2[M_{53}(z_2)\Psi_6(\infty) + M_{56}(z_2)\Psi_7(\infty) + M_{55}(z_2)\Psi_8(\infty)\\ &+ \sum_j N_{5j}(z_2)\Psi_7(\infty)I_j] , \end{aligned} \quad (2.270)$$

where $z_1 = z - i\tilde{\omega}_1$, and $z_2 = z - i\tilde{\omega}_2$.

In the case of the Ξ (or ladder-type) system (see Fig. 2.8 c)), the $2 \to 1$ power spectrum is [56]

$$\hat{\Gamma}_{\Xi 1}^{\rm incoh}(z) = \gamma_{12}^2[M_{11}(z_1)\Psi_4(\infty) + M_{12}(z_1)\Psi_5(\infty) + \sum_j N_{1j}(z_1)\Psi_3(\infty)I_j] , \quad (2.271)$$

and the $3 \to 2$ emission spectrum is given as [56]

$$\begin{aligned} \hat{\Gamma}_{\Xi 2}^{\rm incoh}(z) &= \gamma_{23}^2[M_{53}(z_2)\Psi_6(\infty) + M_{54}(z_2)\Psi_7(\infty) + M_{55}(z_2)\Psi_8(\infty)\\ &+ \sum_j N_{5j}(z_2)\Psi_7(\infty)I_j] . \end{aligned} \quad (2.272)$$

2.6.3 Analytic calculation of the spectra in the strong field approximation

In the following we only consider the case of a resonant interaction of a laser with the $1 \rightarrow 2$ transition, i.e. the detuning is $\tilde{\Delta}_1 = 0$ (see Fig.2.8(a)) and we study the emission spectrum of the $3 \rightarrow 1$ transition. We employ the interaction Hamiltonian of Eq. (2.247) assuming $\tilde{\Delta}_1 = 0$. We consider the dressed atomic states

$$
\begin{aligned}
|r\rangle &= \left[\frac{\lambda_1^2}{\Omega_2^2} + 1 + \left(\frac{\lambda_1^2}{\Omega_1\Omega_2} - \frac{\Omega_2}{\Omega_1}\right)^2\right]^{-1/2} \left[\frac{\lambda_1}{\Omega_2}|1\rangle + |2\rangle + \left(\frac{\lambda_1^2}{\Omega_1\Omega_2} - \frac{\Omega_2}{\Omega_1}\right)|3\rangle\right], \quad (2.273)\\
|s\rangle &= \left[\frac{\lambda_2^2}{\Omega_2^2} + 1 + \left(\frac{\lambda_2^2}{\Omega_1\Omega_2} - \frac{\Omega_2}{\Omega_1}\right)^2\right]^{-1/2} \left[\frac{\lambda_2}{\Omega_2}|1\rangle + |2\rangle + \left(\frac{\lambda_2^2}{\Omega_1\Omega_2} - \frac{\Omega_2}{\Omega_1}\right)|3\rangle\right],\\
|t\rangle &= \left[\frac{\lambda_3^2}{\Omega_2^2} + 1 + \left(\frac{\lambda_3^2}{\Omega_1\Omega_2} - \frac{\Omega_2}{\Omega_1}\right)^2\right]^{-1/2} \left[\frac{\lambda_3}{\Omega_2}|1\rangle + |2\rangle + \left(\frac{\lambda_3^2}{\Omega_1\Omega_2} - \frac{\Omega_2}{\Omega_1}\right)|3\rangle\right],
\end{aligned}
$$

with the λ_i defined as

$$
\begin{aligned}
\lambda_1 &= \frac{\hbar\Omega_2^2\Delta_1}{\Omega_1^2+\Omega_2^2} + \mathscr{O}(\Delta_1)^2, \quad (2.274)\\
\lambda_2 &= \hbar\sqrt{\Omega_1^2+\Omega_2^2} + \frac{\hbar\Omega_1^2\Delta_1}{2(\Omega_1^2+\Omega_2^2)} + \mathscr{O}(\Delta_1)^2,\\
\lambda_3 &= -\hbar\sqrt{\Omega_1^2+\Omega_2^2} + \frac{\hbar\Omega_1^2\Delta_1}{2(\Omega_1^2+\Omega_2^2)} + \mathscr{O}(\Delta_1)^2.
\end{aligned}
$$

In the first order of Δ_1, the dressed atomic states become

$$
\begin{aligned}
|r\rangle &= \frac{\Delta_1}{\Omega_2}\sin\theta^2\cos\theta|1\rangle + \cos\theta|2\rangle - \sin\theta|3\rangle, \quad (2.275)\\
|s\rangle &= \left(\frac{1}{\sqrt{2}} - \frac{1}{\sqrt{32}}\frac{\Delta_1}{\Omega_2}\sin\theta\cos\theta^2\right)|1\rangle + \left(\frac{\sin\theta}{\sqrt{2}} - \frac{3}{\sqrt{32}}\frac{\Delta_1}{\Omega_2}\sin\theta\cos\theta^2\right)|2\rangle\\
&+ \left(\frac{\cos\theta}{\sqrt{2}} + \frac{1}{\sqrt{32}}\frac{\Delta_1}{\Omega_2}\sin\theta\cos\theta(1+3\sin\theta^2)\right)|3\rangle,\\
|t\rangle &= \left(-\frac{1}{\sqrt{2}} - \frac{1}{\sqrt{32}}\frac{\Delta_1}{\Omega_2}\sin\theta\cos\theta^2\right)|1\rangle + \left(\frac{\sin\theta}{\sqrt{2}} + \frac{3}{\sqrt{32}}\frac{\Delta_1}{\Omega_2}\sin\theta\cos\theta^2\right)|2\rangle\\
&+ \left(\frac{\cos\theta}{\sqrt{2}} - \frac{1}{\sqrt{32}}\frac{\Delta_1}{\Omega_2}\sin\theta\cos\theta(1+3\sin\theta^2)\right)|3\rangle,
\end{aligned}
$$

with the angle θ abstractly defined by $\tan\theta = \Omega_2/\Omega_1$. These states are eigenstates of $\mathscr{H}_1'$, i.e.,

$$
\begin{aligned}
\mathscr{H}_1'|r\rangle &= \sin\theta^2\Delta_1|r\rangle, \quad (2.276)\\
\mathscr{H}_1'|s\rangle &= \hbar(\Omega_R + \cos\theta^2\Delta_1)|s\rangle,\\
\mathscr{H}_1'|t\rangle &= \hbar(-\Omega_R + \cos\theta^2\Delta_1|t\rangle,
\end{aligned}
$$

and $\Omega_R = (\Omega_1+\Omega_2)^{1/2}$ represents the effective applied Rabi frequency. In fact we show that, while Ω_R must be large for this approximation to hold, no restrictions are posed on the individual magnitudes of the two Rabi frequencies Ω_1 and Ω_2.

In the interaction picture one can write the master equation

$$
\dot{\rho}' = -\frac{i}{\hbar}[\mathscr{H}_1', \rho'] + \Lambda\rho'. \quad (2.277)
$$

The reversible part of the master Eq. (2.277) has a very simple form

$$\left(\frac{d}{dt}\right)_{rev}\begin{pmatrix}\rho'_{st}\\ \rho'_{sr}\\ \rho'_{rt}\\ \rho'_{ss}\\ \rho'_{tt}\end{pmatrix}=\begin{pmatrix}-2i\Omega_R\rho'_{st}\\ -i(\Omega_R+\cos 2\theta\Delta_1)\rho'_{sr}\\ -i(\Omega_R-\cos 2\theta\Delta_1)\rho'_{rt}\\ 0\\ 0\end{pmatrix}, \tag{2.278}$$

with the trace condition

$$\rho'_{rr}=1-\rho'_{ss}-\rho'_{tt}\,, \tag{2.279}$$

and with Hermitian symmetry relations

$$\rho'_{rs}=(\rho'_{sr})^*\,,\quad \rho'_{tr}=(\rho'_{rt})^*\,,\quad \rho'_{ts}=(\rho'_{st})^*\,. \tag{2.280}$$

The irreversible part of the master equation is somewhat more complicated [61]:

$$\left(\frac{d}{dt}\right)_{irrev}\rho'_{ij}=\sum_{pq}\Lambda_{ijpq}\rho'_{pq}\,, \tag{2.281}$$

where Λ_{ijpq} are parameters defined in Eq. (2.14). We use the transformation equation $\rho'_{\mu\nu}=\sum_{ij}\langle\mu|i\rangle\rho'_{ij}\langle j|\nu\rangle$ in order to get [61]

$$\left(\frac{d}{dt}\right)_{irrev}\rho'_{\mu\nu}=\sum_{\sigma\tau}\left(\sum_{ijpq}\langle\mu|i\rangle\langle j|\nu\rangle\langle p|\sigma\rangle\langle\tau|q\rangle\Lambda_{ijpq}\right)\rho'_{\sigma\tau}\equiv\sum_{\sigma\tau}\Gamma_{\mu\nu\sigma\tau}\rho'_{\sigma\tau}\,, \tag{2.282}$$

the matrix elements $\langle\mu|i\rangle$ can be calculated using Eq. (2.275). We now consider the limit when the Rabi frequency dominates over the relaxation rates. We focus on the derivation of an expression for resonance fluorescence with an accuracy of order $1/\Omega_R$. We can define the vector Ψ as

$$\begin{aligned}\Psi_1 &= \rho'_{st}\,,\quad \Psi_2=\rho'_{sr}\,,\quad \Psi_3=\rho'_{rt}\,,\quad \Psi_4=\rho'_{ss}\,,\\ \Psi_5 &= \rho'_{tt}\,,\quad \Psi_6=\rho'_{rs}\,,\quad \Psi_7=\rho'_{tr}\,,\quad \Psi_8=\rho'_{ts}\,,\end{aligned} \tag{2.283}$$

and $\rho'_{rr}=1-\rho'_{ss}-\rho'_{tt}=1-\Psi_4-\Psi_5$. The master equation in terms of Ψ is

$$\frac{d}{dt}\Psi=L\Psi+I\,. \tag{2.284}$$

In the steady state, it takes the form

$$\Psi(\infty)=-L^{-1}I\,. \tag{2.285}$$

In Eq. (2.285) the only dominant terms are

$$\begin{aligned}\Psi_4(\infty) &= \frac{\Gamma_{sstt}\Gamma_{ttrr}-\Gamma_{ssrr}\Gamma_{tttt})}{\Gamma_{sstt}(\Gamma_{ttrr}-\Gamma_{ttss})+\Gamma_{ssrr}(\Gamma_{ttss}-\Gamma_{tttt}+\Gamma_{ssss}(-\Gamma_{ttrr}+\Gamma_{tttt})}\,,\\ \Psi_5(\infty) &= \frac{\Gamma_{ssss}\Gamma_{ttrr}-\Gamma_{ssrr}\Gamma_{ttss})}{\Gamma_{sstt}(\Gamma_{ttrr}-\Gamma_{ttss})+\Gamma_{ssrr}(\Gamma_{ttss}-\Gamma_{tttt}+\Gamma_{ssss}(-\Gamma_{ttrr}+\Gamma_{tttt})}\,.\end{aligned} \tag{2.286}$$

The deviation from the steady state is defined as [61]

$$\delta\Psi=\Psi(t)-\Psi(\infty)\,, \tag{2.287}$$

which fulfil the condition

$$\frac{d}{dt}\delta\Psi(t) = L\delta\Psi(t)\,. \tag{2.288}$$

Up to corrections of order $1/\Omega_R$, the L_0 in the fluctuation equation Eq. (2.288) has a diagonal form. This approximation can be easily understood if we consider the equations for $\delta\rho'_{\mu\nu}$. For simplicity we take the case when $\Delta_1 = 0$. Similar analysis may be done for $\Delta_1 \neq 0$. One can write

$$\begin{aligned}
\frac{d}{dt}\delta\rho'_{st} = &- 2i\Omega_R\delta\rho'_{st} + \Gamma_{strs}\delta\rho'_{rs} + \Gamma_{strt}\delta\rho'_{rt} + \Gamma_{stsr}\delta\rho'_{sr} + \Gamma_{stst}\delta\rho'_{st} + \Gamma_{sttr}\delta\rho'_{tr} \\
&+ \Gamma_{stts}\delta\rho'_{ts} + (\Gamma_{stss} - \Gamma_{strr})\delta\rho'_{ss} + (\Gamma_{sttt} - \Gamma_{strr})\delta\rho'_{tt}\,, \\
\frac{d}{dt}\delta\rho'_{sr} = &- i\Omega_R\delta\rho'_{sr} + \Gamma_{srrs}\delta\rho'_{rs} + \Gamma_{srrt}\delta\rho'_{rt} + \Gamma_{srsr}\delta\rho'_{sr} + \Gamma_{srst}\delta\rho'_{st} + \Gamma_{srtr}\delta\rho'_{tr} \\
&+ \Gamma_{srts}\delta\rho'_{ts} + (\Gamma_{srss} - \Gamma_{srrr})\delta\rho'_{ss} + (\Gamma_{srtt} - \Gamma_{srrr})\delta\rho'_{tt}\,, \\
\frac{d}{dt}\delta\rho'_{rt} = &- i\Omega_R\delta\rho'_{rt} + \Gamma_{rtrs}\delta\rho'_{rs} + \Gamma_{rtrt}\delta\rho'_{rt} + \Gamma_{rtsr}\delta\rho'_{sr} + \Gamma_{rtst}\delta\rho'_{st} + \Gamma_{rttr}\delta\rho'_{tr} \\
&+ \Gamma_{rtts}\delta\rho'_{ts} + (\Gamma_{rtss} - \Gamma_{rtrr})\delta\rho'_{ss} + (\Gamma_{rttt} - \Gamma_{rtrr})\delta\rho'_{tt}\,.
\end{aligned} \tag{2.289}$$

Introducing the notation

$$\begin{aligned}
&\delta\rho'_{st} = e^{-2i\Omega_R t}R_{st}\,, \quad \delta\rho'_{sr} = e^{-i\Omega_R t}R_{sr}\,, \quad \delta\rho'_{rt} = e^{-i\Omega_R t}R_{rt}\,, \quad \delta\rho'_{ss} = R_{ss}\,, \\
&\delta\rho'_{tt} = R_{tt}\,, \quad \delta\rho'_{rs} = e^{i\Omega_R t}R_{rs}\,, \quad \delta\rho'_{tr} = e^{i\Omega_R t}R_{tr}\,, \quad \delta\rho'_{ts} = e^{2i\Omega_R t}R_{ts}\,,
\end{aligned} \tag{2.290}$$

we get

$$\begin{aligned}
\frac{dR_{st}}{dt} &= \Gamma_{stst}R_{st} + \mathscr{O}(1/\Omega_R)\,, \\
\frac{dR_{sr}}{dt} &= \Gamma_{srrt}R_{rt} + \Gamma_{srsr}R_{sr} + \mathscr{O}(1/\Omega_R)\,, \\
\frac{dR_{rt}}{dt} &= \Gamma_{rtrt}R_{rt} + \Gamma_{rtsr}R_{sr} + \mathscr{O}(1/\Omega_R)\,.
\end{aligned} \tag{2.291}$$

Dropping the rapidly oscillating terms $\mathscr{O}(1/\Omega_R)$, one gets

$$\begin{aligned}
\frac{d}{dt}\delta\rho'_{st} &= (\Gamma_{stst} - 2i\Omega_R)\delta\rho'_{st}\,, \\
\frac{d}{dt}\delta\rho'_{sr} &= (\Gamma_{srsr} - i\Omega_R)\delta\rho'_{sr} + \Gamma_{srrt}\delta\rho'_{rt}\,, \\
\frac{d}{dt}\delta\rho'_{rt} &= \Gamma_{rtsr}\delta\rho'_{sr} + (\Gamma_{rtrt} - i\Omega_R)\delta\rho'_{rt}\,.
\end{aligned} \tag{2.292}$$

Thus the new matrix L_0 can be obtained after neglecting the off-diagonal elements

$$L_0 = \begin{pmatrix}
(1\times 1) & & & & \\
& (2\times 2) & & & \\
& & (2\times 2) & & \\
& & & (2\times 2) & \\
& & & & (1\times 1)
\end{pmatrix}. \tag{2.293}$$

One can write Ψ

$$\frac{d}{dt}\Psi(t) = L_0\Psi(t) + I_\infty\,, \tag{2.294}$$

where $I_\infty = -L_0\Psi(\infty)$. The L_0 components are

$$
\begin{aligned}
(L_0)_1 &= \Gamma_{stst} - 2i\Omega_R\,, \qquad (2.295)\\
(L_0)_2 &= \begin{pmatrix} \Gamma_{srsr} - i(\Omega_R + \Delta_1\cos 2\theta) & \Gamma_{srrt} \\ \Gamma_{stsr} & \Gamma_{rtrt} - i(\Omega_R - \Delta_1\cos 2\theta) \end{pmatrix},\\
(L_0)_3 &= \begin{pmatrix} \Gamma_{ssss} - \Gamma_{ssrr} & \Gamma_{sstt} - \Gamma_{ssrr} \\ \Gamma_{ttss} - \Gamma_{ttrr} & \Gamma_{tttt} - \Gamma_{ttrr} \end{pmatrix},\\
(L_0)_4 &= \begin{pmatrix} \Gamma_{rsrs} + i(\Omega_R + \Delta_1\cos 2\theta) & \Gamma_{rstr} \\ \Gamma_{trrs} & \Gamma_{trtr} + i(\Omega_R - \Delta_1\cos 2\theta) \end{pmatrix},\\
(L_0)_5 &= \Gamma_{tsts} + 2i\Omega_R\,.
\end{aligned}
$$

The quantities $\Gamma_{\mu\nu\sigma\tau}$ are calculated in the first order of Δ_1

$$
\begin{aligned}
\Gamma_{stst} &= \tfrac{1}{8}(-4\Gamma_{31}\cos\theta^2 - 2\Gamma_{32}\cos\theta^2 - \gamma_1\cos\theta^2 - 2\Gamma_{31}\cos\theta^4 - 2\Gamma_{32}\cos\theta^4 - 4\Gamma_{21}\sin\theta^2\\
&- 2\Gamma_{21}\cos\theta^2\sin\theta^2 - 2\Gamma_{31}\cos\theta^2\sin\theta^2 - 2\Gamma_{21}\sin\theta^4) + \mathscr{O}(\Delta_1)\,, \qquad (2.296)
\end{aligned}
$$

$$
\begin{aligned}
\Gamma_{tsts} &= \tfrac{1}{8}(-4\Gamma_{31}\cos\theta^2 - 2\Gamma_{32}\cos\theta^2 - \gamma_1\cos\theta^2 - 2\Gamma_{31}\cos\theta^4 - 2\Gamma_{32}\cos\theta^4 - 4\Gamma_{21}\sin\theta^2\\
&- 2\Gamma_{21}\cos\theta^2\sin\theta^2 - 2\Gamma_{31}\cos\theta^2\sin\theta^2 - 2\Gamma_{21}\sin\theta^4) + \tfrac{1}{16}(-\gamma_1\cos\theta^2\sin\theta - \gamma_1\cos\theta^4\sin\theta\\
&- 3\gamma_1\cos\theta^2\sin\theta^3)\frac{\Delta_1}{\Omega_2} + \mathscr{O}(\Delta_1)^2\,,
\end{aligned}
$$

$$
\begin{aligned}
\Gamma_{srsr} &= \tfrac{1}{4}(-\Gamma_{21}\cos\theta^2 - \Gamma_{21}\cos\theta^4 - \Gamma_{31}\cos\theta^4 - \Gamma_{32}\cos\theta^4 - \Gamma_{31}\sin\theta^2 - \Gamma_{32}\sin\theta^2\\
&- \gamma_1\sin\theta^2 - 2\Gamma_{21}\cos\theta^2\sin\theta^2 - 2\Gamma_{31}\cos\theta^2\sin\theta^2 - 4\Gamma_{32}\cos\theta^2\sin\theta^2 - \Gamma_{21}\sin\theta^4 - \Gamma_{31}\sin\theta^4\\
&- \Gamma_{32}\sin\theta^4) + \tfrac{1}{8}(-\Gamma_{31}\cos\theta^4\sin\theta - \Gamma_{32}\cos\theta^4\sin\theta + 6\Gamma_{21}\cos\theta^4\sin\theta^2 + 3\Gamma_{32}\cos\theta^4\sin\theta^2\\
&+ 4\Gamma_{21}\cos\theta^2\sin\theta^3 - 5\Gamma_{31}\cos\theta^2\sin\theta^3 - 2\Gamma_{32}\cos\theta^2\sin\theta^3 + \gamma_1\cos\theta^2\sin\theta^3 - 3\Gamma_{21}\cos\theta^4\sin\theta^3\\
&- 3\Gamma_{31}\cos\theta^4\sin\theta^3 - 3\Gamma_{32}\cos\theta^4\sin\theta^3 + 3\Gamma_{21}\cos\theta^2\sin\theta^4 + 3\Gamma_{31}\cos\theta^2\sin\theta^4 + 3\Gamma_{32}\cos\theta^2\sin\theta^4\\
&- 6\Gamma_{31}\cos\theta^2\sin\theta^5 - 9\Gamma_{32}\cos\theta^2\sin\theta^5)\frac{\Delta_1}{\Omega_2} + \mathscr{O}(\Delta_1)^2\,,
\end{aligned}
$$

$$
\begin{aligned}
\Gamma_{trtr} &= \tfrac{1}{4}(-\Gamma_{21}\cos\theta^2 - \Gamma_{21}\cos\theta^4 - \Gamma_{31}\cos\theta^4 - \Gamma_{32}\cos\theta^4 - \Gamma_{31}\sin\theta^2 - \Gamma_{32}\sin\theta^2\\
&- \gamma_1\sin\theta^2 - 2\Gamma_{21}\cos\theta^2\sin\theta^2 - 2\Gamma_{31}\cos\theta^2\sin\theta^2 - 4\Gamma_{32}\cos\theta^2\sin\theta^2 - \Gamma_{21}\sin\theta^4 - \Gamma_{31}\sin\theta^4\\
&- \Gamma_{32}\sin\theta^4) - \tfrac{1}{8}(-\Gamma_{31}\cos\theta^4\sin\theta - \Gamma_{32}\cos\theta^4\sin\theta + 6\Gamma_{21}\cos\theta^4\sin\theta^2 + 3\Gamma_{32}\cos\theta^4\sin\theta^2\\
&+ 4\Gamma_{21}\cos\theta^2\sin\theta^3 - 5\Gamma_{31}\cos\theta^2\sin\theta^3 - 2\Gamma_{32}\cos\theta^2\sin\theta^3 + \gamma_1\cos\theta^2\sin\theta^3 - 3\Gamma_{21}\cos\theta^4\sin\theta^3\\
&- 3\Gamma_{31}\cos\theta^4\sin\theta^3 - 3\Gamma_{32}\cos\theta^4\sin\theta^3 + 3\Gamma_{21}\cos\theta^2\sin\theta^4 + 3\Gamma_{31}\cos\theta^2\sin\theta^4 + 3\Gamma_{32}\cos\theta^2\sin\theta^4\\
&- 6\Gamma_{31}\cos\theta^2\sin\theta^5 - 9\Gamma_{32}\cos\theta^2\sin\theta^5)\frac{\Delta_1}{\Omega_2} + \mathscr{O}(\Delta_1)^2\,,
\end{aligned}
$$

$$
\begin{aligned}
\Gamma_{rtrt} &= \tfrac{1}{4}(-\Gamma_{21}\cos\theta^2 - \Gamma_{21}\cos\theta^4 - \Gamma_{31}\cos\theta^4 - \Gamma_{32}\cos\theta^4 - \Gamma_{31}\sin\theta^2 - \Gamma_{32}\sin\theta^2\\
&- 2\Gamma_{21}\cos\theta^2\sin\theta^2 - 2\Gamma_{31}\cos\theta^2\sin\theta^2 - 4\Gamma_{32}\cos\theta^2\sin\theta^2 - \Gamma_{21}\sin\theta^4 - \Gamma_{31}\sin\theta^4\\
&- \Gamma_{32}\sin\theta^4) - \tfrac{1}{8}(-\Gamma_{31}\cos\theta^4\sin\theta - \Gamma_{32}\cos\theta^4\sin\theta + 6\Gamma_{21}\cos\theta^4\sin\theta^2 + 3\Gamma_{32}\cos\theta^4\sin\theta^2\\
&+ 4\Gamma_{21}\cos\theta^2\sin\theta^3 - 5\Gamma_{31}\cos\theta^2\sin\theta^3 - 2\Gamma_{32}\cos\theta^2\sin\theta^3 - 3\Gamma_{21}\cos\theta^4\sin\theta^3\\
&- 3\Gamma_{31}\cos\theta^4\sin\theta^3 - 3\Gamma_{32}\cos\theta^4\sin\theta^3 + 3\Gamma_{21}\cos\theta^2\sin\theta^4 + 3\Gamma_{31}\cos\theta^2\sin\theta^4 + 3\Gamma_{32}\cos\theta^2\sin\theta^4\\
&- 6\Gamma_{31}\cos\theta^2\sin\theta^5 - 9\Gamma_{32}\cos\theta^2\sin\theta^5)\frac{\Delta_1}{\Omega_2} + \mathscr{O}(\Delta_1)^2\,,
\end{aligned}
$$

$$\begin{aligned}\Gamma_{rsrs} &= \tfrac{1}{4}(-\Gamma_{21}\cos\theta^2 - \Gamma_{21}\cos\theta^4 - \Gamma_{31}\cos\theta^4 - \Gamma_{32}\cos\theta^4 - \Gamma_{31}\sin\theta^2 - \Gamma_{32}\sin\theta^2\\ &- 2\Gamma_{21}\cos\theta^2\sin\theta^2 - 2\Gamma_{31}\cos\theta^2\sin\theta^2 - 4\Gamma_{32}\cos\theta^2\sin\theta^2 - \Gamma_{21}\sin\theta^4 - \Gamma_{31}\sin\theta^4\\ &- \Gamma_{32}\sin\theta^4) + \tfrac{1}{8}(-\Gamma_{31}\cos\theta^4\sin\theta - \Gamma_{32}\cos\theta^4\sin\theta + 6\Gamma_{21}\cos\theta^4\sin\theta^2 + 3\Gamma_{32}\cos\theta^4\sin\theta^2\\ &+ 4\Gamma_{21}\cos\theta^2\sin\theta^3 - 5\Gamma_{31}\cos\theta^2\sin\theta^3 - 2\Gamma_{32}\cos\theta^2\sin\theta^3 - 3\Gamma_{21}\cos\theta^4\sin\theta^3\\ &- 3\Gamma_{31}\cos\theta^4\sin\theta^3 - 3\Gamma_{32}\cos\theta^4\sin\theta^3 + 3\Gamma_{21}\cos\theta^2\sin\theta^4 + 3\Gamma_{31}\cos\theta^2\sin\theta^4 + 3\Gamma_{32}\cos\theta^2\sin\theta^4\\ &- 6\Gamma_{31}\cos\theta^2\sin\theta^5 - 9\Gamma_{32}\cos\theta^2\sin\theta^5)\frac{\Delta_1}{\Omega_2} + \mathscr{O}(\Delta_1)^2\,,\end{aligned}$$

$$\begin{aligned}\Gamma_{srrt} &= -\tfrac{1}{2}\Gamma_{32}\cos\theta^2\sin\theta^2 + \tfrac{1}{8}(3\Gamma_{32}\cos\theta^4\sin\theta^2 + 4\Gamma_{21}\cos\theta^2\sin\theta^3 - 4\Gamma_{31}\cos\theta^2\sin\theta^3\\ &+ \Gamma_{32}\cos\theta^2\sin\theta^3 + 2\gamma_1\cos\theta^2\sin\theta^2 + 3\Gamma_{32}\cos\theta^2\sin\theta^5)\frac{\Delta_1}{\Omega_1} + \mathscr{O}(\Delta_1)^2\,,\end{aligned}$$

$$\begin{aligned}\Gamma_{rtsr} &= -\tfrac{1}{2}\Gamma_{32}\cos\theta^2\sin\theta^2 + \tfrac{1}{8}(-3\Gamma_{32}\cos\theta^4\sin\theta^2 - 4\Gamma_{21}\cos\theta^2\sin\theta^3 + 4\Gamma_{31}\cos\theta^2\sin\theta^3\\ &+ -\Gamma_{32}\cos\theta^2\sin\theta^3 + 2\gamma_1\cos\theta^2\sin\theta^2 - 3\Gamma_{32}\cos\theta^2\sin\theta^5)\frac{\Delta_1}{\Omega_2} + \mathscr{O}(\Delta_1)^2\,,\end{aligned}$$

$$\begin{aligned}\Gamma_{rstr} &= -\tfrac{1}{2}\Gamma_{32}\cos\theta^2\sin\theta^2 + \tfrac{1}{8}(3\Gamma_{32}\cos\theta^4\sin\theta^2 + 4\Gamma_{21}\cos\theta^2\sin\theta^3 - 4\Gamma_{31}\cos\theta^2\sin\theta^3\\ &+ \Gamma_{32}\cos\theta^2\sin\theta^3 - 2\gamma_1\cos\theta^2\sin\theta^3 - 3\Gamma_{32}\cos\theta^2\sin\theta^5)\frac{\Delta_1}{\Omega_2} + \mathscr{O}(\Delta_1)^2\,,\end{aligned}$$

$$\begin{aligned}\Gamma_{trrs} &= -\tfrac{1}{2}\Gamma_{32}\cos\theta^2\sin\theta^2 + \tfrac{1}{8}(-3\Gamma_{32}\cos\theta^4\sin\theta^2 - 4\Gamma_{21}\cos\theta^2\sin\theta^3 + 4\Gamma_{31}\cos\theta^2\sin\theta^3\\ &- \Gamma_{32}\cos\theta^2\sin\theta^3 - 2\gamma_1\cos\theta^2\sin\theta^3 - \Gamma_{32}\cos\theta^2\sin\theta^5)\frac{\Delta_1}{\Omega_2} + \mathscr{O}(\Delta_1)^2\,,\end{aligned}$$

$$\begin{aligned}\Gamma_{ssss} - \Gamma_{ssrr} &= \tfrac{1}{8}(-4\Gamma_{21}\cos\theta^2 - 2\Gamma_{32}\cos\theta^2 - \gamma_1\cos\theta^2 - 2\Gamma_{31}\cos\theta^4 - 2\Gamma_{32}\cos\theta^4 - 4\Gamma_{31}\sin\theta^2\\ &- 2\Gamma_{21}\cos\theta^2\sin\theta^2 - 2\Gamma_{31}\cos\theta^2\sin\theta^2 - 2\Gamma_{21}\sin\theta^4 - 4\Gamma_{32}\sin\theta^4)\\ &+ \tfrac{1}{16}(-2\Gamma_{32}\cos\theta^2\sin\theta - \gamma_1\cos\theta^2\sin\theta + 4\Gamma_{21}\cos\theta^4\sin\theta - 4\Gamma_{31}\cos\theta^4\sin\theta\\ &- 2\Gamma_{32}\cos\theta^4\sin\theta + \gamma_1\cos\theta^4\sin\theta + 12\Gamma_{31}\cos\theta^4\sin\theta^2 + 6\Gamma_{32}\cos\theta^4\sin\theta^2\\ &+ 4\Gamma_{21}\cos\theta^2\sin\theta^3 - 4\Gamma_{31}\cos\theta^2\sin\theta^3 - 12\Gamma_{32}\cos\theta^2\sin\theta^3 - 7\gamma_1\cos\theta^2\sin\theta^3\\ &- 12\Gamma_{31}\cos\theta^4\sin\theta^3 - 12\Gamma_{32}\cos\theta^4\sin\theta^3 + 12\Gamma_{21}\cos\theta^2\sin\theta^4 + 12\Gamma_{32}\cos\theta^2\sin\theta^4\\ &- 12\Gamma_{21}\cos\theta^2\sin\theta^5 + 6\Gamma_{32}\cos\theta^2\sin\theta^5)\frac{\Delta_1}{\Omega_2} + \mathscr{O}(\Delta_1)^2\,,\end{aligned}$$

$$\begin{aligned}\Gamma_{tttt} - \Gamma_{ttrr} &= \tfrac{1}{8}(-4\Gamma_{21}\cos\theta^2 - 2\Gamma_{32}\cos\theta^2 - \gamma_1\cos\theta^2 - 2\Gamma_{31}\cos\theta^4 - 2\Gamma_{32}\cos\theta^4 - 4\Gamma_{31}\sin\theta^2\\ &- 2\Gamma_{21}\cos\theta^2\sin\theta^2 - 2\Gamma_{31}\cos\theta^2\sin\theta^2 - 2\Gamma_{21}\sin\theta^4 - 4\Gamma_{32}\sin\theta^4)\\ &- \tfrac{1}{16}(-2\Gamma_{32}\cos\theta^2\sin\theta - \gamma_1\cos\theta^2\sin\theta + 4\Gamma_{21}\cos\theta^4\sin\theta - 4\Gamma_{31}\cos\theta^4\sin\theta\\ &- 2\Gamma_{32}\cos\theta^4\sin\theta + \gamma_1\cos\theta^4\sin\theta + 12\Gamma_{31}\cos\theta^4\sin\theta^2 + 6\Gamma_{32}\cos\theta^4\sin\theta^2\\ &+ 4\Gamma_{21}\cos\theta^2\sin\theta^3 - 4\Gamma_{31}\cos\theta^2\sin\theta^3 - 12\Gamma_{32}\cos\theta^2\sin\theta^3 - 7\gamma_1\cos\theta^2\sin\theta^3\\ &- 12\Gamma_{31}\cos\theta^4\sin\theta^3 - 12\Gamma_{32}\cos\theta^4\sin\theta^3 + 12\Gamma_{21}\cos\theta^2\sin\theta^4 + 12\Gamma_{32}\cos\theta^2\sin\theta^4\\ &- 12\Gamma_{21}\cos\theta^2\sin\theta^5 + 6\Gamma_{32}\cos\theta^2\sin\theta^5)\frac{\Delta_1}{\Omega_2} + \mathscr{O}(\Delta_1)^2\,,\end{aligned}$$

$$\begin{aligned}
\Gamma_{sstt}-\Gamma_{ssrr} &= \tfrac{1}{8}(-4\Gamma_{21}\cos\theta^2+4\Gamma_{31}\cos\theta^2+\gamma_1\cos\theta^2+2\Gamma_{32}\cos\theta^2-2\Gamma_{31}\cos\theta^4-2\Gamma_{32}\cos\theta^4\\
&+ 4\Gamma_{21}\sin\theta^2-4\Gamma_{31}\sin\theta^2-2\Gamma_{21}\cos\theta^2\sin\theta^2-2\Gamma_{31}\cos\theta^2\sin\theta^2-2\Gamma_{21}\sin\theta^4\\
&- 4\Gamma_{32}\sin\theta^4)+\tfrac{1}{8}(-\Gamma_{31}\cos\theta^2\sin\theta+2\Gamma_{21}\cos\theta^4\sin\theta-\Gamma_{31}\cos\theta^4\sin\theta\\
&+ 3\Gamma_{21}\cos\theta^2\sin\theta^2-3\Gamma_{21}\cos\theta^4\sin\theta^2+3\Gamma_{31}\cos\theta^4\sin\theta^2+2\Gamma_{21}\cos\theta^2\sin\theta^3\\
&- 4\Gamma_{31}\cos\theta^2\sin\theta^3-4\Gamma_{32}\cos\theta^2\sin\theta^3-2\gamma_1\cos\theta^2\sin\theta^3+6\Gamma_{32}\cos\theta^2\sin\theta^4\\
&- 3\Gamma_{21}\cos\theta^2\sin\theta^5+3\Gamma_{31}\cos\theta^2\sin\theta^5)\frac{\Delta_1}{\Omega_2}+\mathscr{O}(\Delta_1)^2\,,
\end{aligned}$$

$$\begin{aligned}
\Gamma_{ttss}-\Gamma_{ttrr} &= \tfrac{1}{8}(-4\Gamma_{21}\cos\theta^2+4\Gamma_{31}\cos\theta^2+\gamma_1\cos\theta^2+2\Gamma_{32}\cos\theta^2-2\Gamma_{31}\cos\theta^4-2\Gamma_{32}\cos\theta^4\\
&+ 4\Gamma_{21}\sin\theta^2-4\Gamma_{31}\sin\theta^2-2\Gamma_{21}\cos\theta^2\sin\theta^2-2\Gamma_{31}\cos\theta^2\sin\theta^2-2\Gamma_{21}\sin\theta^4\\
&- 4\Gamma_{32}\sin\theta^4)-\tfrac{1}{8}(-\Gamma_{31}\cos\theta^2\sin\theta+2\Gamma_{21}\cos\theta^4\sin\theta-\Gamma_{31}\cos\theta^4\sin\theta\\
&+ 3\Gamma_{21}\cos\theta^2\sin\theta^2-3\Gamma_{21}\cos\theta^4\sin\theta^2+3\Gamma_{31}\cos\theta^4\sin\theta^2+2\Gamma_{21}\cos\theta^2\sin\theta^3\\
&- 4\Gamma_{31}\cos\theta^2\sin\theta^3-4\Gamma_{32}\cos\theta^2\sin\theta^3-2\gamma_1\cos\theta^2\sin\theta^3+6\Gamma_{32}\cos\theta^2\sin\theta^4\\
&- 3\Gamma_{21}\cos\theta^2\sin\theta^5+3\Gamma_{31}\cos\theta^2\sin\theta^5)\frac{\Delta_1}{\Omega_2}+\mathscr{O}(\Delta_1)^2\,,
\end{aligned}$$

where γ_1 is the decoherence rate of the laser having the frequency ω_1.

The only nonzero elements of the vector I_∞ (to order $1/\Omega_R$) are

$$I_{\infty 4}=I_{\infty 5}=\Gamma_{ssrr}\,. \tag{2.297}$$

One can write the solution of Eq. (2.294)

$$\hat{\Psi}(z)=M^0(z)\Psi(t_0)+\frac{1}{z}M^0(z)I_\infty\,, \tag{2.298}$$

where the matrix M^0 is given as

$$M^0(z)=(z-L_0)^{-1}. \tag{2.299}$$

The polarization operator is defined as

$$P^{(+)}=\gamma_{13}|1\rangle\langle 3|\,,\quad P^{(-)}=\gamma_{13}|3\rangle\langle 1|\,. \tag{2.300}$$

The single-time average is

$$\langle P^{(-)}(t_1)\rangle=\gamma_{13}Tr[\rho'(t_1)|3\rangle\langle 1|]\exp(I\omega_{31}t_1)\,. \tag{2.301}$$

Using the relations

$$|3\rangle\langle 1|r\rangle = \frac{\Delta_1}{\Omega_2}\sin\theta^2\cos\theta\left(-\sin\theta|r\rangle+\frac{1}{\sqrt{2}}\cos\theta|s\rangle+\frac{1}{\sqrt{2}}\cos\theta|t\rangle\right)\,, \tag{2.302}$$

$$\begin{aligned}
|3\rangle\langle 1|s\rangle &= \frac{1}{2}\cos\theta(|s\rangle+|t\rangle)-\frac{1}{\sqrt{2}}\sin\theta|r\rangle\\
&+ \frac{1}{\sqrt{32}}\frac{\Delta_1}{\Omega_2}\sin 2\theta(\sqrt{2}\sin 2\theta|r\rangle+8\sin\theta^2|s\rangle-4(1+\sin\theta^2)|t\rangle)\,,\\
|3\rangle\langle 1|t\rangle &= -\frac{1}{2}\cos\theta(|s\rangle+|t\rangle)+\frac{1}{\sqrt{2}}\sin\theta|r\rangle\\
&+ \frac{1}{\sqrt{32}}\frac{\Delta_1}{\Omega_2}\sin 2\theta(\sqrt{2}\sin 2\theta|r\rangle+8\sin\theta^2|s\rangle-4(1+\sin\theta^2)|t\rangle)\,,
\end{aligned}$$

we can write the expression for $P^{(-)}(z)$ as

$$\begin{aligned}\langle P^{(-)}(z)\rangle &= \frac{1}{2}\cos\theta(\hat{\Psi}_4(z_1)+\hat{\Psi}_1(z_1)-\hat{\Psi}_8(z_1)-\hat{\Psi}_5(z_1))-\frac{1}{\sqrt{2}}\sin\theta(\hat{\Psi}_2(z_1)-\hat{\Psi}_7(z_1)) \qquad (2.303)\\ &+ \frac{\Delta_1}{\Omega_2}\sin\theta^2\cos\theta\left[\sin\theta(-\frac{1}{z_1}+\hat{\Psi}_4(z_1)+\hat{\Psi}_5(z_1))+\frac{1}{\sqrt{2}}\cos\theta(\hat{\Psi}_6(z_1)+\hat{\Psi}_3(z_1)+\frac{1}{4}\hat{\Psi}_2(z_1)\right.\\ &+ \left.\frac{1}{4}\hat{\Psi}_7(z_1))+\cos\theta\sin\theta^2(\hat{\Psi}_4(z_1)+\hat{\Psi}_8(z_1))-\frac{1}{2}\cos\theta(\hat{\Psi}_1(z_1)+\hat{\Psi}_5(z_1))\right],\end{aligned}$$

where $z_1 = z - i\omega_{31}$. We apply the regression theorem

$$\begin{aligned}\Psi_1(t_0)\to\gamma_{13}Tr[\rho(t_0)|\overline{t\rangle\langle s}|1\rangle\langle 3|] &= \gamma_{13}Tr[\rho'(t_0)|t\rangle\langle s|\overline{1\rangle\langle 3}|] \qquad (2.304)\\ &= \gamma_{13}\exp(-i\omega_{31}t_0)\langle s|1\rangle\langle 3|\rho'(t_0)|t\rangle\,,\end{aligned}$$

$$\begin{aligned}&\Psi_1(t_0)\to\gamma_{13}exp(-i\omega_{31}t_0)\left(\tfrac{1}{2}\cos\theta(\rho'_{st}+\rho'_{tt})-\frac{1}{\sqrt{2}}\sin\theta\rho'_{rt}\right) \qquad (2.305)\\ &+\gamma_{13}\frac{\Delta_1}{\Omega_2}\exp(-i\omega_{31}t_0)\left(\frac{1}{\sqrt{32}}\sin\theta^3\cos\theta^2\rho'_{rt}+\frac{1}{2}\sin\theta^3\cos\theta\rho'_{st}-\frac{1}{4}\sin\theta\cos\theta(1+\sin\theta^2)\rho'_{tt}\right).\end{aligned}$$

Again, with over-bars we indicate the operators in the interaction picture. Appling the same procedure, one can get

$$\begin{aligned}&\Psi_2(t_0)\to\gamma_{13}\exp(-i\omega_{31}t_0)\left(\tfrac{1}{2}\cos\theta(\rho'_{sr}+\rho'_{tr})-\frac{1}{\sqrt{2}}\sin\theta\rho'_{rr}\right) \qquad (2.306)\\ &+\gamma_{13}\frac{\Delta_1}{\Omega_2}\exp(-i\omega_{31}t_0)\left(\frac{1}{\sqrt{32}}\sin\theta^2\cos\theta^2\rho'_{rr}+\frac{1}{2}\sin\theta^3\cos\theta\rho'_{sr}-\frac{1}{4}\sin\theta\cos\theta(1+\sin\theta^2)\rho'_{tr}\right),\\ &\Psi_3(t_0)\to\gamma_{13}\frac{\Delta_1}{\Omega_2}\exp(-i\omega_{31}t_0)\left(-\sin\theta^3\cos\theta\rho'_{rt}+\frac{1}{\sqrt{2}}\sin\theta^2\cos\theta^2\rho'_{st}+\frac{1}{\sqrt{2}}\sin\theta^2\cos\theta^2\rho'_{tt}\right),\\ &\Psi_4(t_0)\to\gamma_{13}\exp(-i\omega_{31}t_0)\left(\tfrac{1}{2}\cos\theta(\rho'_{ss}+\rho'_{ts})-\frac{1}{\sqrt{2}}\sin\theta\rho'_{rs}\right)\\ &+\gamma_{13}\frac{\Delta_1}{\Omega_2}\exp(-i\omega_{31}t_0)\left(\frac{1}{\sqrt{32}}\sin\theta^3\cos\theta^2\rho'_{rs}+\frac{1}{2}\sin\theta^2\cos\theta\rho'_{ss}-\frac{1}{4}\sin\theta\cos\theta(1+\sin\theta^2)\rho'_{ts}\right),\\ &\Psi_5(t_0)\to\gamma_{13}\exp(-i\omega_{31}t_0)\left(-\tfrac{1}{2}\cos\theta(\rho'_{st}+\rho'_{tt})+\frac{1}{\sqrt{2}}\sin\theta\rho'_{rt}\right)\\ &+\gamma_{13}\frac{\Delta_1}{\Omega_2}\exp(-i\omega_{31}t_0)\left(\frac{1}{\sqrt{32}}\sin\theta\cos\theta^2\rho'_{rt}-\frac{1}{4}\sin\theta\cos\theta(1+\sin\theta^2)\rho'_{st}+\frac{1}{2}\sin\theta^3\cos\theta\rho'_{tt}\right),\\ &\Psi_6(t_0)\to\gamma_{13}\frac{\Delta_1}{\Omega_2}\exp(-i\omega_{31}t_0)\left(-\sin\theta^3\cos\theta\rho'_{rs}+\frac{1}{\sqrt{2}}\sin\theta^2\cos\theta^2\rho'_{ss}+\frac{1}{\sqrt{2}}\sin\theta^2\cos\theta^2\rho'_{ts}\right),\\ &\Psi_7(t_0)\to\gamma_{13}\exp(-i\omega_{31}t_0)\left(-\tfrac{1}{2}\cos\theta(\rho'_{sr}+\rho'_{tr})+\frac{1}{\sqrt{2}}\sin\theta\rho'_{rr}\right)\\ &+\gamma_{13}\frac{\Delta_1}{\Omega_2}\exp(-i\omega_{31}t_0)\left(\frac{1}{\sqrt{32}}\sin\theta^2\cos\theta^2\rho'_{rr}-\frac{1}{4}\sin\theta\cos\theta(1+\sin\theta^2)\rho'_{sr}+\frac{1}{2}\sin\theta^3\cos\theta\rho'_{tr}\right),\\ &\Psi_8(t_0)\to\gamma_{13}\exp(-i\omega_{31}t_0)\left(-\tfrac{1}{2}\cos\theta(\rho'_{ss}+\rho'_{ts})+\frac{1}{\sqrt{2}}\sin\theta\rho'_{rs}\right)\\ &+\gamma_{13}\frac{\Delta_1}{\Omega_2}\exp(-i\omega_{31}t_0)\left(\frac{1}{\sqrt{32}}\sin\theta^2\cos\theta^2\rho'_{rs}-\frac{1}{4}\sin\theta\cos\theta(1+\sin\theta^2)\rho'_{ss}+\frac{1}{2}\sin\theta^3\cos\theta\rho'_{ts}\right).\end{aligned}$$

In the stationary limit, the only nonzero elements are

$$\rho'_{ss} = \Psi_{4\infty}\,, \quad \rho'_{tt} = \Psi_{5\infty}\,, \tag{2.307}$$

and the equation (2.304) becomes

$$\begin{aligned}
\Psi_1(t_0\to\infty) &= \gamma_{13}\exp(-i\omega_{31}t_0)\left(\frac{1}{2}\cos\theta - \frac{1}{4}\frac{\Delta_1}{\Omega_2}\sin\theta\cos\theta(1+\sin\theta^2)\right)\Psi_5(\infty)\,, \qquad (2.308)\\
\Psi_2(t_0\to\infty) &= -\gamma_{13}\exp(-i\omega_{31}t_0)\left(\frac{1}{\sqrt{2}}\sin\theta - \frac{1}{\sqrt{32}}\frac{\Delta_1}{\Omega_2}\sin\theta^2\cos\theta^2\right)(1-\Psi_4(\infty)-\Psi_5(\infty))\,,\\
\Psi_3(t_0\to\infty) &= \gamma_{13}\exp(-i\omega_{31}t_0)\frac{1}{\sqrt{2}}\frac{\Delta_1}{\Omega_2}\sin\theta^2\cos\theta^2\Psi_5(\infty)\,,\\
\Psi_4(t_0\to\infty) &= \gamma_{13}\exp(-i\omega_{31}t_0)\left(\frac{1}{2}\cos\theta + \frac{1}{2}\frac{\Delta_1}{\Omega_2}\sin\theta^2\cos\theta^2\right)\Psi_5(\infty)\,,\\
\\
\Psi_5(t_0\to\infty) &= -\gamma_{13}\exp(-i\omega_{31}t_0)\left(\frac{1}{2}\cos\theta - \frac{1}{2}\frac{\Delta_1}{\Omega_2}\sin\theta^3\cos\theta\right)\Psi_5(\infty)\,,\\
\Psi_6(t_0\to\infty) &= \gamma_{13}\exp(-i\omega_{31}t_0)\frac{1}{\sqrt{2}}\frac{\Delta_1}{\Omega_2}\sin\theta^2\cos\theta^2\Psi_4(\infty)\,,\\
\Psi_7(t_0\to\infty) &= \gamma_{13}\exp(-i\omega_{31}t_0)\left(\frac{1}{\sqrt{2}}\sin\theta + \frac{1}{\sqrt{32}}\frac{\Delta_1}{\Omega_2}\sin\theta^2\cos\theta^2\right)(1-\Psi_4(\infty)-\Psi_5(\infty))\,,\\
\Psi_8(t_0\to\infty) &= -\gamma_{13}\exp(-i\omega_{31}t_0)\left(\frac{1}{2}\cos\theta + \frac{1}{4}\frac{\Delta_1}{\Omega_2}\sin\theta\cos\theta(1+\sin\theta^2)\right)\Psi_5(\infty)\,,
\end{aligned}$$

in the first order of $1/\Omega_R$. Now one can write the correlation function as

$$\begin{aligned}
&\langle\hat{P}^{(-)}(z)P^{(+)}(\infty)\rangle = \tfrac{\gamma_{13}^2}{32z_1}[16(I_{\infty4}M_{44}+I_{\infty5}M_{45}-I_{\infty4}M_{54}-I_{\infty5}M_{55})\cos\theta \qquad (2.309)\\
+\;& 8z(M_{44}\Psi_4(\infty)-M_{54}\Psi_4(\infty)+M_{88}\Psi_4(\infty)+M_{11}\Psi_5(\infty)-M_{45}\Psi_5(\infty)+M_{55}\Psi_5(\infty))\cos\theta^2\\
-\;& 16(M_{22}+M_{77})z_1(-1+\Psi_4(\infty)+\Psi_5(\infty))\sin\theta^2] + \tfrac{\gamma_{13}^2}{32z_1}\{-8M_{54}z_1\Psi_4(\infty)\cos\theta^3\sin\theta^2\\
-\;& 8M_{11}z_1\Psi_5(\infty)\cos\theta^3\sin\theta^2 + 32[-1+I_{\infty4}(M_{44}+M_{54})+I_{\infty5}(M_{45}+M_{55})]\cos\theta\sin\theta^3\\
+\;& 4\cos\theta^2[M_{88}z_1\Psi_4(\infty)\sin\theta - M_{11}z_1\Psi_5(\infty)\sin\theta - z_1(M_{22}+(M_{11}+2M_{45})\Psi_5(\infty)\\
+\;& 2M_{77}(-1+\Psi_4(\infty)+\Psi_5(\infty)))\sin\theta^3 + (8I_{\infty4}M_{44}+8I_{\infty5}M_{45}+M_{22}z_1(-1+\Psi_4(\infty)\\
+\;& \Psi_5(\infty)))\sin\theta^4] + (-4I_{\infty4}M_{54}-4I_{\infty5}M_{55}+2M_{44}z_1\Psi_4(\infty)-2M_{54}z_1\Psi_4(\infty)\\
+\;& 2M_{55}z_1\Psi_5(\infty)\cos\theta)\sin2\theta^2 + z_1\sin\theta\sin2\theta^2[4M_{67}+M_{22}\Psi_4(\infty)+4M_{44}\Psi_4(\infty)+4M_{54}\Psi_4(\infty)\\
-\;& 4M_{67}\Psi_4(\infty)+4M_{76}\Psi_4(\infty)+M_{88}\Psi_4(\infty)+M_{22}\Psi_5(\infty)-4M_{23}\Psi_5(\infty)-6M_{55}\Psi_5(\infty)\\
-\;& 4M_{67}\Psi_5(\infty)+4M_{32}(-1+\Psi_4(\infty)+\Psi_5(\infty))+2(M_{44}\Psi_4(\infty)-M_{88}\Psi_4(\infty)\\
-\;& M_{45}\Psi_5(\infty))\sin2\theta]\}\frac{\Delta_1}{\Omega_2} + \mathscr{O}(\Delta_1)^2
\end{aligned}$$

When the detuning Δ_1 is zero, we get the well-known expression [61]

$$\begin{aligned}
\langle\hat{P}^{(-)}(z)P^{(+)}(\infty)\rangle = \tfrac{\gamma_{13}^2}{4}\cos^2\theta\Psi_\infty(M_{11}^0+M_{44}^0-M_{54}^0+M_{55}^0+M_{88}^0) \qquad (2.310)\\
+\tfrac{\gamma_{13}^2}{4}\sin^2\theta(1-2\Psi_\infty)(M_{22}^0+M_{77}^0)\,.
\end{aligned}$$

In order to calculate the matrix elements M_{ij}^0, one uses the formula

$$\begin{pmatrix} a & b\\ b & a\end{pmatrix}^{-1} \to \frac{1}{a^2-b^2}\begin{pmatrix} a & -b\\ -b & a\end{pmatrix}\,. \tag{2.311}$$

It is easy to put equation (2.310) in the form [61]

$$\langle \hat{P}^{(-)}(z)\hat{P}^{(+)}(\infty)\rangle = \tfrac{\gamma_{13}^2}{4}\cos^2\theta\Psi_\infty\left(\frac{1}{z_1-\gamma_1+2i\Omega_R}+\frac{2}{z_1-\gamma_4+\gamma_5}+\frac{1}{z_1-\gamma_1-2i\Omega_R}\right)$$
$$+\tfrac{\gamma_{13}^2}{2}\sin^2\theta(1-2\Psi_\infty)\left(\frac{z_1-\gamma_2+i\Omega_R}{(z_1-\gamma_2+i\Omega_R)^2-\gamma_3^2}+\frac{z_1-\gamma_2-i\Omega_R}{(z_1-\gamma_2-i\Omega_R)^2-\gamma_3^2}\right), \tag{2.312}$$

and the emission spectrum will then be given by [61]

$$S(\omega) = Re\langle \hat{P}^{(-)}(z)\hat{P}^{(+)}(\infty)\rangle|_{z=i(\omega-\omega_{31})}\,. \tag{2.313}$$

We list the set of constants that are needed to discuss this result [61]:

$$\begin{aligned}
&\Gamma_{stst} = \Gamma_{tsts} = \gamma_1\,, \\
&\Gamma_{srsr} = \Gamma_{rtrt} = \Gamma_{rsrs} = \Gamma_{trtr} = \gamma_2\,, \\
&\Gamma_{srrt} = \Gamma_{rtsr} = \Gamma_{rstr} = \Gamma_{trrs} = \gamma_3\,, \\
&\Gamma_{ssss} - \Gamma_{ssrr} = \Gamma_{tttt} - \Gamma_{ttrr} = \gamma_4\,, \\
&\Gamma_{sstt} - \Gamma_{ssrr} = \Gamma_{ttss} - \Gamma_{ttrr} = \gamma_5\,,
\end{aligned} \tag{2.314}$$

with the γ-s given as

$$\begin{aligned}
\gamma_1 &= -\Gamma_{32}\tfrac{1}{4}\cos^2\theta(1+\cos^2\theta) - \Gamma_{31}\tfrac{3}{4}\cos^2\theta - \Gamma_{21}\tfrac{3}{4}\sin^2\theta\,, \\
\gamma_2 &= -\Gamma_{32}\tfrac{1}{4}[1+\sin^2\theta(1+2\cos^2\theta)] - \Gamma_{31}\tfrac{1}{4}(1+\sin^2\theta) - \Gamma_{21}\tfrac{1}{4}(1+\cos^2\theta)\,, \\
\gamma_3 &= -\Gamma_{32}\tfrac{1}{2}\sin^2\theta\cos^2\theta\,, \\
\gamma_4 &= -\Gamma_{32}(\tfrac{1}{4}\cos^2\theta+\tfrac{1}{4}\cos^4\theta+\tfrac{1}{2}\sin^4\theta) - \Gamma_{31}\tfrac{1}{4}(1+\sin^2\theta) - \Gamma_{21}\tfrac{1}{4}(1+\cos^2\theta)\,, \\
\gamma_5 &= \Gamma_{32}\tfrac{1}{2}\sin^2\theta(\tfrac{1}{2}\cos^2\theta-\sin^2\theta) + \Gamma_{31}(\tfrac{1}{4}\cos^2\theta-\tfrac{1}{2}\sin^2\theta) + \Gamma_{21}(\tfrac{1}{4}\sin^2\theta-\tfrac{1}{2}\cos^2\theta)\,.
\end{aligned} \tag{2.315}$$

The peak heights of the central component and of the outer sidebands can be calculated using the formula [61]

$$P(0) = \tfrac{\gamma_{13}^2}{4}\cos^2\theta\frac{2}{\gamma_5-\gamma_4}\Psi_\infty\,, \quad P(\pm\Omega_R) = \tfrac{\gamma_{13}^2}{2}\sin^2\theta(1-2\Psi_\infty)\frac{|\gamma_2|}{|\gamma_2^2-\gamma_3^2|}\,, \tag{2.316}$$
$$P(\pm 2\Omega_R) = \tfrac{\gamma_{13}^2}{4}\cos^2\theta\frac{1}{|\gamma_1|}\Psi_\infty\,.$$

The full widths of the spectral features are given in an analytic representation by [61]

$$\begin{aligned}
\Delta\omega(0) &= 2(\gamma_5-\gamma_4) = \Gamma_{32}\cos^2\theta + \Gamma_{31}\cos^2\theta + \Gamma_{21}\sin^2\theta\,, \\
\Delta\omega(\pm\Omega_R) &= 2\{[4\gamma_3^4+(\gamma_2^2-\gamma_3^2)]^{1/2} - 2\gamma_3^2\}^{1/2}\,, \\
\Delta\omega(\pm 2\Omega_R) &= 2|\gamma_1| = \Gamma_{32}\tfrac{1}{2}\cos^2\theta(1+\cos^2\theta) + \Gamma_{31}\tfrac{3}{2}\cos^2\theta + \Gamma_{21}\tfrac{3}{2}\sin^2\theta\,.
\end{aligned} \tag{2.317}$$

Now, we consider only the emission process for the $2 \to 1$ transition so that

$$P^{(+)} = \gamma_{12}|1\rangle\langle 2|\,, \quad P^{(-)} = \gamma_{12}|2\rangle\langle 1|\,. \tag{2.318}$$

The single-time average is

$$\langle P^{(-)}(t_1)\rangle = \gamma_{12}Tr[\rho'(t_1)|2\rangle\langle 1|]\exp(i\omega_{21}t_1)\,. \tag{2.319}$$

Using the relations

$$\begin{aligned} |2\rangle\langle 1|r\rangle &= 0\,, \\ |2\rangle\langle 1|s\rangle &= \frac{1}{2}\sin\theta(|s\rangle+|t\rangle)+\frac{1}{\sqrt{2}}\cos\theta|r\rangle\,, \\ |2\rangle\langle 1|t\rangle &= -\frac{1}{2}\sin\theta(|s\rangle+|t\rangle)-\frac{1}{\sqrt{2}}\cos\theta|r\rangle\,, \end{aligned} \tag{2.320}$$

the power spectrum becomes

$$\begin{aligned} \langle P^{(-)}(z)\rangle &= \frac{\gamma_{12}}{2}\sin\theta(\hat{\Psi}_4(z_2)+\hat{\Psi}_1(z_2)-\hat{\Psi}_8(z_2)-\hat{\Psi}_5(z_2)) \\ &+\frac{\gamma_{12}}{\sqrt{2}}\cos\theta(\hat{\Psi}_2(z_2)-\hat{\Psi}_7(z_2))\,, \end{aligned} \tag{2.321}$$

where $z_2 = z - i\omega_{21}$. The regression theorem yields

$$\begin{aligned} \Psi_1(t_0) &\rightarrow \gamma_{12}\exp(-i\omega_{21}t_0)\left(\tfrac{1}{2}\sin\theta(\rho'_{st}+\rho'_{tt})-\frac{1}{\sqrt{2}}\cos\theta\rho'_{rt}\right)\,, \\ \Psi_2(t_0) &\rightarrow \gamma_{12}\exp(-i\omega_{21}t_0)\left(\tfrac{1}{2}\sin\theta(\rho'_{sr}+\rho'_{tr})+\frac{1}{\sqrt{2}}\cos\theta\rho'_{rr}\right)\,, \\ \Psi_3(t_0) &\rightarrow 0\,, \\ \Psi_4(t_0) &\rightarrow \gamma_{12}\exp(-i\omega_{21}t_0)\left(\tfrac{1}{2}\sin\theta(\rho'_{ss}+\rho'_{ts})+\frac{1}{\sqrt{2}}\cos\theta\rho'_{rs}\right)\,, \\ \Psi_5(t_0) &\rightarrow -\gamma_{12}\exp(-i\omega_{21}t_0)\left(\tfrac{1}{2}\sin\theta(\rho'_{st}+\rho'_{tt})+\frac{1}{\sqrt{2}}\cos\theta\rho'_{rt}\right)\,, \\ \Psi_6(t_0) &\rightarrow 0\,, \\ \Psi_7(t_0) &\rightarrow -\gamma_{12}\exp(-i\omega_{21}t_0)\left(\tfrac{1}{2}\sin\theta(\rho'_{sr}+\rho'_{tr})+\frac{1}{\sqrt{2}}\cos\theta\rho'_{rr}\right)\,, \\ \Psi_8(t_0) &\rightarrow -\gamma_{12}\exp(-i\omega_{21}t_0)\left(\tfrac{1}{2}\sin\theta(\rho'_{ss}+\rho'_{ts})+\frac{1}{\sqrt{2}}\cos\theta\rho'_{rs}\right)\,. \end{aligned} \tag{2.322}$$

In the stationary limit, the off-diagonal elements of $\rho'_{\mu\nu}$ vanish and the only nonzero elements are

$$\rho'_{ss} = \rho'_{tt} = \Psi_\infty\,. \tag{2.323}$$

One may write Eqs. (2.322) as

$$\begin{aligned} \Psi_1(t_0\rightarrow\infty) &= \gamma_{12}\exp(-i\omega_{21}t_0)\tfrac{1}{2}\sin\theta\rho'_{tt}+\mathscr{O}(1/\Omega_R)\,, \\ \Psi_2(t_0\rightarrow\infty) &= \gamma_{12}\exp(-i\omega_{21}t_0)\tfrac{1}{\sqrt{2}}\cos\theta\rho'_{rr}+\mathscr{O}(1/\Omega_R)\,, \\ \Psi_4(t_0\rightarrow\infty) &= \gamma_{12}\exp(-i\omega_{21}t_0)\tfrac{1}{2}\sin\theta\rho'_{ss}+\mathscr{O}(1/\Omega_R)\,, \\ \Psi_5(t_0\rightarrow\infty) &= \gamma_{12}\exp(-i\omega_{21}t_0)\tfrac{1}{2}\sin\theta\rho'_{tt}+\mathscr{O}(1/\Omega_R)\,, \\ \Psi_7(t_0\rightarrow\infty) &= -\gamma_{12}\exp(-i\omega_{21}t_0)\tfrac{1}{\sqrt{2}}\cos\theta\rho'_{rr}+\mathscr{O}(1/\Omega_R)\,, \\ \Psi_8(t_0\rightarrow\infty) &= -\gamma_{12}\exp(-i\omega_{21}t_0)\tfrac{1}{2}\sin\theta\rho'_{ss}+\mathscr{O}(1/\Omega_R)\,. \end{aligned} \tag{2.324}$$

As a result, one obtains the correlation function [61]

$$\begin{aligned} \langle\hat{P}^{(-)}(z)\hat{P}^{(+)}(\infty)\rangle &= \tfrac{\gamma_{12}^2}{4}\sin^2\theta\Psi_\infty(M^0_{11}+M^0_{44}-M^0_{54}-M^0_{45}+M^0_{55}+M^0_{88}) \\ &+ \tfrac{\gamma_{12}^2}{4}\cos^2\theta(1-2\Psi_\infty)(M^0_{22}+M^0_{77})\,. \end{aligned} \tag{2.325}$$

The final form of Eq. (2.325) is [61]

$$\langle \hat{P}^{(-)}(z)\hat{P}^{(+)}(\infty)\rangle = \tfrac{\gamma_{12}^2}{4}\sin^2\theta\Psi_\infty\left(\frac{1}{z_2-\gamma_1+2i\Omega_R}+\frac{2}{z_2-\gamma_4+\gamma_5}+\frac{1}{z_2-\gamma_1-2i\Omega_R}\right)$$
$$+\tfrac{\gamma_{12}^2}{2}\cos^2\theta(1-2\Psi_\infty)\left(\frac{z_2-\gamma_2+i\Omega_R}{(z_2-\gamma_2+i\Omega_R)^2-\gamma_3^2}+\frac{z_2-\gamma_2-i\Omega_R}{(z_2-\gamma_2-i\Omega_R)^2-\gamma_3^2}\right). \quad (2.326)$$

By definition, the emission spectrum is [61]

$$S(\omega) = Re\langle \hat{P}^{(-)}(z)\hat{P}^{(+)}(\infty)\rangle|_{z=i(\omega-\omega_{21})}. \quad (2.327)$$

The formula for the peak heights are given by [61]

$$P(0) = \tfrac{\gamma_{12}^2}{4}\sin^2\theta\frac{2}{\gamma_5-\gamma_4}\Psi_\infty, \quad P(\pm\Omega_R) = \tfrac{\gamma_{12}^2}{2}\cos^2\theta(1-2\Psi_\infty)\frac{|\gamma_2|}{|\gamma_2^2-\gamma_3^2|}, \quad (2.328)$$
$$P(\pm 2\Omega_R) = \tfrac{\gamma_{12}^2}{4}\sin^2\theta\frac{1}{|\gamma_1|}\Psi_\infty,$$

and the widths of the spectral features are as follows:

$$\begin{aligned}\Delta\omega(0) &= 2(\gamma_5-\gamma_4) = \Gamma_{32}\cos^2\theta+\Gamma_{31}\cos^2\theta+\Gamma_{21}\sin^2\theta, \quad (2.329)\\ \Delta\omega(\pm\Omega_R) &= 2\{[4\gamma_3^4+(\gamma_2^2-\gamma_3^2)]^{1/2}-2\gamma_3^2\}^{1/2},\\ \Delta\omega(\pm 2\Omega_R) &= 2|\gamma_1| = \Gamma_{32}\tfrac{1}{2}\cos^2\theta(1+\cos^2\theta)+\Gamma_{31}\tfrac{3}{2}\cos^2\theta+\Gamma_{21}\tfrac{3}{2}\sin^2\theta.\end{aligned}$$

In the following, for completeness, we consider the Λ model (see Fig. 2.8 b)). The correlation function for $3\to 1$ transition is [56]

$$\begin{aligned}\hat{\Gamma}_{\Lambda 1}^{\rm incoh}(z) &= \tfrac{\gamma_{13}^2}{4}\cos^2\theta\Psi_\infty\left(\frac{1}{z_1-\gamma_1+2i\Omega_R}+\frac{2}{z_1-\gamma_4+\gamma_5}+\frac{1}{z_1-\gamma_1-2i\Omega_R}\right) \quad (2.330)\\ &+ \tfrac{\gamma_{13}^2}{2}\sin^2\theta\Psi_\infty\left(\frac{z_1-\gamma_2+i\Omega_R}{(z_1-\gamma_2+i\Omega_R)^2-\gamma_3^2}+\frac{z_1-\gamma_2-i\Omega_R}{(z_1-\gamma_2-i\Omega_R)^2-\gamma_3^2}\right),\end{aligned}$$

and for the $3\to 2$ transition it is

$$\begin{aligned}\hat{\Gamma}_{\Lambda 2}^{\rm incoh}(z) &= \tfrac{\gamma_{12}^2}{4}\cos^2\theta\Psi_\infty\left(\frac{1}{z_2-\gamma_1+2i\Omega_R}+\frac{2}{z_2-\gamma_4+\gamma_5}+\frac{1}{z_2-\gamma_1-2i\Omega_R}\right) \quad (2.331)\\ &+ \tfrac{\gamma_{12}^2}{2}\sin^2\theta\Psi_\infty\left(\frac{z_2-\gamma_2+i\Omega_R}{(z_2-\gamma_2+i\Omega_R)^2-\gamma_3^2}+\frac{z_2-\gamma_2-i\Omega_R}{(z_2-\gamma_2-i\Omega_R)^2-\gamma_3^2}\right),\end{aligned}$$

with

$$\Psi_\infty = \frac{\Gamma_{21}\cos^4\theta}{\Gamma_{21}(\sin^4\theta+2\cos^4\theta)+\Gamma_{32}\cos^2\theta+\Gamma_{31}\sin^2\theta}, \quad (2.332)$$

and with the expressions

$$\begin{aligned}\gamma_1 &= -\tfrac{1}{4}[\Gamma_{21}\sin^2\theta(1+\sin^2\theta)+\Gamma_{32}(2+\sin^2\theta)+\Gamma_{31}(2+\cos^2\theta)], \quad (2.333)\\ \gamma_2 &= -\tfrac{1}{4}\{\Gamma_{21}[1+\cos^2\theta(1+2\sin^2\theta)]+\Gamma_{32}+\Gamma_{31}\},\\ \gamma_3 &= -\tfrac{1}{2}\Gamma_{21}\cos^2\theta\sin^2\theta,\\ \gamma_4 &= -\tfrac{1}{4}\{\Gamma_{21}[\sin^2\theta(1+\sin^2\theta)+2\cos^2\theta]+\Gamma_{32}(1+\cos^2\theta)+\Gamma_{31}(1+\sin^2\theta)\},\\ \gamma_5 &= \tfrac{1}{4}[\Gamma_{21}(\cos^2\theta\sin^2\theta-2\cos^4\theta)+\Gamma_{32}\sin^2\theta+\Gamma_{31}\cos^2\theta].\end{aligned}$$

The full widths at half maximum of the spectral features are given analytically by [56]

$$\begin{aligned} \Delta\omega(0) &= 2|\gamma_5-\gamma_4| = \Gamma_{21}\sin^2\theta+\Gamma_{32}+\Gamma_{31}\,, \\ \Delta\omega(\pm\Omega_R) &= 2\{-2\gamma_3^2+[4\gamma_3^4+(\gamma_2^2-\gamma_3^2)^2]^{1/2}\}^{1/2}\,, \\ \Delta\omega(\pm 2\Omega_R) &= 2|\gamma_1|\,. \end{aligned} \tag{2.334}$$

The peak heights of the central component and the outer sidebands may be calculated using the formula [56]

$$\begin{aligned} &P(0) = \tfrac{\gamma_{13}^2}{4}\cos^2\theta\frac{2}{|\gamma_5-\gamma_4|}\Psi_\infty\,, \quad P(\pm\Omega_R) = \tfrac{\gamma_{13}^2}{2}\sin^2\theta\left|\frac{\gamma_2}{\gamma_2^2-\gamma_3^2}\right|\Psi_\infty\,, \\ &P(\pm 2\Omega_R) = \tfrac{\gamma_{13}^2}{4}\cos^2\theta\frac{1}{|\gamma_1|}\Psi_\infty\,. \end{aligned} \tag{2.335}$$

In order to get the formulas for the spectrum $3\rightarrow 2$, one should replace $\sin\theta$ with $\cos\theta$, and γ_{13} with γ_{12}.

For the Ξ model (see Fig. 2.8 c)), the final result for the correlation function is [56]

$$\begin{aligned} \hat{\Gamma}_{\Xi 1}^{\rm incoh}(z) &= \tfrac{\gamma_{13}^2}{4}\cos^2\theta\Psi_\infty\left(\frac{1}{z_1-\gamma_1+2i\Omega_R}+\frac{2}{z_1-\gamma_4+\gamma_5}+\frac{1}{z_1-\gamma_1-2i\Omega_R}\right) \\ &+ \tfrac{\gamma_{13}^2}{2}\sin^2\theta\Psi_\infty\left(\frac{z_1-\gamma_2-i\Omega_R}{(z_1-\gamma_2-i\Omega_R)^2-\gamma_3^2}+\frac{z_1-\gamma_2+i\Omega_R}{(z_1-\gamma_2+i\Omega_R)^2-\gamma_3^2}\right)\,. \end{aligned} \tag{2.336}$$

Now, we consider the emission process for the $3\rightarrow 2$ transition so that [56]

$$\begin{aligned} \hat{\Gamma}_{\Xi 2}^{\rm incoh}(z) &= \tfrac{\gamma_{12}^2}{4}\sin^2\theta\Psi_\infty\left(\frac{1}{z_2-\gamma_1+2i\Omega_R}+\frac{2}{z_2-\gamma_4+\gamma_5}+\frac{1}{z_2-\gamma_1-2i\Omega_R}\right) \\ &+ \tfrac{\gamma_{12}^2}{2}\cos^2\theta(1-2\Psi_\infty)\left(\frac{z_2-\gamma_2-i\Omega_R}{(z_2-\gamma_2-i\Omega_R)^2-\gamma_3^2}+\frac{z_2-\gamma_2+i\Omega_R}{(z_2-\gamma_2+i\Omega_R)^2-\gamma_3^2}\right)\,, \end{aligned} \tag{2.337}$$

with

$$\Psi_\infty = \frac{\frac{1}{2}(\Gamma_{31}\cos^4\theta+\Gamma_{32}\cos^2\theta)}{\Gamma_{31}(\frac{1}{2}\sin^4\theta+\cos^4\theta)+\frac{1}{2}\Gamma_{21}\sin^2\theta+\Gamma_{32}\cos^2\theta}\,, \tag{2.338}$$

and with

$$\begin{aligned} \gamma_1 &= -\tfrac{1}{4}[\Gamma_{31}\sin^2\theta(1+\sin^2\theta)+3\Gamma_{32}\sin^2\theta+\Gamma_{21}(2+\cos^2\theta)]\,, \\ \gamma_2 &= -\tfrac{1}{4}\{\Gamma_{31}[1+\cos^2\theta(1+2\sin^2\theta)]+\Gamma_{32}(1+\cos^2\theta)+\Gamma_{21}\}\,, \\ \gamma_3 &= -\tfrac{1}{2}\Gamma_{31}\cos^2\theta\sin^2\theta\,, \\ \gamma_4 &= -\tfrac{1}{4}[\Gamma_{31}(\sin^2\theta+\sin^4\theta+2\cos^4\theta)+\Gamma_{32}(1+\cos^2\theta)+\Gamma_{21}(1+\sin^2\theta)]\,, \\ \gamma_5 &= \tfrac{1}{4}[\Gamma_{31}\cos^2\theta(\sin^2\theta-2\cos^2\theta)+\Gamma_{32}(\sin^2\theta-2\cos^2\theta)+\Gamma_{21}\cos^2\theta]\,. \end{aligned} \tag{2.339}$$

The full widths at half maximum of the spectral features are the given by [56]

$$\begin{aligned} \Delta\omega(0) &= \Gamma_{31}\sin^2\theta+\Gamma_{32}\sin^2\theta+\Gamma_{21}\,, \\ \Delta\omega(\pm\Omega_R) &= 2\{-2\gamma_3^2+[4\gamma_3^4+(\gamma_2^2-\gamma_3^2)^2]^{1/2}\}^{1/2}\,, \\ \Delta\omega(\pm 2\Omega_R) &= \tfrac{1}{2}[\Gamma_{31}\sin^2\theta(1+\sin^2\theta)+3\Gamma_{32}\sin^2\theta+\Gamma_{21}(2+\cos^2\theta)]\,. \end{aligned} \tag{2.340}$$

The peak heights of the central component and of the outer sidebands are given by the formulas [56]

$$P_{21}(0) = \tfrac{\gamma_{13}^2}{4}\cos^2\theta\frac{2}{|\gamma_5-\gamma_4|}\Psi_\infty\,, \quad P_{21}(\pm\Omega_R) = \tfrac{\gamma_{13}^2}{2}\sin^2\theta\left|\frac{\gamma_2}{\gamma_2^2-\gamma_3^2}\right|\Psi_\infty\,, \tag{2.341}$$
$$P_{21}(\pm 2\Omega_R) = \tfrac{\gamma_{13}^2}{4}\cos^2\theta\frac{1}{|\gamma_1|}\Psi_\infty\,, \quad P_{32}(0) = \tfrac{\gamma_{12}^2}{4}\sin^2\theta\frac{2}{|\gamma_5-\gamma_4|}\Psi_\infty\,,$$
$$P_{32}(\pm\Omega_R) = \tfrac{\gamma_{12}^2}{2}\cos^2\theta(1-2\Psi_\infty)\left|\frac{\gamma_2}{\gamma_2^2-\gamma_3^2}\right|\,, \quad P_{32}(\pm 2\Omega_R) = \tfrac{\gamma_{12}^2}{4}\sin^2\theta\frac{1}{|\gamma_1|}\Psi_\infty\,.$$

2.7 Total fluorescence and steady-state population

Now, we calculate the total fluorescence of transition $1-3$ which is defined, following Ref. [49], as

$$I_{13} = \int_{-\infty}^{\infty} d\omega S(\omega)\,. \tag{2.342}$$

From Eq. (2.312) and (2.313) we obtain

$$I_{13} = \frac{\gamma_{13}^2}{4}\cos^2\theta\Psi_\infty(\pi+2\pi+\pi) + \frac{\gamma_{13}}{2}\sin^2\theta(1-2\Psi_\infty)(\pi+\pi)\,, \tag{2.343}$$

or, by using the expression (2.286) for the Ψ_∞, one may gets the following:

$$I_{13} = \frac{\gamma_{13^2}\pi}{2}\cos^2\frac{\Gamma_{32}\sin^2\theta+\Gamma_{31}\sin^2\theta+\Gamma_{21}\cos^2\theta}{\Gamma_{32}(\frac{1}{2}\cos^4\theta+\sin^4\theta)+\Gamma_{31}\sin^2\theta+\Gamma_{21}\cos^2\theta}\,. \tag{2.344}$$

In the case of the $1-2$ transition, starting with the formulas (2.326) and (2.327), and using the same procedure, we get

$$I_{12} = \frac{\gamma_{12}^2\pi}{2}\frac{\Gamma_{32}(\sin^6\theta+\cos^6\theta)+\Gamma_{31}\sin^4\theta+\Gamma_{21}\sin^2\theta\cos^2\theta}{\Gamma_{32}(\frac{1}{2}\cos^4\theta+\sin^4\theta)+\Gamma_{31}\sin^2\theta+\Gamma_{21}\cos^2\theta}\,. \tag{2.345}$$

Applying Eq. (2.283) and (2.275) it is easy to see that

$$\frac{I_{13}}{\rho_{33}} = \pi\gamma_{13}^2\,, \quad \frac{I_{12}}{\rho_{22}} = \pi\gamma_{12}^2\,. \tag{2.346}$$

2.8 High-precision metrology of highly charged ions via relativistic resonance fluorescence

As an application of our relativistic formalism for describing resonance fluorescence in a three-level setting, we describe line narrowing phenomena obsevable in highly charged ions and its application for the accurate metrology of properties of highly charged ions.

In Fig. 2.9 (a) we plot the power spectrum of resonance fluorescence for the case of the $2s\leftrightarrow 2p_{3/2}$ electric dipole transition in Li-like ^{209}Bi (Z=83) ions. The dynamic (AC) Stark shift leads to a splitting of the central peak, giving rise to a Mollow spectrum. Due to the long lifetime of the upper level of the hyperfine-split ground state, level 2, almost 100 % of the population is trapped in this level if only the $3\leftrightarrow 1$ transition is driven coherently with an x-ray laser. The calculation yields for the population of the uppermost state a value of approx. $\Gamma_{21}/(\Gamma_{32}+2\Gamma_{21}) \approx 10^{-12} \ll 1$, resulting in a negligibly small total

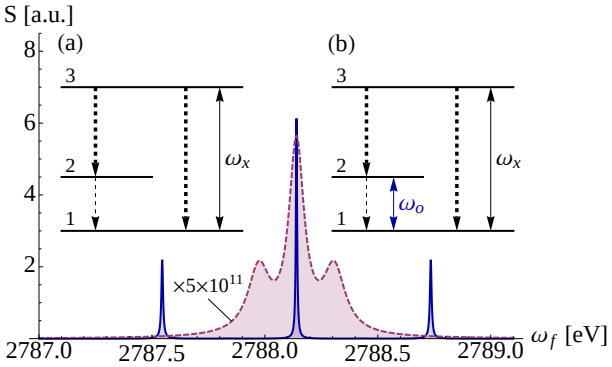

Figure 2.9: Fluorescence photon spectrum for the $2s \leftrightarrow 2p_{3/2}$ transition in Li-like ^{209}Bi as a function of the fluorescence photon frequency ω_f. (a) Dashed (red) curve: An x-ray laser ($I_x = 5 \times 10^{11}$ W/cm^2) is in resonance with the ionic electric dipole (E1) transition at $\omega_x = 2788.1$ eV between the hyperfine-split ground state 1 ($2s$ with $F = 4$, $M_F = 4$) and the uppermost state 3 ($2p_{3/2}$ with $F = 5$, $M_F = 5$). This curve is multiplied by a factor of 5×10^{11}. Thick (thin) dashed arrows represent fast E1 x-ray (slow M1 optical) decays. (b) Continuous (blue) curve: an additional optical driving ($I_o = 10^{14}$ W/cm^2) is applied on the $\omega_o = 0.797$ eV [76] M1 transition between the hyperfine-split magnetic sublevels 1 ($F = 4$, $M_F = 4$) and 2 ($F = 5$, $M_F = 5$). The inner sidebands are suppressed. See text for more details.

x-ray fluorescence [1]. This undesirable effect may be reversed if additionally the $2 \leftrightarrow 1$ optical transition is coherently driven (see Fig. 2.9), leading to an efficient re-population of level 3.

Furthermore, the spectral lines become substantially narrower due to coherence and interference effects (see [61] for the pioneering non-specific treatment). The width of the central peak and the outer sidebands are given, following our derivations in the previous sections, by $\Gamma_C = (\Gamma_{31} + \Gamma_{32} + \gamma_D)R + \Gamma_{21}(1 - R)$ and $\Gamma_{SB} = |\frac{3}{2}(\Gamma_{31} - \frac{1}{3}\gamma_D)R + \frac{1}{2}\Gamma_{32}(R + R^2) + \frac{3}{2}\Gamma_{21}(1 - R)|$, respectively, with the ratio R being $g_{31}^2/(g_{31}^2 + g_{21}^2)$. This effect is shown in Fig. 2.9 (b). Further increasing the intensity of the long-wavelength driving field and thus g_{21} could even assign the narrow linewidth of $7.7 \cdot 10^{-15}$ eV of the M1 hyperfine transition to the E1 x-ray transition of interest. The above line width formulas also imply that the dephasing width γ_D – typically on the order of 0.1 eV for XFELs [1] – does not hamper the observation of sub-natural linewidths in the x-ray regime as their contribution scales with the same factor R.

Transition lifetimes – and related quantities like the atomic dipole or multipole moments – are of great interest for astrophysical applications and for testing fundamental theories. Measurements of these quantities are particularly necessary since they are especially sensitive to the long-range behavior of atomic wave functions. Currently, even the best measurements do not exceed the 10^{-3} level of accuracy [53]. In our scheme, the narrowed central and outer lines enable in principle an even more accurate determination of the atomic Rabi frequencies: the outer sideband peaks' distance is given by $D_s(0) = 4G = 4\sqrt{g_{31}^2 + g_{21}^2}$ (in the secular limit and when the x-ray laser is on resonance, i.e. its detuning $\Delta = \omega_x - \omega_{31}$ from the transition frequency is 0). In this formula, the optical Rabi frequency g_{21} is usually known, therefore, determining its counterpart g_{31} for the x-ray transition is only limited by the accuracy of measuring the peak distance D. Fig. 2.10 (b) shows the ratio of the width of the narrowed outer lines to their distance $D_s(0)$. As shown, this ratio, characterizing the relative accuracy for the determination of atomic multipole moments, can be improved by several orders of magnitude for

[1] Our current discussion is valid in the secular limit $G = \sqrt{g_{31}^2 + g_{21}^2} \gg \max\{\Gamma_{31}, \Gamma_{32}, \Gamma_{21}\}$. If the effective Rabi frequency G can not be rendered high enough for a sufficient applicability of this approximation, one has to work with the more accurate and lengthy expressions of the spectral features.

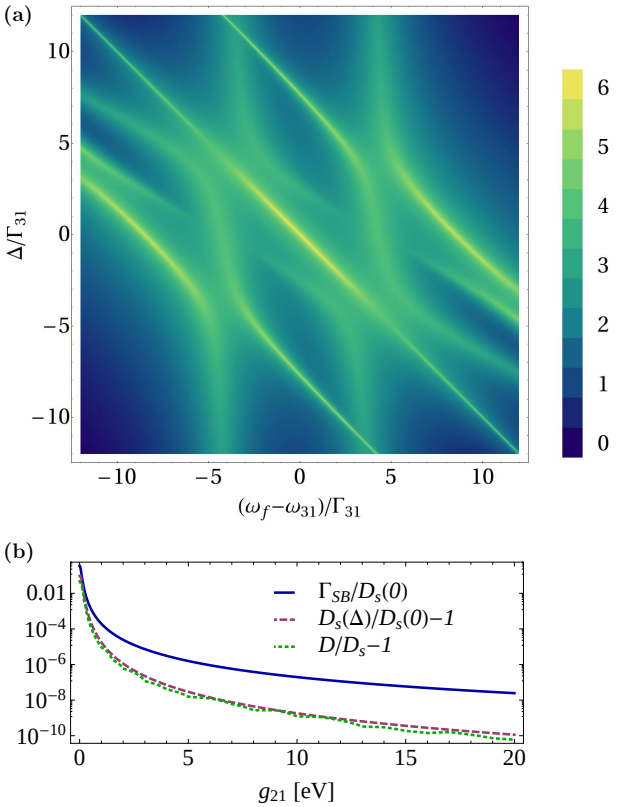

Figure 2.10: (a) Density plot of the fluorescence spectrum (logarithmic scale, arb. units) as a function of the fluorescence photon frequency ω_f with respect to the x-ray transition frequency ω_{31} (abscissa) and the laser detuning $\Delta = \omega_x - \omega_{31}$ (ordinate), with the frequencies normalized by the Γ_{31} rate. The parameters are for Bi as in Fig. 2.9. (b) Continuous (blue) curve: ratio of the interference-narrowed width Γ_{SB} of the outer sideband peaks to their distance $D_s(0) = 4G = 4\sqrt{g_{31}^2 + g_{21}^2}$ as a function of the optical Rabi frequency g_{21}, with further parameters for the Bi three-level system as given in the third line of Table 2.2. Dashed (red) curve: deviation of the sideband distance D_s, with $\Delta = \Gamma_{31}$. Dotted (green) curve: deviation of the exact sideband distance D from its value in the secular limit D_s.

higher optical laser intensities.

Our calculation shows that the detuning dependence of the outer sideband distance is given by $D_s(\Delta) = 4G + \frac{G}{2}\left(4R - 3R^2\right)(\Delta/G)^2 + \mathcal{O}\left((\Delta/G)^4\right)$. This weak dependence is also illustrated in Fig. 2.10 (a). Hence, the experimental sensitivity on the potentially inaccurately known detuning may be reduced by orders of magnitude by increasing the optical intensity (Rabi frequency), as also shown on Fig. 2.10 (b). The multipole matrix elements of the ionic transitions can thus be determined in principle to a high accuracy on the order of 10^{-4}–10^{-6}, once the intensity of the driving field is accurately known. Conversely, the intensity may be measured to high accuracy if the multipole moments are reliably known from an independent experiment (e.g. lifetime measurements). At the same time, knowing the Rabi frequencies, the dependence of sideband positions on the x-ray detuning could allow to measure in principle the ionic x-ray transition energy in an independent way. Table 2.2 lists values for some elements and atomic transitions.

Our above results have been demonstrated on the example of highly charged ions with non-vanishing nuclear spins, i.e. when hyperfine splitting of the electronic ground state occurs. However, certainly, the

Table 2.2: Parameters for $2s \leftrightarrow 2p_{3/2}$ transitions in the Li-like ions $^{203}Tl^{78+}$ (ω_{31}=2236.5 eV), $^{209}Bi^{80+}$ (2788.1 eV) and $^{235}U^{89+}$ (4459.4 eV). Optical transition energies (ω_{21}), natural line widths (Γ_{31}, Γ_{21}) and Rabi frequencies (g_{31}, g_{21}) as well as the interference-narrowed outer sideband width (Γ_{SB}) of the x-ray transition are given for the laser intensities I_x, I_o. $x(y)$ stands for $x \times 10^y$.

	ω_{21}	Γ_{31}	Γ_{SB}	Γ_{21}	g_{31}	g_{21}	I_x	I_o
			[meV]				[W/cm^2]	
Tl	499	6.6	7.1(-2)	1.1(-12)	1.8(2)	2.1(3)	1(12)	1(16)
			7.2(-4)		1.8(2)	2.1(4)	1(12)	1(18)
Bi	797	7.2(1)	9.7(-2)	7.7(-12)	8.3(1)	2.9(3)	5(11)	1(16)
			1.9(-1)		1.2(3)	2.9(4)	1(14)	1(18)
U	136	2.4(1)	3.7(-2)	3.7(-14)	7.7(1)	2.8(3)	5(11)	1(16)
			1.3		3.3(4)	1.9(5)	9(16)	5(19)

results may be applied to further three-level configurations. For example, such configurations may also be prepared by applying (strong) external magnetic fields, which gives rise to a large Zeeman splitting of the ground-state level, addressable by long-wavelength coherent radiation such as masers (or even CO_2 lasers). Furthermore, the results can be generalized to other physical systems with high transition energies, such as electromagnetic transitions in nuclei. In this setting, nuclear multipole moments and transition energies may in principle be determined by an independent method.

–III–

RELATIVISTIC LIGHT SHIFTS IN HYDROGENIC IONS

Energy shifts of atomic levels due to laser fields play an important role in high-precision laser spectroscopy. The dynamic Stark shift is one of the inherent systematic effects that shifts atomic energy levels in a laser spectroscopic experiment. In contrast to other shifting effects which may in principle be experimentally controllable, the dynamic Stark shift is due to the probing laser field itself and as such it cannot be eliminated. For this reason, it received considerable attention. The dynamic (AC) Stark shift is also present in laser-induced processes like ionization [7, 19, 50, 78]. Theoretical investigations so far apply nonrelativistic approaches and are restricted to electric dipole transitions.

In this Chapter we calculate light field shifts in a fully relativistic manner. This allows one to extend the field of investigations to stronger laser fields, higher frequencies – e.g., x-ray lasers [27] –, and to the highest nuclear charges.

3.1 Dynamic shift by means of perturbation theory

Let us consider the effect of adding the interaction Hamiltonian $V(\epsilon,t)$ to the sum of relativistic hydrogen-like ion H_0:

$$\begin{aligned} H &= H_0 + V(\epsilon,t)\,, \\ H_0 &= c\boldsymbol{\alpha}\boldsymbol{p} + \boldsymbol{\beta}m_0c^2 - \frac{Ze^2}{4\pi\epsilon_0 r}\,, \\ V(\epsilon,t) &= -\left(A_0\boldsymbol{\alpha}\hat{\epsilon}_\nu e^{i\boldsymbol{k}\boldsymbol{r}-i\omega t} + c.c.\right)e^{\epsilon t}\,. \end{aligned} \tag{3.1}$$

Here, ϵ is an infinitesimal damping parameter [68]. The introduction of an adiabatic damping parameter is a key element of time-dependent perturbation theory. In the interaction picture (denoted by the subscript I), the interaction V is represented by [14]:

$$V_I(\epsilon,t) = e^{\frac{i}{\hbar}H_0 t}V(\epsilon,t)e^{-\frac{i}{\hbar}H_0 t}\,. \tag{3.2}$$

We calculate the time evolution operator U_I up to second order in V_I from the Dyson series:

$$\begin{aligned} U_I &= \lim_{t\to\infty} U_I(\epsilon,t)\,, \\ U_I(\epsilon,t) &= 1 - \frac{i}{\hbar}\int_{-\infty}^{t} dt' V_I(\epsilon,t) + \\ &\quad \left(-\frac{i}{\hbar}\right)^2 \int_{-\infty}^{t} dt' \int_{-\infty}^{t'} dt'' V_I(\epsilon,t')V_I(\epsilon,t")\,. \end{aligned} \tag{3.3}$$

Let Φ_n represent an eigenfunction of the unperturbed Hamiltonian H_0 with an eigenvalue E_n. We denote the complete set of eigenstates of H_0 by $\{|\Phi_n\rangle\}$. $|\Phi_I(t)\rangle$ is a time-dependent atomic state in the interaction picture. The state function before interaction is an eigenstate of H_0: $|\Phi_I(t=-\infty)\rangle = |\Phi_a\rangle$, where Φ_a is an eigenstate of the unperturbed Hamiltonian H_0. Thus the state function at any time can be constructed by applying the evolution operator as

$$|\Phi_I(t)\rangle = U_I(\epsilon,t)|\Phi_I(t=-\infty)\rangle = \sum_n c_n(t)|\Phi_n\rangle\,. \tag{3.4}$$

This condition is also true for the degenerate case [14] without loss of generality. The time-dependent expansion coefficients $c_n(t)$ are given as the projections

$$c_n(t) = \langle\Phi_n|\Phi_I(t)\rangle\,. \tag{3.5}$$

For calculating the light shift of a given atomic state a, we are interested in the projection [68]

$$c_a(t) = \langle\Phi_a|\Phi_I(t)\rangle = \langle\Phi_a|U_I(\epsilon,t)|\Phi_a\rangle\,. \tag{3.6}$$

The first-order perturbation $\langle\Phi_a|V|\Phi_a\rangle$ vanishes. Substituting $U_I(\epsilon,t)$ from Eq. (3.3), the leading order of the perturbation expansion is V^2 and the problem reduces to calculating the matrix element

$$\begin{aligned} M = &\int_{-\infty}^{t} dt' \int_{-\infty}^{t'} dt''\langle\Phi_a|V_I(\epsilon,t')V_I(\epsilon,t'')|\Phi_a\rangle = \\ &\sum_n \int_{-\infty}^{t} dt' \int_{-\infty}^{t'} dt''\langle\Phi_a|V_I(\epsilon,t')|\Phi_n\rangle\langle\Phi_n|V_I(\epsilon,t'')|\Phi_a\rangle\,. \end{aligned} \tag{3.7}$$

The index n counts all bound and continuum states of the unperturbed hydrogen-like ion. After carrying out the time integration, the matrix element is given as

$$\begin{aligned} M = -\frac{\hbar}{i}\sum_n \Bigg(& A_0^2 \frac{\langle\Phi_a|V_1|\Phi_n\rangle\langle\Phi_n|V_1|\Phi_a\rangle e^{2t(\epsilon-i\omega)}}{2(\epsilon-i\omega)(E_a-E_n+\hbar\omega-i\hbar\epsilon)} \\ &+|A_0|^2 \frac{\langle\Phi_a|V_2|\Phi_n\rangle\langle\Phi_n|V_1|\Phi_a\rangle}{2\epsilon(E_a-E_n-\hbar\omega-i\hbar\epsilon)} e^{2\epsilon t} \\ &+|A_0|^2 \frac{\langle\Phi_a|V_1|\Phi_n\rangle\langle\Phi_n|V_2|\Phi_a\rangle}{2\epsilon(E_a-E_n+\hbar\omega-i\hbar\epsilon)} e^{2\epsilon t} \\ &+(A_0^*)^2 \frac{\langle\Phi_a|V_2|\Phi_n\rangle\langle\Phi_n|V_2|\Phi_a\rangle e^{2t(\epsilon+i\omega)}}{2(\epsilon+i\omega)(E_a-E_n-\hbar\omega-i\hbar\epsilon)} \Bigg)\,. \end{aligned} \tag{3.8}$$

For simplicity the notation $V_1 = -\boldsymbol{\alpha}\hat{\epsilon}_\nu e^{i\boldsymbol{kr}}$ and $V_2 = -\boldsymbol{\alpha}^*\hat{\epsilon}_\nu^* e^{-i\boldsymbol{kr}}$ is introduced above. In the second order of perturbation theory one can write

$$c_a(t) = -\frac{i}{\hbar}M'(t)\,, \tag{3.9}$$

with $M' = -\frac{i}{\hbar}M$. Neglecting higher-order terms, the logarithmic derivative of the expansion coefficient is

$$\frac{d}{dt}\ln(c_a(t)) = -\frac{i}{\hbar}\frac{dM'}{dt}\,. \tag{3.10}$$

In the limit $\epsilon \to 0$, the time derivative of the matrix element is

$$\begin{aligned}\frac{dM'}{dt} &= \sum_n \left(A_0^2 \frac{\langle\Phi_a|V_1|\Phi_n\rangle\langle\Phi_n|V_1|\Phi_a\rangle}{E_a - E_n + \hbar\omega} e^{-2i\omega t} \right. \\ &+ |A_0|^2 \frac{\langle\Phi_a|V_2|\Phi_n\rangle\langle\Phi_n|V_1|\Phi_a\rangle}{E_a - E_n - \hbar\omega} \\ &+ |A_0|^2 \frac{\langle\Phi_a|V_1|\Phi_n\rangle\langle\Phi_n|V_2|\Phi_a\rangle}{E_a - E_n + \hbar\omega} \\ &+ \left. (A_0^*)^2 \frac{\langle\Phi_a|V_2|\Phi_n\rangle\langle\Phi_n|V_2|\Phi_a\rangle}{E_a - E_n - \hbar\omega} e^{2i\omega t} \right) . \end{aligned} \tag{3.11}$$

In the static limit $\omega \to 0$ of the electromagnetic field, this expression simplifies to

$$\begin{aligned}\frac{dM'_{(\omega=0)}}{dt} &= \sum_n \left(A_0^2 \frac{\langle\Phi_a|V_1|\Phi_n\rangle\langle\Phi_n|V_1|\Phi_a\rangle}{E_a - E_n} \right. \\ &+ |A_0|^2 \frac{\langle\Phi_a|V_2|\Phi_n\rangle\langle\Phi_n|V_1|\Phi_a\rangle}{E_a - E_n} \\ &+ |A_0|^2 \frac{\langle\Phi_a|V_1|\Phi_n\rangle\langle\Phi_n|V_2|\Phi_a\rangle}{E_a - E_n} \\ &+ \left. (A_0^*)^2 \frac{\langle\Phi_a|V_2|\Phi_n\rangle\langle\Phi_n|V_2|\Phi_a\rangle}{E_a - E_n} \right) . \end{aligned} \tag{3.12}$$

For $\omega \neq 0$ we use the property $e^{2i\omega t} = \frac{1}{2i\omega}\int_0^t dt' e^{2i\omega t'}$. Using relation (3.3) (see Ref. [46]) to form the Dyson series, we get

$$\begin{aligned}\frac{dM'_{\omega\neq 0}}{dt} &= \sum_n \left(|A_0|^2 \frac{\langle\Phi_a|V_2|\Phi_n\rangle\langle\Phi_n|V_1|\Phi_a\rangle}{E_a - E_n - \hbar\omega} \right. \\ &+ \left. |A_0|^2 \frac{\langle\Phi_a|V_1|\Phi_n\rangle\langle\Phi_n|V_2|\Phi_a\rangle}{E_a - E_n + \hbar\omega} \right) . \end{aligned} \tag{3.13}$$

Because $\frac{dM'_{\omega\neq 0}}{dt}$ and $\frac{dM'_{(\omega=0)}}{dt}$ are time independent, one can make the ansatz [68]

$$\frac{\dot{c}_a}{c_a} = -\frac{i}{\hbar}\Delta_a^{AC} \tag{3.14}$$

and define the energy shift of the state a due to interaction with the light field as

$$\begin{aligned}\Delta_a^{AC} &= |A_0|^2 \sum_n \left(\frac{\langle\Phi_a|V_2|\Phi_n\rangle\langle\Phi_n|V_1|\Phi_a\rangle}{E_a - E_n - \hbar\omega} \right. \\ &+ \left. \frac{\langle\Phi_a|V_1|\Phi_n\rangle\langle\Phi_n|V_2|\Phi_a\rangle}{E_a - E_n + \hbar\omega} \right) . \end{aligned} \tag{3.15}$$

A_0 is given as $|A_0|^2 = \frac{|\boldsymbol{E}|^2 c^2}{\omega^2}$, with $\boldsymbol{E}$ being the electric field strength. On Fig. 3.1, the diagrams representing the two terms in the above equations are shown.

3.2 Evaluation of matrix elements

In this section we describe how the relativistic wave functions, the vector potential of the electromagnetic field and the interaction matrix elements in Eq. (3.15) are treated. Our description is fully relativistic and

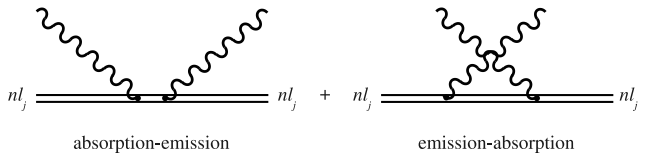

Figure 3.1: Diagrams representing the lowest-order perturbative light shift corrections. The Coulomb-dressed electron is depicted by a double line and the wavy lines represent photons.

accounts for spin and magnetic field effects. A similar description is used for the relativistic theoretical study of the spontaneous emission in Refs. ([6, 34, 36, 46]).

The principal task in calculating the light shift is the evaluation of the matrix element

$$M = \sum_n \frac{\langle \Phi_a | \hat{\alpha}^* \hat{\epsilon}_\nu^* e^{-i\boldsymbol{kr}} | \Phi_n \rangle \langle \Phi_n | \hat{\alpha} \hat{\epsilon}_\nu e^{i\boldsymbol{kr}} | \Phi_a \rangle}{E_a - E_n - \hbar\omega} \,. \tag{3.16}$$

We apply the multipole decomposition of the transverse electromagnetic plane wave as

$$\hat{\alpha} \hat{\epsilon_\nu} e^{i\boldsymbol{kr}} = 4\pi \hat{\alpha} \sum_{lm} \sum_{\lambda=0}^{1} i^{l-\lambda} \left(\boldsymbol{Y}_{lm}^{(\lambda)}(\hat{k}) \cdot \hat{\epsilon}_\nu \right)^\dagger \boldsymbol{a}_{lm}^{(\lambda)}(\boldsymbol{r}) \,, \tag{3.17}$$

thus M becomes

$$\begin{aligned} M &= 16\pi^2 \sum_{nlm\lambda l'm'\lambda'} \langle \Phi_a | \hat{\alpha}^* i^{\lambda - l} (\hat{\epsilon_\nu} \boldsymbol{Y}_{lm}^{(\lambda)}(\hat{k})) \boldsymbol{a}_{lm}^{(\lambda)\dagger}(\boldsymbol{r}) | \Phi_n \rangle \\ &\times \frac{\langle \Phi_n | \hat{\alpha} (i^*)^{l' - \lambda'} (\boldsymbol{Y}_{l'm'}^{(\lambda')}(\hat{k}) \hat{\epsilon_\nu})^\dagger \boldsymbol{a}_{l'm'}^{(\lambda')}(\boldsymbol{r}) | \Phi_a \rangle}{E_a - E_n - \hbar\omega} \,. \end{aligned} \tag{3.18}$$

To obtain the level shift, a summation over polarization states and integration over photon directions has to be performed:

$$M = \frac{1}{2} \sum_\nu \frac{1}{4\pi} \int d\Omega_k M \,. \tag{3.19}$$

Using the orthogonality property

$$\sum_\nu \int d\Omega_k \left(\boldsymbol{Y}_{l'm'}^{(\lambda')}(\hat{k}) \hat{\epsilon}_\nu \right)^\dagger \left(\hat{\epsilon_\nu} \boldsymbol{Y}_{lm}^{(\lambda)}(\hat{k}) \right) = \delta_{ll'} \delta_{mm'} \delta_{\lambda\lambda'} \,, \tag{3.20}$$

the expression above simplifies to

$$M = 2\pi \sum_{nlm\lambda} \frac{\langle \Phi_a | \hat{\alpha}^* \boldsymbol{a}_{lm}^{(\lambda)\dagger}(\boldsymbol{r}) | \Phi_n \rangle \langle \Phi_n | \hat{\alpha} \boldsymbol{a}_{lm}^{(\lambda)}(\boldsymbol{r}) | \Phi_a \rangle}{E_a - E_n - \hbar\omega} \,. \tag{3.21}$$

Using the spectral representation of Green's function

$$G(\boldsymbol{r}, \boldsymbol{r}'; z) = \sum_n \frac{\Phi_n(\boldsymbol{r}) \Phi_n(\boldsymbol{r})^\dagger}{E_n - z} \,, \tag{3.22}$$

and splitting Eq. (3.21) into an electric ($\lambda = 1$) and a magnetic ($\lambda = 0$) part we get:

$$\begin{aligned} M &= -2\pi \sum_{lm} \int d\boldsymbol{r} d\boldsymbol{r}' \Phi_a^\dagger(\boldsymbol{r}) \hat{\alpha}^* \boldsymbol{a}_{lm}^{(0)\dagger}(\boldsymbol{r}) G(\boldsymbol{r}, \boldsymbol{r}'; z) \\ &\quad \times \hat{\alpha} \boldsymbol{a}_{lm}^{(0)}(\boldsymbol{r}) \Phi_a(\boldsymbol{r}') \\ &\quad -2\pi \sum_{lm} \int d\boldsymbol{r} d\boldsymbol{r}' \Phi_a^\dagger(\boldsymbol{r}) \hat{\alpha}^* \boldsymbol{a}_{lm}^{(1)\dagger}(\boldsymbol{r}) G(\boldsymbol{r}, \boldsymbol{r}'; z) \\ &\quad \times \hat{\alpha} \boldsymbol{a}_{lm}^{(1)}(\boldsymbol{r}) \Phi_a(\boldsymbol{r}') \,, \end{aligned} \tag{3.23}$$

where the energy variable is $z = E_a - \hbar\omega$.

We perform a gauge transformation of the matrix elements. The transformed multipole potential can be written as

$$\begin{aligned} \boldsymbol{a}_{JM}^{\lambda}(\hat{r}) &\longrightarrow \boldsymbol{a}_{JM}^{\lambda}(\hat{r}) + \nabla \chi_{JM}(\hat{r}) \,, \\ \Phi_{JM}(\hat{r}) &\longrightarrow i\omega \chi_{JM}(\hat{r}) \,. \end{aligned} \tag{3.24}$$

where the gauge function $\chi_{JM}(\hat{r})$ (and the multipole potential) is a solution to the Helmholtz equation. We choose the gauge function to be

$$\chi_{JM}(\hat{r}) = -\frac{1}{k} G_J j_J(kr) Y_{JM}(\hat{r}) \,. \tag{3.25}$$

With the choice of $G_J = \sqrt{J+1/J}$, the so-called Babushkin gauge, i.e. a relativistic generalization of the length form interaction, is adopted [5, 34, 36]. This transformation has no effect on the magnetic multipole potentials, but transforms electric potentials to the form

$$\begin{aligned} \boldsymbol{a}_{JM}^{(1)}(\hat{r}) &= -j_{J+1}(kr) \left(\boldsymbol{Y}_{JM}^{(1)}(\hat{r}) - \sqrt{\frac{J+1}{J}} \boldsymbol{Y}_{JM}^{(-1)}(\hat{r}) \right) \,, \\ \Phi_{JM}^{(1)}(\hat{r}) &= -ic \sqrt{\frac{J+1}{J}} j_J(kr) Y_{JM}(\hat{r}) \,. \end{aligned} \tag{3.26}$$

The electric multipole potentials can be rewritten as

$$\boldsymbol{a}_{JM}^{(1)}(\hat{r}) = -\sqrt{\frac{2J+1}{J}} \boldsymbol{a}_{JJ+1M}(\hat{r}) \,, \tag{3.27}$$

with $\boldsymbol{a}_{JJ+1M}(\hat{r})$ given in [46].

Denoting with M^m the magnetic part and with M^e the electric part and after some algebraic manipula-

tions we obtain

$$
\begin{aligned}
M^m &= \frac{4\pi}{\hbar c}\sum_{lm\kappa_n}\Big\{(R_1^m+R_4^m)K_{JJM}^{\kappa_n-\kappa_a}K_{JJM}^{-\kappa_n\kappa_a} \\
&\quad -R_2^m\left(K_{JJM}^{-\kappa_n\kappa_a}\right)^2-R_3^m\left(K_{JJM}^{\kappa_n-\kappa_a}\right)^2\Big\}, \\
M^e &= \frac{4\pi}{\hbar c}\sum_{lm\kappa_n}\left\{\frac{2J+1}{J}\Big[(R_1^e+R_4^e)K_{JJ+1M}^{\kappa_n-\kappa_a}K_{JJ+1M}^{-\kappa_n\kappa_a}\right. \\
&\quad -R_2^e\left(K_{JJ+1M}^{-\kappa_n\kappa_a}\right)^2-R_3^e\left(K_{JJ+1M}^{\kappa_n-\kappa_a}\right)^2\Big] \\
&\quad -\frac{J+1}{J}\Big[R_{1'}^e\left(K_{JM}^{\kappa_n\kappa_a}\right)^2+\left(R_{2'}^e+R_{3'}^e\right)K_{JM}^{\kappa_n\kappa_a}K_{JM}^{-\kappa_n-\kappa_a} \\
&\quad \left.+R_{4'}^e\left(K_{JM}^{-\kappa_n-\kappa_a}\right)^2\Big]\right\}. \qquad (3.28)
\end{aligned}
$$

We shall refer to the K's as the angular matrix elements and to the R's as the radial matrix elements.

The matrix element

$$
M'=\sum_n\frac{\langle\Phi_a|\hat{\alpha}\hat{\epsilon}_\nu e^{i\boldsymbol{kr}}|\Phi_n\rangle\langle\Phi_n|\hat{\alpha}^*\hat{\epsilon}_\nu^* e^{-i\boldsymbol{kr}}|\Phi_a\rangle}{E_a-E_n+\hbar\omega} \qquad (3.29)
$$

can readily be found from Eq. (3.28) by the substitutions $K^{\kappa_n-\kappa_a}\to K^{-\kappa_a-\kappa_n}$, $K^{\kappa_n\kappa_a}\to K^{\kappa_a-\kappa_n}$, $K^{\kappa_n\kappa_a}\to K^{\kappa_a\kappa_n}$ and $K^{-\kappa_n-\kappa_a}\to K^{-\kappa_a-\kappa_n}$. In the radial part, the energy variable $z=E_a+\hbar\omega$ has to be substituted.

3.2.1 Radial matrix elements

The following notations are introduced for the two-dimensional radial integrals:

$$
\begin{aligned}
R_1^m &= \int drdr'r^2r'^2F_a(r)j_J(kr)g_{12}(r,r';E)j_J(kr')G_a(r'), \\
R_2^m &= \int drdr'r^2r'^2G_a(r)j_J(kr)g_{22}(r,r';E)j_J(kr')G_a(r'), \\
R_3^m &= \int drdr'r^2r'^2F_a(r)j_J(kr)g_{11}(r,r';E)j_J(kr')F_a(r'), \\
R_4^m &= \int drdr'r^2r'^2G_a(r)j_J(kr)g_{21}(r,r';E)j_J(kr')F_a(r'), \\
R_{1'}^e &= \int drdr'r^2r'^2G_a(r)j_J(kr)g_{11}(r,r';E)j_J(kr')G_a(r'), \\
R_{2'}^e &= \int drdr'r^2r'^2F_a(r)j_J(kr)g_{21}(r,r';E)j_J(kr')G_a(r'), \\
R_{3'}^e &= \int drdr'r^2r'^2G_a(r)j_J(kr)g_{12}(r,r';E)j_J(kr')F_a(r'), \\
R_{4'}^e &= \int drdr'r^2r'^2F_a(r)j_J(kr)g_{22}(r,r';E) \\
&\quad \times j_J(kr')F_a(r'). \qquad (3.30)
\end{aligned}
$$

In these integrals, $j_J(kr)$ is the spherical Bessel function [3] and the g_{ij} $(i,j = 1,2)$ are the radial components of the Coulomb-Dirac Green's function.

All radial matrix elements can be evaluated analytically by the help of the substitution

$$j_l(kr) = \left(\frac{\pi}{2kr}\right)^{1/2} J_{l+1/2}(kr) \tag{3.31}$$

and the Taylor expansion of the Bessel functions $J_{l+1/2}$:

$$j_l(kr) = \sqrt{\frac{\pi}{2kr}} \sum_{n=0} \frac{(-1)^n}{2^{2n+l+1/2} n! \Gamma(n+l+3/2)} (kr)^{2n+l+1/2}. \tag{3.32}$$

The final results are as follows:

$$\begin{aligned} R_1^m = & \left(1 - \frac{E_a^2}{m^2c^4}\right)^{1/2} U_a^2 \frac{1}{2} (2\lambda_n)^{(2\gamma_n)} \sum_n \\ & \left(- (\kappa_n + \nu/\epsilon_n) \frac{n!(I_{A_1J}^2 - I_{B_1J}^2)}{\Gamma(2\gamma_n + 1 + n)(n + \gamma_n + 1 - \nu)} \right. \\ & -(\kappa_n - \nu/\epsilon_n) \frac{n!(I_{A_1J}^2 - I_{B_1J}^2)}{\Gamma(2\gamma_n + 1 + n)(n + \gamma_n - \nu)} \\ & \left. - \frac{n!2}{\Gamma(2\gamma_n + n)(n + \gamma_n - \nu)} (I_{A_2J} I_{B_1J} - I_{A_1J} I_{B_2J}) \right), \end{aligned} \tag{3.33}$$

$$\begin{aligned} R_2^m = & \left(1 + \frac{E_a}{mc^2}\right) U_a^2 \frac{\varepsilon}{2} (2\lambda_n)^{(2\gamma_n)} \sum_n \\ & \left((\kappa_n + \nu/\epsilon_n) \frac{n!'(I_{A_1J} - I_{B_1J})^2}{\Gamma(2\gamma_n + 1 + n)(n + \gamma_n + 1 - \nu)} - \right. \\ & [(\kappa_n - \nu/\epsilon_n) - 2(\gamma_n + \nu)] \frac{n!(I_{A_1J} - I_{B_1J})^2}{\Gamma(2\gamma_n + 1 + n)(n + \gamma_n - \nu)} \\ & - \frac{n!2}{\Gamma(2\gamma_n + n)(n + \gamma_n - \nu)} \\ & \left. \times (I_{A_2J} I_{A_1J} - I_{A_1J} I_{B_2J} - I_{A_2J} I_{B_1J} + I_{B_1J} I_{B_2J}) \right), \end{aligned} \tag{3.34}$$

$$\begin{aligned} R_3^m = & \left(1 - \frac{E_a}{mc^2}\right) U_a^2 \frac{1}{2\varepsilon} (2\lambda_n)^{(2\gamma_n)} \sum_n \\ & \left((\kappa_n + \nu/\epsilon_n) \frac{n!(I_{A_1J} + I_{B_1J})^2}{\Gamma(2\gamma_n + 1 + n)(n + \gamma_n + 1 - \nu)} - \right. \\ & [(\kappa_n - \nu/\epsilon_n) + 2(\gamma_n + \nu)] \frac{n!(I_{A_1J} + I_{B_1J})^2}{\Gamma(2\gamma_n + 1 + n)(n + \gamma_n - \nu)} \\ & + \frac{n!2}{\Gamma(2\gamma_n + n)(n + \gamma_n - \nu)} \\ & \left. \times (I_{A_2J} I_{A_1J} + I_{A_1J} I_{B_2J} + I_{A_2J} I_{B_1J} + I_{B_1J} I_{B_2J}) \right), \end{aligned} \tag{3.35}$$

$$R_4^m = \left(1 - \frac{E_a^2}{m^2c^4}\right) U_a^2 \frac{1}{2} (2\lambda_n)^{(2\gamma_n)} \sum_n \tag{3.36}$$
$$\left(- (\kappa_n + \nu/\epsilon_n) \frac{n!(I_{A_1J}^2 - I_{B_1J}^2)}{\Gamma(2\gamma_n + 1 + n)(n + \gamma_n + 1 - \nu)} \right.$$
$$-(\kappa_n - \nu/\epsilon_n) \frac{n!(I_{A_1J}^2 - I_{B_1J}^2)}{\Gamma(2\gamma_n + 1 + n)(n + \gamma_n - \nu)}$$
$$\left. - \frac{n!2}{\Gamma(2\gamma_n + n)(n + \gamma_n - \nu)} (I_{A_2J} I_{B_1J} - I_{A_1J} I_{B_2J}) \right),$$

$$R_{1'}^e = \left(1 + \frac{E_a}{mc^2}\right) U_a^2 \frac{1}{2\varepsilon} (2\lambda_n)^{(2\gamma_n)} \sum_n \tag{3.37}$$
$$\left((\kappa_n + \nu/\epsilon_n) \frac{n!(I_{A_1J} - I_{B_1J})^2}{\Gamma(2\gamma_n + 1 + n)(n + \gamma_n + 1 - \nu)} - \right.$$
$$[(\kappa_n - \nu/\epsilon_n) + 2(\gamma_n + \nu)] \frac{n!(I_{A_1J} - I_{B_1J})^2}{\Gamma(2\gamma_n + 1 + n)(n + \gamma_n - \nu)}$$
$$+ \frac{n!2}{\Gamma(2\gamma_n + n)(n + \gamma_n - \nu)}$$
$$\left. \times (I_{A_2J} I_{A_1J} - I_{A_1J} I_{B_2J} - I_{A_2J} I_{B_1J} + I_{B_1J} I_{B_2J}) \right),$$

$$R_{2'}^e = \left(1 - \frac{E_a^2}{m^2c^4}\right)^{1/2} U_a^2 \frac{1}{2} (2\lambda_n)^{(2\gamma_n)} \sum_n \tag{3.38}$$
$$\left(- (\kappa_n + \nu/\epsilon_n) \frac{n!(I_{A_1J}^2 - I_{B_1J}^2)}{\Gamma(2\gamma_n + 1 + n)(n + \gamma_n + 1 - \nu)} \right.$$
$$-(\kappa_n - \nu/\epsilon_n) \frac{n!(I_{A_1J}^2 - I_{B_1J}^2)}{\Gamma(2\gamma_n + 1 + n)(n + \gamma_n - \nu)}$$
$$\left. + \frac{n!2}{\Gamma(2\gamma_n + n)(n + \gamma_n - \nu)} (I_{A_2J} I_{B_1J} - I_{A_1J} I_{B_2J}) \right),$$

$$R_{3'}^e = \left(1 - \frac{E_a^2}{m^2c^4}\right)^{1/2} U_a^2 \frac{1}{2} (2\lambda_n)^{(2\gamma_n)} \sum_n \tag{3.39}$$
$$\left(- (\kappa_n + \nu/\epsilon_n) \frac{n!(I_{A_1J}^2 - I_{B_1J}^2)}{\Gamma(2\gamma_n + 1 + n)(n + \gamma_n + 1 - \nu)} \right.$$
$$-(\kappa_n - \nu/\epsilon_n) \frac{n!(I_{A_1J}^2 - I_{B_1J}^2)}{\Gamma(2\gamma_n + 1 + n)(n + \gamma_n - \nu)}$$
$$\left. + \frac{n!2}{\Gamma(2\gamma_n + n)(n + \gamma_n - \nu)} (I_{A_2J} I_{B_1J} - I_{A_1J} I_{B_2J}) \right),$$

$$
\begin{aligned}
R^e_{4'} = & \left(1-\frac{E_a}{mc^2}\right) U_a^2 \frac{\varepsilon}{2} (2\lambda_n)^{(2\gamma_n)} \sum_n \\
& \left((\kappa_n + \nu/\epsilon_n) \frac{n!(I_{A_1J}+I_{B_1J})^2}{\Gamma(2\gamma_n+1+n)(n+\gamma_n+1-\nu)} - \right. \\
& [(\kappa_n - \nu/\epsilon_n) - 2(\gamma_n+\nu)] \frac{n!(I_{A_1J}+I_{B_1J})^2}{\Gamma(2\gamma_n+1+n)(n+\gamma_n-\nu)} \\
& - \frac{n!2}{\Gamma(2\gamma_n+n)(n+\gamma_n-\nu)} \\
\times \quad & \left. (I_{A_2J}I_{A_1J} + I_{A_1J}I_{B_2J} + I_{A_2J}I_{B_1J} + I_{B_1J}I_{B_2J}) \right) .
\end{aligned} \tag{3.40}
$$

For the one-dimensional radial integrals we obtain the following analytical results:

$$
\begin{aligned}
I_{A_1J} = & \left(\frac{\pi}{2k}\right) \sum_{\alpha,p} \frac{a_r(-1)^\alpha}{\alpha!\Gamma(\alpha+l+3/2)} \frac{(-a_r+1)_p}{(2\gamma_a+1)_p} \\
& \times \frac{\Gamma(\gamma_{an}+l+2\alpha+p+1)\Gamma(2\gamma_n+n+1)}{n!\Gamma(2\gamma_n+1)} \\
& \times \left(\frac{k}{2}\right)^{2\alpha+l+1/2} \frac{(2\lambda_a)^{p+\gamma_a-1}}{p!} \lambda_{an}^{-(\gamma_{an}+p+2)} \\
& \times {}_2F_1(-n, \gamma_{an}+l+2\alpha+p+1, 2\gamma_n+1, \frac{2\lambda_n}{\lambda_{an}}) ,
\end{aligned} \tag{3.41}
$$

$$
\begin{aligned}
I_{A_2J} = & \left(\frac{\pi}{2k}\right) \sum_{\alpha,p} \frac{a_r(-1)^\alpha}{\alpha!\Gamma(\alpha+l+3/2)} \frac{(-a_r+1)_p}{(2\gamma_a+1)_p} \\
& \times \frac{\Gamma(\gamma_{an}+l+2\alpha+p+1)\Gamma(2\gamma_n+n)}{n!\Gamma(2\gamma_n)} \\
& \times \left(\frac{k}{2}\right)^{2\alpha+l+1/2} \frac{(2\lambda_a)^{p+\gamma_a-1}}{p!} \lambda_{an}^{-(\gamma_{an}+p+2)} \\
& \times {}_2F_1(-n, \gamma_{an}+l+2\alpha+p+1, 2\gamma_n, \frac{2\lambda_n}{\lambda_{an}}) ,
\end{aligned} \tag{3.42}
$$

$$
\begin{aligned}
I_{B_1J} = & \left(\frac{\pi}{2k}\right) \sum_{\alpha,p} \frac{(N_a-\kappa_a)(-1)^\alpha}{\alpha!\Gamma(\alpha+l+3/2)} \frac{(-a_r)_p}{(2\gamma_a+1)_p} \\
& \times \frac{\Gamma(\gamma_{an}+l+2\alpha+p+1)\Gamma(2\gamma_n+n+1)}{n!\Gamma(2\gamma_n+1)} \\
& \times \left(\frac{k}{2}\right)^{2\alpha+l+1/2} \frac{(2\lambda_a)^{p+\gamma_a-1}}{p!} \lambda_{an}^{-(\gamma_{an}+p+2)} \\
& \times {}_2F_1(-n, \gamma_{an}+l+2\alpha+p+1, 2\gamma_n+1, \frac{2\lambda_n}{\lambda_{an}}) ,
\end{aligned} \tag{3.43}
$$

$$
\begin{aligned}
I_{B_2 J} &= \left(\frac{\pi}{2k}\right) \sum_{\alpha,p} \frac{(N_a-\kappa_a)(-1)^\alpha}{\alpha!\Gamma(\alpha+l+3/2)} \frac{(-a_r)_p}{(2\gamma_a+1)_p} \\
&\times \frac{\Gamma(\gamma_{an}+l+2\alpha+p+1)\Gamma(2\gamma_n+n)}{n!\Gamma(2\gamma_n)} \\
&\times \left(\frac{k}{2}\right)^{2\alpha+l+1/2} \frac{(2\lambda_a)^{p+\gamma_a-1}}{p!} \lambda_{an}^{-(\gamma_{an}+p+2)} \\
&\times {}_2F_1(-n, \gamma_{an}+l+2\alpha+p+1, 2\gamma_n, \frac{2\lambda_n}{\lambda_{an}}) \,. \qquad (3.44)
\end{aligned}
$$

Here we introduced the notations $\lambda_{an} = \lambda_a + \lambda_n$ and $\gamma_{an} = \gamma_a + \gamma_n$ for simplicity. The remaining radial matrix elements can be calculated from the ones given in Eq. (3.33-3.36) by the substitutions $R_i^e = R_i^m(J \to J+1)$ for all $i \in \{1,2,3,4\}$.

3.2.2 Angular matrix elements

The equations (3.28) contain angular integrals of the form

$$
K_{JkM}^{\kappa_n \kappa_a} = \int do_r \Omega_{\kappa_n}^\dagger(\hat{r}) \hat{\sigma} \boldsymbol{Y}_{JkM}(\hat{r}) \Omega_{\kappa_a}(\hat{r}) \,. \qquad (3.45)
$$

The direct product of the spin operator $\hat{\sigma}$ and the vector spherical harmonic is a spherical tensor operator and thus its matrix element can be rewritten as

$$
K_{JkM}^{\kappa_n \kappa_a} = \langle l_n \frac{1}{2} j_n | T_J(Y_k \sigma_1) | l_a \frac{1}{2} j_a \rangle \,. \qquad (3.46)
$$

The reduced matrix elements of the tensor T can be calculated using the formula

$$
\begin{aligned}
&\langle l_1 \frac{1}{2} j || T_K(C_k \sigma_1) || l_1' \frac{1}{2} j' \rangle = \\
&= a_K (-1)^{J'-K-1/2} (2j'+1)^{1/2} \begin{pmatrix} j & j' & K \\ \frac{1}{2} & -\frac{1}{2} & 0 \end{pmatrix} , \qquad (3.47)
\end{aligned}
$$

where the coefficients are [15]

$$
\begin{aligned}
a_k &= (\kappa - \kappa')/\sqrt{k(k+1)} \,, \\
a_{k-1} &= -(k+\kappa+\kappa')/\sqrt{2k(k+1)} \,, \\
a_{k+1} &= (k+1-\kappa-\kappa')/\sqrt{(k+1)(2k+1)} \,. \qquad (3.48)
\end{aligned}
$$

These formulas are derived in detail in the Appendix. For the integrals containing the scalar spherical harmonics,

$$
\begin{aligned}
K_{JM}^{\kappa_n \kappa_a} &= \int do_r \Omega_{\kappa_n}^\dagger(\hat{r}) Y_{JM}(\hat{r}) \Omega_{\kappa_a}(\hat{r}) \\
&= \langle l_n \frac{1}{2} j_n | Y_{JM} | l_a \frac{1}{2} j_a \rangle \,, \qquad (3.49)
\end{aligned}
$$

one can compute the reduced matrix elements as [15]

$$
\begin{aligned}
&\langle l_1 \frac{1}{2} j || C_K || l_1' \frac{1}{2} j' \rangle = \\
&= (-1)^{j'-K-1/2} (2j'+1)^{1/2} \begin{pmatrix} j & j' & K \\ \frac{1}{2} & -\frac{1}{2} & 0 \end{pmatrix} . \qquad (3.50)
\end{aligned}
$$

Table 3.1: Comparision of non-relativistic (NR) and relativistic (R) light shifts for K and L shell states in hydrogenic ions, at an optical laser frequency. E_b denotes the binding energy of the orbital and ΔE stands for the light shift contribution.

		$Z = 54$		$Z = 92$	
		E_b	ΔE	E_b	ΔE
NR	$1s$	-39674.2	$-1.02586(-4)$	-115159	$-1.21763(-5)$
R	$1s_{1/2}$	-41347.0	$-8.17337(-5)$	-132280	$-5.63212(-6)$
NR	$2s$	-9918.55	$-2.73564(-3)$	-28789.6	$-3.24700(-4)$
R	$2s_{1/2}$	-10443.5	$-4.94986(-2)$	-34215.5	$-1.40870(-3)$
NR	$2p$	-9918.55	$-4.92415(-3)$	-28789.6	$-5.84460(-4)$
R	$2p_{1/2}$	-10443.5	$-3.17409(-3)$	-34215.5	$-2.17374(-4)$
R	$2p_{3/2}$	-10016.7	$+4.31087(-2)$	-29649.8	$+7.88416(-4)$

3.3 Numerical results

To start our discussion on relativistic results of light shifts, we present results for an atom in a laser field at an infrared frequency ($\lambda = 1054$ nm, $\hbar\omega = 1.176$ eV) and with the widely accessible intensity of $I = 10^{18}$ W/cm^2. We calculate the light shifts in eV, both in relativistic and nonrelativistic treatments, for some heavy elements ($Z = 54, 92$, i.e. Xe and U). Results are shown in Table 3.1. As it is well known, the AC stark shifts, calculated in a non-relativistic way, follow an exact $\propto Z^{-4}$ scaling. It is also intuitively understandable that external field effects in general have a smaller effect if the electrons are bound by stronger central potentials. Still, even for elements as heavy as Xe and U, and for orbitals of the L shell, the light shift exceeds or approaches to the meV range. This is anticipated to be noticeable in near-future experiments. For measurements with lighter elements, the effects are certainly more pronounced.

As the table also clearly shows, the relativistic and nonrelativistic results greatly differ. For these relativistic systems, the non-relativistic calculation can only serve as an order-of-magnitude approximation, since not even the first digits of the results calculated in the two different approaches agree. In some cases, e.g. for the $2p_{3/2}$ state, even the sign of the shift is different, which is originated in the different level structure as described by the relativistic theory.

For soft x-ray frequencies ($\hbar\omega = 50$ eV), for the same intensity, we display the shifts for the elements $Z = 10, 54$ and 92 in Table 3.2. At the heaviest system studied, namely, for U, these results almost coincide with the light shifts calculated with optical laser frequencies. This illustrates that retardation effects are only relevant when the photon energy is comparable to the atomic binding energy: in the case of U, where the binding energies exceed the 10 keV-range, even a photon frequency of 50 eV is negligible in the description of the dynamic Stark shift. However, for lighter systems such as Xe ($Z = 54$), the difference between the optical and the soft x-ray light field is noticeable. This is especially the case for excited states.

In order to avoid a discussion about the intensity I and for a better comparison with existing non-relativistic literature data, in the following we introduce the dynamic Stark shift coefficient β:

$$\Delta_a^{AC} = h\beta_a I, \tag{3.51}$$

where Δ_a^{AC} is the Stark shift of the atomic level $|\Phi_a\rangle$. In Tables 3.3, 3.4 and 3.5, the nonrelativistic and relativistic Stark shift coefficients β_{NR} and β_R are compared for $1s - ns$ two-photon resonance

Table 3.2: Comparison of nonrelativistic (NR) and relativistic (R) light shifts for K and L shell states in hydrogenic ions at a soft x-ray laser frequency. Notations as in Table 3.1.

	$Z=10$		$Z=54$		$Z=92$	
	E_b	ΔE	E_b	ΔE	E_b	ΔE
$1s$	-1360.57	$-8.74042(-2)$	-39674.2	$-1.02587(-4)$	-115159	$-1.21763(-5)$
$1s_{1/2}$	-1362.39	$-8.6767(-2)$	-41347.0	$-8.17339(-5)$	-132280	$-5.63212(-6)$
$2s$	-340.142	-2.47409	-9918.55	$-2.73583(-3)$	-28789.6	$-3.24703(-4)$
$2s_{1/2}$	-340.710	-2.33842	-10443.5	$-5.01577(-2)$	-34215.5	$-1.40885(-3)$
$2p$	-340.142	-4.47426	-9918.55	$-4.92452(-3)$	-28789.6	$-5.84465(-4)$
$2p_{1/2}$	-340.710	-3.61534	-10443.5	$-3.17429(-3)$	-34215.5	$-2.17375(-4)$
$2p_{3/2}$	-340.256	-4.16667	-10016.7	$+4.37674(-2)$	-29649.8	$+7.88564(-4)$

Table 3.3: Comparison of nonrelativistic (NR) and relativistic (R) light shifts for $1s$–ns two-photon transitions for Z=1.

$Z=1$	$\beta_{\rm NR}$ [Hz(W/m^2)$^{-1}$]	$\beta_{\rm R}$ [Hz(W/m^2)$^{-1}$]
	$1s-ns$	$1s_{1/2}-ns_{1/2}$
$1s-2s$	$-2.67827(-5)$	$-2.67808(-5)$
$1s-3s$	$-3.02104(-5)$	$-3.02082(-5)$
$1s-4s$	$-3.18301(-5)$	$-3.18278(-5)$
$1s-5s$	$-3.26801(-5)$	$-3.26778(-5)$
$1s-6s$	$-3.31724(-5)$	$-3.31701(-5)$
$1s-7s$	$-3.34805(-5)$	$-3.34781(-5)$
$1s-8s$	$-3.36851(-5)$	$-3.36827(-5)$
$1s-9s$	$-3.38277(-5)$	$-3.38252(-5)$

transitions for nuclear charge numbers $Z=1, 10$ and 54. The light shift calculated in the non-relativistic limit of the formulas derived in this thesis agree perfectly with the calculations of Haas et al. [40]. Also, they show an exact $\propto Z^{-4}$ scaling with the atomic number Z. However, for the relativistic results, a clear deviation from this law is observable, especially for the highest atomic charge numbers. These tables also illustrate that the light shifts are most relevant for highly excited, weakly bound states, i.e. for Rydberg levels.

As we can see from the Eqs. (3.23,3.26), in the final expression of dipole light shifts we have the following possible combinations of electromagnetic potentials: matrix elements of scalar-scalar, vector-vector and scalar-vector potentials. Because of the selection rules incorporated in the angular matrix elements, the scalar-vector part is zero. In the following tables we give some values of the dynamic Stark shift coefficient β for scalar-scalar and vector-vector parts and for the interaction with the magnetic field component of the laser field, including the retardation contribution caused by the dependence on the photons frequency. If we calculate the Stark shifts with the $\boldsymbol{rE}$ potential, we get for the scalar-scalar part the same results as in Eq. (3.2) for dipole approximation, without including the frequency-dependent retardation. The tables shows that the scalar-scalar contribution is by far the dominant part of the interaction. Thus we can conclude that the $\boldsymbol{rE}$ form is a rather good approximation of the total relativistic interaction operator. At high nuclear charges and frequencies, the dependence of the scalar-scalar term on the photon

Table 3.4: Comparison of nonrelativistic (NR) and relativistic (R) light shifts for $1s$–ns two-photon transitions for Z=10.

$Z = 10$	$\beta_{\rm NR}$ [Hz(W/m^2)$^{-1}$]	$\beta_{\rm R}$ [Hz(W/m^2)$^{-1}$]
	$1s - ns$	$1s_{1/2} - ns_{1/2}$
$1s - 2s$	$-2.67827(-9)$	$-2.65885(-9)$
$1s - 3s$	$-3.02104(-9)$	$-2.99941(-9)$
$1s - 4s$	$-3.18301(-9)$	$-3.16030(-9)$
$1s - 5s$	$-3.26801(-9)$	$-3.24471(-9)$
$1s - 6s$	$-3.31724(-9)$	$-3.29360(-9)$
$1s - 7s$	$-3.34805(-9)$	$-3.32418(-9)$
$1s - 8s$	$-3.36851(-9)$	$-3.34449(-9)$
$1s - 9s$	$-3.38277(-9)$	$-3.35863(-9)$

Table 3.5: Comparison of nonrelativistic (NR) and relativistic (R) light shifts for $1s$–ns two-photon transitions for Z=54.

$Z = 54$	$\beta_{\rm NR}$ [Hz(W/m^2)$^{-1}$]	$\beta_{\rm R}$ [Hz(W/m^2)$^{-1}$]
	$1s - ns$	$1s_{1/2} - ns_{1/2}$
$1s - 2s$	$-3.14978(-12)$	$-2.51398(-12)$
$1s - 3s$	$-3.55288(-12)$	$-2.84491(-12)$
$1s - 4s$	$-3.74337(-12)$	$-3.00038(-12)$
$1s - 5s$	$-3.84334(-12)$	$-3.08132(-12)$
$1s - 6s$	$-3.90124(-12)$	$-3.12789(-12)$
$1s - 7s$	$-3.93747(-12)$	$-3.15688(-12)$
$1s - 8s$	$-3.96153(-12)$	$-3.17606(-12)$
$1s - 9s$	$-3.97829(-12)$	$-3.18937(-12)$

Table 3.6: Different relativistic electric dipole (E1) contributions to the light shift for $1s$-ns two-photon transitions: scalar-scalar (s-s), vector-vector (v-v), and magnetic field contributions, with or without frequency-dependent retardation (ret.) contributions. The results are given for $Z = 10$.

$Z = 10$	s-s	s-s, ret.	v-v	v-v, ret.	Mag.	Mag., ret.
$1s - 2s$	$-2.6588(-9)$	$-2.6579(-9)$	$-6.7879(-16)$	$-6.7848(-16)$	$-9.2665(-13)$	$-9.2635(-13)$
$1s - 3s$	$-2.9994(-9)$	$-2.9978(-9)$	$-1.0200(-15)$	$-1.0193(-15)$	$-1.0973(-12)$	$-1.0968(-12)$
$1s - 4s$	$-3.1603(-9)$	$-3.1584(-9)$	$-1.1667(-15)$	$-1.1658(-15)$	$-1.1753(-12)$	$-1.1746(-12)$
$1s - 5s$	$-3.2447(-9)$	$-3.2427(-9)$	$-1.2402(-15)$	$-1.2393(-15)$	$-1.2156(-12)$	$-1.2149(-12)$
$1s - 6s$	$-3.2936(-9)$	$-3.2915(-9)$	$-1.2818(-15)$	$-1.2808(-15)$	$-1.2387(-12)$	$-1.2380(-12)$
$1s - 7s$	$-3.3241(-9)$	$-3.3220(-9)$	$-1.3075(-15)$	$-1.3064(-15)$	$-1.2531(-12)$	$-1.2524(-12)$
$1s - 8s$	$-3.3444(-9)$	$-3.3423(-9)$	$-1.3243(-15)$	$-1.3233(-15)$	$-1.2627(-12)$	$-1.2619(-12)$
$1s - 9s$	$-3.3586(-9)$	$-3.3564(-9)$	$-1.3360(-15)$	$-1.3349(-15)$	$-1.2693(-12)$	$-1.2685(-12)$

Table 3.7: Different relativistic electric dipole (E1) contributions to the light shift for $1s$-ns two-photon transitions: scalar-scalar (s-s), vector-vector (v-v), and magnetic field contributions, with or without frequency-dependent retardation (ret.) contributions. The results are given for $Z = 54$.

$Z = 54$	s-s	s-s, ret.	v-v	v-v, ret.	Mag.	Mag., ret.
$1s - 2s$	$-2.5139(-12)$	$-2.4873(-12)$	$-6.2890(-16)$	$-6.2032(-16)$	$-2.8362(-14)$	$-2.8093(-14)$
$1s - 3s$	$-2.8449(-12)$	$-2.8013(-12)$	$-9.5338(-16)$	$-9.3473(-16)$	$-3.3758(-14)$	$-3.3284(-14)$
$1s - 4s$	$-3.0003(-12)$	$-2.9488(-12)$	$-1.0922(-15)$	$-1.0683(-15)$	$-3.6223(-14)$	$-3.5646(-14)$
$1s - 5s$	$-3.0813(-12)$	$-3.0255(-12)$	$-1.1615(-15)$	$-1.1347(-15)$	$-3.7490(-14)$	$-3.6859(-14)$
$1s - 6s$	$-3.1278(-12)$	$-3.0697(-12)$	$-1.2004(-15)$	$-1.1720(-15)$	$-3.8214(-14)$	$-3.7552(-14)$
$1s - 7s$	$-3.1568(-12)$	$-3.0972(-12)$	$-1.2243(-15)$	$-1.1949(-15)$	$-3.8664(-14)$	$-3.7982(-14)$
$1s - 8s$	$-3.1760(-12)$	$-3.1153(-12)$	$-1.2400(-15)$	$-1.2099(-15)$	$-3.8960(-14)$	$-3.8266(-14)$
$1s - 9s$	$-3.1893(-12)$	$-3.1280(-12)$	$-1.2508(-15)$	$-1.2202(-15)$	$-3.9166(-14)$	$-3.8462(-14)$

frequency starts to show up; however, the vector-vector and magnetic terms are still orders of magnitude smaller.

For completeness, in the Tables 3.8-3.9 we present values for the quadrupole contributions to the level shift. These terms are also approx. 3 orders of magnitude weaker than the dominant electric dipole interaction. However, with the improvement of experimental accuracy, the thorough understanding of relativistic light shift effects becomes increasingly stringent.

Table 3.8: Different relativistic electric quadrupole (E2) contributions to the light shift for $1s$-ns two-photon transitions: scalar-scalar (s-s), vector-vector (v-v), and magnetic field contributions, with or without frequency-dependent retardation (ret.) contributions. The results are given for $Z = 10$.

$Z = 10$	s-s	s-s, ret.	v-v	v-v, ret.	Mag.	Mag., ret.
$1s - 2s$	$-7.4262(-14)$	$-7.4227(-14)$	$-2.2189(-20)$	$-2.2178(-20)$	$-2.6903(-17)$	$-2.6891(-17)$
$1s - 3s$	$-1.1060(-13)$	$-1.1053(-13)$	$-4.7669(-20)$	$-4.7635(-20)$	$-4.4819(-17)$	$-4.4790(-17)$
$1s - 4s$	$-1.2604(-13)$	$-1.2594(-13)$	$-6.1152(-20)$	$-6.1104(-20)$	$-5.3336(-17)$	$-5.3298(-17)$
$1s - 5s$	$-1.3374(-13)$	$-1.3363(-13)$	$-6.8463(-20)$	$-6.8406(-20)$	$-5.7793(-17)$	$-5.7749(-17)$
$1s - 6s$	$-1.3808(-13)$	$-1.3797(-13)$	$-7.2755(-20)$	$-7.2693(-20)$	$-6.0368(-17)$	$-6.0320(-17)$
$1s - 7s$	$-1.4075(-13)$	$-1.4064(-13)$	$-7.5459(-20)$	$-7.5394(-20)$	$-6.1975(-17)$	$-6.1926(-17)$
$1s - 8s$	$-1.4251(-13)$	$-1.4239(-13)$	$-7.7263(-20)$	$-7.7195(-20)$	$-6.3042(-17)$	$-6.2991(-17)$
$1s - 9s$	$-1.4372(-13)$	$-1.4360(-13)$	$-7.8522(-20)$	$-7.8452(-20)$	$-6.3784(-17)$	$-6.3732(-17)$

Table 3.9: Different relativistic electric quadrupole (E2) contributions to the light shift for $1s$-ns two-photon transitions: scalar-scalar (s-s), vector-vector (v-v), and magnetic field contributions, with or without frequency-dependent retardation (ret.) contributions. The results are given for $Z = 54$.

$Z = 10$	s-s	s-s, ret.	v-v	v-v, ret.	Mag.	Mag., ret.
$1s - 2s$	$-2.1019(-15)$	$-2.0727(-15)$	$-6.0334(-19)$	$-5.9420(-19)$	$-2.4280(-17)$	$-2.3956(-17)$
$1s - 3s$	$-3.1586(-15)$	$-3.0960(-15)$	$-1.3122(-18)$	$-1.2840(-18)$	$-4.0816(-17)$	$-4.0029(-17)$
$1s - 4s$	$-3.6054(-15)$	$-3.5255(-15)$	$-1.6853(-18)$	$-1.6449(-18)$	$-4.8642(-17)$	$-4.7588(-17)$
$1s - 5s$	$-3.8269(-15)$	$-3.7378(-15)$	$-1.8859(-18)$	$-1.8384(-18)$	$-5.2707(-17)$	$-5.1505(-17)$
$1s - 6s$	$-3.9511(-15)$	$-3.8566(-15)$	$-2.0028(-18)$	$-1.9511(-18)$	$-5.5040(-17)$	$-5.3750(-17)$
$1s - 7s$	$-4.0272(-15)$	$-3.9294(-15)$	$-2.0761(-18)$	$-2.0217(-18)$	$-5.6489(-17)$	$-5.5144(-17)$
$1s - 8s$	$-4.0771(-15)$	$-3.9770(-15)$	$-2.1248(-18)$	$-2.0686(-18)$	$-5.7447(-17)$	$-5.6065(-17)$
$1s - 9s$	$-4.1115(-15)$	$-4.0099(-15)$	$-2.1587(-18)$	$-2.1012(-18)$	$-5.8112(-17)$	$-5.6704(-17)$

–IV–

HIGHER-ORDER RESONANT RECOMBINATION PROCESSES

In the dielectronic recombination process involving two interacting electrons, as sketched in Fig. 4.1, the kinetic energy of the recombined electron is transferred to a single bound electron by a radiationless excitation to an intermediate autoionizing state. The recombination is completed by its radiative stabilization. For the case of highly charged ions (HCIs), radiative transition probabilities are high, and the competition of radiative deexcitation and Auger decay of the intermediate state is biased towards the first mechanism.

Beyond the well-known DR, resonant recombination processes involving higher-order correlations are relevant, too. Here, as displayed in Fig. 4.1, two or even three bound electrons can be simultaneously excited by the resonantly captured electron in trielectronic or even quadruelectronic recombination (TR and QR, respectively). The higher-order recombination mechanisms can be summarized by the equation

$$A^{q+} + e^- \rightarrow \left[A^{(q-1)+}\right]^{(n+1)*} \rightarrow A^{(q-1)+} + \text{photons}\,, \tag{4.1}$$

where n represents the number of simultaneously excited bound electrons, respectively the order of the resonant capture process.

Resonant mechanisms are highly efficient in either ionizing or recombining ions and hence already DR is of paramount importance for the physics of outer planetary atmospheres and interstellar clouds as well as an important radiative cooling mechanism in astrophysical and laboratory high-temperature plasmas [16,17,57]. DR often represents the dominant pathway for populating excited states in plasmas and, consequently, for inducing easily observable x-ray lines which are used as diagnostic tools for fusion plasmas (whereby Kr as well as Ar were chosen as ideal candidates) [22, 80], triggering a range of DR studies with highly charged Kr ions [11, 29, 66]. From a more fundamental point of view, the selectivity of DR [13] allows testing stringently sophisticated atomic structure and dynamics calculations, in particular of relativistic and quantum electrodynamic (QED) effects in bound electronic systems.

Investigating HCIs with DR offers additional important advantages including large cross sections and the magnification of relativistic and QED contributions by several orders of magnitude. These have been exploited in experiments both at electron beam ion traps (EBITs) (see, e.g., [32, 33, 42, 51, 60, 85]) and in storage rings (SRs). The $2s_{1/2} - 2p_{1/2}$ splitting in lithiumlike ions was determined in a SR with an accuracy capable of testing second-order QED corrections [13]. Direct EBIT spectroscopic measurements have achieved even higher precision [8]. Similarly, using DR in an ultra-cold electron target at a SR, the same splitting in Li-like Sc^{18+} has been indirectly determined with a precision of 4.6

ppm [55]. DR measurements have recently become sensitive to isotopic shifts in Li-like ^{142,150}Nd [12] and to the contribution of the generalized Breit interaction [60].

It is important to mention that in general TR and QR offer new photorecombination channels and their contribution to the radiative cooling of plasmas needs to be considered in the theoretical modeling. However, very scarce experimental data are available. At interaction energies of less than 52 eV, intra-shell TR resonances involving L-shell electrons of Cl^{13+} ions were observed at the TSR [70]. Contributions of roughly 10% to the total photorecombination rate at temperatures $T_e \approx 1$ to 100 eV (a range interesting for astrophysical photoionized plasmas) were found.

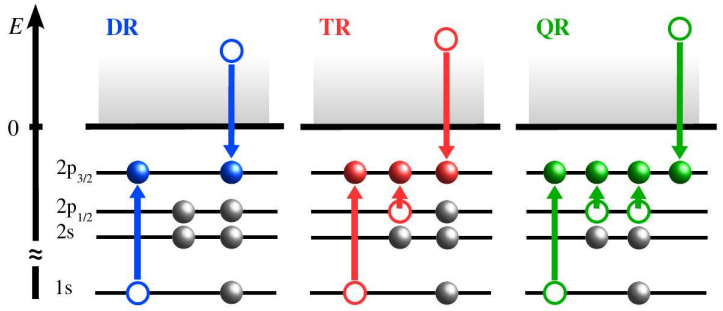

Figure 4.1: Scheme of correlated resonant electron recombination processes: In dielectronic recombination (blue) one bound electron is excited by the captured electron, in trielectronic recombination (red) two and in quadruelectronic recombination (green) three electrons are promoted to higher states by the captured electron (K-LL, KL-LLL and KLL-LLLL processes, respectively, where the initial and final shells of the bound and active electrons are specified).

4.1 Total cross section for resonant recombination processes

Cross section formulas for dielectronic recombination have been derived in the framework of several formalisms, including non-relativistic [41] and relativistic [74, 84] approaches. These results can be generalized to describe the higher-order correlated processes of trielectronic, quadruelectronic etc. processes as well. One can express the differential cross section in the solid angle Ω_k of the emitted photon as

$$\frac{d\sigma_{i\to f}}{d\Omega_k} = \frac{2\pi}{F_i}\sum_{dd'}\frac{\langle\Phi_f|H_{er}|\Phi_d\rangle\langle\Phi_d|V_{capt}|\Phi_i\rangle}{E-E_d+i\Gamma_d/2}\frac{\langle\Phi_f|H_{er}|\Phi'_d\rangle^*\langle\Phi'_d|V_{capt}|\Phi_i\rangle^*}{E-E_{d'}-i\Gamma_{d'}/2}\rho_f\,, \tag{4.2}$$

with H_{er} being the electron-radiation field interaction Hamiltonian and V_{capt} being the sum of the Coulomb and Breit interactions. In the above formula, E is the total initial energy of the system, and Φ_i, Φ_d and Φ_f (just as their counterparts with primed indices) denote the initial, intermediate and final states of a given recombination channel. E_d denotes the energy of the intermediate state including radiative corrections, and Γ_d is total decay width of that state. F_i and ρ_f stand for the incoming electron flux and the density of final photonic states, respectively. In the isolated resonances – or two-level – approximation the non-diagonal elements of the double sum above are neglected. The differential cross section becomes [84]

$$\frac{d\sigma_{i\to f}}{d\Omega_k} = \frac{2\pi}{F_i}\sum_{d}\frac{|\langle\Phi_f|H_{er}|\Phi_d\rangle|^2|\langle\Phi_d|V_{capt}|\Phi_i\rangle|^2}{(E-E_d)^2+\Gamma_d^2/4}\rho_f\,, \tag{4.3}$$

By definition the expression of cross section has to be averaged over the initial states and summed over the final states. This means an averaging over the magnetic sub-states M_i of the target ion and over the two spin projections m_s of the incoming electron, and summing over the magnetic sub-states M_f of the final state ion, integrating over the directions Ω_k and summing over the polarizations λ of the outgoing photon. We shall perform an extra averaging over the electron's emission solid angle, because the total cross section does not depend on the direction of the electron to be captured. These can be summarized as [41]

$$\sigma_{i\to f}^{DR} = \frac{2\pi^2}{p^2}\frac{A_r}{\Gamma_d} L_d(E - E_d - \Delta E_d) V_a \,, \tag{4.4}$$

with the rate of radiative decay from the state d to the final state f

$$A_r = \frac{2\pi}{2J_d+1}\sum_{M_f\lambda}\sum_{M_d}\int d\Omega_k |\langle \Psi_f; J_f M_f, \mathbf{k}, \lambda | H_{er} | \Psi_d; J_d M_d\rangle|^2 \rho_f \,, \tag{4.5}$$

where the total angular momentum of the intermediate state, J_d was introduced, and the normalized Lorentz resonance profile

$$L_d(E - E_d) = \frac{\Gamma_d/2\pi}{(E-E_d)^2 + \Gamma_d^2/4} \,. \tag{4.6}$$

The rate of resonant capture into the state d is given by [41]

$$V_a = \frac{p^2}{4\pi^2 F_i}\frac{1}{2(2J_i+1)}\sum_{M_i m_s M_d}\int d\Omega_p |\langle \Psi_d; J_d M_d | V_{capt} | \Psi_i; J_i M_i, \mathbf{p} m_s\rangle|^2 \,, \tag{4.7}$$

with the initial state total angular momentum J_i, and it is connected to its time-reversed analogue, the Auger (autoionization) rate A_a, by the principle of detailed balance [84]

$$V_a = \frac{2J_d+1}{2(2J_i+1)} A_a \,. \tag{4.8}$$

By definition the autoionization (Auger) rate is [84]

$$A_a = \frac{2\pi}{2J_d+1}\sum_{M_i m_s M_d}\int d\Omega_p |\langle \Psi_d; J_d M_d | V_{capt} | \Psi_i; J_i M_i, \mathbf{p} m_s\rangle|^2 \rho_i \,, \tag{4.9}$$

where $F_i\rho_i = p^2/(2\pi)^3$.

The appearance of higher-order processes, i.e. the trielectronic and quadruelectronic recombination channels with more than two active electrons can be understood as follows: Let us consider recombination with an initially C-like ion in its ground state, labeled by the dominant $|1s^2 2s^2 2p_{1/2}^2\rangle$ configuration. When describing TR, the autoionizing state can be approximated as a minimal linear combination of two configurations sharing total angular momentum and parity [10], $|\mathrm{TR}\rangle = c_1|1s2s^2 2p_{1/2} 2p_{3/2}^3\rangle + c_2|1s2s^2 2p_{1/2}^2 2p_{3/2}^2\rangle$. Here, the first term is the dominant one, as represented in the simplified scheme of Fig. 4.1. The neglect of the second term, i.e. the independent-particle (e.g. Hartree-Fock) approximation, would in the first order lead to a vanishing transition amplitude, $\langle 1s2s^2 2p_{1/2} 2p_{3/2}^3 | V_{Coul} | 1s^2 2s^2 2p_{1/2}^2\rangle = 0$. Only the inclusion of configuration mixing, a means of accounting for all-order electron correlation, leads to a non-vanishing amplitude $\langle \mathrm{TR}|V_{Coul}|1s^2 2s^2 2p_{1/2}^2\rangle = c_2\langle 1s2s^2 2p_{1/2}^2 2p_{3/2}^2|V_{Coul}|1s^2 2s^2 2p_{1/2}^2\rangle$. Thus higher-order processes appear only if correlation effects are taken into account and their measurement can benchmark more thoroughly their theoretical description both in terms of structure and dynamics. In spite of their relevance, the exact quantitative description of such correlations and their scaling with the number of involved electrons remains an open theoretical problem.

The resonance strength, which is defined as the integrated area under the peak for a given resonance, can be expressed as follows – provided the fluorescence x-rays are observed at 90° to the incoming electron beam as in case of a typical EBIT experiment [30]:

$$S_{idf}^{DR} = \frac{\pi\hbar^3}{2p^2}\left(1 - \frac{\beta_{df}}{2}\right)\frac{2J_d+1}{2(2J_i+1)}\frac{A_r^{df}A_a^{di}}{\sum_f A_r^{df} + A_a^{di}}\,. \tag{4.10}$$

In Eq. (4.10), the dipole angular distribution factor for photon detection perpendicular to the electron beam direction was taken into account by means of the anisotropy parameter β_{df} [30].

4.2 Description of the relativistic many-body system: the multiconfiguration Dirac-Fock method

For the description of bound atomic states present in the recombination channels we employ the widely used and versatile multiconfiguration Dirac-Fock (MCDF) method [24, 36]. The Dirac-(Hartree)-Fock (DF) method is the relativistic generalization of the well-known Hartree-Fock self-consistent procedure, as it is based on the Dirac equation rather than the Schrödinger wave equation.

In the DF scheme, an atomic state function is approximated in terms of a single Slater determinant, i.e. antisymmetrized product of Dirac single-electron orbitals, coupled to a well-defined total angular momentum J. Also, such a configuration state function, denoted by $|\gamma JP\rangle$, possesses a well-defined parity P, given as the product of individual parities of the single-electron orbitals involved in the determinant. The index γ represents here the set of quantum numbers necessary to fully define the configuration state function, i.e. the principal and angular momentum quantum numbers of the single-electron orbitals, the number of electrons in a given orbital, and the way the single-electron angular momenta j are coupled to the total angular momentum J.

In the multiconfiguration case, i.e. in the MCDF method, the DF approximation is extended by employing a linear combination of configuration state functions instead of a single one, i.e. the atomic state function is given by the ansatz

$$|\Gamma JP\rangle = \sum_i |\gamma_i JP\rangle\,. \tag{4.11}$$

Here, the different configuration state functions $|\gamma_i JP\rangle$ have different orbital occupations, however, they have the same symmetry, i.e. the same total angular momentum J and parity P.

We use the GRASP suite of codes (General Relativistic Atomic Structure Package) for the generation of these bound many-electron wave functions [24]. Further details on the method and the numerics used can be found in Ref. [24, 36].

4.3 Evaluation of Coulomb-Dirac continuum wave functions

In the initial state of the recombination process one has an electron in the positive continuum, and all other electrons are in the bound state of the target ion. One can make the ansatz [84]

$$\Psi(\gamma_i J_i M_i \mathbf{p} m_s) = \mathscr{A}[\Psi(\gamma_i J_i M_i) \otimes \psi_{\mathbf{p}m_s}(\mathbf{r})]\,. \tag{4.12}$$

The $\Psi(\gamma_i J_i M_i)$ is the wave function of the bound electrons of the ion with the angular momentum J_i and its projection M_i, and $\psi_{\mathbf{p}m_s}(\mathbf{r})$ is the wave function of the incoming electron, with a momentum $\mathbf{p}$ and

spin projection $m_s = \pm 1/2$. Just as in the previous section, the symbol γ_i summarizes all information necessary to specify the orbital occupation and the coupling.

For the continuum solutions one can use a partial wave expansion for the electron with asymptotic momentum $\mathbf{p}$ and the spin projection m_s [25]

$$\psi_{\mathbf{p}m_s}(\mathbf{r}) = \sum_{\kappa\mu} i^l e^{i\Delta_\kappa} \sum_{m_l} Y_l^{m_l *}(\hat{p}) C(l\tfrac{1}{2}j; m_l m_s \mu) \psi_{p\kappa\mu}(\mathbf{r})\,. \tag{4.13}$$

The phases Δ_κ are chosen in such a way that the wave function satisfies the boundary condition of an incoming plane wave and an outgoing spherical wave.

The Dirac bispinor wave function $\psi_{p\kappa\mu}(\mathbf{r})$ is calculated in the frozen orbital approximation. This means to solve numerically the Dirac equation with the nuclear potential screened by the bound electrons in the initial state in which the ionic states are assumed to be weakly influenced by the continuum electron. For highly charged ions, this assumption is well justified. By integrating the radial Dirac equations, one obtains the continuum radial functions $F_{p\kappa_p}(r)$ and $G_{p\kappa_p}(r)$ [36, 38]

$$\begin{aligned} \left(\frac{d}{dr} + \frac{\kappa_p}{r}\right) F_{p\kappa_p}(r) - \left(2c + \frac{\epsilon_p}{c} + \frac{Y_p(r)}{cr}\right) G_{p\kappa_p}(r) &= 0\,, \\ \left(\frac{d}{dr} - \frac{\kappa_p}{r}\right) G_{p\kappa_p}(r) + \left(\frac{\epsilon_p}{c} + \frac{Y_p(r)}{cr}\right) F_{p\kappa_p}(r) &= 0\,, \end{aligned} \tag{4.14}$$

with Y_p the screened potential. One should impose the boundary conditions

$$F_{p\kappa_p}(0) = 0\,, \quad G_{p\kappa_p}(0) = 0\,. \tag{4.15}$$

The normalization condition for these solutions is given as

$$\int_0^\infty dr \left(G_{p\kappa_p}(r) G_{p'\kappa'_p}(r) + F_{p\kappa_p}(r) F_{p'\kappa'_p}(r) \right) = \delta_{\kappa_p \kappa'_p} \delta(E - E')\,. \tag{4.16}$$

4.4 Calculation of Auger rates

The Auger decay rate of the autoionizing intermediate state d is, as defined previously,

$$A_a = \frac{2\pi}{2J_d + 1} \sum_{M_i m_s M_d} \int d\Omega_p |\langle \Psi_d; J_d M_d | V_{capt.} | \Psi_i; J_i M_i, \mathbf{p} m_s \rangle|^2 \rho_i\,, \tag{4.17}$$

where $V_{capt.}$ is the sum of the Coulomb potential and the Breit interaction. In the case of energy-normalized wave functions, $\rho_i = 1$. For coordinate representation of the initial state $|\Psi_i; J_i M_i, \mathbf{p} m_s\rangle$, after applying the partial wave expansion (4.13) one can obtain [84]

$$\begin{aligned} \Psi(\gamma_i J_i M_i \mathbf{p} m_s) = \sum_{\kappa\mu} i^l e^{i\Delta_\kappa} \sum_{m_l} Y_l^{m_l *}(\hat{p}) C(l\tfrac{1}{2}j; m_l m_s \mu) \\ \times \sum_{JM} C(J_i j J; M_i \mu M) \Psi(\gamma_i J_i M_i, p\kappa; JM)\,. \end{aligned} \tag{4.18}$$

The angular momentum J_i and its magnetic quantum number M_i corespond to the initial state. The configuration state function $\Psi(\gamma_i J_i M_i, p\kappa; JM)$ is an antisymmetrized product of the bound multi-electron state also including the continuum state. Knowing this, the Auger rate becomes [84]:

$$A_a = 2\pi \sum_\kappa |\langle \Psi_d; J_d || V_{capt} || \Psi_i; J_i, p\kappa; J_d \rangle|^2\,. \tag{4.19}$$

The reduced matrix element $\langle \Psi_d; J_d || V_{capt} || \Psi_i; J_i, p\kappa; J_d \rangle$ is defined as in Ref. [15]. It is independent of the magnetic quantum numbers. These matrix elements have been computed numericaly by using an adopted version of the code AUGR [83], an extension of the GRASP 1.0 suite of codes [24].

In particular, the matrix elements of the Coulomb potential with configuration state functions can be written as a linear combination of products of angular coefficients and two-electron radial integrals:

$$\langle \gamma_r J_r | \sum_{i<j} \frac{1}{|\mathbf{r}_i - \mathbf{r}_j|} | \gamma_s J_s \rangle = \sum_{abcd} \sum_k V_{rs}^k(abcd) R^k(abcd) \,, \tag{4.20}$$

The rather involved coefficients $V_{rs}^k(abcd)$ have been evaluated by the MCP code [35]. The radial integrals $R^k(abcd)$ are defined as [24]

$$R^k(abcd) = \int_0^\infty dr \left[(F_{n_a\kappa_a}(r) F_{n_c\kappa_c}(r) + G_{n_a\kappa_a}(r) G_{n_c\kappa_c}(r)) \frac{1}{r} Y^k(bd; r) \right] \,, \tag{4.21}$$

with the relativistic Hartree Y-functions

$$Y^k(ac; r) = r \int_0^\infty ds \frac{r_<^k}{r_>^{k+1}} [F_{n_a\kappa_a}(r) F_{n_c\kappa_c}(r) + G_{n_a\kappa_a}(r) G_{n_c\kappa_c}(r)] \,. \tag{4.22}$$

The Breit interaction between the electrons 1 and 2 is defined as [36]

$$V_{\rm Breit}(1,2) = -\boldsymbol{\alpha}_1 \boldsymbol{\alpha}_2 \frac{\cos(\omega R)}{R} + (\boldsymbol{\alpha}_1 \nabla_1)(\boldsymbol{\alpha}_2 \nabla_2) \frac{\cos(\omega R) - 1}{\omega^2 R} \,, \tag{4.23}$$

where ω denotes the energy of the virtual photon exchanged and the distance of the electronic vectors is $R = |\mathbf{r}_1 - \mathbf{r}_2|$. The matrix element can be expressed as [24]

$$\langle \gamma_r J_r | \sum_{i<j} V_{Breit}(i,j) | \gamma_s J_s \rangle = \sum_{abcd} \sum_{k\tau} V_{rs}^{k\tau}(abcd) S^{k\tau}(abcd) \,. \tag{4.24}$$

In the angular coefficients $V_{rs}^{k\tau}$ the index τ differentiates different types of integrals. They can be evaluated using the MCBP code [37]. The expressions for the radial integrals $S^{k\tau}(abcd)$ can be found in Ref. [24], and they are calculated numerically by the code BENA [37].

4.5 Radiative transitions between many-electron states

In this section we outline the calculation of radiative transition probabilities between many-electron states as described by MCDF state vectors. This can be regarded as a straightforward generalization of the calculation of radiative rates involving single-electron states as derived in Chapter 2. In Section 4.1, the electromagnetic transition probability from the intermediate state d to the final state f by the emission of a photon with all possible wave number vectors $\mathbf{k}$ and polarizations λ was defined as

$$A_r^{d\to f} = \frac{2\pi}{2J_d + 1} \sum_{M_d} \sum_{M_f \lambda} \int d\Omega_k |\langle \Gamma_f J_f M_f; \mathbf{k}, \lambda | H_{er} | \Gamma_d J_d M_d; 0 \rangle|^2 \rho_f \,, \tag{4.25}$$

where H_{er} is the electromagnetic interaction operator. We can express the matrix element between two atomic state functions d and f as [24]

$$\langle \Gamma_f J_f M_f; \mathbf{k}, \lambda | H_{er} | \Gamma_d J_d M_d; 0 \rangle = \sum_{r,s=1}^{n_c} c_{r\Gamma_f}^* c_{s\Gamma_d} \langle \gamma_r J_r M_r; \mathbf{k}, \lambda | H_{er} | \gamma_s J_s M_s; 0 \rangle \,. \tag{4.26}$$

In order to be able to evaluate the matrix elements of H_{er}, one should expand it in multipole components. This means to decompose it in a sum of electric and magnetic multipoles, i.e., $\mathbf{a}^{(0)}_{LM}(r)$ and $\mathbf{a}^{(1)}_{LM}(r)$. The matrix element becomes [36, 46]

$$\begin{aligned}\langle\gamma_r J_r M_r;\mathbf{k},\lambda|H_{er}|\gamma_s J_s M_s;0\rangle &= \sqrt{\frac{2\pi c^2}{\omega_{\mathbf{k}} V}}\sum_L\sum_M \sqrt{2\pi}(-i)^L\sqrt{2L+1}D^L_{M,-\lambda}(\hat{k}) \\ &\times \left[\langle\gamma_r J_r M_r|\boldsymbol{\alpha}\mathbf{a}^{(0)}_{LM}(r)+i\lambda\boldsymbol{\alpha}\mathbf{a}^{(1)}_{LM}(r)|\gamma_s J_s M_s\rangle\right].\end{aligned} \tag{4.27}$$

The rotation matrix $D^L_{M,-\lambda}(\hat{k})$ is defined in Ref. [67].

Introducing the re-coupling coefficients $d^L_{ab}(rs)$ (Ref. [65]), one can write the reduced matrix elements between configuration state functions as a linear combination of single-electron reduced matrix elements in the following way:

$$\langle\gamma_r J_r M_r||O^{(L)}||\gamma_s J_s M_s\rangle = \sum_{ab} d^L_{ab}(rs)\langle n_a\kappa_a||O^{(L)}||n_b\kappa_b\rangle\,, \tag{4.28}$$

with $O^{(L)}$ the spherical tensor operator defined in Ref. [67]. The magnetic and electric one-particle matrix elements are in the Coulomb gauge [36]

$$\begin{aligned}\langle f||\boldsymbol{\alpha}\mathbf{a}^{(0)}_{LM}||i\rangle &= i(-1)^{j_i+L+1/2}\sqrt{\frac{(2j_i+1)(2L+1)}{4\pi L(L+1)}} \\ &\times \begin{pmatrix} j_f & j_i & L \\ \frac{1}{2} & -\frac{1}{2} & 0\end{pmatrix}(\kappa_f+\kappa_i)\left[\int dr(F_f(r)G_i(r)+F_i(r)G_f(r))j_L(kr)\right],\end{aligned} \tag{4.29}$$

$$\begin{aligned}\langle f||\boldsymbol{\alpha}\mathbf{a}^{(1)}_{LM}||i\rangle &= i(-1)^{j_i+L+1/2}\sqrt{\frac{2j_i+1}{4\pi}}\begin{pmatrix} j_f & j_i & L \\ \frac{1}{2} & -\frac{1}{2} & 0\end{pmatrix} \\ &\times \left[\sqrt{\frac{L+1}{L(2L+1)}}\left(LI^-_{L-1}-(\kappa_f-\kappa_i)I^+_{L-1}\right)\right. \\ &+ \left.\sqrt{\frac{L}{(L+1)(2L+1)}}\left((L+1)I^-_{L+1}+(\kappa_f-\kappa_i)I^+_{L+1}\right)\right],\end{aligned} \tag{4.30}$$

with the integrals

$$I^{\pm} = \int dr\,(F_f(r)G_i(r)\pm F_i(r)G_f(r))\,j_L(kr)\,. \tag{4.31}$$

The radial orbital functions $F_i(r)$, $G_i(r)$, $F_f(r)$ and $G_f(r)$ are generated numerically in the MCDF procedure as summarized before, and these functions are used to evaluate the radial integrals by numerical quadrature. This task is performed by the OSCL module of the GRASP 1.0 package of codes [24].

4.6 Comparision of theoretical and experimental results

Once the bound-state wave functions and energies, and the radiative and Auger transition rates have been calculated, the cross section and related quantites like the resonance strength can be evaluated. Fig. 4.2

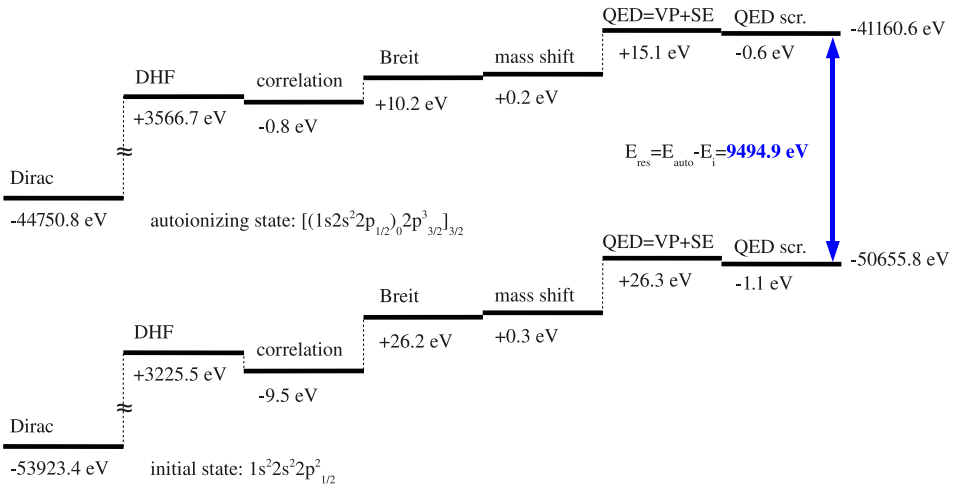

Figure 4.2: Different contributions to the energy of the ground state and the excited autoionizing state of a given transition in C-like Kr, as calculated with the methods presented in the previous sections.

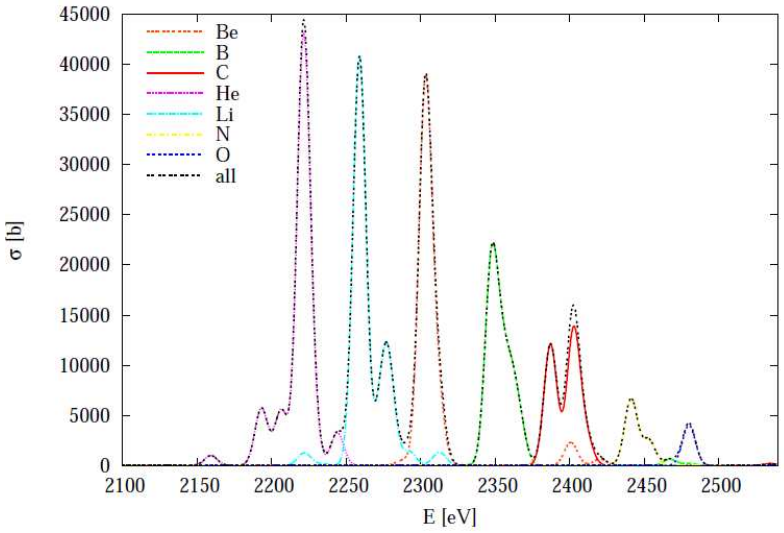

Figure 4.3: Total calculated cross section for resonant recombination, involving DR, TR and QR channels, for few-electron Ar ions. The electron energy range of the K-LL resonances is shown. The Lorentzian peaks have been convoluted with a Gaussian line shape with a FWHM of 10 eV for better comparision with experiments.

illustrates the magnitude of contributions to the transition energy of a trielectronic resonance in the C-like krypton ion. Such calculations have been performed to all possible transitions in the relevant K-LL energy range for He-, Li-, Be-, B-, C-, N-, and O-like Ar, Fe, and Kr ions, however, we do not list all numbers here. In Figs. 4.3 and 4.4 we show total theoretical cross sections for resonance recombination in highly charged Ar- and Fe-ions, respectively, as a function of the electron beam energy.

Fig. 4.5 shows the relative strength of certain TR transitions as compared to the dominant DR process in some few-electron charge states.

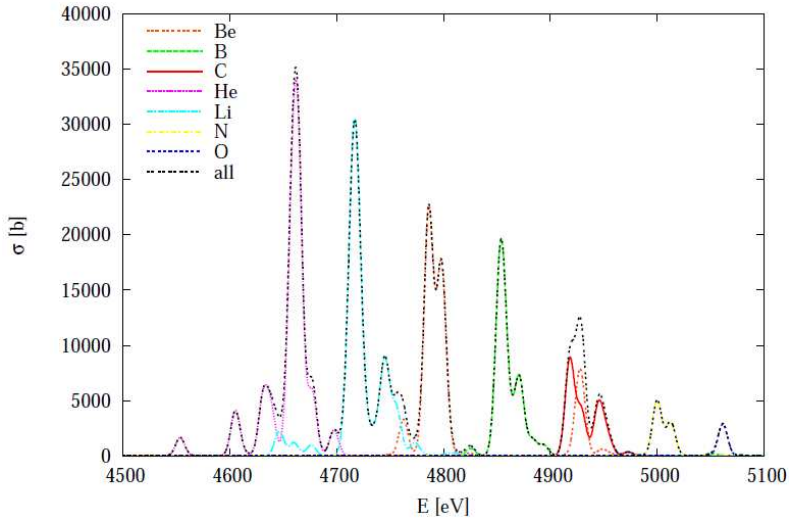

Figure 4.4: Total calculated cross section for resonant recombination, involving DR, TR and QR channels, for few-electon Fe ions. The electron energy range of the K-LL resonances is shown.

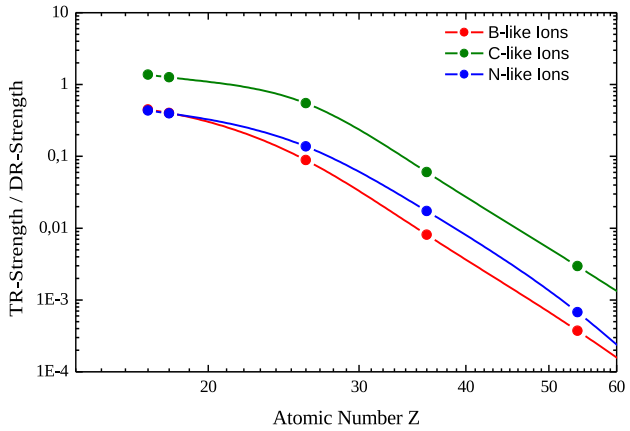

Figure 4.5: Ratio of trielectronic to dielectronic recombination resonance strengths for elements with different atomic numbers Z for certain transitions involving the B-, C- and N-like charge states. As expected, the relative weight of the TR process which is due to higher-order electron correlation decreases for stronger central Coulomb fields.

The experiment was performed at the Heidelberg EBIT [20] where highly charged Kr, Fe and Ar ions were produced and radially trapped by an electron beam, as explained at the end of Chapter 2. A magnetic field of 8 T compresses the beam to a radius of ≈ 22 μm. The ions were axially confined by electrostatic potentials applied to a set of drift tubes. The electron beam energy was swept over the expected range of resonance energies. Photons emitted as signature of the direct and indirect photorecombination and their cascades were detected with a high-purity germanium x-ray detector having a resolution of about 350 eV viewing the trap in a direction perpendicular to the exciting beam. The photons counted are

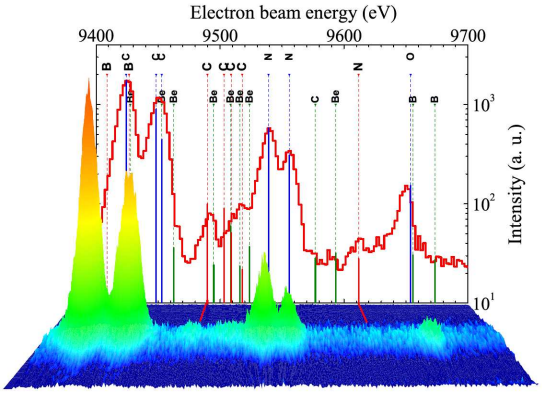

Figure 4.6: DR and TR resonances in the K-LL DR region of C- to O-like Kr ions as a projection and in three-dimensional illustration (photon intensity against electron beam energy and photon energy). Predictions (this work) for DR, TR and QR resonances and their strength are marked by blue, red and green lines, respectively. At the top the calculated resonances (color coded) for differently charged ion species are indicated.

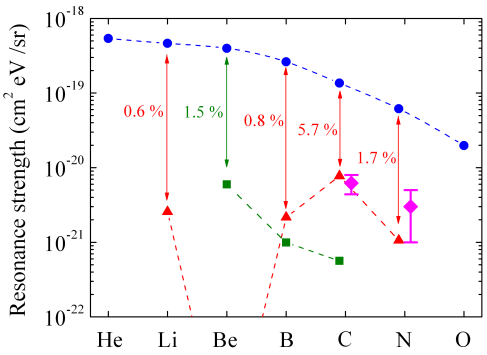

Figure 4.7: DR, TR and QR resonances strengths for He- to O-like Kr ions. Theory: DR, blue circles; TR, red triangles; QR, green squares. Measured TR strength: magenta diamonds. The relative strengths of the higher-order recombination processes with respect to total DR are indicated.

represented in a two-dimensional intensity plot as a function of the electron beam energy. Bright spots at well-defined electron and photon energies reveal the recombination resonances in the illustration in Fig. 4.6. Projecting the counts within a certain photon energy region around the energy difference of the K and L shell (about 13 keV) onto the beam energy axis yields the energy-differential cross section of the photorecombination under perpendicular observation. An excellent electron energy resolution of about 13 eV FWHM at 10 keV was accomplished in the EBIT and actually was prerequisite to resolve the weak peaks corresponding to inter-shell TR and separate them from the roughly twenty times stronger DR features.

Fig. 4.6 presents an example of resonances appearing in the electron energy region of C- to O-like K-LL DR. Well-resolved DR and TR resonances of C- to O-like Kr ions are found. Close to their theoretically expected positions, signatures of C- and Be-like inter-shell QR resonances are indicated as well. The experimental resonance energies for inter-shell TR as well as the signatures of QR are compared to the theoretical values in Table 4.1. Our predictions agree very well within error bars with the inter-shell TR

Table 4.1: Predicted and measured energies of selected dielectronic (TR), trielectronic (TR) and quadruelectronic (QR) resonances for Be-like to O-like Kr ions. The autoionizing configurations are given in the jj coupling notation; subscripts following round brackets denote the angular momentum of coupled subshells and subscripts following square brackets stand for the total angular momentum of the level. The experimental errors correspond to statistical uncertainties.

Process	charge state	intermediate state	E_{exp} (eV)	E_{theo} (eV)
DR	C	$[1s2s^22p_{1/2}^2(2p_{3/2}^2)_2]_{5/2}$	9429.0(2)	9429(5)
DR	C	$\left\{ \begin{array}{l} [1s2s^22p_{1/2}^2(2p_{3/2}^2)_2]_{3/2} \\ [1s2s^22p_{1/2}^2(2p_{3/2}^2)_0]_{1/2} \end{array} \right\}$	9455.0(3)	9455(5)
DR	N	$[1s2s^22p_{1/2}^2 2p_{3/2}^3]_2$	9543.9(3)	9543(6)
DR	N	$[1s2s^22p_{1/2}^2 2p_{3/2}^3]_1$	9561.6(4)	9560(6)
DR	O	$[1s2s^22p_{1/2}^2 2p_{3/2}^4]_{1/2}$	9653.8(4)	9653(7)
TR	C	$[(1s2s^22p_{1/2})_0 2p_{3/2}^3]_{3/2}$	9496.3(3)	9495(4)
TR	C	(blend)	9514.3(3)	9514(5)
TR	N	$[(1s2s^22p_{1/2})_1 2p_{3/2}^4]_1$	9617.5(7)	9616(6)
QR	Be	$[1s2p_{3/2}^4]_{1/2}$	9594(2)	9598(4)
QR	C	$[1s2s^22p_{3/2}^4]_{1/2}$	9576(2)	9582(4)

results and reasonably with the weaker QR signatures.

In Fig. 4.6 the theoretical resonance strengths were also normalized to the earlier mentioned C-like DR resonance line for Be-like, B-like and C-like Kr and to the first corresponding DR line for N-like and O-like ions. These values also show a good agreement with our predictions, thus further confirming the identification of the features as inter-shell TR resonances.

An overview on the calculated and measured DR, TR and QR resonance strengths is shown on Fig. 4.7. The DR strength decreases monotonically with a growing number of L electrons. For inter-shell TR, the possible range of ion charge states spans from the Li- to the N-like isoelectronic sequence. It is noteworthy that the predicted KL-LLL TR strength vanishes for initially Be-like ions due to parity reasons: while the TR resonances should necessarily be described by $|1s2s2p^3\rangle$ configurations possessing negative parity, the nearby K-LL DR configurations $|1s2s^22p^2\rangle$ are of positive parity, forbidding the requested admixtures. For this case, QR is the dominant higher-order recombination process. Interestingly, the ratio of inter-shell TR to the *total* DR resonance strength reaches values of up to 6% for C-like Kr^{30+}. This demonstrates that higher-order recombination processes of such mid-Z HCI contribute in the $1-10\,\%$ range to the total resonant photorecombination at interaction energies as high as 10 keV, which are relevant in the temperature range from $T_e = 500\,\mathrm{eV}$ upwards. The measured values confirm this statement. Experimental total TR resonance strengths of $(6.2\pm1.8)\times10^{-21}$ cm^2 eV sr^{-1} for C-like and $(3\pm2)\times10^{-21}$ cm^2 eV sr^{-1} for N-like ions agree reasonably well with theoretical values, as seen on Fig. 4.7. Moreover, they are remarkably large for a higher-order process in an inter-shell reaction involving a K-shell excitation. Studying HCIs at lower and higher Z values and, therefore, shifting from the nonrelativistic to the relativistic regime helps quantifying these contributions for the benefit of fundamental aspects and of plasma physics applications.

These considerations lead to the EBIT measurement of resonant recombination cross sections with the somewhat lighter Fe ions. Fig. 4.8 shows an experimental spectrum for this case. Beyond the TR

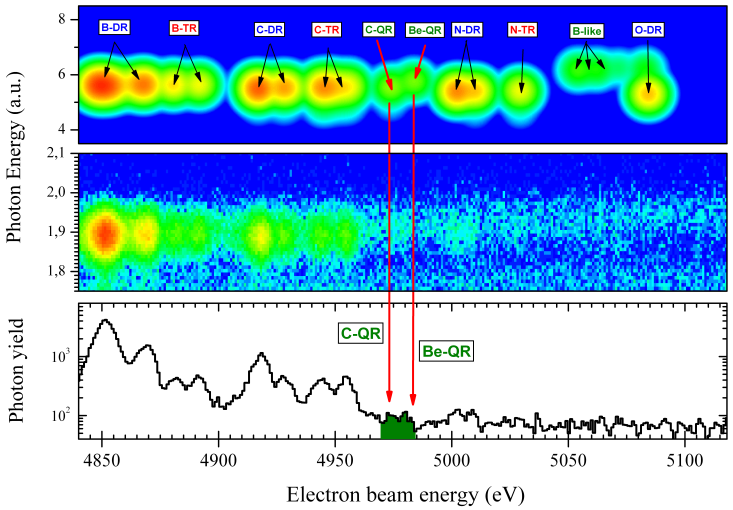

Figure 4.8: Theoretical (uppermost panel) and experimental (middle panel) intensity (arbitrary units) of x-ray emission as a function of the x-ray photon energy and the electron beam energy, for B- to O-like Fe ions [9]. Also, the photon yield integrated over the x-ray energies is shown in the bottom panel. The light spots correspond to DR, TR and QR resonances. QR resonances, indicated by the long red arrows and the green area, have been observed for the first time.

peaks observed just as in the case of Kr, by the help of our theoretical calculations QR peaks have been unambiguously identified for the first time. They appear in the spectral range of the C- and Be-like Fe ions.

–V–

CONCLUSIONS AND OUTLOOK

5.1 Conclusions

In this thesis we theoretically investigated relativistic processes in highly charged ions, where strong electromagnetic fields play a decisive role.

In Chapter 2 we developed a fully relativistic ab initio theory of the bound dynamics of atomic systems in laser fields ranging to the x-ray domain. This study completes and extends a number of earlier investigations on the response of three-level atoms to external driving fields. Due to the interference effects, multilevel atoms may feature much more effects than two-level systems. In this thesis we have studied the spontaneous emission characteristics of a V-model atom. The presence of two driving fields can largely modify the shape of the emission spectrum.

As relativistic effects on the bound electronic wave function increase rapidly with the nuclear charge number Z, one needs to formulate a fully relativistic theory of coherent laser-atom interaction. The bare atomic states are constructed from solutions of the Dirac equation. This approach allows for exploiting the sensitivity of inner-shell electrons to relativistic electron correlation, QED and nuclear effects in strong Coulomb fields. Also the description of the theory beyond dipole approximation allowed us to describe forbidden transitions such as $M1$ transitions. As a demonstrative example, a means to determine ionic transition multipole moments and frequencies via a three-level configuration driven by an x-ray and an optical field has been put forward. Current or near-future laser systems are expected to increase the accuracy of multipole moment determinations from the current 10^{-3} level (via lifetime measurements) to the 10^{-4} range or better. Furthermore, the undesirable trapping of atomic population in a long-lived metastable state – naturally occurring in certain three-level systems – can be reversed by the scheme presented here. Other scenarios developed for the quantum control of non-relativistic resonance fluorescence emission [48, 64, 71, 81, 82] are anticipated to yield further improvement of detection and accuracy.

The inner-shell electrons in highly charged ions have a large overlap with the nuclear matter. Also, the relative simplicity of electronic shell structure in such few-electron ions allows for the accurate theoretical extraction of nuclear proton distribution parameters from isotope shift data, as shown in the first half of Chapter 2. Here, we have investigated isotope shifts measurements and we have extracted information on heavy nuclei via resonance fluorescence of a two-level atomic configuration driven by a short-wavelength laser field.

For the case of ions or atoms driven by lasers with off-resonant frequencies, shifts of hydrogenic energy levels were calculated in Chapter 3 in an analytical way. Interaction with the monofrequent laser field is

treated by second-order time-dependent perturbation theory. Our formalism goes beyond the Stark long-wavelength dipole approximation and takes into account non-dipole effects of retardation and interaction with the magnetic field components of the laser beam. The technics is based on the adiabatically damped Babushkin gauge interaction. This procedure is based on using the unperturbed Hamiltonian, and treating the interaction $\boldsymbol{\alpha} \cdot \boldsymbol{A}$ as the perturbation. This interaction gives rise to a dynamic Stark shift. In order to calculate the matrix elements, we used the fully relativistic wavefunction, solutions of the Dirac-Coulomb equation. Because the transition is off-resonant, a Green function representing an infinite sum over virtual bound states and integration over all virtual continuum states is involved. The computation takes advantage of an expansion over a Sturmian basis of the first-order Dirac-Coulomb Green function.

At high laser intensities, the light shifts are found to be sizable, especially for excited states with lower binding energies. These results are relevant in current and near-future spectroscopic experiments, especially for experiments employing advanced light sources in the x-ray regime. This motivates further study of the interaction of heavy atoms or ions with an intense, high frequency, radiation field. The result of the Stark shift calculation shows that the relativistic contributions are indeed significant. In comparison with the usual nonrelativistic dipole treatment, the influence of relativity is to decrease the magnitude of the transition matrix elements in two-photon processes. It appears also that retardation effects cannot be neglected. The relativistic corrections should be included even for small $Z \approx 20$ and become clearly necessary for higher nuclear charges. We saw also that the dipole approximation is a reasonable approximation in most cases, where only the retardation effects should be added.

A further central point of this work has been the process of dielectronic (DR), trielectronic (TR) and quadruelectronic (QR) recombination via the KLL resonant channels. We have analyzed various effects which contribute to the resonance energies observed in DR, TR and QR into He-, Li-, Be-, B-, C-, N-, and O-like Ar, Fe, and Kr ions. We applied the multiconfiguration Dirac-Fock method to determine atomic state functions and energies. Our calculations include Coulomb and Breit correlation contributions, approximations for the many-electron QED terms as well as finite nuclear size effects. The comparison of our theoretical values with the experimental data shows a good overall agreement.

Due to the complex nature of the physical problem, results in many-body theories are commonly provided without error estimates in the literature. In our work we assigned theoretical uncertainties to the transition energies. On the theoretical side, the largest error bars are due to QED screening effects and electron correlation contributions. As electron interaction terms to DR, TR and QR energies beyond the no-pair approximation may not be negligible in the case of heavy ions, the calculation of such terms is necessary in the future to improve the accuracy of theoretical results.

The previously unobserved processes of TR and QR have been unambiguously identified in EBIT measurements performed at the Max Planck Institute for Nuclear Physics [10], involving for the first time a K-shell electron as one of the actors. By investigating the electronic rearrangements taking place in such multiple excitations, new access to the study of dynamic correlations of bound electrons is presented. In the case of Kr ions, the inclusion of these hitherto unexplored contributions raises the total resonant photorecombination x-ray yield by up to 6% at temperatures in the $T_e > 500\,\mathrm{eV}$ range, an effect which has to be considered in the quantitative modeling of fusion and other hot, e. g. , astrophysical plasmas. Future improvements experimental in resolution – e.g. by means of the forced evaporative cooling technique [10] to decrease Doppler broadening due to ionic motion – may even enable A A.detailed studies of the hyperfine structure as well as of isotopic shifts.

5.2 Outlook

In this thesis, a versatile fully relativistic theory of correlated electronic dynamics in strong Coulomb and laser fields has been developed. Beyond the dynamic processes and level shifts investigated in this work, a range of other phenomena may be theoretically studied using the same framework.

As seen in Chapter 2, the resonance fluorescence spectrum bears the signature of the driving process. For monochromatic x-ray light, the spectrum exhibits sidebands with positions determined by the Rabi frequency. By superimposing a second color, e.g., an optical laser, an efficient manipulation of the fluorescence spectrum could be achieved, e.g., in a V-type system the spectral line widths can be narrowed by several orders of magnitude. For future investigations, one may think of other schemes in which an x-ray transition is strongly driven and the fluorescence spectrum is manipulated with optical light. This should imprint a clear signature on the fluorescence spectrum as seen in our V-type system. Specifically, one may ask the question what effect an optical twin pulse or a frequency comb have on the fluorescence spectrum. To this end, the formalism of Chapter 2 needs to be extended to describe the dynamics in the time domain. This may offer the opportunity for novel frequency combs at x-ray wavelengths, a finer control over the comb and novel spectroscopic methods. A potential application is a more accurate spectroscopy of highly charged ions.

Diffraction of x rays represents a salutary method to learn about ionic structure since the photons that are irradiated and scattered interact only weakly with other ions or electrons in the interaction volume. This is particularly beneficial for the spectroscopy of highly charged ions. In this context, one may investigate Raman scattering (Stokes and anti-Stokes processes) of highly charged ions with transitions in the x-ray range. A high x-ray flux from free electron lasers [1, 2] appears to be necessary to compensate for the somewhat lower cross sections.

The perturbative description of non-resonant light shifts, described in Chapter 3, may be employed with little modifications to further two-photon processes: excitation, ionization and electron-positron (or, in general, fermion-antifermion) pair creation. These processes are illustrated in Fig. 5.1. In case of excitation, the second-order electrodynamic process promotes a bound electron initially in the ground state to an excited bound state. For ionization, this final state is replaced by an electronic wave function belonging to the continuous part of the spectrum with an electron energy above $+mc^2$. Pair creation in a Coulomb field occurs when the initial electronic state has an energy below $-mc^2$ („Dirac sea“), and then photon absorption promotes the fermion into a bound or positive continuum state (bound-free and free-free pair production, respectively).

These processes are not only interesting from an academic point of view but they also have important experimental applications. The theoretical understanding of relativistic two-photon excitation is required to conceive Doppler-free two-photon spectroscopic experiments with trapped ions, especially for highly charged ions where a relativistic treatment is mandatory. Our treatment applies for a broad range of transition energies, also allowing to perform studies in the x-ray range. The scheme of such experiments, allowing for the determination of ionic transition energies with accuracies much higher than presently possible, is shown in Fig. 5.2. As the laser intensities required for two-photon excitation are anticipated to be rather high, the levels involved in the transition are shifted by the polarization effects discussed in Chapter 3, therefore, the light shift effect calculated in the present work plays an important role in the interpretation and analysis of such experiments.

The two-photon ionization of highly charged ions is anticipated to become feasible by the use of upcoming intense x-ray free electron lasers such us the LCLS [2] and XFEL [1] facilities, equipped with transportable EBITs providing the trapped ions as targets. Experiments of this type are planned by the Max Planck Institute for Nuclear Physics, therefore, thorough theoretical investigation are necessary.

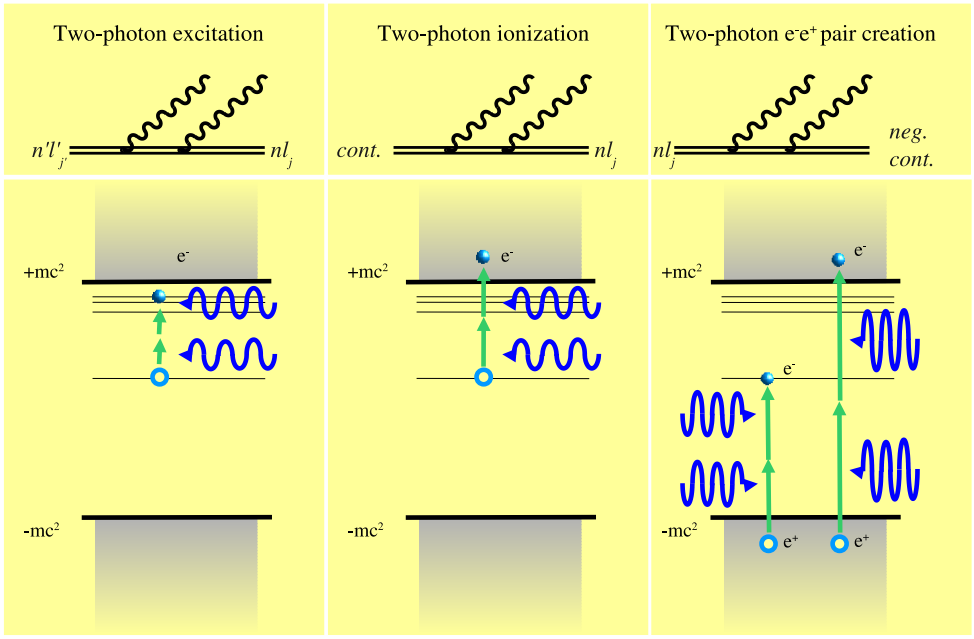

Figure 5.1: Two-photon processes involving highly charged ions: excitation, ionization, and free-free and bound-free electron-positron pair creation, respectively. The panels in the upper row show the Feynman diagrams of the corresponding processes, while the panels in the lower row show the level structures involved. See text for further details.

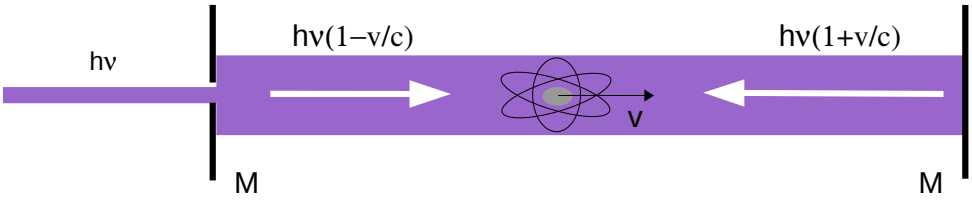

Figure 5.2: Scheme of a Doppler-free spectroscopic experiment with two-photon excitation. The atomic transition corresponds to two times the photon energy $h\nu$. The incoming laser light is split into two counter-propagating beams by the use of two parallel planar mirrors (M). The atoms (or ions), trapped in the interaction region between the mirrors, move with a random thermal velocity v. In the reference frame of the ion, the photons arriving from the two different directions have slightly Doppler-shifted frequencies; however, as the shifts have different signs in the dominant linear order in v/c, the blue and red shifts largely cancel. As a consequence, all ions (possessing different velocities) can absorb two laser photons and emit fluorescence photons.

The perturbative treatment developed for the calculation of light shift of energy levels (Chapter 3) can be extended to bound-continuum transitions in a straightforward way. Also, the inclusion of resonance pathways (resonant excitation-ionization) is feasible by means of a density operator approach such as that applied for relativistic resonance fluorescence in Chapter 2.

The direct production of electron-positron or even the heavier muon-antimuon pairs by two-photon absorption from a high-frequency laser wave colliding with an atomic nucleus has been investigated recently [59]. The process is sensitive to the nuclear form factor, i.e. electrodynamic nuclear properties

such as charge radii and other parameters of the protonic charge distribution. It could be realized experimentally by combining radiation from upcoming x-ray free electron or high harmonic generation [58] laser sources with an ultra-relativistic ion beam from the present accelerator generation. In Ref. [59], the strong field approximation has been employed, i.e. the created fermionic pair was described by Volkov wave functions accounting for interaction with the intense laser field but fully neglecting interaction with the nucleus. This description may be refined by our formalism described in Chapter 3, taking into account the nuclear potential to all orders. In the case of $\mu^+\mu^-$ pairs, the wave functions and the analytic Sturmian basis set corresponding to a pointlike nucleus have to be substituted with their counterparts integrated in the potential of an extended nucleus.

–APPENDIX A–

COULOMB-DIRAC GREEN'S FUNCTION IN THE STURMIAN REPRESENTATION

Given a Hermitian operator H, the corresponding resolvent or Green operator $G(z)$ is defined by [79]

$$(H - z)G(z) = 1, \tag{A.1}$$

where z is a complex number and corespond to the energy variable. Let us assume that H possesses a complete set of eigenfunctions Φ_n corresponding to eigenvalues E [79]:

$$(H - E_n)\Phi_n = 0\,, \tag{A.2}$$

$$\sum_n \Phi_n \Phi_n^\dagger = 1\,. \tag{A.3}$$

In the spectral representation, $G(z)$ is formally given by [79]

$$G(z) = -\sum_n \frac{\Phi_n \Phi_n^\dagger}{z - E_n}\,. \tag{A.4}$$

Generally, the summation is performed over a discrete and a continuous spectrum of eigenfunctions.

Let us represent H by a differential operator H_r acting on a Hilbert space of functions on R^3, and $G(z)$ represented by a function $G(\boldsymbol{r_1}, \boldsymbol{r_2}; z)$ on $R^3 \times R^3$. They satisfies the equation

$$(H_{\boldsymbol{r_1}} - z)G(\boldsymbol{r_1}, \boldsymbol{r_2}; z) = \delta(\boldsymbol{r_1} - \boldsymbol{r_2})\,. \tag{A.5}$$

For a certain class of Hamiltonians, the Green's function can be given analytically, without explicitly carrying out the summation over a complete spectrum. The Green's function associated with the Dirac-Coulomb Hamiltonian can be decomposed into radial and angular parts as [44]

$$G(\boldsymbol{r}_1, \boldsymbol{r}_2; E_n) = \frac{1}{c\hbar} \begin{pmatrix} G^{11} & G^{12} \\ G^{21} & G^{22} \end{pmatrix}\,, \tag{A.6}$$

where in the components G^{ij}, $i, j \in \{1, 2\}$, which are 2×2 matrices, we omitted the coordinate and

energy arguments for brevity. They can be decomposed as

$$\begin{aligned} G^{11} &= \sum_{\kappa_n m_n} g^{11}_{\kappa_n}(r_1, r_2; E_n)\Omega_{\kappa_n m_n}(\hat{r})\Omega^*_{\kappa_n m_n}(\hat{r'})\,, \\ G^{12} &= \sum_{\kappa_n m_n} -ig^{12}_{\kappa_n}(r_1, r_2; E_n)\Omega_{\kappa_n m_n}(\hat{r})\Omega^*_{-\kappa_n m_n}(\hat{r'})\,, \\ G^{21} &= \sum_{\kappa_n m_n} ig^{21}_{\kappa_n}(r_1, r_2; E_n)\Omega_{-\kappa_n m_n}(\hat{r})\Omega^*_{\kappa_n m_n}(\hat{r'})\,, \\ G^{22} &= \sum_{\kappa_n m_n} g^{22}_{\kappa_n}(r_1, r_2; E_n)\Omega_{-\kappa_n m_n}(\hat{r})\Omega^*_{-\kappa_n m_n}(\hat{r'})\,. \end{aligned} \tag{A.7}$$

The radial components g^{ij} can be represented as an expansion involving Laguerre polynomials [44]:

$$\begin{aligned} g^{11}_{\kappa_n} &= \frac{1}{2\varepsilon}(2\lambda_n)^{2\gamma_n}(rr')^{\gamma_n-1}e^{-\lambda_n(r+r')}\sum_{n=0}^{\infty}\Bigg((\kappa_n+\nu/\epsilon_n)\frac{n!}{\Gamma(2\gamma_n+1+n)}\frac{L_n^{2\gamma_n}(2\lambda_n r)L_n^{2\gamma_n}(2\lambda_n r')}{n+\gamma_n+1-\nu} \\ &- [(\kappa_n-\nu/\epsilon_n)+2(\gamma_n+\nu)]\frac{n!}{\Gamma(2\gamma_n+1+n)}\frac{L_n^{2\gamma_n}(2\lambda_n r)L_n^{2\gamma_n}(2\lambda_n r')}{n+\gamma_n-\nu} \\ &+ \frac{n!}{\Gamma(2\gamma_n+n)}\frac{L_n^{2\gamma_n-1}(2\lambda_n r)L_n^{2\gamma_n}(2\lambda_n r')+L_n^{2\gamma_n}(2\lambda_n r)L_n^{2\gamma_n-1}(2\lambda_n r')}{n+\gamma_n-\nu}\Bigg)\,, \end{aligned} \tag{A.8}$$

$$\begin{aligned} g^{12}_{\kappa_n} &= \frac{1}{2}(2\lambda_n)^{2\gamma_n}(rr')^{\gamma_n-1}e^{-\lambda_n(r+r')}\sum_{n=0}^{\infty}\Bigg((\kappa_n+\nu/\epsilon_n)\frac{n!}{\Gamma(2\gamma_n+1+n)}\frac{L_n^{2\gamma_n}(2\lambda_n r)L_n^{2\gamma_n}(2\lambda_n r')}{n+\gamma_n+1-\nu} \\ &+ (\kappa_n-\nu/\epsilon_n)\frac{n!}{\Gamma(2\gamma_n+1+n)}\frac{L_n^{2\gamma_n}(2\lambda_n r)L_n^{2\gamma_n}(2\lambda_n r')}{n+\gamma_n-\nu} \\ &- \frac{n!}{\Gamma(2\gamma_n+n)}\frac{L_n^{2\gamma_n-1}(2\lambda_n r)L_n^{2\gamma_n}(2\lambda_n r')-L_n^{2\gamma_n}(2\lambda_n r)L_n^{2\gamma_n-1}(2\lambda_n r')}{n+\gamma_n-\nu}\Bigg)\,, \end{aligned} \tag{A.9}$$

$$g^{21}_{\kappa_n} = g^{12}_{\kappa_n}(r \leftrightarrow r')\,, \tag{A.10}$$

$$\begin{aligned} g^{22}_{\kappa_n} &= \frac{\varepsilon}{2}(2\lambda_n)^{2\gamma_n}(rr')^{\gamma_n-1}e^{-\lambda_n(r+r')}\sum_{n=0}^{\infty}\Bigg((\kappa_n+\nu/\epsilon_n)\frac{n!}{\Gamma(2\gamma_n+1+n)}\frac{L_n^{2\gamma_n}(2\lambda_n r)L_n^{2\gamma_n}(2\lambda_n r')}{n+\gamma_n+1-\nu} \\ &- [(\kappa_n-\nu/\epsilon_n)-2(\gamma_n+\nu)]\frac{n!}{\Gamma(2\gamma_n+1+n)}\frac{L_n^{2\gamma_n}(2\lambda_n r)L_n^{2\gamma_n}(2\lambda_n r')}{n+\gamma_n-\nu} \\ &- \frac{n!}{\Gamma(2\gamma_n+n)}\frac{L_n^{2\gamma_n-1}(2\lambda_n r)L_n^{2\gamma_n}(2\lambda_n r')+L_n^{2\gamma_n}(2\lambda_n r)L_n^{2\gamma_n-1}(2\lambda_n r')}{n+\gamma_n-\nu}\Bigg)\,. \end{aligned} \tag{A.11}$$

Here, we introduced the notations

$$\varepsilon = \sqrt{\frac{mc^2-E}{mc^2+E}}\,, \epsilon = \frac{E}{mc^2}\,, \nu = \frac{\alpha Z\epsilon}{\sqrt{1-\epsilon^2}}\,. \tag{A.12}$$

–APPENDIX B–

REDUCTION OF ANGULAR MATRIX ELEMENTS

We collect some formulas which will be important in the calculation of the angular part of matrix elements. In a general two-component system like a Dirac wave function possessing an orbital and a spin part, with the tensor $R_{k_1}(1)$ acting only on the first part and $S_{k_2}(2)$ only on the second component, a tensor acting on the composite system can be written as [15]

$$\begin{aligned} &T_{KQ}(k_1 k_2) = \\ &= \sum_{q_1 q_2} R_{k_1 q_1}(1) S_{k_2 q_2}(2) C(k_1 k_2 K; q_1 q_2 Q)\,, \end{aligned} \tag{B.1}$$

with the $C(k_1 k_2 K; q_1 q_2 Q)$ being the Clebsch-Gordan coefficients. The reduced matrix element of the spherical tensor operator can be written as [15]

$$\begin{aligned} &\langle j_1 j_2 j || T_K(k_1 k_2) || j_1' j_2' j' \rangle = \\ &= [(2j'+1)(2K+1)(2j_1+1)(2j_2+1)]^{1/2} \\ &\times \left\{ \begin{array}{ccc} j & j' & K \\ j_1 & j_1' & k_1 \\ j_2 & j_2' & k_2 \end{array} \right\} \langle j_1 || R_{k_1} || j_1' \rangle \langle j_2 || S_{k_2} || j_2' \rangle\,. \end{aligned} \tag{B.2}$$

Here, the $9j$ symbol was introduced in its usual notation. We apply this general theorem to an electron, i.e. a particle with its spin equal to $1/2$, coupled with the orbital angular momentum l (l') to the quantum number j (j') (i.e. we substitute in the above equation $j_1 = l_1$, $j_1' = l_1'$, and $j_2 = j_2' = 1/2$):

$$\begin{aligned} &\langle l_1 \frac{1}{2} j || T_K(C_{k_1} \sigma_1) || l_1' \frac{1}{2} j' \rangle = \\ &= [(2j'+1)(2K+1)(2l_1+1)2]^{1/2} \\ &\times \left\{ \begin{array}{ccc} j & j' & K \\ l_1 & l_1' & k_1 \\ \frac{1}{2} & \frac{1}{2} & 1 \end{array} \right\} \langle l_1 || C_{k_1} || l_1' \rangle \langle \frac{1}{2} || \sigma_1 || \frac{1}{2} \rangle\,. \end{aligned} \tag{B.3}$$

Using the matrix elements [15]

$$\langle l_1 || C_{k_1} || l_1' \rangle = (2l_1'+1)^{1/2} (-1)^{l_1} \left(\begin{array}{ccc} l_1 & k_1 & l_1' \\ 0 & 0 & 0 \end{array} \right) \tag{B.4}$$

and

$$\langle \frac{1}{2} || \sigma_1 || \frac{1}{2} \rangle = 2 \langle \frac{1}{2} || \boldsymbol{S} || \frac{1}{2} \rangle = \sqrt{3}\,, \tag{B.5}$$

we get

$$\langle l_1 \frac{1}{2} j || T_K(C_{k_1}\sigma_1) || l_1' \frac{1}{2} j' \rangle =$$
$$= \sqrt{(2j'+1)(2K+1)(2l_1+1)6} \left\{ \begin{array}{ccc} j & j' & K \\ l_1 & l_1' & k_1 \\ \frac{1}{2} & \frac{1}{2} & 1 \end{array} \right\}$$
$$\times (2l_1'+1)^{1/2} (-1)^{l_1} \left(\begin{array}{ccc} l_1 & k_1 & l_1' \\ 0 & 0 & 0 \end{array} \right), \tag{B.6}$$

where $\boldsymbol{S}$ is the spin operator.

In the case of $k_1 = K$, the expression relating the $9j$-symbol to the Racah W-coefficient simplifies to [15]

$$\left\{ \begin{array}{ccc} j & j' & K \\ l_1 & l_1' & K \\ \frac{1}{2} & \frac{1}{2} & 1 \end{array} \right\} =$$
$$= \frac{j(j+1) - l_1(l_1+1) - j'(j'+1) + l_1'(l_1'+1)}{[6K(K+1)(2K+1)]^{1/2}}$$
$$\times (-1)^{K+1/2-j-l_1'} W\left(jj'l_1l_1'; K1/2\right). \tag{B.7}$$

Thus, the reduced matrix element can be rewritten as [15]

$$\langle l_1 \frac{1}{2} j || T_K(C_K\sigma_1) || l_1' \frac{1}{2} j' \rangle =$$
$$= \frac{j(j+1) - l_1(l_1+1) - j'(j'+1) + l_1'(l_1'+1)}{\sqrt{K(K+1)}}$$
$$\times (-1)^{K+1/2-j-l_1'+l_1} \sqrt{(2j'+1)(2l_1+1)(2l_1'+1)}$$
$$\times W\left(jj'l_1l_1'; K1/2\right) \left(\begin{array}{ccc} l_1 & k_1 & l_1' \\ 0 & 0 & 0 \end{array} \right). \tag{B.8}$$

Let us pay attention to the product of the Racah coefficient and the $3j$ symbol. The $6j$ symbol is invariant under the interchange of any two columns, and also for interchange of the upper and lower arguments in each of any two columns. Thus the following relation holds: $W\left(abcd; e1/2\right) = W\left(dcba; e1/2\right)$. If $a+b+e$ is even, a special case is [15]

$$W\left(abcd; e\frac{1}{2}\right) \left(\begin{array}{ccc} a & b & e \\ 0 & 0 & 0 \end{array} \right) = \tag{B.9}$$
$$= -\frac{1}{[(2a+1)(2b+1)]^{1/2}} \left(\begin{array}{ccc} c & d & e \\ -\frac{1}{2} & \frac{1}{2} & 0 \end{array} \right).$$

In our case the corresponding expression is as follows:

$$W\left(l_1'l_1j'j; K\frac{1}{2}\right) \left(\begin{array}{ccc} K & l_1 & l_1' \\ 0 & 0 & 0 \end{array} \right) = \tag{B.10}$$
$$= -(-1)^{K+l_1+l_1'} \frac{1}{[(2l_1'+1)(2l_1+1)]^{1/2}} \left(\begin{array}{ccc} j' & j & K \\ -\frac{1}{2} & \frac{1}{2} & 0 \end{array} \right).$$

The reduced matrix element thus becomes

$$\langle l_1 \frac{1}{2} j || T_K(C_K \sigma_1) || l_1' \frac{1}{2} j' \rangle =$$
$$= \frac{j(j+1) - l_1(l_1+1) - j'(j'+1) + l_1'(l_1'+1)}{[K(K+1)]^{1/2}}$$
$$\times (-1)^{j'-K-1/2} (2j'+1)^{1/2} \begin{pmatrix} j & j' & K \\ \frac{1}{2} & -\frac{1}{2} & 0 \end{pmatrix}. \tag{B.11}$$

Using the relation $j(j+1) - l_1(l_1+1) - j'(j'+1) + l_1'(l_1'+1) = \kappa - \kappa'$, we arrive to [15]

$$\langle l_1 \frac{1}{2} j || T_K(C_K \sigma_1) || l_1' \frac{1}{2} j' \rangle = \frac{\kappa - \kappa'}{[K(K+1)]^{1/2}}$$
$$\times (-1)^{j'-K-1/2} (2j'+1)^{1/2} \begin{pmatrix} j & j' & K \\ \frac{1}{2} & -\frac{1}{2} & 0 \end{pmatrix}. \tag{B.12}$$

In the case of $k_1 = K+1$, the reduced matrix element of the spherical tensor operator can be written as [15]

$$\langle l_1 \frac{1}{2} j || T_K(C_{K+1} \sigma_1) || l_1' \frac{1}{2} j' \rangle =$$
$$= [(2j'+1)(2K+1)(2l_1+1)6]^{1/2} \begin{Bmatrix} j & j' & K \\ l_1 & l_1' & K+1 \\ \frac{1}{2} & \frac{1}{2} & 1 \end{Bmatrix}$$
$$\times (2l_1'+1)^{1/2} (-1)^{-K-1-l_1'} \begin{pmatrix} K+1 & l_1 & l_1' \\ 0 & 0 & 0 \end{pmatrix}. \tag{B.13}$$

If $c+d+e$ is odd, the following relation holds:

$$\begin{pmatrix} c+1 & d & e \\ 0 & 0 & 0 \end{pmatrix} \begin{Bmatrix} a & b & c \\ d & e & c+1 \\ \frac{1}{2} & \frac{1}{2} & 1 \end{Bmatrix} =$$
$$= \frac{(d-a)(2a+1) + (e-b)(2b+1) + c + 1}{[6(c+1)(2c+1)(2c+3)(2d+1)(2e+1)]^{1/2}}$$
$$\times (-1)^{b+e+1/2} \begin{pmatrix} a & b & c \\ \frac{1}{2} & -\frac{1}{2} & 0 \end{pmatrix}, \tag{B.14}$$

thus the product of the $3j$ and $9j$ symbols in our case can be written as

$$\begin{pmatrix} K+1 & l_1 & l_1' \\ 0 & 0 & 0 \end{pmatrix} \begin{Bmatrix} j & j' & K \\ l_1 & l_1' & K+1 \\ \frac{1}{2} & \frac{1}{2} & 1 \end{Bmatrix} =$$
$$= \frac{(l_1 - j)(2j+1) + (l_1' - j')(2j'+1) + K + 1}{[6(K+1)(2K+1)(2K+3)(2l_1+1)(2l_1'+1)]^{1/2}}$$
$$\times (-1)^{j'+l_1'+1/2} \begin{pmatrix} j & j' & K \\ \frac{1}{2} & -\frac{1}{2} & 0 \end{pmatrix}. \tag{B.15}$$

Using the formula $\kappa = (l_1 - j)(2j + 1)$, this can be further simplified to [15]

$$\begin{aligned}
&\langle l_1 \frac{1}{2} j || T_K(C_{K+1}\sigma_1) || l_1' \frac{1}{2} j' \rangle = \\
&= -\frac{\kappa + \kappa' + K + 1}{[(K+1)(2K+3)]^{1/2}} (-1)^{j'-K-1/2} \\
&\times (2j'+1)^{1/2} \begin{pmatrix} j & j' & K \\ \frac{1}{2} & -\frac{1}{2} & 0 \end{pmatrix} .
\end{aligned} \tag{B.16}$$

Finally, in the case of $k_1 = K - 1$, the reduced matrix element is given as [15]

$$\begin{aligned}
&\langle l_1 \frac{1}{2} j || T_K(C_{K+1}\sigma_1) || l_1' \frac{1}{2} j' \rangle = \\
&= [(2j'+1)(2K+1)(2l_1+1)6]^{1/2} \begin{Bmatrix} j & j' & K \\ l_1 & l_1' & K-1 \\ \frac{1}{2} & \frac{1}{2} & 1 \end{Bmatrix} \\
&\times (2l_1'+1)^{1/2} (-1)^{-K-1-l_1'} \begin{pmatrix} K-1 & l_1 & l_1' \\ 0 & 0 & 0 \end{pmatrix} .
\end{aligned} \tag{B.17}$$

When the sum $c + d + e$ is odd, the product of the algebraic symbols can be written as

$$\begin{aligned}
&\begin{pmatrix} c+1 & d & e \\ 0 & 0 & 0 \end{pmatrix} \begin{Bmatrix} a & b & c \\ d & e & c-1 \\ \frac{1}{2} & \frac{1}{2} & 1 \end{Bmatrix} = \\
&= \frac{(d-a)(2a+1) + (e-b)(2b+1) - c}{[6c(2c+1)(2c-1)(2d+1)(2e+1)]^{1/2}} \\
&\times (-1)^{b+e+1/2} \begin{pmatrix} a & b & c \\ \frac{1}{2} & -\frac{1}{2} & 0 \end{pmatrix} .
\end{aligned} \tag{B.18}$$

Applying this relation to the case of interest,

$$\begin{aligned}
&\begin{pmatrix} K-1 & l_1 & l_1' \\ 0 & 0 & 0 \end{pmatrix} \begin{Bmatrix} j & j' & K \\ l_1 & l_1' & K-1 \\ \frac{1}{2} & \frac{1}{2} & 1 \end{Bmatrix} = \\
&= \frac{(l_1 - j)(2j+1) + (l_1' - j')(2j'+1) - K}{[6K(2K+1)(2K-K)(2l_1+1)(2l_1'+1)]^{1/2}} \\
&\times (-1)^{j'+l_1'+1/2} \begin{pmatrix} j & j' & K \\ \frac{1}{2} & -\frac{1}{2} & 0 \end{pmatrix} ,
\end{aligned} \tag{B.19}$$

and applying again the formula $\kappa = (l_1 - j)(2j + 1)$, one arrives to [15]

$$\begin{aligned}
&\langle l_1 \frac{1}{2} j || T_K(C_{K+1}\sigma_1) || l_1' \frac{1}{2} j' \rangle = \\
&= \frac{\kappa + \kappa' - K}{[K(2K-1)]^{1/2}} (-1)^{j'-K-1/2} \\
&\times (2j'+1)^{1/2} \begin{pmatrix} j & j' & K \\ \frac{1}{2} & -\frac{1}{2} & 0 \end{pmatrix}
\end{aligned} \tag{B.20}$$

The results in Eq. (B.11), (B.16) and (B.20) can be summarized as [15]

$$\begin{aligned}
&\langle l_1 \frac{1}{2} j || T_K(C_k\sigma_1) || l_1' \frac{1}{2} j' \rangle = \\
&= a_K (-1)^{j'-K-1/2} (2j'+1)^{1/2} \begin{pmatrix} j & j' & K \\ \frac{1}{2} & -\frac{1}{2} & 0 \end{pmatrix} ,
\end{aligned} \tag{B.21}$$

with the factors

$$\begin{aligned} a_k &= (\kappa - \kappa')/\sqrt{k(k+1)}\,, \\ a_{k-1} &= -(k + \kappa + \kappa')/\sqrt{2k(k+1)}\,, \\ a_{k+1} &= (k + 1 - \kappa - \kappa')/\sqrt{(k+1)(2k+1)}\,. \end{aligned} \tag{B.22}$$

–APPENDIX C–

ALLOWED COUPLINGS OF SUBSHELL ANGULAR MOMENTA IN RELATIVISTIC ATOMIC STATES

	q	v	J
$j=\frac{1}{2}$	0,2	0	0
	1	1	$\frac{1}{2}$
$j=\frac{3}{2}$	0,4	0	0
	1,3	1	$\frac{3}{2}$
	2	0	0
		2	2
$j=\frac{5}{2}$	0,6	0	0
	1,5	1	$\frac{5}{2}$
	2,4	0	0
		2	2,4
	3	1	$\frac{5}{2}$
		3	$\frac{3}{2},\frac{9}{2}$
$j=\frac{7}{2}$	0,8	0	0
	1,7	1	$\frac{7}{2}$
	2,6	0	0
		2	2,4,6
	3,5	1	$\frac{7}{2}$
		3	$\frac{3}{2},\frac{5}{2},\frac{9}{2},\frac{11}{2},\frac{15}{2}$
	4	0	0
		2	2,4,6
		4	2,4,5,8
$j=\frac{9}{2}$	0,10	0	0
	1,9	1	$\frac{9}{2}$
	2,8	0	0
		2	2,4,6,8
	3,7	1	$\frac{9}{2}$
		3	$\frac{3}{2},\frac{5}{2},\frac{7}{2},\frac{9}{2},\frac{11}{2},\frac{13}{2},\frac{15}{2},\frac{17}{2},\frac{21}{2}$
	4,6	0	0
		2	2,4,6,8

	q	v	J
$j = \frac{9}{2}$		4	0,2,3,4^2,5,6^2,7,8,9,10,12
	5	1	$\frac{9}{2}$
		3	$\frac{3}{2},\frac{5}{2},\frac{7}{2},\frac{9}{2},\frac{11}{2},\frac{13}{2},\frac{15}{2},\frac{17}{2},\frac{21}{2}$
		5	$\frac{1}{2},\frac{5}{2},\frac{7}{2},\frac{9}{2},\frac{11}{2},\frac{13}{2},\frac{15}{2},\frac{17}{2},\frac{19}{2},\frac{25}{2}$

Table C.1: Allowed coupling of states j^q for $j = \frac{1}{2} - \frac{9}{2}$.The seniority of the coupling and the subshell angular momentum are denoted, respectively, by v and J. The superscript 2 that follows $J = 4, 6$ for $j^q = \left(\frac{9}{2}\right)^{4,6}$, $v = 4$ indicates a two-fold degeneracy with respect to this classification scheme [24].

Bibliography

[1] European XFEL Project, http://xfel.desy.de/technical_information/photon_beam_para-meter/.

[2] Stanford LCLS Specifications, https://slacportal.slac.stanford.edu/sites/lcls_public/Instruments/SXR/Pages/Specifications.aspx.

[3] M. Abramowitz and I. A. Stegun. *Handbook of mathematical functions*. National Bureau of Standards, 1972.

[4] V. Ayvazyan, N. Baboi, J. Bahr, V. Balandin, B. Beutner, A. Brandt, I. Bohnet, A. Bolzmann, R. Brinkmann, O. I. Brovko, J. P. Carneiro, S. Casalbuoni, M. Castellano, P. Castro, L. Catani, E. Chiadroni, S. Choroba, A. Cianchi, H. Delsim-Hashemi, G. Di Pirro, M. Dohlus, S. Dusterer, H. T. Edwards, B. Faatz, A. A. Fateev, J. Feldhaus, K. Flottmann, J. Frisch, L. Frohlich, T. Garvey, U. Gensch, N. Golubeva, H. J. Grabosch, B. Grigoryan, O. Grimm, U. Hahn, J. H. Han, M .V. Hartrott, K. Honkavaara, M. Huning, R. Ischebeck, E. Jaeschke, M. Jablonka, R. Kammering, V. Katalev, B. Keitel, S. Khodyachykh, Y. Kim, V. Kocharyan, M. Korfer, M. Kollewe, D. Kostin, D. Kramer, M. Krassilnikov, G. Kube, L. Lilje, T. Limberg, D. Lipka, F. Lohl, M. Luong, C. Magne, J. Menzel, P. Michelato, V. Miltchev, M. Minty, W. D. Moller, L. Monaco, W. Muller, M. Nagl, O. Napoly, P. Nicolosi, D. Nolle, T. Nunez, A. Oppelt, C. Pagani, R. Paparella, B. Petersen, B. Petrosyan, J. Pfluger, P. Piot, E. Plonjes, L. Poletto, D. Proch, D. Pugachov, K. Rehlich, D. Richter, S. Riemann, M. Ross, J. Rossbach, M. Sachwitz, E. L. Saldin, W. Sandner, H. Schlarb, B. Schmidt, M. Schmitz, P. Schmuser, J. R. Schneider, E. A. Schneidmiller, H. J. Schreiber, S. Schreiber, A. V. Shabunov, D. Sertore, S. Setzer, S. Simrock, E. Sombrowski, L. Staykov, B. Steffen, F. Stephan, F. Stulle, KP. Sytchev, H. Thom, K. Tiedtke, M. Tischer, R. Treusch, D. Trines, I. Tsakov, A. Vardanyan, R. Wanzenberg, T. Weiland, H. Weise, M. Wendt, I. Will, A. Winter, K. Wittenburg, M. V. Yurkov, I. Zagorodnov, P. Zambolin, and K Zapfe. First operation of a free-electron laser generating GW power radiation at 32 nm wavelength. *Eur. Phys. J. D*, 37:297, 2006.

[5] F. A. Babushkin. A relativistic treatment of radiation transitions. *Opt. Spectr.*, 13:77, 1962.

[6] A. O. Barut and Y. I. Salamin. Relativistic theory of spontaneous emission. *Phys. Rev. A*, 37:2284, 1988.

[7] D. Bauer and P. Koval. Qprop: A Schrödinger-solver for intense laseratom interaction. *Comput. Phys. Comm.*, 174:396, 2006.

[8] P. Beiersdorfer, H. Chen, D. B. Thorn, and E. Träbert. Measurement of the two-loop lamb shift in Lithiumlike U^{89+}. *Phys. Rev. Lett.*, 95:233003, 2005.

[9] C. Beilmann. Measurement of higher-order resonant recombination processes. in preparation.

[10] C. Beilmann, O. Postavaru, L. H. Arntzen, R. Ginzel, C. H. Keitel, V. Mäckel, P. H. Mokler, M. C. Simon, H. Tawara, I. I. Tupitsyn, J. Ullrich, J. R. Crespo López-Urrutia, and Z. Harman. Intershell trielectronic recombination with K-shell excitation in Kr^{30+}. *Phys. Rev. A*, 80:050702(R), 2009.

[11] M. Bitter, H. Hsuan, C. Bush, S. Cohen, C. J. Cummings, B. Grek, K. W. Hill, J. Schivell, M. Zarnstorff, P. Beiersdorfer, A. Osterheld, A. Smith, and B. Fraenkel. Spectra of Heliumlike Krypton from Tokamak fusion test reactor plasmas. *Phys. Rev. Lett.*, 71:1007, 1993.

[12] C. Brandau, C. Kozhuharov, Z. Harman, A. Müller, S. Schippers, Y. S. Kozhedub, D. Bernhardt, S. Böhm, J. Jacobi, E. W. Schmidt, P. H. Mokler, F. Bosch, H.-J. Kluge, Th. Stöhlker, K. Beckert, P. Beller, F. Nolden, M. Steck, A. Gumberidze, R. Reuschl, U. Spillmann, F. J. Currell, I. I. Tupitsyn, V. M. Shabaev, U. D. Jentschura, C. H. Keitel, A. Wolf, and Z. Stachura. Isotope shifts in the dielectronic recombination of three-electron $^{A}Nd^{57+}$. *Phys. Rev. Lett.*, 100:073201, 2008.

[13] C. Brandau, C. Kozhuharov, A. Müller, W. Shi, S. Schippers, T. Bartsch, S. Böhm, C. Böhme, A. Hoffknecht, H. Knopp, N. Grün, W. Scheid, T. Steih, F. Bosch, B. Franzke, P. H. Mokler, F. Nolden, M. Steck, T. Stöhlker, and Z. Stachura. Precise determination of the $2s_{1/2} - 2p_{1/2}$ splitting in very heavy Lithiumlike ions utilizing dielectronic recombination. *Phys. Rev. Lett.*, 91:073202, 2003.

[14] B. M. Brandsen and C. J. Joachain. *Introduction to Quantum Mechanics*. Longman, 1989.

[15] D. M. Brink and G. R. Satchler. *Angular Momentum*. Oxford Science Publications, 2002.

[16] A. Burgess. A general formula for the estimation of dielectronic recombination co-efficients in low-density plasmas. *Astr. Jour.*, 139:886, 1964.

[17] S. A. Cohen, K.A. Werley, D.E. Posta, B.J. Braams, J.L. Perkins, and D. Pearlstein. Two-dimensional fluid simulations of the ITER SOL plasma. *Jour. Nucl. Mater.*, 176 & 177:909, 1990.

[18] N. D. Cook. *Models of the Atomic Nucleus*. Springer, Berlin, Heidelberg, New York, 2006.

[19] J. T. Costello. Photoionization experiments with the ultrafast EUV laser 'FLASH' free electron laser in Hamburg. *J. Phys.: Conf. Ser.*, 88:012057, 2007.

[20] J. R. Crespo López-Urrutia, A. Dorn, R. Moshammer, and J. Ullrich. The Freiburg electron beam ion trap/source project FreEBIT. *Phys. Scr.*, T80:502, 1999.

[21] R. Şchiopu, Z. Harman, W. Scheid, and N. Grün. Isotope shifts of dielectronic resonances for heavy few-electron ions. *Eur. Phys. J. D.*, 31:21, 2004.

[22] J. Cummings, S.A. Cohen, R. Hulse, D.E. Post, M.H. Redi, and J. Perkins. Power radiated from ITER by impurities. *Jour. Nucl. Mater.*, 176 & 177:916, 1990.

[23] P.A.M. Dirac. The quantum theory of the electron. *P. Roy. Soc. Lond. A Mat.*, 117:610, 1928.

[24] K. G. Dyall, I. P. Grant, C. T. Johnson, F. A. Parpia, and E. P. Plummer. Grasp: A general-purpose relativistic atomic structure program. *Comput. Phys. Commun.*, 55:425, 1989.

[25] J. Eichler and W.E. Meyerhof. *Relativistic Atomic Collisions*. Academic Press San Diego, 1995.

[26] S.R. Elliott, P. Beiersdorfer, and M.H. Chen. Trapped-ion technique for measuring the nuclear charge radii of highly charged radioactive isotopes. *Phys. Rev. Lett.*, 76:1031, 1996.

[27] S. W. Epp, J. R. Crespo López-Urrutia, G. Brenner, V. Mäckel, P. H. Mokler, R. Treusch, M. Kuhlmann, M. V. Yurkov, J. Feldhaus, J. R. Schneider, M. Wellhöfer, M. Martins, W. Wurth, and J. Ullrich. Soft X-Ray laser spectroscopy on trapped highly charged iones at FLASH. *Phys. Rev. Lett.*, 98:183001, 2007.

[28] G. Fricke, C. Bernhardt, K. Heilig, L.A. Schellenberg, E.B. Shera, and C.W. Dejager. Nuclear ground state charge radii from electromagnetic interactions. *At. Data. Nucl. Data. Tables 60*, 2:177, 1995.

[29] T. Fuchs, C. Biedermann, and R. Radtke. Channel-specific dielectronic recombination of highly charged Krypton. *Phys. Rev. A*, 58:4518, 1998.

[30] M. Gail, N. Grün, and W. Scheid. Angular distribution of radiation emitted after resonant transfer and excitation. *J. Phys. B: At. Mol. Opt. Phys.*, 31:4645, 1998.

[31] W. Geithner, T. Neff, G. Audi, K. Blaum, P. Delahaye, H. Feldmeier, S. George, C. Guénaut, F. Herfurth, A. Herlert, S. Kappertz, M. Keim, A. Kellerbauer, H.-J. Kluge, M. Kowalaska, P. Livens, D. Lunney, K. Marinova, R. Neugart, L. Schweikhard, S. Wibert, and C. Yazidjian. Masses and charge radii of $^{17-22}$Ne and the two-proton-halo candidate ^{17}Ne. *Phys. Rev. Lett.*, 101:252502, 2008.

[32] A. J. González Martínez, J. R. Crespo López-Urrutia, J. Braun, G. Brenner, H. Bruhns, A. Lapierre, V. Mironov, R. Soria Orts, H. Tawara, M. Trinczek, and J. Ullrich. State-selective quantum interference observed in the recombination of highly charged $Hg^{75+-78+}$ Mercury ions in an electron beam ion trap. *Phys. Rev. Lett.*, 94:203201, 2005.

[33] A. J. González Martínez, J. R. Crespo López-Urrutia, J. Braun, G. Brenner, H. Bruhns, A. Lapierre, V. Mironov, R. Soria Orts, H. Tawara, M. Trinczek, J. Ullrich, A. N. Artemyev, Z. Harman, U. D. Jentschura, C. H. Keitel, J. H. Scofield, and I. I. Tupitsyn. Benchmarking high-field few-electron correlation and QED contributions in Hg^{75+} to Hg^{78+} ions. i. experiment. *Phys. Rev. A*, 73:052710, 2006.

[34] I. P. Grant. Gauge invariance and relativistic radiative transitions. *J. Phys. B*, 7:1458, 1974.

[35] I. P. Grant. A program to calculate angular momentum coefficients in relativistic atomic structure - revised version. *Comput. Phys. Commun.*, 11:397, 1976.

[36] I. P. Grant. *Relativistic Quantum Theory of Atoms and Molecules*. Springer, Berlin, Germany, 2006.

[37] I. P. Grant, B.J. McKenzie, P. H. Norrington, D. F. Mayer, and N. C. Pyper. An atomic multiconfigurational Dirac-Fock package. *Comput. Phys. Commun.*, 21:233, 1980.

[38] W. Greiner. *Relativistic Quantic Mechanics*. Springer, Berlin, Germany, 2000.

[39] A. Gumberidze, Th. Stöhlker, D. Banaś, K. Beckert, P. Beller, H. F. Beyer, F. Bosch, S. Hagmann, C. Kozhuharov, D. Liesen, F. Nolden, X. Ma, P. H. Mokler, M. Steck, D. Sierpowski, and S. Tashenov. Quantum electrodynamics in strong electric fields: The ground-state Lamb shift in Hydrogenlike Uranium. *Phys. Rev. Lett.*, 94:223001, 2005.

[40] M. Haas, U. D. Jentschura, C. H. Keitel, N. Kolachevsky, M. Herrmann, P. Fendel, M. Fischer, Th. Udem, R. Holzwarth, T. W. Hänsch, M. O. Scully, and G. S. Agarwal. Two-photon excitation dynamics in bound two-body Coulomb systems including ac Stark shift and ionization. *Phys. Rev. A*, 73:052501, 2006.

[41] Y. Hahn. Theory of dielectronic recombination. *Adv. At. Mol. Phys.*, 21:123, 1985.

[42] Z. Harman, I. I. Tupitsyn, A. N. Artemyev, U. D. Jentschura, C. H. Keitel, J. R. Crespo López-Urrutia, A. J. González Martínez, H. Tawara, and J. Ullrich. Benchmarking high-field few-electron correlation and QED contributions in $Hg^{75+...78+}$ ions. II. theory. *Phys. Rev. A*, 73:052711, 2006.

[43] H. G. Hetzheim and C. H. Keitel. Ionization dynamics versus laser intensity in laser-driven multiply charged ions. *Phys. Rev. Lett.*, 102:083003, 2009.

[44] D.J. Hylton and N.J. Snyderman. Analytic basis set for high-z atomic qed calculations: Heavy he-like ions. *Phys. Rev. A*, 55:2651, 1997.

[45] J. D. Jackson. *Classical Electrodynamics*. John Wiley and Sons, Inc., New Jersy, 1999.

[46] W. R. Johnson. Atomic physics. lecture notes, see `http://www.nd.edu/~johnson/Publications/book.pdf`.

[47] W. R. Johnson and G. Soff. The lamb shift in hydrogen-like atoms , $1 \leq z \leq 110$. *Atomic Data and Nuclear Data Tables*, 33:405–446, 1985.

[48] C. H. Keitel. Narrowing spontaneous emission without intensity reduction. *Phys. Rev. Lett.*, 83:1307, 1999.

[49] C. H. Keitel, L. M. Narducci, and M. O. Scully. Origin of the sub-natural line-narrowing effect in resonance fluorescence. *Phys. Rev. B*, 60:153, 1995.

[50] M. Klaiber, K. Z. Hatsagortsyan, and C. H. Keitel. Gauge-invariant relativistic strong-field approximation. *Phys. Rev. A*, 73:053411, 2006.

[51] A. D. Knapp, P. Beiersdorfer, M. H. Chen, J. H. Scofield, and D. Schneider. Observation of interference between dielectronic recombination and radiative recombination in highly charged Uranium Ions. *Phys. Rev. Lett.*, 74:54, 1995.

[52] L. D. Landau and E. M. Lifshitz. *Quantum Mechanics, non-relativistic theory*. Pergamon Press, 1991.

[53] A. Lapierre, U. D. Jentschura, J. R. Crespo López–Urrutia, J. Braun, G. Brenner, H. Bruhns, D. Fischer, A. J. González Martínez, Z. Harman, W. R. Johnson, C. H. Keitel, V. Mironov, C. J. Osborne, G. Sikler, R. Soria Orts, V. Shabaev, H. Tawara, I. I. Tupitsyn, J. Ullrich, and A. Volotka. Relativistic electron correlation, quantum electrodynamics, and the lifetime of the $1s^2 2s^2 2p\ ^2P^o_{3/2}$ level in Boronlike Argon. *Phys. Rev. Lett.*, 95:183001, 2005.

[54] M. Lax. *Statistical Physics, Phase Transitions and Superfluidity*. Gordon and Breach, New York, 1968.

[55] M. Lestinsky, E Lindroth, D.A. Orlov, E.W. Schmidt, S. Schippers, S. Böhm S, C. Brandau, F. Sprenger, A.S. Terekhov, A. Müller, and A. Wolf. Screened radiative corrections from hyperfine-split dielectronic resonances in Lithiumlike Scandium. *Phys. Rev. Lett.*, 100(3):033001, 2008.

[56] M. S. Manka, H. M. Doss, L. M. Narducci, P. Ru, and G. L. Oppo. Spontaneous emission and absorption properties of a driven three-level system ii. the λ and cascade models. *Phys. Rev. A*, 43:3748, 1991.

[57] H. S. W. Massey and R. R. Bates. The properties of neutral and ionized atomic Oxygen and their influence on the upper atmosphere. *Rep. Prog. Phys.*, 9:62, 1942.

[58] C. Müller. Nonlinear Bethe-Heitler pair creation with attosecond laser pulses at the LHC. *Phys. Lett. B*, 672:56, 2009.

[59] C. Müller, C. Deneke, and C. H. Keitel. Muon-pair creation by two X-Ray laser photons in the field of an atomic nucleus. *Phys. Rev. Lett.*, 101:060402, 2008.

[60] N. Nakamura et al. Evidence for strong Breit interaction in dielectronic recombination of highly charged heavy ions. *Phys. Rev. Lett.*, 100(7):073203, 2008.

[61] L. M. Narducci, M. O. Scully, G.-L. Oppo, P. Ru, and J. R. Tredicce. Spontaneous emission and absorption properties of a driven three-level system. *Phys. Rev. A*, 42:1630, 1990.

[62] A. Palffy. Nuclear effects in atomic transitions. *Contemporary Physics*, 51:471–496, 2010.

[63] C. W. P. Palmer. Reformulation of the theory of the mass shift. *J. Phys. B*, 20:5987, 1987.

[64] E. Paspalakis and P. L. Knight. Phase control of spontaneous emission. *Phys. Rev. Lett.*, 81:293, 1998.

[65] N. C. Pyper, I. P. Grant, and N. Beatham. A new program for calculating matrix elements of one-particle operators in jj-coupling. *Comput. Phys. Commun.*, 15:387, 1978.

[66] R. Radtke, C. Biedermann, T. Fuchs, G Fussmann, and P. Beiersdorfer. Measurement of the radiative cooling rates for high-ionization species of Krypton using an electron beam ion trap. *Phys. Rev. E*, 61:1966, 2000.

[67] M. E. Rose. *Elementary Theory of Angular Momentum*. John Wiley & Sons, 1967.

[68] J. J. Sakurai. *Modern Quantum Mechanics*. Addison-Wesley Publishing Company, Inc., 1994.

[69] R. Sánchez, W. Nötershäuser, G. Ewald, D. Albers, J. Behr, P. Bricault, B. A. Bushaw, A. Dax, J. Dilling, M. Dombsky, G. W. F. Drake, S. Götte, R. Kirchner, H.-J. Kluge, Th. Kühl, J. Lassen, C. D. P. Levy, M. R. Pearson, E. J. Prime, V. Ryjkov, A. Wojtaszek, Z.-C. Yan, and C. Zimmermann. Nuclear charge radii of ^{9,11}Li: The influence of halo neutrons. *Phys. Rev. Lett.*, 96:033002, 2006.

[70] M. Schnell, G. Gwinner, N. R. Badnell, M. E. Bannister, S. Böhm, J. Colgan, S. Kieslich, S. D. Loch, D. Mitnik, A. MÏller, M. S. Pindzola, S. Schippers, D. Schwalm, W. Shi, A.Wolf, and S.-G. Zhou. Observation of trielectronic recombination in Be-like Cl Ions. *Phys. Rev. Lett.*, 91:043001, 2003.

[71] M. O. Scully and S.-Y. Zhu. Quantum control of the inevitable. *Science*, 281:1973, 1998.

[72] M. O. Scully and M. S. Zubairy. *Quantum Optics*. Cambridge University Press, 1997.

[73] V. M. Shabaev. QED theory of nuclear recoil effects in atoms. *Phys. Rev. A*, 57:59, 1998.

[74] V. M. Shabaev. Two-time Green function method in the quantum electrodynamics of high-Z few-electron atoms. *Phys. Rep.*, 356:119, 2002.

[75] V. M. Shabaev and A. N. Artemyev. Relativistic nuclear recoil corrections to the energy levels of multicharged ions. *J. Phys. B*, 27:1307, 1995.

[76] V. M. Shabaev, M. B. Shabaeva, I. I. Tupitsyn, V. A. Yerokhin, A. N. Artemyev, T. Kühl, M. Tomaselli, and O. M. Zherebtsov. Transition energy and lifetime for the ground-state hyperfine splitting of high-Z Lithiumlike ions. *Phys. Rev. A*, 57:149, 1998.

[77] R. Soria Orts, Z. Harman, J. R. Crespo López-Urrutia, A. N. Artemyev, H. Bruhns, A. J. González Martínez, U. D. Jentschura, C. H. Keitel, A. Lapierre, V. Mironov, V. M. Shabaev, H. Tawara, I. I. Tupitsyn, J. Ullrich, and A. V. Volotka. Exploring relativistic many-body recoil effects in highly charged ions. *Phys. Rev. Lett.*, 97:103002, 2006.

[78] A. A. Sorokin, S. V. Bobashev, T. Feigl, K. Tiedtke, H. Wabnitz, and M. Richter. Photoelectric effect at ultrahigh intensities. *Phys. Rev. Lett.*, 99:213002, 2007.

[79] R. A. Swainson and G W F Drake. A unified treatment of the non-relativistic and relativistic hydrogen atom ii: the green function. *J. Phys. A: Math. Gen*, 24:95–120, 1991.

[80] K. Widmann, P. Beiersdorfer, V. Decaux, S.R. Elliott, D. Knapp, A. Osterheld, M. Bitter, and A. Smith. Studies of He-like Krypton for use in determining electron and ion temperatures in very-high-temperature plasmas. *Rev. Sci. Instrum.*, 66:761, 1995.

[81] P. Zhou and S. Swain. Ultranarrow spectral lines via quantum interference. *Phys. Rev. Lett.*, 77:3995, 1996.

[82] S.-Y. Zhu and M. O. Scully. Spectral line elimination and spontaneous emission cancellation via quantum interference. *Phys. Rev. Lett.*, 76:388, 1996.

[83] P. Zimmerer. *Relativistische Theorie für die dielektronische Rekombination bei sehr schweren hochgeladenen Ionen*. PhD thesis, Justus-Liebig-Universität Giessen, 1992.

[84] M. Zimmermann. *Photo-Rekombination bei sehr schweren hochgeladenen Ionen*. PhD thesis, Justus-Liebig-Universität Giessen, 1996.

[85] Y. Zou, J. R. Crespo López-Urrutia, and J. Ullrich. Observation of dielectronic recombination through two-electron one-photon correlative stabilization in an electron-beam ion trap. *Phys. Rev. A*, 67:042703, 2003.

[86] J.D. Zumbro, E.B. Shera, Y. Tanaka, C.E. Bemis, Jr., R.A. Naumann, M.V. Hoehn, W. Reuter, and R.M. Steffen. E2 and E4 deformation in ^{233,234,235,238}U. *Phys. Rev. Lett.*, 53:1888, 1984.

ACKNOWLEDGMENTS

Firstly, I must thank my two supervisors Prof. Dr. Christoph H. Keitel and Dr. Zoltán Harman who have kept me on the right track throughout my research.

I express my gratitude to my parents, Dan and Raica, and my brother Silviu, who have been a constant support to me through my whole life.

To my friends Benjamin Galow, Dr. Mihai Macovei and Dr. Bennaceur Najjari, thank you for teaching me something new each day. I hope we will work on interesting things together in the future.

I thank my previous advisors, Prof. Dr. Sorin Ciulli and Prof. Dr. Adrian Costescu, whose help and advice was invaluable for my scientifical career.

I extend my aknowledgments to my colleagues from the EBIT group of MPIK: Christian Beilmann, PD Dr. José R. Crespo López-Urrutia, Dr. Volkhard Mäckel, Prof. Dr. Paul Mokler and Prof. Dr. Hiroyuki Tawara for such a nice collaboration.

At not last, I would like to say thanks to Sven Bernitt, PD Dr. Jörg Evers, Mircea Girju, Markus Kohler, Dr. Adriana Pálffy, Dr. Sergey Popruzhenko, Prof. Dr. Yousef Salamin, Dr. Andrey Surzhykov, Qurrat-ul-Ain and Dr. Jacek Zatorski for helpful conversations.